TECHNICAL REPORT FOR LABORATORY RESULTS OF SEALING ASSEMBLIES AND CEMENT SYSTEM

AUTHORS:

Saeed Salehi (PhD), Principal Investigator

Ramadan Ahmed (PhD), Co-Principal Investigator

Catalin Teodoriu (PhD), Co-Principal Investigator

Chinedum Peter Ezeakacha, Graduate Research Assistant

George Kwatia, Graduate Research Assistant

Shawgi Ahmed, Graduate Research Assistant

Mustafa Al-Ramadan, Graduate Research Assistant

Prepared under BSEE Project NO: E17PC00005

by

THE UNIVERSITY OF OKLAHOMA

July 2018

1 EXECUTIVE SUMMARY

This report presents the accomplishments and laboratory results of sealing assemblies and cement systems under the Bureau of Safety and Environmental Enforcement (BSEE) Project #E17PC00005. In this report, the term "barrier(s)" defines the use of cement sheath and the liner hanger sealing assembly to prevent uncontrolled influx and migration of formation fluid to a shallow formation or surface facilities. This report is divided into three major sections with three laboratory-scaled test setups. A comprehensive literature review was conducted for all the sections. These reviews provide a road map to addressing the integrity of sealing assemblies and cement systems in downhole conditions.

Cement Tests (Setup I)

This project section discusses different approaches to evaluate and improve cement sealability. In oil and gas drilling operations, set cement is a barrier used to maintain the integrity of a wellbore by preventing influx and the movement of formation fluids through the annular space. Cement sealability is important for regular well operation and safety, while the reduced sealability of a cement sheath can allow formation fluid (gas) to flow in and migrate. The objectives of this project section are: i) Evaluate annular cement integrity and its ability to seal as a primary barrier, by using different classes of Portland cements and gas migration additives; ii) Verify the reliability of current liner overlap pressure test and investigate the critical liner-casing overlap length; and iii) Characterize and report critical cement properties for different anti-gas migration slurry designs.

The results showed that neat Class H and Class G cements are not enough to prevent gas migration and seal as a primary barrier. The physical properties of various anti-gas migration slurry designs have provided a holistic characterization of the slurries. A gas tight cement slurry that was designed with a commercial additive proved to mitigate gas flow through a set cement sheath. Analytical results revealed that the combined annular cement permeability increases as the cement age increases. The leakage scenarios that were evaluated showed an increase in leakage time as the liner-casing overlap increases. Liner-casing overlap ranging from 50 ft to 250 ft may not provide longer duration for detecting and controlling gas influx when the cement sheath is faulty. The leakage time increases as the combined permeability decreases. Finally, the current liner-casing pressure test duration of 30 minutes may not be adequate to detect a faulty cement barrier, should the elastomer in the liner hanger be faulty. All the recommendations from this section of the project are documented in the draft recommendation report.

Elastomer Aging Cell Tests (Setup III)

Elastomers are essential for zonal isolation in the exploration and production of hydrocarbon. They degrade when exposed to harsh downhole conditions. Elastomer degradation can be due to physical and/or chemical changes. Physical degradation can occur when an elastomer is exposed to extreme stress loading conditions (e.g. pressure, temperature, ultra-violet rays, and atmospheric ozone and moisture). Besides physical degradation, elastomers are susceptible to chemical attacks.

Downhole conditions can create pathways for corrosive gases including hydrogen sulfide (H_2S), methane (CH_4), and carbon dioxide (CO_2). When elastomers are exposed to such harsh chemical conditions, they are prone to deteriorate because of changes in their molecular structure. The objectives of this project section are: i) Investigate elastomer integrity as "fit for service" in shallow well construction applications; and ii) Determine elastomer performances under downhole corrosive conditions (temperature, pressure, and corrosive gases). The intrinsic elastomer properties that were investigated include: hardness, volumetric swelling, and compression.

The results showed that elastomer's hardness deteriorates with exposure to the downhole corrosive conditions. The order of corrosive gas effect on elastomer hardness from high to low is CO_2 > All gases > H_2S > CH_4. The H_2S used in this study is 500 ppm H_2S in CH_4 carrier. The term "All gases" stands for a combination of 50% CO_2 and 50% H_2S with CH_4 carrier. Elastomers tend to swell when exposed to these corrosive conditions. This change in property is due to the initial chain rupture in the elastomer, followed by chain growth. Chain rupture increases the elastomer size (swelling), while chain growth causes the elastomer to shrink. H_2S and CH_4 had the least effect on volumetric swelling, while a combination of CO_2, H_2S, and CH_4 had the most detrimental swelling effect on the elastomers. Elastomer compression is characterized by how much strain is recorded at various stresses. Compression results revealed that exposing an elastomer to the least aging condition is enough to compromise its sealing integrity to the point where altering aging parameters becomes redundant. The order of corrosive gas impact on elastomer compression from high to low is CO_2 > All gases > H_2S > CH_4. All the recommendations from this section of the project are documented in the draft recommendation report.

Sealing Assemblies Tests (Setup II)

One of the multiple barriers that is installed during drilling and completions is the liner hanger seal assembly. The liner hanger is used to engage the liner, connect it to the previous casing, and sealed off with cement before a pressure test is performed. Typically, the liner hanger sealing assembly is placed up-stream to the cement column. This arrangement prevents the evaluation of both the cement and liner hanger seal assembly independently, since the sealing element isolates the cement sheath and there is no direct or indirect way of assessing its integrity. Verifying the integrity of elastomeric element and cement at the top of a liner hanger is critical. The performance verification processes and tests in this section of the project/report were performed based on the critical reviews of literature, current regulations, and applicable industry standards. The experimental objectives are: i) Evaluate the performance of common elastomeric seals used in liner hanger sealing systems as independent barrier element, ii) Evaluate the performance of a liner hanger seal assembly and cement sheath to determine which of them acts as a primary barrier; and iii) Develop testing protocols for proper testing of different barriers.

The results from the experiments revealed that the elastomeric seals, such as ethylene propylene diene monomer (EPDM) and nitrile butadiene rubber (NBR), did not exhibit any leakage when they were independently subjected to a pressure test of 40 psig. However, both elastomers failed the pressure test and leaked when a mechanical defect was intentionally created.

Elastomer energization plays a critical role in maintaining their seal integrity. Leakage was observed when NBR samples were subjected to a pressure cycling test and the elastomers were energized by pre-compression force that were generated from the friction between the pipes (inner and outer) and the elastomers. The results also showed that prolonged pressure test duration (up to 60 minutes) did not affect the elastomers performance for pressures up to 40 psig. The independent sealing performance of EPDM and NBR after surfactant degradation was not impaired for the test conditions used in this study. However, the independent sealing performance of EPDM was completely compromised after CO_2 chemical degradation. The pressure tests showed instantaneous decline with no sealing effect. The details of all the results are discussed in this report and all the recommendations from this section of the project are documented in the draft recommendation report.

TABLE OF CONTENTS

LIST OF FIGURES

LIST OF TABLES

2 CEMENT TESTS USING SET UP I

2.1 INTRODUCTION

Cement plays a major role in the oil and gas industry, especially during the drilling and completion phase. The placement of cement in the annulus between the casing and wellbore serves to create zonal isolation and provide casing support. Therefore, a proper placement of cement is crucial to achieve excellent zonal isolation. On the other hand, the loss of zonal isolation can cause serious problems that may result in a loss of well control (Bios et al. 2011). Losing zonal isolation can come from improper placement of cement and changes in wellbore conditions from drilling or formation strength tests (formation integrity test and leak-off test). These conditions tend to generate microannuli, and/or induced fractures in the cement sheath, leading to annular gas migration in the case of uncontrolled formation fluid influx. Thus, it is important that a cement sheath seals the annulus to provide excellent zonal isolation and prevent fluid movement to surface facilities or adjacent shallow formation. This section of the report evaluates annular cement integrity, critical cement properties test with time, and reliability verification of the current liner lap pressure testing.

2.1.1 Overview

Cement sealability helps to maintain the integrity of a well and prevent subsurface fluid movement/migration to other formations and surface. The cement's ability to withstand mechanical and chemical deteriorations while maintaining its properties is known as cement durability. Cement durability and sealability strongly depends on the cement properties such permeability, thickening time, rheology, static gel strength (SGS), and unconfined compressive strength (UCS). While some of these properties are more critical than others during the pumping phase of cement, others are more crucial during the setting phase. A slurry with excellent thickening time and SGS is desired during cement pumping. An ultra-low permeable cement is usually desired during the setting phase to prevent fluid movement and provide excellent zonal isolation. A cement sheath with high UCS is typically required over time to withstand the thermal and pressure cycling that occurs in the life time of a well.

However, during the pumping and setting phase of cement, especially in gas prone zones, annular gas flow through the cemented annulus can occur and this is known as gas migration. Annular gas flow can lead to catastrophic events such as loss of well control, broaching of the shallow formation or a blowout. Most times, these flows are encountered before the blowout preventer in installed (Murray et al. 1995). In most cases, gas will migrate through a cemented annulus if the cement matrix is permeable and has poor bonding with the casing and rock surface. In addition, the development of microannuli, channels, and induced fractures (even with an ultra-low-permeable cement matrix) allows formation fluid migration through these features rather than the cement matrix itself. Gas migration control additives are usually mixed into cement slurries to increase seability, bonding, and help prevent the evolution of microannuli. Cement sealability can

be evaluated by quantifying the cemented annulus total permeability. Limited laboratory studies have been conducted to evaluate the oil well cement sealability (Christian et al. 1976; Tarco and Asghari 2010; Omosebi 2016; Stormont et al. 2017).

2.1.2 Problem Statement

The concept of gas migration has been of major concern since the 1960's. Various aspects of experimental and field case studies (Cook et al. 1983; Al-Buraik et al. 1998), development of new products and techniques (Watters and Sabins 1980; Siedel and Greene 1985), and technical recommendations (Cheung and Beirute 1985; Dean and Brennen 1992) have been discussed to try to mitigate gas migration. Shallow gas migration through a cement sheath in the early stages of setting endangers the integrity of a well by creating flow paths in the cement sheath such as microannuli and channels. Shallow gas flow can lead to blowouts in the open-hole section, usually below the conductor or surface casing because of gas migration through the cement (Adams and Kuhlman 1990). Nelson and Guillot (2006) and Talabani et al. (1997) stressed that the root cause of gas migration is the pathways in the annulus through which the gas can migrate.

This is especially relevant today as the oil and gas industry is exploring and producing hydrocarbon from harsh environments. This has made shallow gas incidents much more of a concern in many regions of the world, including the Pacific Rim, the Norwegian Continental Shelf (NCS), UK Continental Shelf, and the Gulf of Mexico (Moore and Hamilton 1993). Lécolier et al. (2010) argued that a substantial amount of the world's remaining gas reserves has over 2% of CO_2 and substantial amounts of H_2S. The presence of these gases has complicated well construction design. Deepwater cementing operations present several challenges all around the world because of shallow flow. Appropriate well design procedures require a cement system that can mitigate gas migration.

2.1.3 Objectives

A neat Portland cement is often thought of as been the primary barrier to prevent formation fluid influx during the early setting phase. This is not completely certain considering the loss of well control incidents that have been reported because of gas migration during this phase. The possible failure of a neat cement questions the need to develop a cement slurry capable of mitigating gas influx and migration. The objectives of the tasks in this section include:

- Evaluate annular cement integrity and ability to seal as a primary barrier, by using Portland cement and gas migration additives.
- Verify the reliability of current liner overlap pressure test and investigate the critical liner-casing overlap length.
- Characterize and report critical cement properties for different anti-gas migration slurry designs.

2.2 LITERATURE REVIEW

Shallow flows usually occur because of high pore pressures from under-compaction and over-pressurization of sands during rapid depositions. Shallow flows can consist of water, gas, and formation fines. One out of every five potential surface casing hazards were identified to be shallow flows (Bogaerts et al. 2012). Shallow gas is usually encountered at shallow subsurface depths of 300 ft with low fracture gradients. They often result in cratering and blowouts in the open-hole sections. Gas leakage in the annulus has been recorded as a major hazard in drilling and completions operations, and records show that one out of three blowouts occur because of a shallow influx (Adams and Kuhlman 1990; Prince 1990). Danenberger's study in 1993 showed that 58 out of the 83 blowouts that were encountered between the years of 1971 and 1991 on the outer continental shelf (OCS) of the United States had gases associated with them. This was a strong indication of the severity of shallow gas flows and cratering which costed significant expenditure to the operators. To curb some of these problems, steps have been taken by the industry over the years to improve shallow well casing and cement designs. These include API RP 65 (Cementing Shallow Water Flow Zones in Deepwater Wells) and API RP 65 – Part 2 (Isolating Potential Flow Zones During Well Construction). Some other new standards such as the API Recommended Practice (RP) 19LH (Liner Hangers) is currently being drafted by an API subcommittee. Specifications of downhole liner hangers will be specified in this new standard.

2.2.1 Gas Migration

Gas migration is defined as gas entry into a cemented annulus with the potential to provide a flow path into the wellbore for gas, water, and hydrocarbons. Gas migration can cause fluid flow through the annulus to the surface. If gas goes undetected, it can lead severe consequences such as underground blowouts and sustained casing pressure. Aspects of gas migration have been described in the literatures as the following:

- Experimental and field case studies (Stone and Christian 1974; Garcia and Clark 1976; Cook et al. 1983; Al-Buraik et al. 1998; Bour and Wilkinson 1992).
- Development of technical recommendations (Levine et al. 1979; Tinsley et al. 1980; Cheung and Beirute 1985; Dean and Brennen 1992).
- Developments of new products and techniques (Kucyn et al. 1997; Watters and Sabins 1980; Cheung and Myrick 1983; Siedel and Green 1985; Matthews and Copeland 1986).
- Empirical prediction techniques (Sutton et al. 1984; Rae et al. 1989)

Gas migration phenomenon can be caused by numerous factors at any given time. The root causes of gas migration have been attributed to i) a decline in annulus hydrostatic pressure; and ii) pathways in the annulus through which gas can migrate (Nelson and Guillot 2006). Primary causes of gas migration are related to the cementing process. Gas migration through a cemented annulus can be categorized into three types based on their migration pathways (Talabani et al. 1997). The first type occurs between the casing and the cement; a situation whereby gas molecules migrate

through the void created between the casing and cement. A common practice to remedy this problem is adding the appropriate amount of magnetite to the cement slurry. The second type of gas migration occurs through the void created between the cement and the wellbore wall. This void is created when the filter cake that is formed at the wellbore adversely affects the bonding process. Anchorage Clay and some other additives can be used to eliminate this problem in drilling. The third gas migration path exists because of hydrostatic pressure changes that appear in the cement during the setting phase. This is also referred to as primary gas migration when gas molecules migrate into the cement because of loss of the hydrostatic head.

To better understand gas migration, Stiles and Baret (1993) proposed three stages of cementing: i) during placement; ii) post-placement (short); and iii) post-setting (long). It is important to understand all the physical and chemical processes that a cement slurry goes through from liquid slurry to semi-solid and solid states. When the cement hydrostatic pressure in front of a large volume of gas "pocket" drops below the pressure in the gas zone, gas influx takes place (Pinto et al. 2012). On the other hand, secondary gas migration occurs much later after cement placement is complete. This is because of mechanical and thermal stresses which compromises the integrity of the hydraulic bond or the integrity of the cementing material (Rupak 2007). According to the Mineral Management Service (MMS) safety alert (2003), annular flow related to cementing surface casing has been identified as one of the most frequent causes of the loss of well control incidents in the Gulf of Mexico (GoM). When zonal isolation is not achieved, and gas molecules migrate behind the casing, it charges the shallow formations. These shallow formations become a formidable challenge when there is little proximity between the pore pressure and fracture gradients in the operational mud window. In such situations, the gas can broach the casing, leading to a blowout. The following reviews are major studies in literature regarding gas migration:

Carter et al. (1973) presented a laboratory model of gas migration in deviated boreholes by focusing on properties of cement slurries needed for successful primary cementing jobs. Their research showed that the parameters directly related to gas migration include: cement filtration control, borehole mud removal, and effective hydrostatic head (hydrostatic pressure exerted by the mud, spacer, and cement slurry). In addition, the study presented factors that reduce gas migration during and after primary cementing. These factors are summarized as centralization of casing strings and increased flow rates during displacement amongst others.

Garcia and Clark (1976) presented their findings from a field study. This study was done to trace gas migration as it occurred in the wellbore. The investigations showed that gas migration occurs under two conditions. The first is when there is fluid loss in the cement slurry. The second is when there is an uneven setting of the slurry, such that there is no hydrostatic head communication between the bottom of the hole and the mud column directly above the set cement. The authors provided guidelines to predict formations that have potentials for gas migration. Furthermore, they recommended practices to curb annular gas flow.

Christian et al. (1976) presented a method to calculate the allowable filtrate loss rate for a cement slurry during various stages of cementing. They stated that without fluid-loss control, cement slurries may be unsuccessful in transmitting full hydrostatic pressure before their initial set. The authors showed that increasing the concentration of fluid-loss additives results to lower cement permeability and lower gas migration potentials. In addition, their field results demonstrated that gas migration can be successfully prevented with cement slurries that have a fluid loss rate less or equal to 50 ml/30 minutes. Cook and Cunningham (1977) in a similar study showed that filtrate loss control is just as important as the slurry thickening time or its compressive strength development. Both studies concluded that maximum fluid loss control additive should be used in cement slurries when cementing across abnormal pressure zones. This would help to minimize gas leakage.

Webster and Eikerts (1979) identified the relationship between water separation in a cement slurry and loss of hydrostatic head of the cement. Their study was based on laboratory tests and field results. They observed that the use of clay in regulated amounts can control the amount of free water in cement slurries. They concluded that reduction of free water to zero eliminates the potential of flow after a cementing job.

Bannister et al. (1983) simulated a wellbore model to study the incursion of gas into cement. Two design approaches were used to reduce gas conductivity (the relationship between gas flow and loss of hydrostatic pressure). One of these approaches was to deposit impermeable cement filter cake against the formation. The other approach involved the use of a self-activating slurry that interacts with incoming gas to form an impermeable barrier. Results from their investigation showed that the impermeable filter cake deposition hinders gas invasion as long as it is in place. However, once it ruptures, gas flow becomes unhindered and rapid.

Cooke et al. (1983) presented field measurements of annular pressure and temperature during primary cementing operations. Pressure and temperature measurements were conducted in seven wells via sensors to investigate the causes of fluid migration behind casings. They highlighted multiple causes of fluid migration but focused on one which is: the loss of pressure in a cement before the cement sets. Their investigations disclosed that annular pressure measurements indicated fluid entry into the wellbore when the formation pore pressure exceeds the pressure exerted by the cement. The sensors showed the extent of vertical movement of the migrated fluid. The authors concluded their study with practical steps that can be followed to help minimize flow induced by loss in annular pressure.

Beirute and Cheung (1990) developed a method to scale down field wellbore parameters to laboratory conditions for accurate testing of cement recipes to be used for controlling gas migration. Their method assumed the gas bearing formation to have substantial permeability, gas volume, and thickness to invade the annulus and pressure-charge the cement. The authors concluded with some criteria for selecting cement slurries for wells with potential gas migration problems.

Bour and Wilkinson (1992) presented an analytical method to quantify the potential and severity of gas flow. They showed that appropriate gas migration control cementing systems can be designed once the flow potential has been established. Compressible cement was recommended for combating gas migration problems. Al-Buraik et al. (1998) also discussed solutions to shallow gas migration problems with the use of lightweight latex slurries and right-angle set (RAS) latex slurries amongst others.

Recently, Bois et al. (2017) developed a gas migration model that investigates two different stages of fluid and porous solid in the life of a cement slurry. Their model allowed for computing cement properties and the state of stress at any depth and time. In addition, their model showed that the opening of a micro-annulus is not necessarily associated with gas migration. However, gas will invade the cement sheath when the cement pore pressure drops below the pore pressure of the formation. The authors highlighted the importance of gas flow rate and diffusivity in the cement sheath. They concluded that gas may use multiple leakage paths during migration to reach the surface, leading to a shallow gas blow out or a leak into another reservoir.

Overall, optimizing cement mix designs and the mixing process can help in mitigating gas migration. It must be noted that a single factor cannot prevent gas migration. Rather a combination of factors, depending on the well condition, is required. Some of the key properties of cement in context of controlling gas migration are enumerated as follows:

- Fluid loss
- Gel strength development
- Cement shrinkage
- Permeability
- Free fluid (free water)
- Mud removal
- Microannulus
- Mechanical and chemical failure of cement sheath

2.2.2 Gas Migration Additives

One common gas migration additive is microsilica (silica fume). It is a byproduct of silicon and ferrosilicon production. It has a bulk density between 400 and 500 kg/m^3 and specific gravity of 2.2. It is composed primarily of vitreous silica, having SiO_2 content ranging from 85 to 95%, and a particle size distribution range of 0.02 to 0.5 μm (average of 0.15 μm). This fine particle size allows packing between the cement grains resulting in an improved microstructure of the cement matrix. Grinrod et al. (1988) discussed the use of microsilica in the creation of a gas tight cement slurry. When it is used in various concentrations with varying densities (Figure 2.2), the authors discovered that microsilica had the ability to mitigate gas migration. However, with a constant

density, the concentration of microsilica had to be increased in tandem with an increase in gas pressure (Figure 2.2). Although microsilica can control free water, the authors proved that the material stopped gas migration by immobilizing the pore water within the cement matrix. They explained that microsilica gives better strength and bonding, reduced permeability, improved durability, and provides less strength retrogression (Figure 2.3). They also presented three field case studies where microsilica was used as an anti-gas migration additive and proved to be effective.

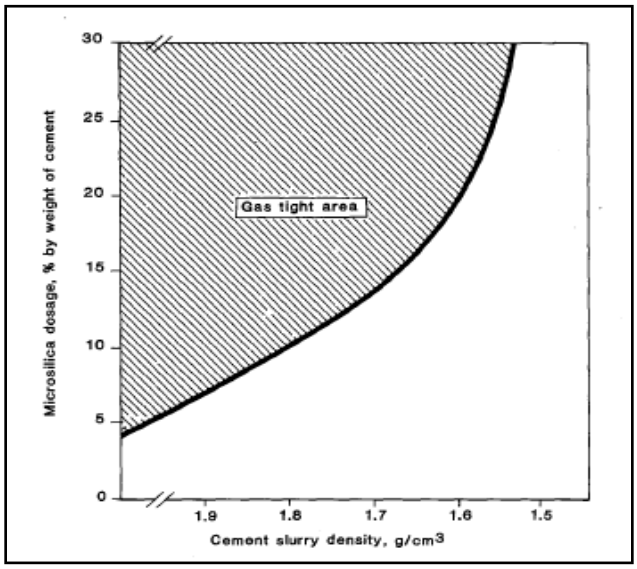

Figure 2.1: Dosage of microsilica needed at different cement slurry densities to withstand a maximum gas pressure of 125% of the water gradient (Grinrod et al. 1988).

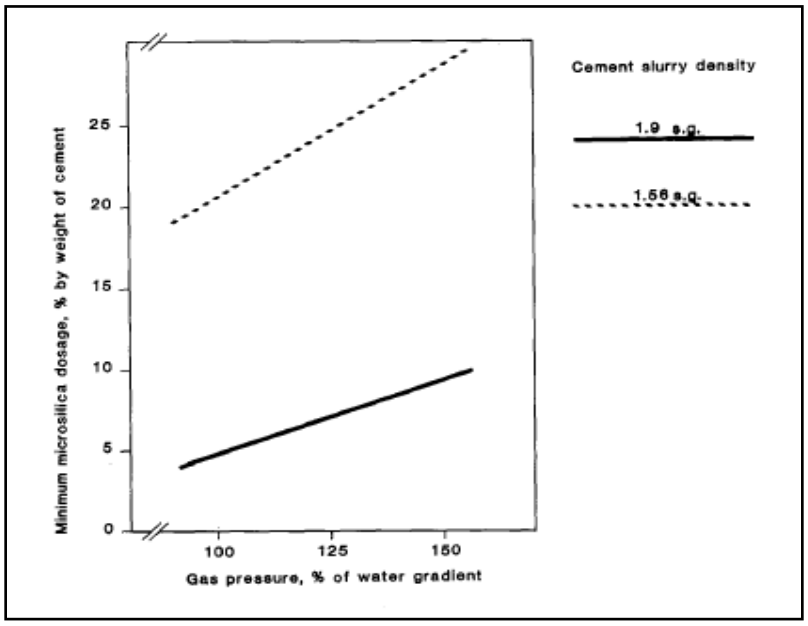

Figure 2.2: Minimum dosage of mirosilica needed to withstand increasing gas pressure (Grinrod et al. 1988).

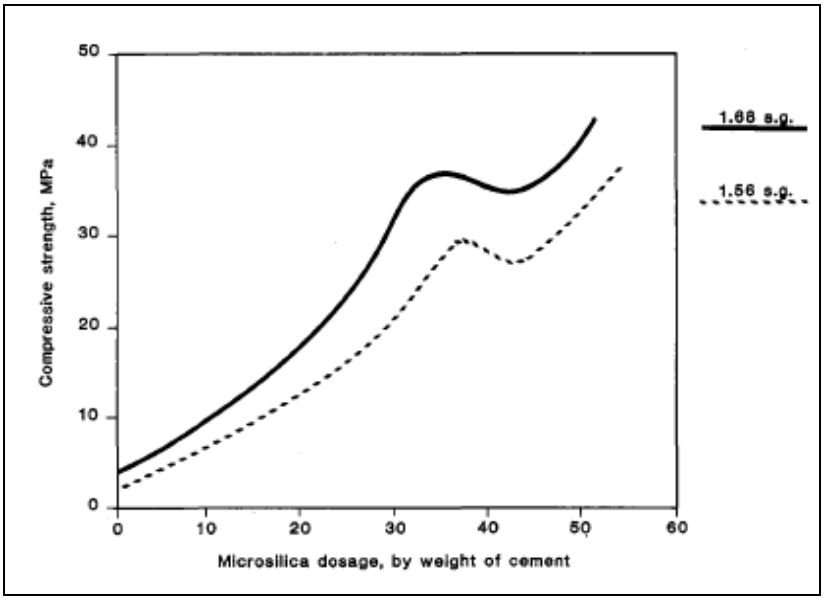

Figure 2.3: Effect of microsilica on compressive strength (284°F, 28 days) for light-weight cements.

Although microsilica has a positive effect on cement permeability, Skalle and Sveen (1991) reported that it did not produce gas-tight cement at elevated temperatures. They investigated other cement additives and documented that bentonite reduced the amount of free water. However, it acted as a contaminant because it reduced the bonding strength of the cement. The authors also highlighted that Latex reduces bonding strength significantly. Daou and Piot (2009) reviewed typical uses of microsilica in oilfield cements. They paid particular attention to the influence of material grade - degree of densification on slurry behavior and set cement properties. They clarified the dispersability of densified microsilica in cement slurry by analyzing the set microsilcia cement microstructure. This was done with a scanning electron microscope (SEM) coupled with an energy dispersive spectrometer (EDS). Contrary to general opinion, the authors reported that not all microsilica are the same. Microsilica comes in two major forms – undensified and densified microsilica. Undensified microsilica has a bulk density typically within the range of 200 to 350 kg/m^3 while densified microsilica has a bulk density typically within the range of 500 to 700 kg/m^3. The authors documented that densified microsilica does not disperse into small particles when mixed in a cement slurry. Therefore, densified and partially densified grades which are popular because they can be handled easily, do not provide the performance required for adequate zonal isolation which is expected of a microsilica cement. According to their research, densified microsilica behaves as a complete inert material and not as a reactive one. Thus, it is practically not useful as a light-weight material or an anti-settling agent. They presented the particle size distribution of varied densification of microsilica as shown in Figure 2.4.

Figure 2.5 shows the particle size distribution of cement with undensified and densified microsilica. Daou and Piot (2009) concluded that only moderately compacted microsilica with a bulk density of approximately 300 kg/m^3 would be helpful in developing a good cement performance.

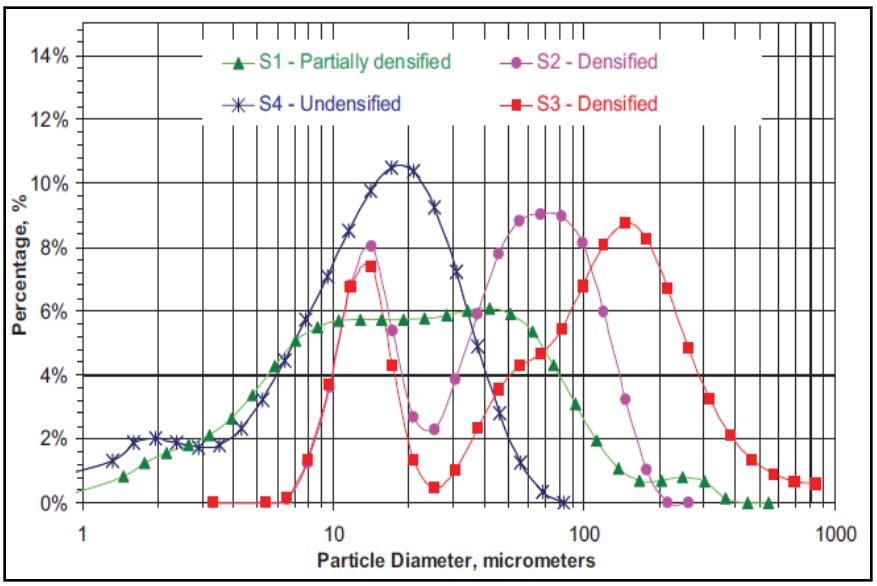

Figure 2.4: Particle size distribution of raw samples. S1 – 333 kg/m^3, S2 – 719 kg/m^3, S3 – 582 kg/m^3, S4 – 167 kg/m^3 (Daou and Piot 2009).

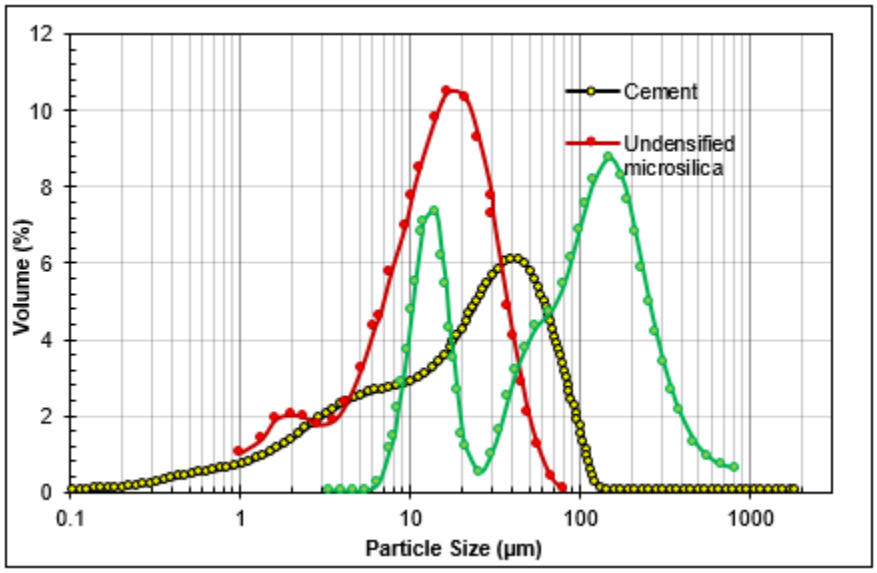

Figure 2.5: Particle size distribution of cement and various cement additives (after Daou and Piot 2009; Dylan Moore 2015).

Al-Yami et al. (2009) proposed a cement formulation to prevent gas migration in high pressure – high temperature (HP/HT) wells. The additives they used included: silica, manganese tetraoxide, expansion additives (magnesium oxides burned at 219.2 °F), hematite, and silica sand. The cement slurries that prevented gas migration had formulations composed of 45% BWOC of Mn_3O_4 and 45% CWOC hematite with different ratios of silica sand and silica flour. The best formulation was Class G cement with 45% BWOC hematite, 5% BWOC expansion additive, 10% BWOC silica sand, 25% BWOC silica flour, 45% BWOC Mn_3O_4, 3.5 gals/sack gas blocker, 0.5 gals/sack gas block stabilizer, 1.2% BWOC high temperature retarder, 0.45% BWOC low temperature retarder,

and 0.3% BWOC fluid loss additive. The authors concluded that a cement with this formulation would prevent gas migration in a HP/HT well. Shakirah (2008) highlighted that magnesium oxide (MgO) provides an expansion force in the cement matrix at high temperature; thereby, decreasing the probability of microannuli creation. This expansive force within the cement matrix is because the magnesium oxide hydrates to form magnesium hydroxide – which occupies more space than the original MgO. However, this hydration is only achievable at high temperatures up to 550°F and would not be beneficial at temperatures below 140°F.

Abbas et al. (2013) highlighted the use of hydroxypropyl methylcellulose (HPMC) – a cellulose based gelling and thickening agent – as a gas migration agent. They reported that HPMC can develop an impervious barrier while preventing free water in the cement system. With laboratory experiments, they confirmed that HPMC-based cement slurries were gas tight, having the ability to prevent gas migration up to 150 psi. Their results showed that for HPMC polymer concentrations between 0.2 and 0.55 gals/sack, the cement pore pressure remained at a constant 16 psi with a continuous injection of 150 psi for up to 8 hours. Two additional advantages of using HPMC slurry includes: ability to control fluid loss up to 190°F and increase thickening time for up to 2 hours.

The use of carbon black as a gas migration additive in cement was discussed by Calloni et al. (1995). Carbon black is a paracrystalline carbon that is produced as a byproduct of incomplete combustion of heavy petroleum products like coal tar that is often used due to its economic advantages. They documented that concentrations as low as 4% BWOC of carbon black was enough to prevent gas migration in all formulations. The particle size of carbon black ranges from 10 to 200 nm. A surfactant (formaldehyde-condensed naphthalene sulfonate, sulfonated cumarone, or indene resins) is necessary for its dispersion (Petroleum Engineer's Guide). The authors presented a field case scenario where carbon black was used in cementing a well in the Adriatic Sea. A CBL/VDL run after 3 days showed correct top of cement and good bond to the pipe and formation. Some patents on the chemicals used for cement gas migration inhibition include: Jassal et al (2004) – a copolymer of 2-acrylamido-2-methyl-1-propane sulfonic acid (AMPS), *N*-vinylacylamide, and acrylamide (AAm) that reduced the occurrence of gas channeling, and Kuksov et al. (1992) – a mixture of lignosulfonates, alkali-treated brown coal, and organic silicon compounds that was able to reduce the permeability of cements.

Phosphorated aluminum powder can also be used as an anti-gas migration additive. The calcium hydroxide in the cement slurry reacts with the phosphorated aluminum powder. This reaction produces hydrogen gas that swells the cement slurry, which prevents the channeling of gas in the cement (Wang 1996; Bortsov 1997a; Bortsov 1997b).

2.2.3 Cement Permeability

Permeability is a term generally used to describe the state of a material which allows fluid (liquid or gas) to flow through it. Cement permeability and porosity are good indicators of cement sealability. Ultra-low permeability is usually desired to prevent formation fluid influx and

migration. According to Kiran et al. (2017), alteration of cement properties (such as permeability) can occur due to the reaction of invaded fluids and cement contamination. Christian et al. (1976) studied the effect of fluid loss control on cement and presented a method to calculate the allowable filtrate-loss rate for a cement slurry during different stages of cementing. The authors measured the permeability of Class H cement versus gas flow time. Class H cement permeability was measured as 0.01 mD after 10 minutes of nitrogen injection. They concluded that cement with low fluid loss exhibited lower permeability values. Tarco and Asghari (2010) conducted several experiments to study the stability and integrity of cement. They used two classes of cement ("Type 10" and Class G). They reported the permeability of the neat Type 10 and neat Class G cement samples as 0.0627 mD and 0.0453 mD, respectively.

In addition to these studies on cement permeability, Omosebi (2016) studied the degradation of oilfield cement in high pressure high temperature (HPHT) environments. The author used two types of cement (Class G and Class H) and measured their porosity and permeability. The samples were cured for 5 days at 200^{o}F. The porosity and permeability for Class G were reported as 28 % and 0.044 mD respectively, while the porosity and permeability for Class H cement were reported as 29 % and 0.043 mD respectively. Stormont et al. (2017) conducted several experiments to study microannuli response at different confining pressures, pore pressures, and casing pressures. A microannuli in a cement specimen was intentionally created while two other specimens were intact (no microannuli). Class G cement was used with 33% water/cement ratio and the specimens were cured for 7 days at 131^{o}F. The cement permeability for the two intact specimens were less than 0.001 mD. Table 2.1 shows the range of cement permeability from these studies.

Table 2.1: Cement permeability range

Permeability (mD)	<0.001	0.043	0.044	0.045	0.01
Type	Class G	Class H	Class G	Class G	Class H
Curing Time	7 Days at 131 ℉	5 Days at 200 ℉		N/A	N/A
W/C	0.33	0.38	0.44	0.44	0.38
Reference	Stormont et al. 2017	Omosebi 2016		Tarco & Asghari 2010	Christian et al. 1976

2.2.4 Modelling and Simulation for Gas Migration.

Modelling of annular gas flow in a cemented annulus is one way of providing a better understanding on gas migration mechanisms. While some researchers focused on numerical and analytical modelling of pressure buildup associated with sustained casing pressure, others tried to

model gas leakage in CO_2 sequestration. Rocha-Valdez et al. (2014) defined the sustained casing pressure (SCP) as "any measurable casing pressure that rebuilds after being bled down which can be attributed to cause(s) other than artificially applied pressures or temperature fluctuations in the well". Figure 2.6 shows a schematic of gas migration through a cement and mud column. SCP results from poor cementing that leads to losing well integrity, triggering gas flow from a gas formation through the cemented annulus (Xu and Wojtanowicz 2016; Xu 2002). Nishakawa (1999) modeled the gas flow through a cemented annulus to the surface. The author considered the cement as a porous media with gas flowing vertically through the cement column. The effects of gas specific gravity, cement porosity, and temperature on SCP were considered. The results showed that a decrease in cement porosity, gas specific gravity, and temperature leads to higher SCP. The applicability of this model is limited since it was not implemented on field data.

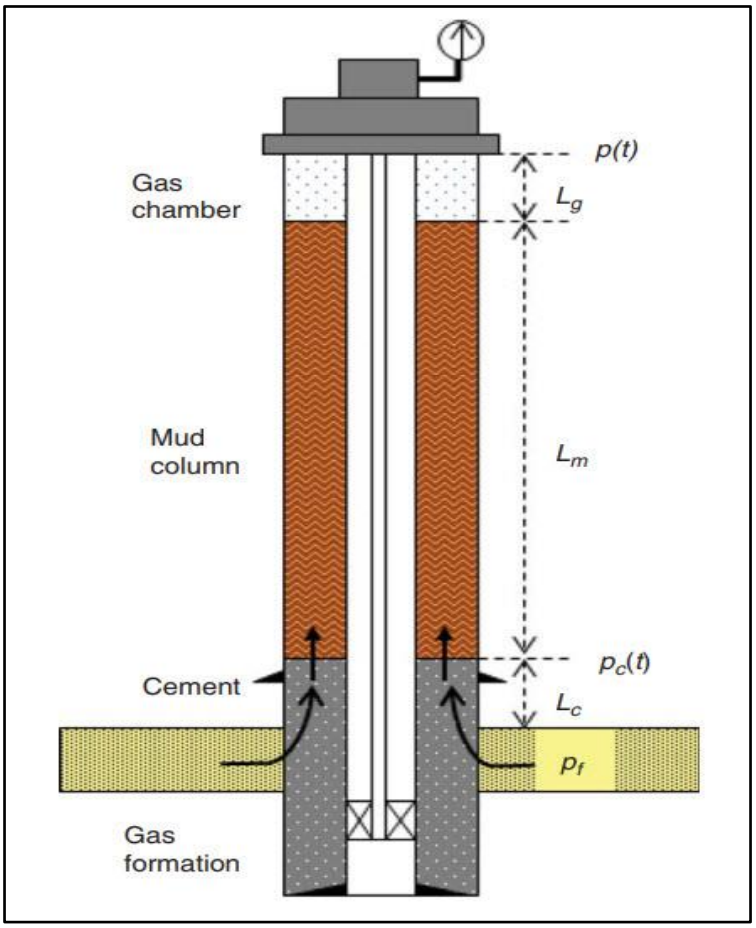

Figure 2.6: Schematic of gas migration through cement and mud columns (after Rocha-Valadez et al. 2014)

Xu and Wojtanowicz (2001) developed a mathematical model for testing SCP. The model objective was to detect the flow mechanism during gas leakage and identify the main parameters associated with gas leakage to be used in choosing corrective measures. The study showed that the pattern of SCP buildup is controlled by several parameters such as cement, mud, and gas invasion zone. They concluded that cement permeability and mud compressibility have a strong effect at

the early stages of SCP, while the gas formation pressure affects the late stages where the maximum value of the stabilized SCP depends on it. Their mathematical model was implemented to match the field data of two wells and their results where within an acceptable estimate.

Xu and Wojtanowicz (2003) expanded their SCP model by considering gas migration in a mud column which affects the early SCP build up and pressure bleed-down. Huerta et al. (2009) simplified this model and used it to quantify the potential of CO_2 well leakage. They were able to match the model with field data and this effort provided important information such as leakage depth and effective cement permeability. The effective cement permeability was transformed to geometries of leakage pathways such as microannulus and gas channels. This model was also implemented by Tao et al. (2010). The authors modified the SCP model to adapt to the CO_2 leakage model. Matching the field pressure data with the model allowed them to determine the cement effective permeability and the gas leakage depth.

Salehi (2013) studied near wellbore leakage pathways in shale gas wells using experimental and modelling approach. A 3-D finite element model specifically for cement leakage modelling and wellbore was developed using a multistage approach (Figure 2.7). The author included all the steps involved in the life cycle of a well to investigate previous deformation that occurred by excessive loads during drilling or stimulation. The model and approach were applied to a well in the Haynesville shale play.

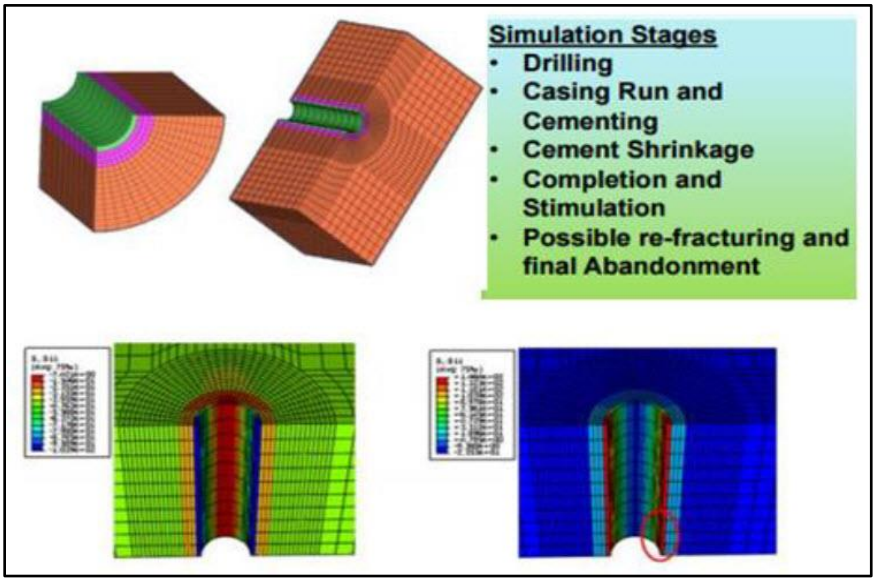

Figure 2.7: 3-D finite element model developed to mimic near wellbore leakage pathways (after Salehi 2013)

Rocha-Valadez et al. (2014) presented an analytical solution for SCP numerical model given by Xu (2002). They assumed a constant gas inflow pressure and the gas flowing from the top of the cement will move immediately to the gas cap. Matching the field data with the model resulted to a cement permeability value that was close to the one obtained from the numerical model.

Stormont et al. (2017) developed a wellbore model to mimic gas invasion into a cemented annulus. They intentionally created a microannulus in a cement specimen to investigate the effect of confining, casing, and pore pressures. They concluded that a microannulus acts like a fracture with respect to deformation under stress. In addition, the authors presented an analytical gas leakage model and assumed that gas only flows through the microannulus. They modelled the flow using the Navier-Strokes equation coupled with the cubic law since the microannulus are fracture-like.

2.3 RESEARCH METHODOLOGY

To achieve the objectives in this section of the project, theoretical, experimental, and analytical approaches were used. An extensive literature review presented in the preceding subsection provided information on cement properties, slurry designs, and additives that can be added to make cement slurries gas tight. The outcomes of reviews and theoretical analysis provided useful information in comprehending the inadequacy of set cement to prevent migration of formation fluids, mainly gas. Sealability of cement strongly depends on the cement to casing bonds and available pores within the cement.

In this study, different slurry designs have been investigated using additives like latex, microsilica, and bentonite. The key properties of cement with regards to gas migration control, mechanisms for wellbore cement failure, and relationship between cement design and its integrity were examined. A gas tight slurry was successfully designed. The gas tight cement slurry was made of the following additives: Class H, 1.5 liters/100 kg commercial additive. The formulation was rigorously tested to evaluate the slurry's performance.

2.3.1 Scope of Work

Two different oil well cements (Class G and Class H) were compared in their ability to seal in the very early stages of cementing. Cement slurries are sensitive to downhole conditions such as temperature and pressure (Ahmed et al. 2009). Besides cement rheology and thickening time test, all the experiments with setup I were performed at ambient temperature and the cement sheath surface was exposed to ambient pressure. Shallow reservoirs have relatively low pressure and temperature. It was difficult to mimic these conditions considering the large scale (field size) setup. To accomplish the specific goals in this section of the report, setup I was split into different setups: big setup I and small setup I.

In the big setup I, two different "wait on cement" (WOC) times were used to investigate the effect of WOC time on the cement sealability: 12 and 24 hours. Nitrogen gas (N_2) was injected at 60 psig to examine and test the integrity of the system. Latex and Bentonite were mixed with oil well cement to evaluate cement integrity and sealability. In each experiment (slurry design), two to three major pressure cycles were performed and each of these cycles contained at least two to three tests. The pressure decline curves were used to generate the combined permeability. Three methods were used to measure the combined permeability of the system for each test. These were used to evaluate cement sealability and in developing a model for the critical liner-casing overlap.

The primary goal for developing the small setup I was to test various combinations of slurry additives. In this setup, pressure was kept constant at 60 psig and WOC was 24 hours. Class H cement was used for the investigations in this setup. Experimental investigations were conducted in two phases. In the first phase, neat Class H cement was used while in the second phase neat Class H cement was mixed with different additives (bentonite, latex, microsilica and nanomaterials). To quantify the level of slurry improvement, leakage time of set cements were measured and compared. In addition, physical properties such as compressive strength, rheology, thickening time, density, and gas transit time tests were conducted to verify the suitability of the new cement mixture.

2.3.2 Test Materials

A brief description of the materials used in the cement experiments and their specific roles are presented below.

Cement

Commercial Class H and Class G oil well cements were used to conduct the experiments. These classes were selected because they are commonly used for cementing the wells drilled in the Gulf of Mexico and North Sea.

Water

Water is a primary material required for mixing and cement hydration. 38% water requirement by weight of Class H cement and 44% water requirement by weight of Class G cement were used in accordance with API RP 10A (2010). Distilled water was used for mixing to control contamination and reduce the degree of uncertainty in the tests conducted. When bentonite and/or some other solid additives were added, the total water requirement was increased accordingly.

Bentonite

Bentonite was used in cement slurry preparation to reduce the fluid loss from the cement. More water was added since bentonite can absorb water and swell. This tends to decrease the overall density of the slurry and reduce the amount of free water. The criteria for adding water when bentonite is used is: for every 1% of bentonite added, mix water was increased by approximately 5.3%.

Silica and Microsilica

Multiple literatures (Lea 1971; Eilers et al. 1983; Grabowski and Gillott 1989) documented that the ratio of CaO/SiO_2 (C/S) is crucial to compressive strength. For a C/S ratio greater than 1, the cement developed low compressive strength because of the formation of di-calcium silicate hydrate. However, a lower C/S ratio leads to the formation of tobermorite gel which has low porosity and permeability. With a low C/S ratio a high compressive strength is attained. 30% BWOC silica should be added to keep the C/S ratio below 1. With the addition of silica, the adequate amount of water must be added. The water requirement is 38.5% (by the weight of the

silica). Microsilica has a particle size range of 0.02 to 0.5 μm, with an average of 0.15 μm. The fine particle sizes of microsilica allows it to be packed between the cement grains, which results to an improved microstructure of the cement matrix. However, microsilica comes in two major forms – undensified and densified microsilica. Undensified microsilica has a typical bulk density between 200 and 350 kg/m^3 while densified microsilica has a typical bulk density between 500 and 700 kg/m^3. The microsilica used for the experiments is the Silica Fume White which has a bulk density of 400 kg/m^3. Adding microsilica into cement without adding a water reducer would entail adding a water requirement. The water requirement ranged from 5% to 12% BWOC based on previous work. However, for these experiments, the Silica Fume White used had manufacturer's requirement of 5% to 20% BWOC replacement.

Latex

Latexes are aqueous dispersions of polymer particles (such as surfactants) which imparts stability to the dispersion. When mixed with cement, latex acts as an impermeable polymer barrier particularly in gas prone zones. It fills the pores in the cement and reduces the permeability of the cement. The latex used in the experiments is the Latex Thin Set Motar Additive. This product comes in liquid form and no water requirement is needed.

Fly ash

Fly ash consists of silt-sized particles which are generally spherical, typically ranging in size between 10 μm and 100 μm. Fly ash is usually classified as Class C or Class F and it consists primarily of silicon oxides, aluminum iron, and calcium. They also contain low amount of magnesium, potassium, sodium, titanium, and sulfur. The small particle size distribution of fly ash and its unique spherical shape makes it a good mineral filler. Fly ash in the presence of water, reacts with calcium hydroxide at ambient temperatures to produce cementitious compounds. A water requirement of 3.6 gal/74 lbm is used for the Fly ash.

When the solid test materials are added together, the particle size distribution of the solid mixture tends to change from one slurry design to another. A laser diffraction particle size analyzer (Mastersizer 2000) was used to measure the particle size distribution of some samples.

Figure 2.8 shows the particle size distribution of neat Class H, neat Class G, and other slurry designs that were used in this study. These were measured in dry state.

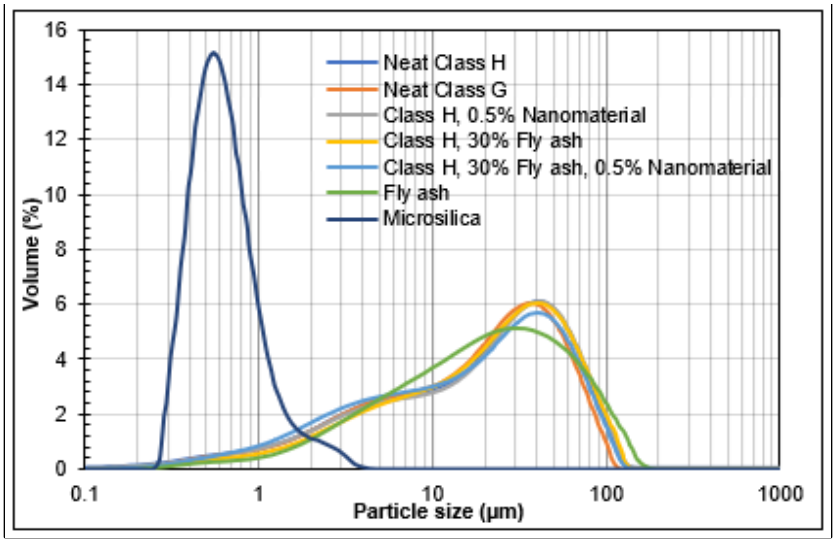

Figure 2.8: Particle size distribution of various samples.

2.3.3 Cement Mixing and Measuring Devices

Blender

A commercial blender with a high horse power of 3½ hp supplied by Waring Co. (Model: MX1500XTX Xtreme) was used. It has a programmable keypad and adjustable speed setting (rpm). Figure 2.9 shows the blender which was used to prepare the cement in batches according to the API Standards.

Figure 2.9: Waring Blender

Mixer

Figure 2.10 shows a large commercial mixer supplied by Hobart Co. (Model: D300) for mixing the batches of cement from the blender. This was done to keep the cement slurry homogeneous before pouring it in any of the setups.

Figure 2.10: Hobart mixer

Mud Balance

An atmospheric standard mud balance shown in Figure 2.11 was used to measure the cement slurry density for each experiment.

Figure 2.11: Mud balance

Viscometer

The rheological properties of the slurries were measured using the viscometer shown in Figure 2.12. Rheological properties were measured at 102°F and according to API standards (R1B1 bob and spindle geometry with spring factor =1).

Figure 2.12: Viscometer (M3600)

Consistometer

Figure 2.13 shows the cement consistometer which was used to measure cement consistency (thickening time) and the static gel strength of the cement slurries at 102°F and 2300 psi. The temperature and pressure were selected from a temperature and pressure gradient profile for different well sections in shallow wells. The consistency limit was set to 50 Bc for all slurries.

Figure 2.13: Cement consistometer (M7540)

2.3.4 Cement Slurry Mixing Procedure

In preparing the cement slurries, standard API cement-water mixing procedures were followed. All dry materials were weighed and mixed thoroughly prior to adding them to the mix fluid. Where latex and other liquid additives are included, the required mass of water and liquid additives were placed in the blender which is turned on to rotate at 4000 rpm for 10 seconds and then shut down. This is done to a create a homogenous liquid mixture before adding cement or other dry materials. Where bentonite and other dry additives were included, all dry additives were added to the cement powder and mixed gently to create a homogenous dry mixture before pouring into the mix fluid or only water. When neat cement or a homogenous mix of neat cement and dry additive(s) is being added, the blender is turned on to rotate at 4000 rpm while the cement powder is added to the fluid within 15 seconds. After adding the dry materials to the fluid, the lid of the mixer is put in place and the mixing continues at 12000 rpm for 35 secs.

2.3.5 Components and Arrangement for Big Setup I

Steel Pipes

Standard wall steel pipes threaded on both sides were used to create the artificial annulus. These were supplied by McMaster company. All the pipes used were not welded seamless to mitigate the variations in wall thickness. Table 2.2 shows all the information for the pipes used in the big setup I experiments including the number of pipes, length, internal diameter, outer diameter, and wall thickness.

Table 2.2: Pipe properties for big setup I

Number of pipes	Length (ft.)	Inner diameter (in)	Outer diameter (in)	Wall thickness (in)
4	3	6.025	6.625	0.28
4	4	4.5	4.026	0.237

Ultrasonic Thickness Gauge

An ultrasonic thickness gauge (Model: GM100) was supplied by Benetech. This equipment was used to measure the wall thickness of the metal pipes used in both the big and small setup I. This was done to ensure that the pipes had uniform wall thickness (Figure 2.14).

Figure 2.14: Ultrasonic thickness gauge

Flanges

The steel pipe flanges were supplied by McMaster Company and were used to construct the big setup I. In each experiment, three flanges were used to create the artificial annulus, two were 4-inch and one was a 6-inch flange.

Flange Caps

6-inch high-pressure stainless-steel flange cap from McMaster was used to cover the 6-inch flange at the bottom of the set up. A 4-inch flange cap was used at the top of the set up to cover the 4-inch flange to create a wellbore.

Gaskets

Rubber gaskets were used at the bottom and at the top of the setup to mitigate any leak from the inner pipe, the outer pipe, and between the flange and flange cap.

High Strength Bolts

20 high-strength grade-9 hexagonal bolts were screwed to tighten the flange to the flange cap.

Nitrogen Gas (N_2)

Nitrogen gas (N_2) was used to pressurize the base of the cement and cause gas to migrate through the pores of the cement. N_2 was selected because of its inert triple bond makes it difficult to react with any substance until some reaction conditions are met (none of which are present in the experiment). It's availability and low cost also made it ideal for experiments.

Video Cameras

Zmodo HD video cameras with 1 Mega Pixel resolution were mounted on top of the setup and focused on the artificial annulus to detect the bubbles coming out of the cement sheath. Two to three of these cameras were used. A network video recorder (NVR) was connected to the video cameras to save all the recordings. Later, these recordings were reviewed and used to detect the first bubble that comes out of the cement sheath from which the leakage time is calculated. The recordings were also used to calculate the gas flow rate and estimate the combined permeability based on the number and diameter of the bubbles.

Pressure Sensors

Four calibrated pressure sensors supplied by McMaster company were mounted on the outer pipe to collect real-time pressure data inside the cement. The pressure data were then used to estimate the combined permeability.

Data Acquisition System

A 16-bit data acquisition system acquired from the Measurement Computing Company was connected to the pressure transmitters and computer to convert signals from pressure transmitters to digital readings in the computer. Figure 2.15 shows a schematic of the big setup I arrangement. The two main steps that were followed in arranging this setup include: fabrication and assembly. This setup is made of two concentric pipes that have an artificial annulus in between. The artificial annulus is open to the atmosphere. Flanges and flange caps were used to prevent the system from leaking and provide an artificial wellbore. The outer pipe has a gas injection port at the bottom of the setup for gas pressure testing. Also, three pressure transmitters were mounted on the outer pipe to measure pressure in the annulus at the time of gas injection.

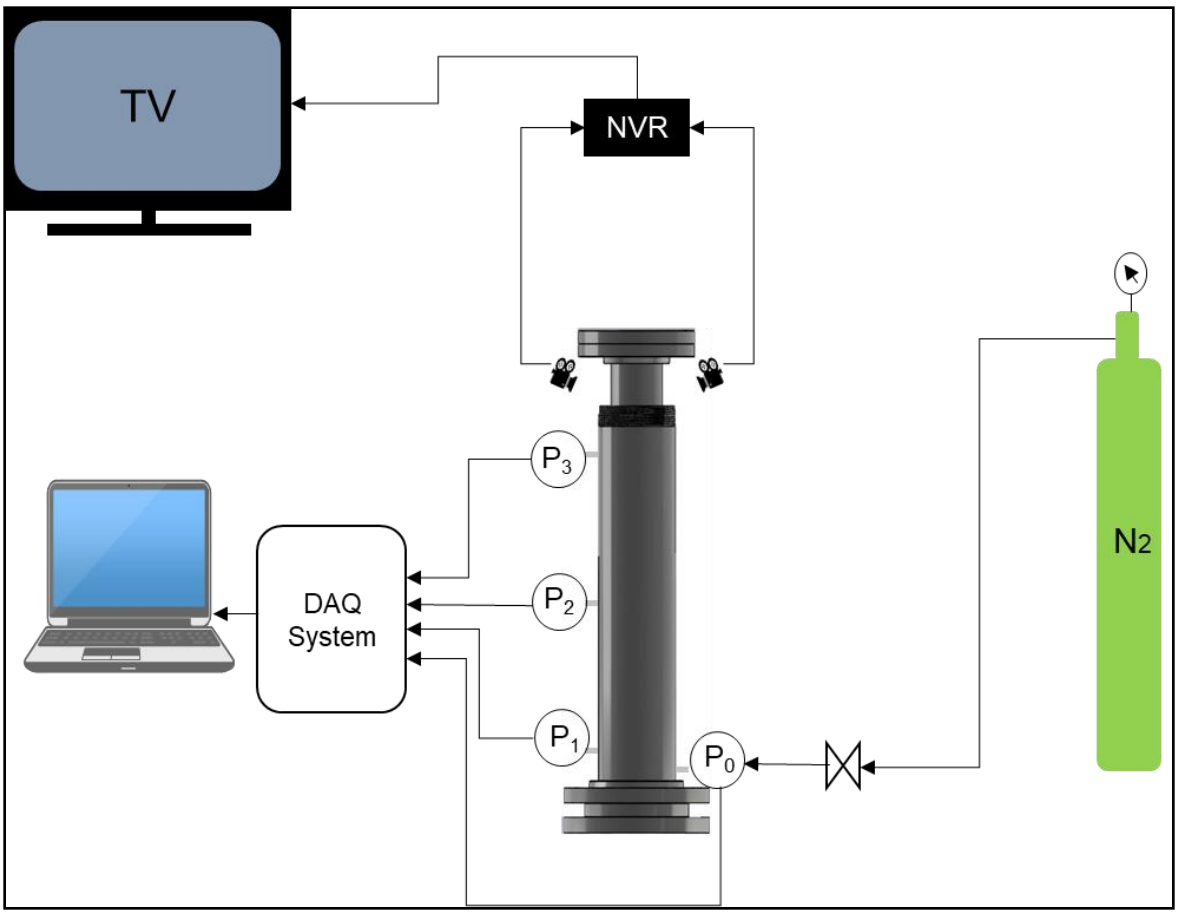

Figure 2.15: Schematic showing the arrangements of the components in big setup I

2.3.6 Experimental Arrangement for Small Setup I

In the small setup I, a constant pipe height of 3 feet was maintained. There were no pressure sensors installed and the pipe diameter was 2-inch. During the preliminary setup and tests, one 1-inch and one 2-inch pipes were used. The results from these tests and material availability informed the decision to continue with the 2-inch pipe for subsequent experiments. Each small setup I were made up of two major components only. The first component is the setup (a hollow pipe with a diameter of 1 inch or 2 inches) and the second component is the N_2 gas cylinder with a pressure exceeding 10 times what is needed for each experiment.

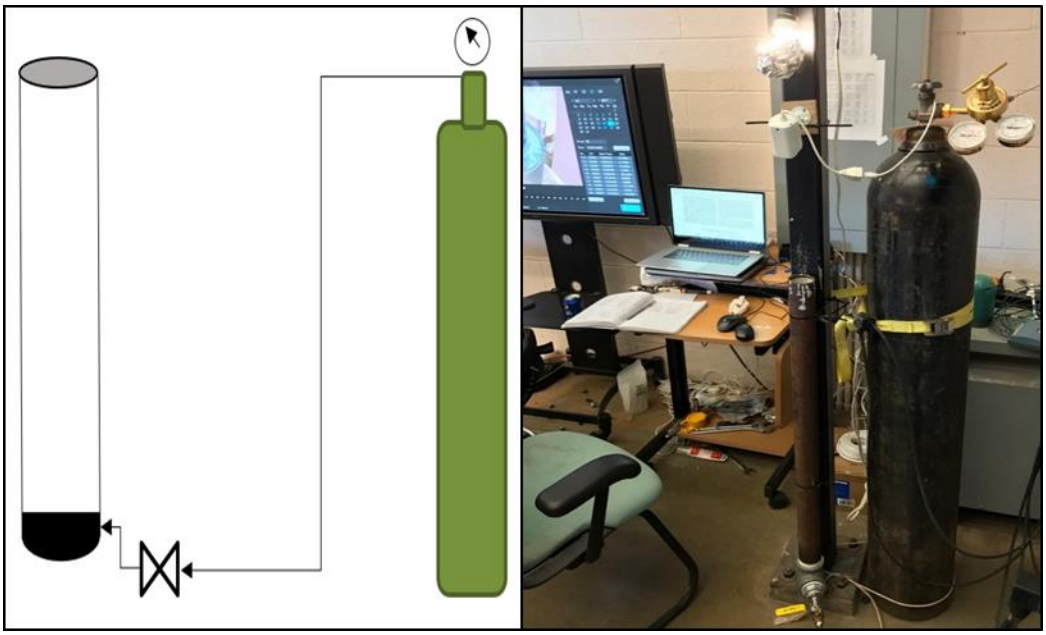

Figure 2.16 shows the arrangement and schematic for the small setup I. At the base of the setup, 6 filter papers, 2 circular wire meshes, and a layer of sponge are placed in the pipe. These were installed to prevent any cement leakage and ensure even distribution of gas pressure at the base of the setup.

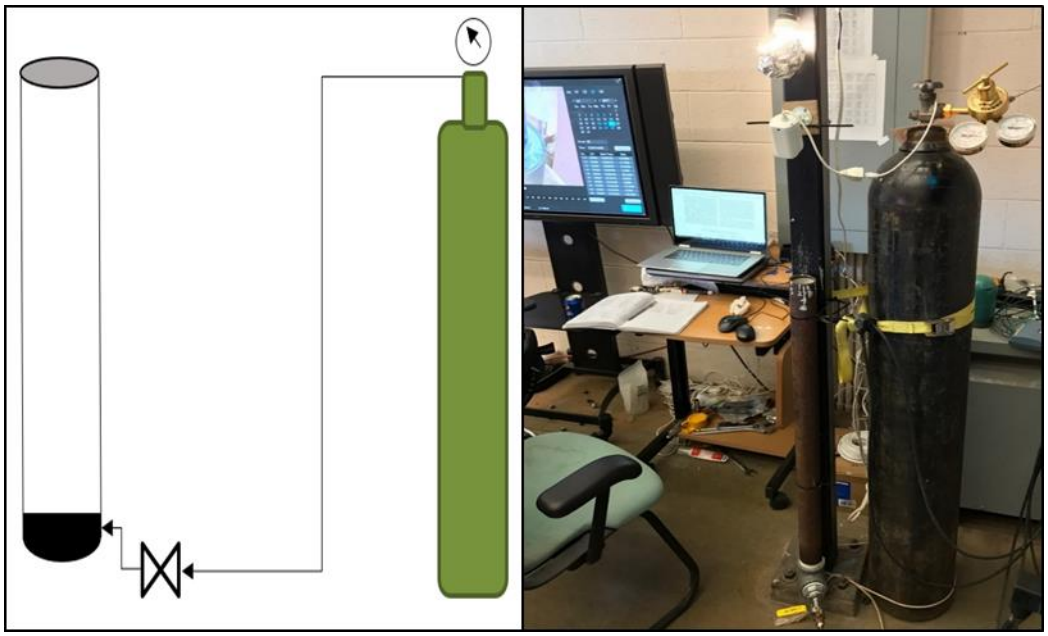

Figure 2.16: Schematic showing the arrangement of components and experimental station for small setup I.

2.3.7 Test Matrix for Big Setup I

Table 2.3 shows the test matrix used for this set up. Class H cement was used in the first three experiments, while Class G was used in the fourth experiment. Experiment 1 and 2 had no additives

but the difference between them was the WOC time. The third experiment had additives (latex and bentonite) and the WOC time was 24 hours as that of experiment 1. Class G was used for experiment 4 and no additives were added to the cement which had 24 hours WOC.

Table 2.3: Test matrix for big setup I

Experiment No.	Set Up Height (ft)	Cement Grade	Additives		WOC (hrs)	Cement Density (ppg)
			Latex (gal/sack)	Bentonite (%)		
1	3	Class H	N/A	N/A	24	16.65
2	3	Class H	N/A	N/A	12	16.65
3	3	Class H	3	1	24	12
4	3	Class G	N/A	N/A	24	16.65

2.3.8 Test Matrix for Small Setup I

Error! Reference source not found. Table 2.4 shows the small setup I test matrix. The only independent variable was the cement additive and for each experiment, the leakage time and degree of bubbling were recorded and compared to assess the performance of a new formulation. The term vibration in the table is defined as the uniform agitation of the cement inside the pipe for a specific time (20 to 30 minutes), using a mechanical vibrator that is attached to the external pipe wall. This is done to ensure that the cement is uniformly distributed inside the pipe and to release any air bubbles that may have been trapped while pouring the cement.

Table 2.4: Test matrix and parameters for studying the effects of additives using small setup I

Small setup I-	WOC (hr)	Vibration (mins)	Material	Height (ft)	Diameter (in.)	Additives					Density (ppg)
						Microsilica (%)	Latex (gal/sack)	Bentonite (%)	Fly ash (%)	Nanomaterial	
Experiment 1	24	12	Steel	3	1	N/A	N/A	N/A	N/A	N/A	16.65
Experiment 2	24	12	Steel	3	2	N/A	N/A	N/A	N/A	N/A	16.65
Experiment 3	24	60	Steel	3	2	N/A	1	0.5	N/A	N/A	16.65
Experiment 4	24	20	Steel	3	2	N/A	1	N/A	30	N/A	14
Experiment 5	24	25	Steel	3	2	5.5	N/A	N/A	N/A	N/A	16.05
Experiment 6	24	25	Steel	3	2	12	N/A	N/A	N/A	N/A	N/A
Experiment 7	24	30	Steel	3	2	N/A	N/A	N/A	N/A	0.5	16.55
Experiment 8	24	25	Steel	3	2	N/A	1	N/A	30	0.5	14.5
Experiment 9	24	25	Steel	3	2	1.5 liters/100 kg commercial additive					16.4

2.3.9 Experimental Test Procedure for Big Setup I

Before describing the test protocols, it is important to define some key terms that would be used subsequently in this section of the report. First, the term “experiment” is used to define different slurry mixes with various additives. The term “test” is used to define the flow of nitrogen gas through the cement and monitor for bubbles at the surface for one day. A “cycle” is used to define two to three consecutive tests. For instance, cycle two test two (C2T2) would mean the second cycle of the second day for a given cement slurry formulation (experiment). Four experiments were performed using the big setup I. Each experiment consists of at least two to three cycles, one to two cycles of injecting nitrogen gas at 60 psig.

The cement slurry is mixed with the mixing procedure described in **2.3.4** and poured into the big setup I. After pouring the slurry in the artificial annulus, the specified WOC time is allowed before the next steps. Before the end of WOC time, the next step was connecting the video cameras and the pressure sensors to the setup and keep them activated for at least 12 hours. After the WOC is completed, a test begins by flowing nitrogen gas through the annulus at the proposed pressure. The nitrogen gas is only injected for 30 minutes. After this time, the inlet gas valve is closed and whatever pressure that is in the cement annuls is allowed to decline with time. The time for the first bubble appearance is recorded and the area around the annulus where the bubble is observed is marked.

2.3.10 Experimental Testing Procedure for Small Setup I

A 24-hour WOC was considered for all the experiments using this setup. After this time, the gas inlet valve is opened, allowing 60 psig into the setup through the sponges for 30 minutes. During this period, the surface of the cement is observed for any gas bubbles. After 30 minutes, the inlet valve is shut and the gas that was pumped into the cement is allowed to migrate. If gas begins to migrate during or after the 30 minutes, the positions are marked and the time at which the bubbles are observed on the surface of the water is recorded. If multiple positions appear, each position is marked, and the time is recorded. In all the tests using small setup I, a maximum of 2 cycles of 60 psig tests are conducted. The test nomenclature or identification code follows a pattern to indicate the type of setup being used, the cement slurry mixture composition, the cycle in which a test is carried out, and finally the day the test is carried out. Table 2.5 describes the nomenclature for identifying both the slurry mixture and the test conducted. Every nomenclature is documented for each test prior to running the test. After all necessary tests are conducted on a setup, it is discarded. A total of 9 setups were put together and 27 tests were conducted at 60 psig.

Table 2.5: Nomenclature for small setup I experiments

S. Experiment 1 C1 T1		
S. Experiment 1	C1	T1
First slurry mixture in test matrix	Cycle Number	Test Number

2.3.11 Data Preparation and Calculation from Big Setup I

In this subheading, the data collection and preparation techniques are discussed. In addition, some analytical equations are highlighted for calculating the systems permeability.

2.3.11.1 Leakage Time

Leakage time can be defined as the time it takes for the nitrogen gas to travel from the bottom of the setup through the cement sheath to the top. In other words, the time it takes for first bubble to appear at the top of cement, considering the time at which the nitrogen gas was injected. In each experiment, one or more positions were bubbling at the same and/or at different times. Positions were marked and monitored during all tests. The first bubble detected in each position is noted as well as the time at which the last bubble appears in these positions. Gas bubble positioning is variable where they stop appearing or may appear in new positions in subsequent test.

2.3.11.2 Pressure Data Cleaning and Denoising

The pressure data collected for all the experiments were cleaned and denoised using the least square denoising method in a commercial software (KAPPA Saphir). Also, the pressure values were converted from psig to psia. Figure 2.17 and Figure 2.18 shows the pressure data for one of the experiments before and after denoising respectively.

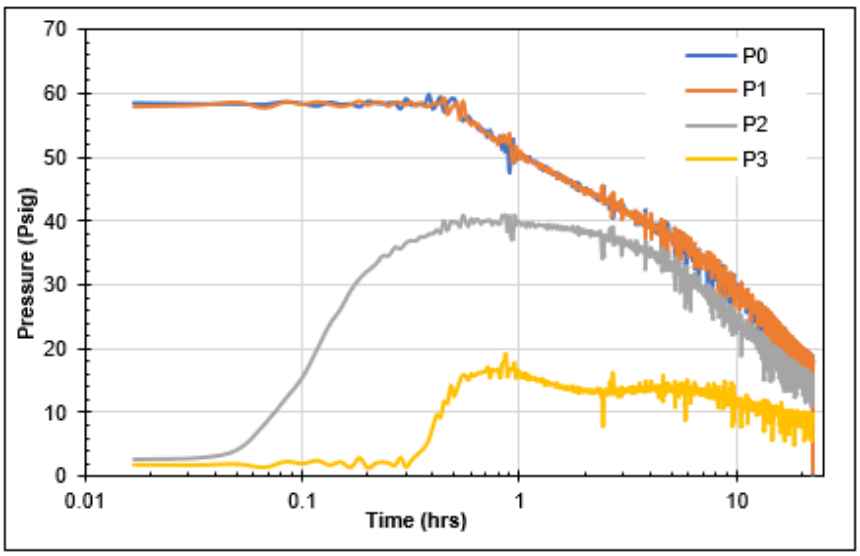

Figure 2.17: Pressure data before denoising

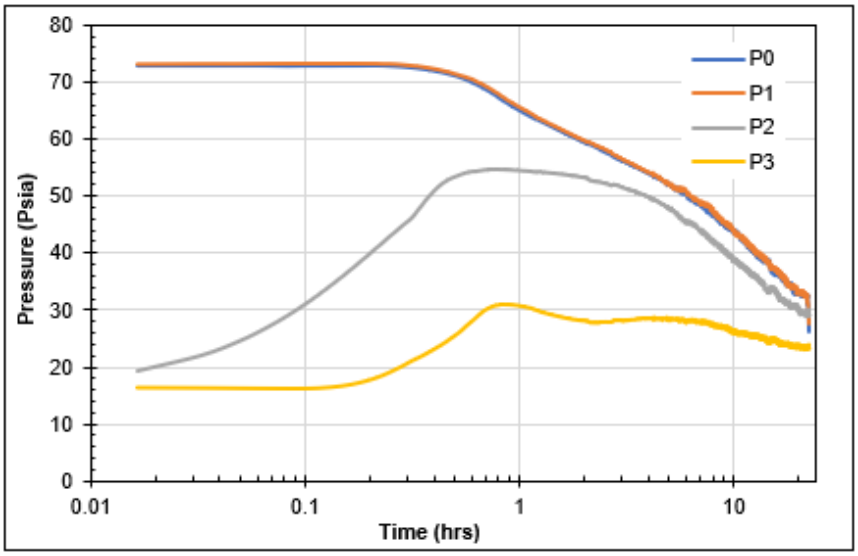

Figure 2.18: Pressure data after denoising

2.3.11.3 Flow Rate Calculation

Gas flow rate was calculated using two different methods. The first method is the bubble counting method while the second is the quasi-steady method. In the bubble counting method, gas flow rate was calculated based on the number of bubbles and bubble's volume using the following equation:

$$q_g = \sum_{j=1}^{m} \frac{n_j V_j}{t} \quad \text{..... (1)}$$

The recorded videos for all the experiments conducted were analyzed to roughly estimate the gas flow rate. Gas flow rate was estimated by counting the number of bubbles coming out from all the bubbling positions. Bubble diameters were measured to get the bubble volume. Each bubbling position was treated separately since the bubbling intensity and volume of bubbles changed from one position to another. To proceed with the permeability calculation, the following assumption was made: gas flow rate is constant after 29 minutes from the time the gas was injected. Therefore, the gas flow rate was estimated from the last minute before stopping the gas injection. In the quasi-steady method, equation 2 below was used. The flow rate can be calculated at different upstream pressures with the equation since there is a fixed volume and a constant downstream pressure which is the atmospheric pressure.

$$q_g = \frac{V}{P_1}\frac{dP}{dt} \quad \text{..... (2)}$$

2.3.11.4 Permeability Calculation

The calculated permeability is not only the cement permeability, but also it includes the permeability of induced cracks, channels, and microannuli. Thus, this permeability is referred to as the combined permeability or system permeability. This permeability was calculated using three different methods with the aid of the estimated gas flow rates. These methods are the Darcy's method, Forchheimer's method, and pulse-decay methods. In the Darcy's method, the combined

permeability is calculated based on Darcy's laws using equation 3. In this equation, the gas flow rate is estimated from an approach referred to as the bubble counting method. It should be noted that the Darcy method which employs the bubble counting method was not used for some of the tests because of the difficulty of counting and/or detecting the bubbles.

$$K = \frac{2000 \times \mu \times q_g \times P_b \times L}{A(P_i^2 - P_o^2)} \quad \text{..... (3)}$$

Using the Forchheimer's method, the combined permeability of the system was calculated using the Forchheimer equation (4). This equation accounts for the inertial flow and is written as:

$$\frac{MA\,(P_u^2 - P_d^2)}{2zRT\mu L\rho q} = \frac{1}{k} + (\frac{\rho q}{\mu A})\beta \quad \text{..... (4)}$$

This equation assumes a steady state condition and can be rewritten as:

$$Y = {}^{1}/_{k} + \beta X \quad \text{..... (5)}$$

where $Y = \frac{MA\,(P_i^2 - P_o^2)}{2zRT\mu L\rho q}$ ..... (6)

and $X = \frac{\rho q}{\mu A}$ ..... (7)

The gas flow rate can be calculated based on the quasi-steady method which will result in multiple sets of x and y. The plotted data will generate a straight line with an intercept that is equal to the reciprocal of permeability.

Pressure pulse-decay measurements have been widely used to measure the permeability of low and ultra-low permeable rocks. Brace et al. (1968) invented this method to measure the permeability of granite under high pressure. This method tends to shorten the time it takes to measure the permeability of tight porous media since the steady state condition is not required. Oilfield cement sheath is known to have low permeability values; thus, this method can be applied to measure the combined permeability of the cement sheath in a shorter time. The combined permeability was calculated based on the pressure decline curves using the following equations:

$$P_{u(t)}^2 = P_d^2 + (P_{u\,(i)}^2 - P_d^2)e^{-\beta t} \quad \text{..... (8)}$$

$$\beta = \frac{KA}{\mu V L C_g} \quad \text{..... (9)}$$

Equation 8 can be rewritten as

$$(P_{u(t)}^2 - P_d^2) = (P_{u\,(i)}^2 - P_d^2)e^{-\beta t} \quad \text{..... (10)}$$

Where the left-hand side of the equation can be plotted against time resulting in an exponential equation with a β exponent. The combined permeability can then be calculated from equation 9. One advantage of using this method is that the gas flow rate is not included in its calculations.

Using this method allows for comparing the combined permeability obtained from the two previous methods, where the flow rates were used in their calculations.

2.4 RESULTS

In this subsection, the results from each experiment using the big setup I and small setup I are presented and discussed. Beginning with the big setup I, the results from the four experiments are discussed and compared, followed by four leakage scenarios and modelling results for gas migration through cement in a liner-casing overlap (**2.4.1** to **2.4.5**). The results from the experiments and tests using small setup I are presented from **2.4.6** to **2.4.12**.

2.4.1 Big Setup I Experiment 1 with Neat Class H and 24 hours WOC

Experiment 1 with big setup I was conducted with neat Class H cement with 38 % water/cement (W/C) ratio and 24 hours WOC. After WOC time, three gas injection tests were performed at 60 psig. Figure 2.19 shows the leakage time versus the cement age for three cycles with three tests in cycles 2 and 3 and two preliminary tests in cycle 1. In the first test within the cycle 1, the first bubble appeared and was recorded after 11 minutes. However, the leakage time decreased to 5 minutes in the second test when the cement age was 2 days. The leakage time increased again to 11 minutes in the first test of cycle 2 when the cement age was 11 days and then decreased afterwards in the second and third tests within this cycle. This trend was also observed in cycle 3. The reason for increase in leakage time between the end of the last test in a cycle and the beginning of the first test in the next cycle can be linked to the fallow period between the cycles. This also contributed to the disappearance of some bubbling positions. The phenomenon of disappearing positions is referred to as “self-healing” and has been reported by Carroll et al. (2016), Carey (2013), and Huerta et al. (2012). The authors attributed this phenomenon to the mobilization and precipitation of minerals along the pathways within the cement sheath.

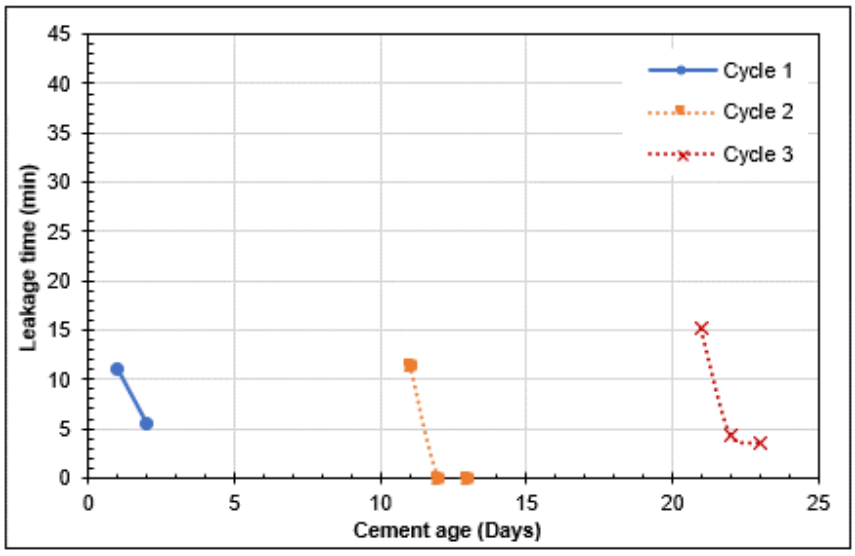

Figure 2.19: Leakage time versus cement age for all the three cycles and tests performed in experiment 1 (Class H, WOC: 24 hours)

The combined permeability values for this experiment were estimated using the three different methods discussed in section **2.3.11.4**. The permeability values in cycle 1 were calculated from only the Darcy's method because of lack of continuous pressure measurements required for the other two methods. In addition, the two tests conducted in this cycle were considered preliminary. Furthermore, the Darcy's method was not used in estimating permeability values in cycle 3 because of the difficulty in counting and detecting the bubbles. Figure 2.20 shows the combined permeability calculated from these methods versus cement age. A general observation is that the combined permeability increases as the cement age increase. Parrott (1995) reported such a trend when measuring the air permeability for different cement specimens for almost 800 days. The calculated permeability values fall under the range of neat Class H cement permeability reported the literature. Neat Class H and G cement permeability value ranges from 0.001mD to 0.045 mD as shown with the red rectangle in Figure 2.20 (Stormont et al. 2017; Omosebi 2016; Tarco and Asghari 2010; Christian et al. 1976).

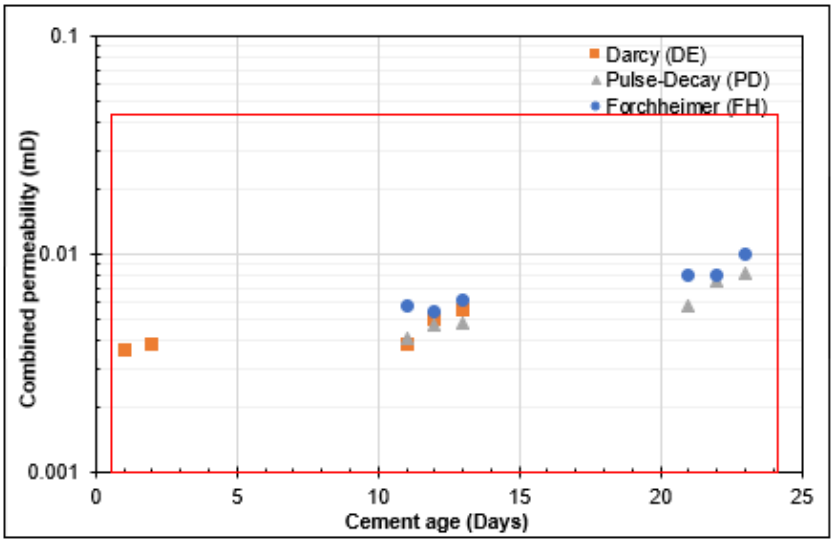

Figure 2.20: Combined permeability using different methods versus cement age for experiment 1 (Class H, WOC: 24 hours)

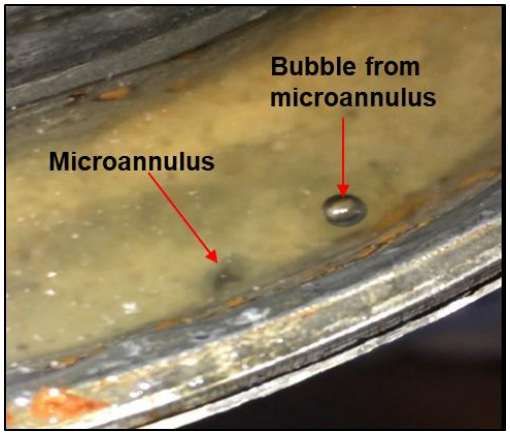

Figure 2.21: A microannulus bubbling from big setup I experiment 1

2.4.2 Big Setup I Experiment 2 with Neat Class H and 12 hours WOC

The major difference between experiment 1 and 2 using big setup I was the WOC time. The first test was performed after 12 hours WOC and the first bubble was detected approximately after 5 minutes. Figure 2.22 shows the leakage time versus the cement age for only one cycle. The second test was performed 8 days after the first test and the "self-sealing" phenomenon was observed with increase in cement aging. The combined permeability values were estimated using the three methods. Figure 2.23 shows that all the calculated permeability values fall between 0.001mD and 0.045 mD, except the value calculated from the Darcy's method in test 1. The values from the Forchheimer and pulse-decay methods were 0.002 mD and 0.003 mD respectively.

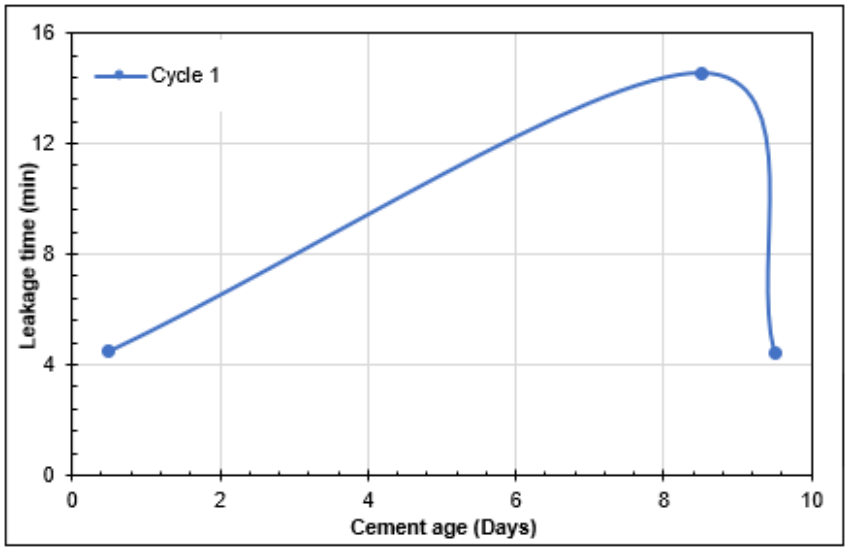

Figure 2.22: Leakage time versus cement age for 60 psig cycle in experiment 2 (Class H, WOC: 12 hours)

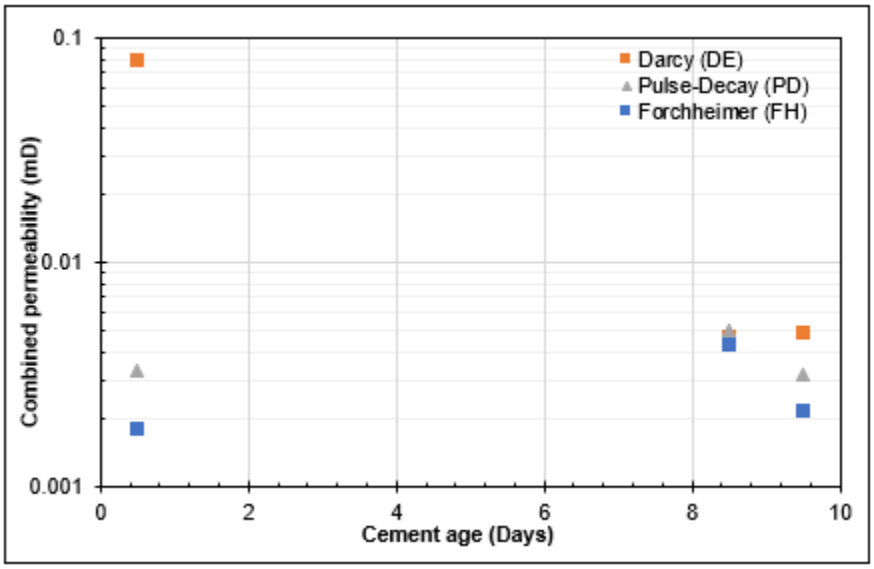

Figure 2.23: Combined permeability using all methods versus cement age for experiment 2 (Class H, WOC: 12 hours)

Table 2.6 compares the results from the first tests in the cycle 1 of each experiment conducted in the big setup I. The difference between experiments 1 and 2 was their WOC time (24 hours WOC time for experiment 1 and 12 hours WOC time for experiment 2). Considering the first test in cycle 1, after the WOC time, experiment 2 had a shorter leakage time (less than half of the leakage time for experiment 1) and a higher combined permeability value (0.079 mD). Thus, a cautious conclusion can be drawn that WOC time affects gas migration rate and cement permeability for neat Class H cement.

Table 2.6: Summary of the results from the first tests in each of the experiments from big setup I

Exp. No.	Cement Grade	WOC (hrs)	Leakage Time (min)	Combined Permeability (mD) Darcy's Method	Combined Permeability (mD) Pulse-Decay Method	Combined Permeability (mD) Forchheimer's Method
1	H	24	11	0.004	N/A	N/A
2	H	12	5	0.079	0.003	0.002
3	H	24	16	0.132	0.070	0.032
4	G	24	0.22	N/A	0.001	0.001

2.4.3 Big Setup I Experiment 3 with Class H, Latex, and 24 hours WOC

Experiment 3 was conducted with Class H cement, 3 gallons/sack Thin Mortar Latex, and 1% of Bentonite. These two additives were added to the cement slurry to prevent gas migration and reduce fluid loss in the cement. The WOC time was 24 hours and other test conditions (60 psig after WOC, for 30 minutes) remained constant. During the first test in cycle 1, the first bubble was detected after 16 minutes as shown in Figure 2.24, while the first bubble was detected after 3 minutes in the second test. Furthermore, the self-healing phenomenon was not observed because of the additives. Latex is a gas migration additive and when mixed with cement forms an impermeable polymer structure within the cement pores which reduces the cement's permeability. Although, experiment 3 had the highest first bubble appearance time (leakage time) compared to experiments 1 and 2, this slurry was expected to have superior performance by preventing gas migration for at least the 30 minutes testing period. Visual observations also suggested that experiment 3 had a higher bubbling intensity compared to experiments 1 and 2, and that the bubble diameters appeared to be larger as shown in Figure 2.25.

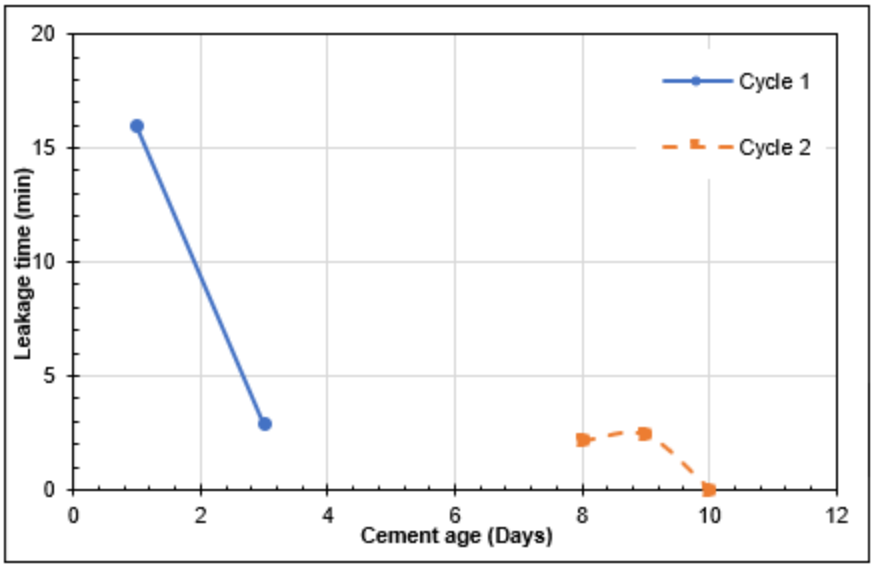

Figure 2.24*:* Leakage time versus cement age for the performed cycles in experiment 3 (Class H with Latex, WOC: 24 hours*)*

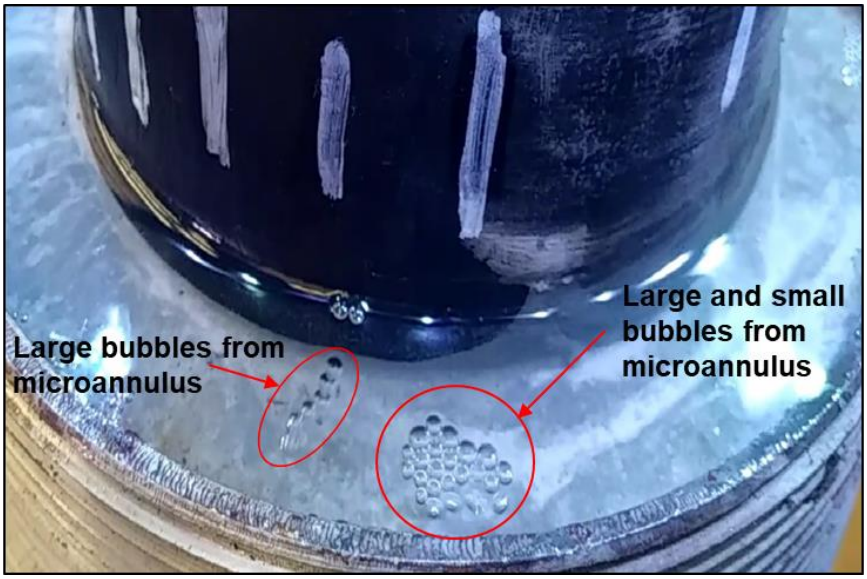

Figure 2.25: Large and small bubbles from microannuli within the set cement sheath from big setup I experiment 3

One possible explanation for the reduced performance of this slurry is that latex, like any other polymer, requires some degree of elevated temperature to activate its polymer chains (Jones and Carpenter 1991; Al-Buraik et al. 1998). It is this temperature activated process that allows the cross linking of latex polymer chains to form impermeable structures within the cement pores; thus, reducing the pore spaces and impeding the development of potential microannuli. This experiment was performed at ambient temperature because it was difficult to mimic the elevated temperature condition considering the big setup I and the arrangement used. Moreover, the latex used in this

experiment was liquid and will most likely act like an additional water requirement (at an ambient temperature).

The performance of this slurry was also evident in the high permeability values obtained. These were much higher compared those calculated from experiments 1 and 2 as shown in Figure 2.26. In addition, all the values except one were higher than the range reported in literature for neat Class H and G. Given that this slurry had additives, its permeability values were expected to be lower than those for neat cement or fall within their range at the very least. The set cement from this slurry had severe microannuli and the combined permeability values shows an increasing trend as the cement age increases.

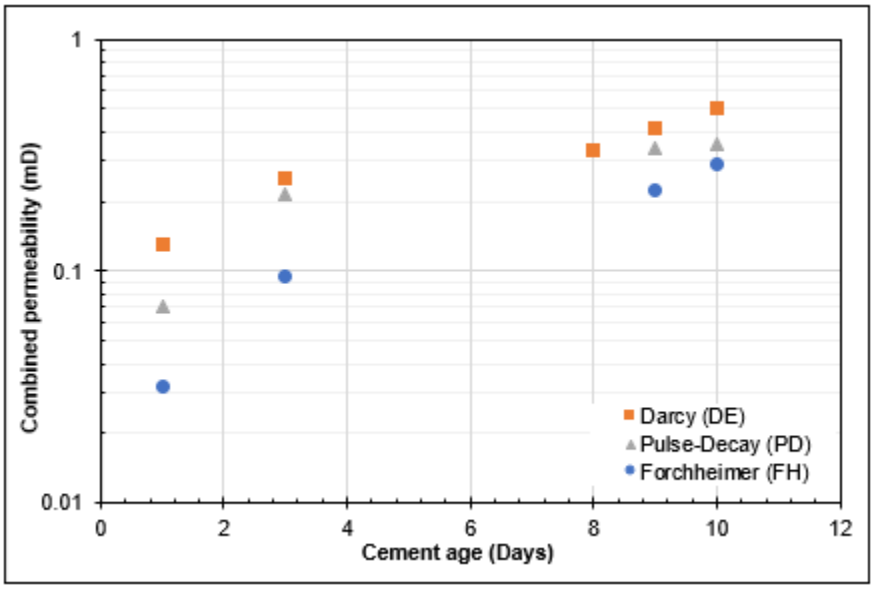

Figure 2.26: Combined permeability using all methods versus cement age for Experiment 3 (Class H with Latex, WOC: 24 hours)

2.4.4 Big Setup I Experiment 4 with Neat Class G and 24 hours WOC

Neat Class G cement with 44% water to cement ratio was used in this experiment. The WOC time was 24 hours and other test conditions (60 psig after WOC, for 30 minutes) remained constant. Of all the experiments using the big setup I, Class G cement showed the lowest value for the leakage time. Figure 2.27 shows the leakage time versus cement age, and the first bubble in the first test was detected after 13 seconds. It was also observed that the leakage time for the set cement sheath was less than one minute for all the tests. The combined permeability values were estimated with only the pulse-decay and Forchheimer's methods. The Darcy's method was not used because the cameras did not detect the bubbles effectively. Figure 2.28 shows an increase in permeability with increase in cement age. The values are within the range of reported permeability values and the values from both methods were very close.

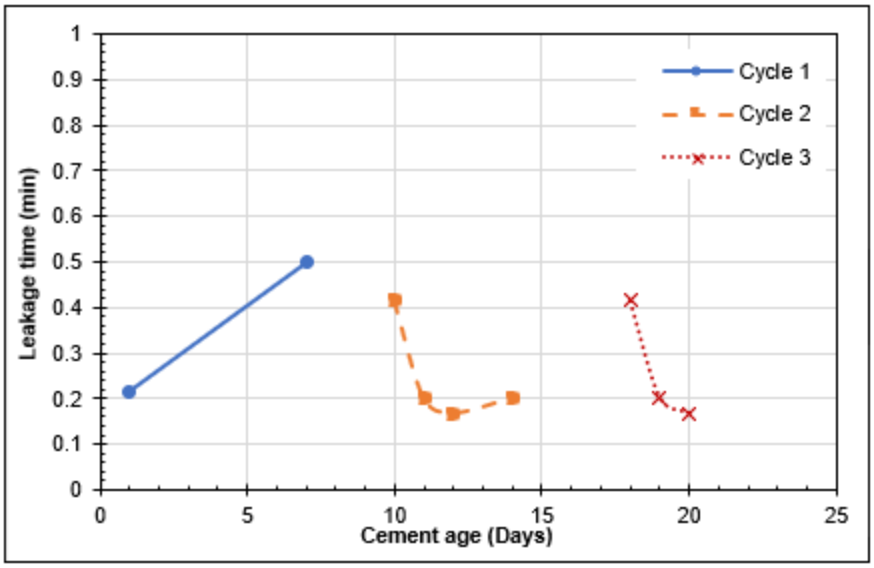

Figure 2.27: Leakage time versus cement age all the performed cycles in experiment 4 (Class G, WOC: 24 hours)

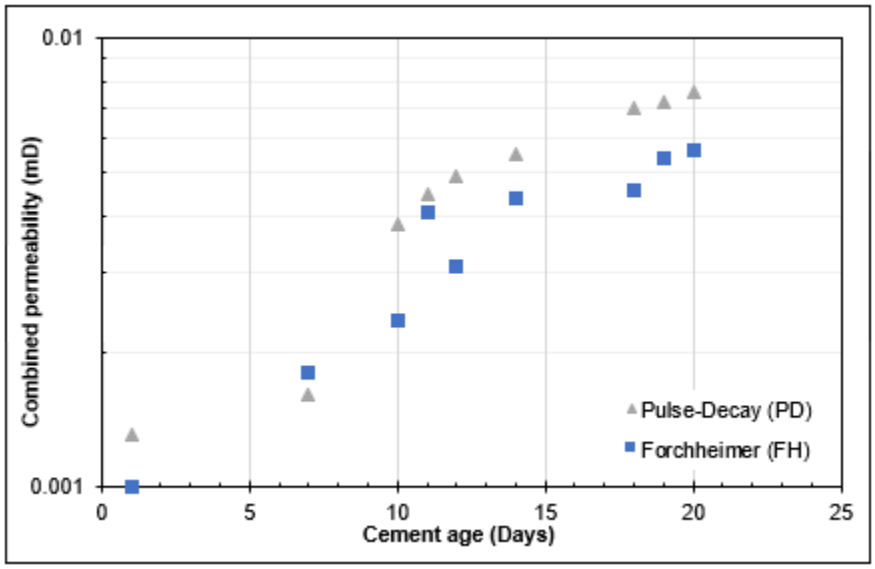

Figure 2.28: Combined permeability versus cement age for experiment 4 (Class G, WOC: 24 hours)

2.4.5 Gas Leakage Scenario Investigation

In this section, four scenarios are presented for gas leakage through a cement sheath. The difference between these scenarios is the differential pressure across the cement behind the liner-casing overlap. The goal of creating these scenarios is to investigate the optimum liner-casing overlap. In each scenario, four permeability values were used to assess the risk associated with each one of them. In addition, the liner-casing overlap was varied to investigate how the overlap length is going to help ensure good well integrity. Figure 2.29 shows gas flowing through different liner-casing overlaps. Select assumptions applied to the scenarios are as follows:

- The last casing shoe is set at 1000 ft.
- Casing diameter is 22 inches.
- Liner hanger diameter is 18 inches.
- Temperature is 100^{o}F.
- Four permeability values of 0.01, 0.1, 0.3, and 0.5 mD.
- Faulty elastomers in the liner hanger.

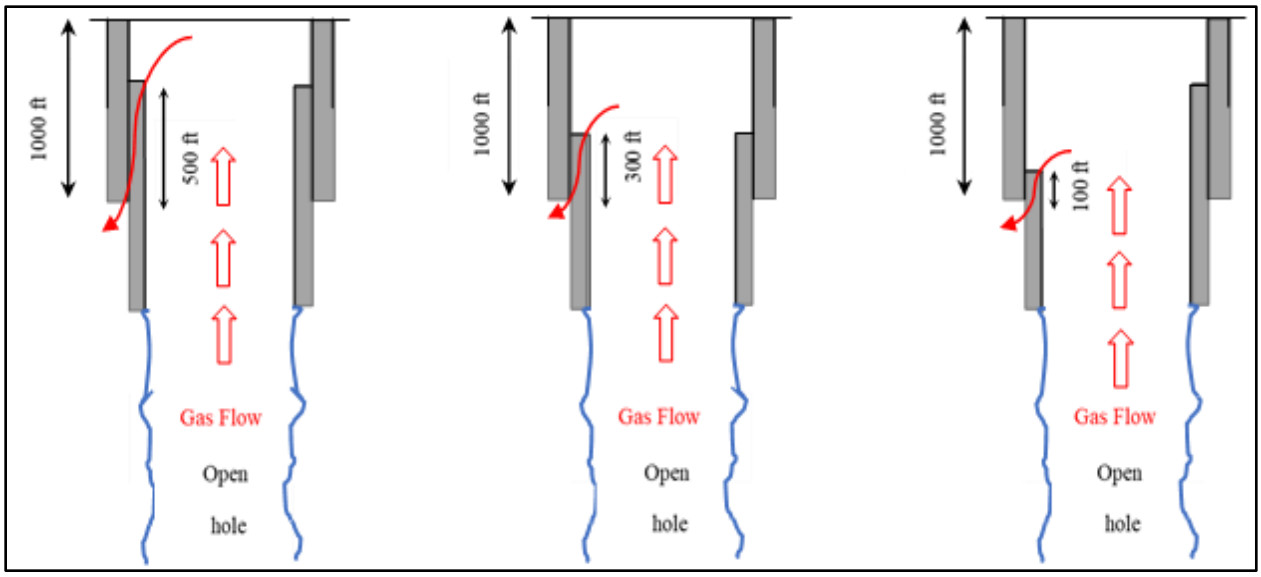

Figure 2.29: Gas leakage through different liner-casing overlap lengths

Stormont et al. (2017) proposed a simple gas leakage model that depends on the hydraulic aperture. They defined the hydraulic aperture as the space between two parallel plates which allows fluid flow. The hydraulic aperture can be calculated based on the cubic law using the following equation:

$$h^3 = \frac{12\,kA}{\omega} \quad \text{..... (11)}$$

Where h is the hydraulic aperture, A is the annular area, and ω is hydraulic aperture length. The hydraulic aperture length which corresponds to the inner pipe can be expressed as $2\pi r_1$. The hydraulic aperture can also be expressed as $(r_2\text{-}r_1)$, where r_2 is the radius of the annular gap. The flow is assumed to only go through the microannulus. The flow was modelled using the Navier-Strokes equation coupled with the cubic law and it is given by:

$$q = -\frac{\nabla P}{12\mu}\omega h^3 \quad \text{..... (12)}$$

The four permeability values used were plugged in equation (11) to calculate the hydraulic aperture for each case. Then, the hydraulic aperture values were used in equation (12) to obtain the flow rate. The leakage time can then be calculated based on the flow rate from equation (12) as:

$$t = \frac{L_c A_m}{q} \quad \text{..... (13)}$$

Where A_m is the flow area and L_c is the liner-casing overlap length. In the scenarios that were investigated, the leakage time was considered the primary variable for determining the optimum liner-casing overlap length. According to API Bulletin E3 (1993), the liner-casing overlap length can vary from 50 to 500 ft. Therefore, the overlap lengths in the scenarios were varied from 50 to 500 ft with 50 ft increment.

In the first scenario, a differential pressure of 250 psi across the cement column behind the liner-casing overlap was assumed. Figure 2.30 shows the leakage time versus the overlap length for 250 psi differential pressure across the cement column. For 50 ft overlap, the leakage time was approximately 3 hours for a permeability of 0.01 mD, while the leakage time decreased below 30 minutes for the rest of the permeability values. A general trend that was observed is that as the liner-casing overlap length increases, the leakage time increases. For 0.3 mD, the gas takes almost 25 minutes to leak when the overlap length is 100 ft, while it takes 95 minutes for 200 ft overlap length.

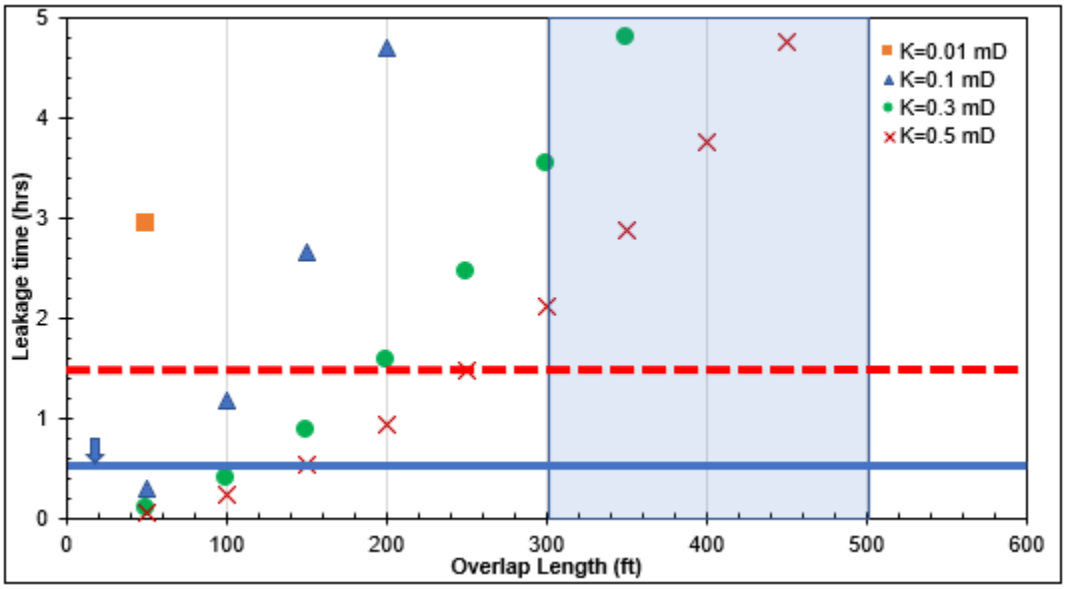

Figure 2.30: Leakage time versus liner-casing overlap length for 250 psi pressure differential across the cement.

The second scenario assumes a differential pressure of 500 psi across the cement column behind the liner-casing overlap. Figure 2.31 shows how the leakage time varies with the overlap length for 500 psi differential pressure across the cement column. For 50 ft of overlap, the leakage time was approximately 1 ½ hours (with a permeability of 0.01 mD), while it was less than 30 minutes for the rest of the permeability values. The leakage time increases as the liner-casing overlap increases. For a permeability of 0.3 mD, the leakage time is 15 minutes when the overlap is 100 ft, while it is 55 minutes for 200 ft of overlap. It can be observed that as the differential pressure across the cement (within the overlap) increases, the leakage time decreases.

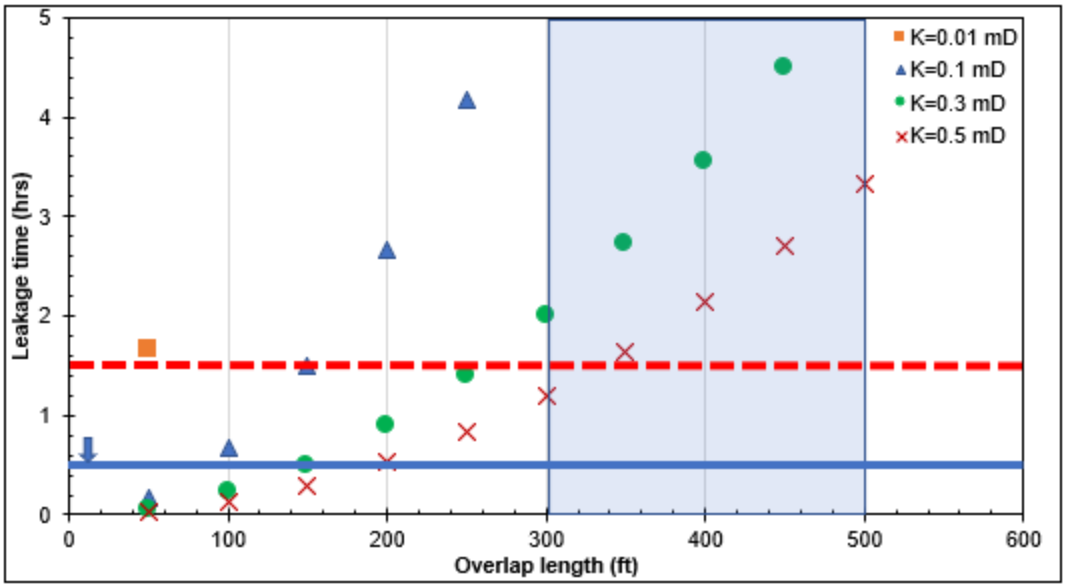

Figure 2.31: Leakage time versus liner-casing overlap length for 500 psi pressure differential across the cement.

The third and fourth leakage scenarios assumed differential pressures of 1000 psi and 1500 psi respectively across the cement column behind the liner-casing overlap. Figure 2.32 and Figure 2.33 show the leakage time versus the overlap length for 1000 psi and 1500 psi differential pressures respectively. It can be observed that the 50 ft overlap has the lowest leakage time especially for permeability values ranging from 0.1 to 0.5 mD.

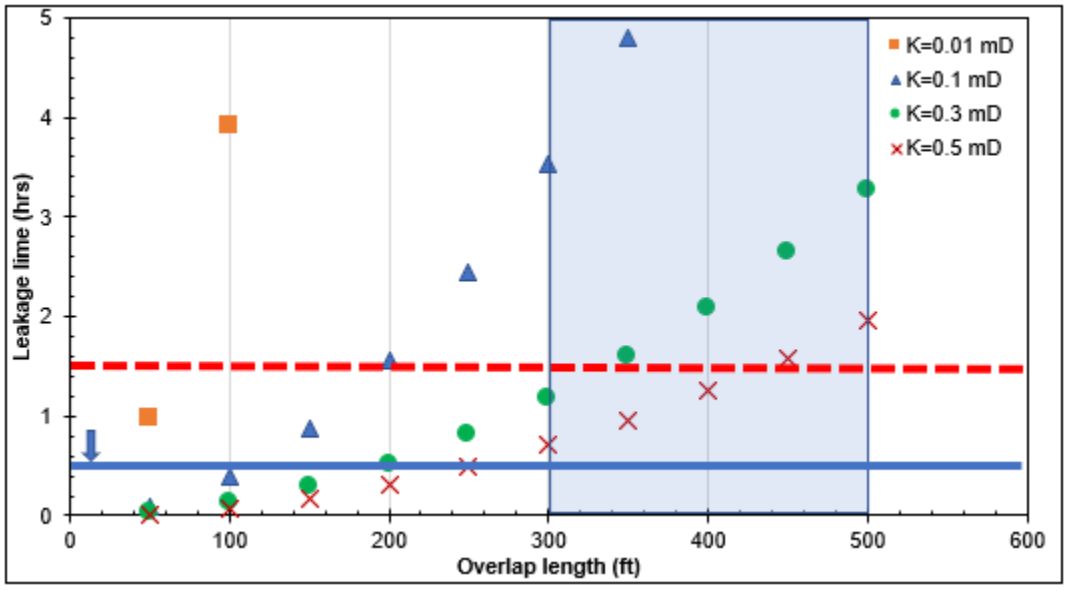

Figure 2.32: Leakage time versus liner-casing overlap length for 1000 psi pressure differential across the cement.

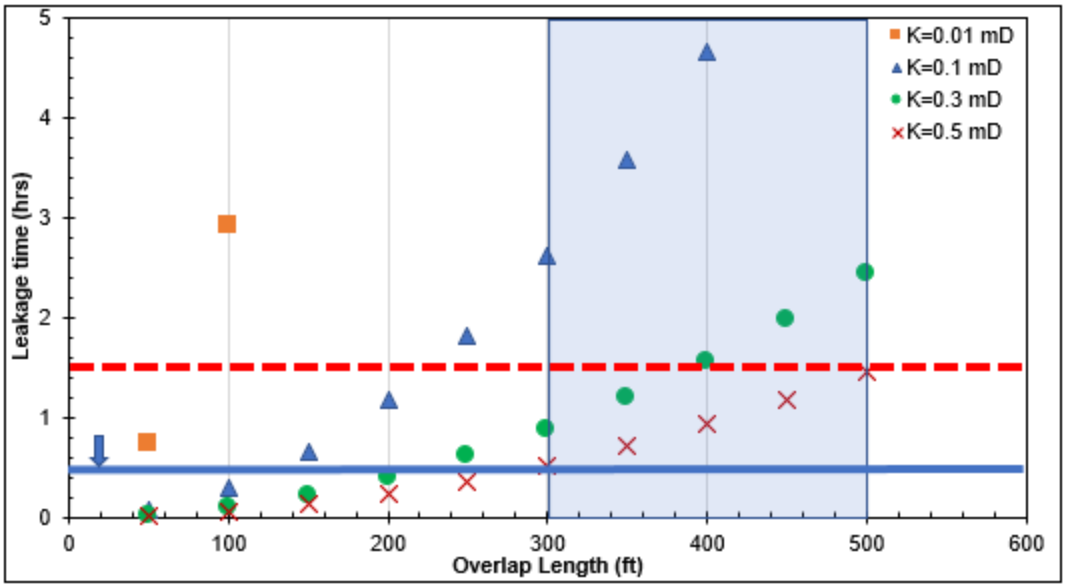

Figure 2.33: Leakage time versus liner-casing overlap length for 1500 psi pressure differential across the cement.

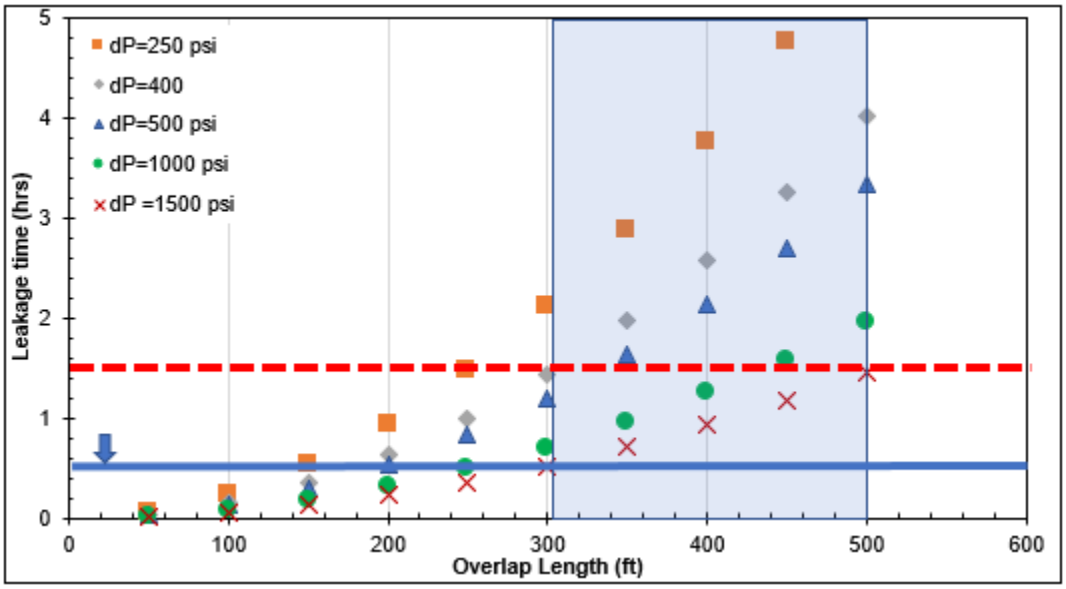

Figure 2.34: Leakage time versus liner-casing overlap length for 0.5 mD combined permeability for several differential pressures.

Figure 2.34 shows how the leakage time will vary with the overlap length for various differential pressures at 0.5 mD combined permeability. It can be observed that as the differential pressure across the overlap increases, the leakage time decreases. For 150 ft overlap and 250 psi differential, the leakage time is 30 minutes, while for 1000 psi it is 10 minutes. However, as the overlap length increases, the difference in leakage time is increases. For 300 ft overlap and 250 psi differential the leakage time is approximately 2 hours 7 minutes, while for 1000 psi differential it is 42 minutes.

The recommendations from the leakage scenario results are documented in the draft recommendation report.

2.4.6 Small Setup I with Neat Class H Cement Sample

In all the small setups, a maximum of two 60 psig cycles were performed before discarding it. The mixing, curing, and testing procedures for all tests with the small setups are the same. One of the major observations that was documented during tests was that the leakage time decreased within a cycle as time elapsed. Another observation was that some bubble positions disappeared, and some appeared as time elapsed. Figure 2.35 shows the leak positions on small setup I experiment 1 (a) and experiment 2 (b). In the experiments, the positions that disappeared in cycle 1 were positions 2, 3, 4, and 5. In cycle 2, position 6 disappeared. In small setup I experiment 2, positions 3 and 4 disappeared in cycle 1.

One of the objectives of small setup I was to investigate the effect of pipe size. Looking at Table 2.7 and comparing the leakage times of small setup I experiment 1 and 2 to big setup I experiment 1, a significant deviation in leak times were observed. The small setups had faster leak times than the big setup. An explanation for this could be the total volume to be filled with 60 psig of the inlet gas. Big setup I had a volume of 8303 ml to be filled while the small setup I had a volume of 463.33 ml (1-inch) and 1853.3 ml (2-inch) to be filled with N_2 gas. The volume difference allows the gas to migrate faster in the small setups; thus, the shorter leak time recorded. In Table 2.7, a shorter leak time is observed for the small setup I experiment 1 compared to experiment 2. The volume difference – small setup I experiment 1 (463.33 ml) and small setup I experiment 2 (1853.3 ml) – accounts for the change in time, since the pressure was kept constant at 60 psig throughout the experiments.

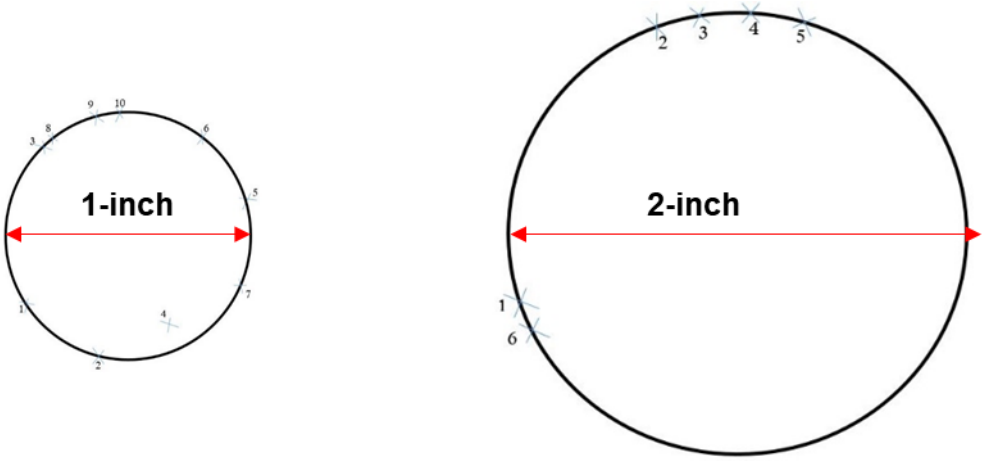

a **b**

Figure 2.35: Small setup I showing experiment 1 (a) and experiment 2 (b)

Table 2.7: Leakage time for big setup I experiment 1 and small setup I experiment 1 and 2.

Experimental Setup	Leakage Time (minutes)
Big setup I experiment 1	11
Small setup I experiment 1	1
Small setup I experiment 2	5

2.4.7 Small Setup 1 with Class H, Latex, and Bentonite Cement Sample

Using this setup, experiment 3 was performed with neat Class H cement, 1 gal/sack Thin Mortar Latex, and 0.5% bentonite. The first test was performed after 24 hours WOC. Before the test, water was poured on the cement surface to help track the bubbling. Prior to flowing the gas into the system, just after pouring water on top of the set cement, there were bubbles already emanating from the surface of the cement. This observation was deemed to be normal since a similar experience was encountered in big setup I experiment 3.

The cement surface bubbled for over 45 minutes; thus, delaying the commencement of the test. After most bubbles disappeared, the setup was connected, and the first test was performed. 21 minutes after beginning the test, the first bubble and position were observed. Position 2 started bubbling 1 hour 32 minutes after the test began. However, the bubbles from this position were not consistent and were coming out intermittently. The second test was performed the following day, there was one bubble from positions 2 and 3. There were also 3 random bubbles observed from various positions on the cement surface. These were not classified as leaks because a leak is considered to be a continuous bubbling of the gas. After 9 minutes 53 seconds, position 2 experienced its first gush of bubbles. After 1 hour, there were random bubbles that appeared from time to time but no consistent bubbles were observed.

A third test (72 WOC) was conducted on small setup I experiment 3. After 9 minutes 31 seconds of starting the test, the first random bubble was observed followed by other random bubbles with one of them coming from position 3. None of these were recorded as the leak time because no constant bubbling was observed. The leak time was recorded as 20 minutes 9 seconds because position 3's bubbling became more pronounced and consistent at this time. In this study, the consistency and pronouncement of a leak is defined when there is a 7 to 20 seconds delay between one bubble and the next coming from the same leak position. Since the bubbling in small setup I experiment 3 was inconsistent, an extended experiment was carried on the setup. The valve was opened at 3:42 pm on September 26, 2017 (8 days WOC). The first leak occurred after 8 hours of testing and after 20 hours of testing, two constant leak positions were observed.

2.4.8 Small Setup I with Class H and Fly Ash Cement Sample

Fly ash cement slurry was one of the recipes that was tested. The composition of fly ash has been discussed under section **2.3.2**, and Figure 2.36 shows that fly ash particles are generally spherical (Federal Highway Administration, 2017). In small setup I experiment 4, 30% fly ash BWOC and

1 gal/sack latex was used. A water requirement of 3.6 gal/74 lbm was used for the fly ash. The first test was performed on November 10, 2017 (24 hours WOC), using the standard testing procedure. During the first test, a rise in the water level was visually observed and shortly after, there was a leak. The leak was recorded at position 1, 21 minutes 26 seconds after commencing the test. After bubbling continuously for about an hour, the bubbling seized but continued almost immediately. This was approximately 1 hour 18 minutes from the test commencement. Two other tests were conducted on this sample, one on November 11, 2017 (48 hours WOC) and the last on November 14, 2017. Their leak times were recorded as 14 minutes 25 seconds and 20 minutes 48 seconds respectively. Visual observation suggests that the bubbling intensity in the last experiment was lower compared to the 48 hours WOC test. This indicates an improvement in the cement compressive strength and a potential decrease in cement permeability with hydration. The shorter leak time is attributed to residual gas in the cement from the test performed the day before. The 2-day fallow period allows all the gas to escape the setup and an increase in leakage time was observed once again. This observation directly corresponds to the self-healing effect discussed in big setup I experiment 1. It is to be noted that all through the tests with this slurry, only one leak position was observed (as shown in Figure 2.37).

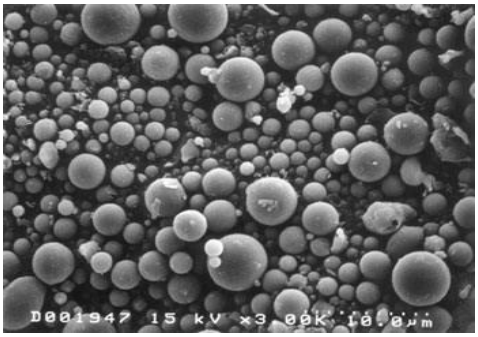

Figure 2.36: Fly ash particles at 2000x magnification (Federal Highway Administration, 2017).

(a) **(b)**

Figure 2.37: Fly ash cement showing gas bubbles during test (a) and leak position after test (b) for small setup I experiment 4.

2.4.9 Small Setup I with Microsilica Cement Sample

Microsilica cement slurry was investigated with small setup I experiment 5. The cement slurry was formulated with Portland cement, 38% water requirement, 5.5% microsilica (Silica Fume White) BWOC, and a 5% water requirement for the microsilica. A 5% water requirement was selected because no water reducers were used during the mixing. Prior to this selection, a range of 5% to 12% water requirement could have been used for the experiment. Both low and high ranges were prepared, but the sample with 5% water requirement was used so that the slurry density (16.05 ppg) is kept close to that of neat Class H base (16.65 ppg). The resulting density from the 12% water requirement sample was 15.5 ppg

The first test was performed after 24 hours WOC and the first leak was observed 15 seconds into the test. This indicates poor bonding between the microsilica cement and the casing since the leak occurred at the wall (position 1). The test continued for 30 minutes, and no subsequent leaks were recorded. The second test was conducted the following day and two new leak positions were recorded, making a total of 3 leak positions. The second and third leaks occurred 57 seconds and 2 minutes 11 seconds respectively, after starting the test. After 72 hours WOC, test 3 was performed and the first leak occurred 11 seconds after beginning the test. The leak in position 2 was recorded 35 seconds into the test. Figure 2.38 (b) shows the three leak positions in small setup I experiment 5. Position 3 was identified within the cement sheath and this can translate to a faulty cement. Images of the cement sheath were obtained with a Dino-Lite Digital Microscope. Figure 2.38 (a) shows the surface of the slurry before the first test while Figure 2.38 (c) shows leak position 1 observed during the test. The leak came from beneath the cement crack and steel pipe wall as shown by the red circle and arrow.

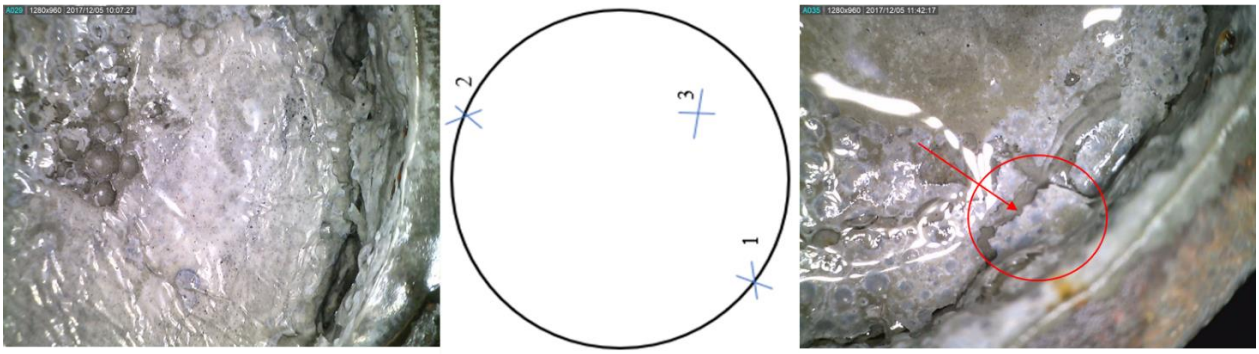

(a) **(b)** **(c)**

Figure 2.38: Microsilica cement before the first test (a), leak positions (b), and leak position 1 during a test (c) for small setup I experiment 5

To verify the inadequacy of Silica Fume White, the slurry for small setup I experiment 6 was designed. This was similar to the slurry design for small setup I experiment 5, except that 12% of microsilica was used instead of 5.5% used in experiment 5. The microsilica concentration was increased in a bid to create an improved cement slurry. No water requirement was needed for this experiment. After 24 hours WOC, the first test was conducted, and a leak was observed within the

first 7 to 10 seconds. The second test (48 hours WOC) that was conducted on this setup had the first leak within 10 seconds of commencing the test. Both tests had the gas leaking through the same position (between the cement and the steel wall) similar to experiment 5. The leak times which were almost instantaneous indicated poor bonding through the entire length of the cement column.

One plausible mechanism for the cement failure is slurry densification. It was highlighted in literature that microsilica has a particle size ranging from 0.02 to 0.5 μm, with an average of 0.15 μm. Cement on the other hand has a particle size ranging from 1 μm to 90 μm, with 10 wt% of the cement being made of particles larger than 50 μm and only a few wt% consisting of particles larger than 90 μm. On the fine end, less than 10% of the cement particles were smaller than 2 μm. Figure 2.5 juxtaposes the plots of particle size distribution of cement, undensified, and densified microsilica. The fine particle size of microsilica allows packing between the cement grains, resulting to an improved microstructure within the cement matrix. Undensified microsilica has a typical bulk density between 200 kg/m^3 and 350 kg/m^3, while densified microsilica has a typical bulk density between 500 kg/m^3 and 700 kg/m^3. The microsilica used in this study had an approximate density of 400 kg/m^3. Per Daou and Piot (2009), "only microsilica with a bulk density of approximately 300 kg/m^3 is the adequate compromise between proper handling characteristics and good slurry performance".

2.4.10 Small Setup I with Nanomaterial Cement Sample

Nanomaterial was used as an additive in small setup I experiment 7. A 0.5% BWOC concentration of nanomaterial was used in combination with Class H cement. As a result of the fine nature of the nanomaterial, the mixing procedure was slightly modified to effectively homogenize the slurry. After completing the standard API mixing procedure, an additional 15 seconds of shearing at 4000 rpm was done, followed by another 15 seconds of shearing at 12000 rpm. This modification allowed for complete dispersion of the nanomaterial within the new slurry. The normal curing and testing procedures were followed. The first leak was detected after 9 minutes 54 seconds into the first test and the bubbles that were observed were extremely tiny. Position 2 was recorded 11 minutes after position 1 was marked. The bubbles at position 2 were also miniscule and had an average of 1 minute 28 seconds delay between one bubble and the next. This delay was determined by an average of the time between 4 consecutive bubbles. Two other tests were conducted after 48 hours and 72 hours WOC. No bubbles were recorded on the second day of testing. On the third day of testing, continuous bubbling was recorded after 2 hours 4 minutes and 35 seconds of beginning the test. This leak was small and was spotted on a different surface location of the set cement which was marked position 3. Figure 2.39 (a) shows the surface of the set cement before the test and Figure 2.39 (b) shows position 1 where the first leak was detected.

(a) **(b)**

Figure 2.39: Nanomaterial cement sample before test without leaks (a) and during the test showing position 1 within the cement

After allowing the nanomaterial cement to fallow for 5 days, another test was conducted on the sample. The first leak was detected at position 3 after 1 minute and 11 seconds into the test. Five new positions were spotted after the first leak, some being at the center of the set cement while others were between the cement and casing. Figure 2.40 shows all the leak positions on small setup I experiment 7 during the test conducted after the fallow period.

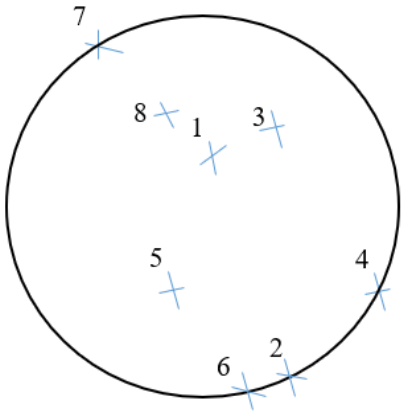

Figure 2.40: Leak positions in small setup 1 experiment 7 during the test conducted after the fallow period

2.4.11 Small Setup I with Class H, Flyash, Latex, and Nanomaterial Cement Sample

To improve on the previous slurry designs, a combination of additives was tried. In small setup I experiment 8, a cement slurry with Class H cement, 30% fly ash, 1 gal/sack Latex, and 0.5% nanomaterial was formulated. The water requirement for fly ash was kept at 3.6 gal/74 lbm. The first leak during the test was recorded at 1 minute 14 seconds, while the second leak was recorded at 1 minute 20 seconds. The bubbling intensity observed on the first day of the test was high and the bubbles were coming from multiple positions as shown in Figure 2.41 (a and b). Three tests were performed for 3 consecutive days on the sample and the bubbling intensity appeared to have decreased as the number of days increased. By the end of the 3-day testing period, a total of eight

bubbling positions were identified. Five of these were within the set cement while the other 3 were located at the interface between the set cement and the steel pipe. Figure 2.41 (c) shows the identified leak positions in small setup I experiment 8 after all the tests.

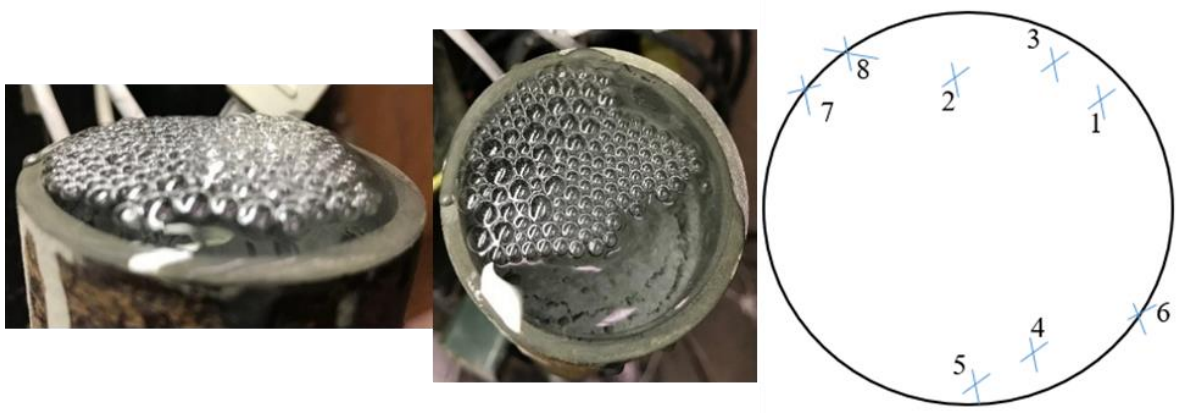

(a) **(b)** **(c)**

Figure 2.41: Side and top view of gas bubbles (a and b) and bubble positions (c) in small setup I experiment 8

2.4.12 Small Setup I with Class H, 1.5 liters/100 kg Commercial Additive Cement Sample

A commercial additive from a major service company was used to design a new slurry for small setup I experiment 9. The recommended range was 4.5 liters to 9 liters of the additive per 100 kg of cement. 6 and 3 liters/100 kg were tried but both concentrations made the cement slurry too viscous to be used in the lab. A concentration of 1.5 liters/100 kg was finally used. The new slurry revealed a high static gel strength (SGS) but regular thickening time. These results are discussed in detail in **2.5**. No leaks were observed during the first test which was after 24 hours WOC. After 48 hours WOC, the set cement was pressurized for 6 hours – 4 hours followed by a 2-hour session. No leaks were noticed as the system remained gas tight. The last test was conducted for 2 hours after 72 hours WOC and the system still proved to be gas tight.

Figure 2.42: Small setup I experiment 9 showing no bubbles after two tests.

Table 2.8. Summary of results for all the tests using setup I

Big setup I					
Setup/Experiment	**WOC (hrs.)**	**Density (ppg)**	**Composition**	**Leak time (mins:secs)**	**Bubbling description**
S1E1	24	16.65	Neat Class H	11 mins 08 secs	3
S1E2	12	16.65	Neat Class H	4 mins 28 secs	3
S1E3	24	12.5	3 gals/sack latex, 1% bentonite	16 mins 17 secs	5
S1E4	24	16.65	Neat Class G	13 secs	3
Small setup I					
Setup Experiment	**WOC (hrs.)**	**Density (ppg)**	**Composition**	**Leak time (mins:secs)**	**Bubbling description**
SS1E1	24	16.65	Neat Class H	1 min	3
SS1E2	24	16.65	Neat Class H	5 mins	3
SS1E3	24	16.65	1 gal/sack latex, 0.5% bentonite	21 mins	1
SS1E4	24	14	1 gal/sack latex, 30% flyash	21 mins 26 secs	2
SS1E5	24	16.05	5.5% microsilica	15 secs	4
SS1E6	24		12% microsilica	7 secs	1
SS1E7	24	16.55	0.5% nanomaterial	9 mins 54 secs	1
SS1E8	24	14.5	1 gal/sack latex, 30% fly ash, 0.5% nanomaterial	1 min 14 secs	5
SS1E9	24	16.4	1.5 liters/ 100 kg commercial additive from a service company	N/A	0

1 - Tiny inconsistent bubbling, 2 - Tiny consistent bubbling, 3 - Regular bubbling, 4 - Intense bubbling, 5 - Intense bubbling with multiple locations.

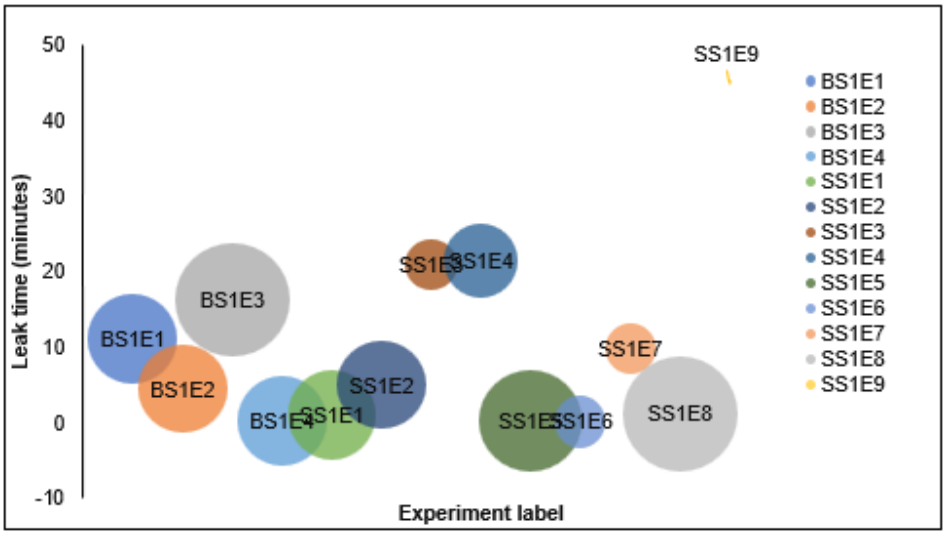

Figure 2.43: Bubble graph showing the leak times for all the tests using setup I

Figure 2.43 depicts the bubble graph for Table 2.8. The level at which the center of the bubble stands, represents the leak time of that experiment. The size of the bubble in the bubble graph indicates the degree of bubbling. The bubbling degree is on a scale of 1 to 5. '1' indicates tiny and consistent bubbling, whereas '5' indicates intense bubbling with multiple locations. The bubble graph provides a pictorial view of the tests conducted with the big setup I and small setup I. For the big setup I, the nomenclature "BS1E1" represents big setup I experiment 1, while for the small setup I, SS1E1 represents small setup I experiment 1.

2.5 PHYSICAL PROPERTIES OF CEMENT SAMPLES

2.5.1 Rheology

Rheology is the science and study of the deformation and flow of matter, especially the flow of non-Newtonian fluids. The rheology of a fluid also describes the interrelation between forces, deformation, and time. All cement slurries are considered non-Newtonian and they can be shear thinning or shear thickening. In equation 14, n > 1 indicates shear thickening or pseudoplastic while n < 1 indicates shear thinning or dilatant fluids.

$$\sigma = K\gamma^n \quad \text{(14)}$$

The addition of some additives like fly ash and nanomaterial can make the formulated slurries develop higher viscosity. A combination of nanomaterial and fly ash in the same slurry increases the viscosity of the slurry. Although cement slurries with additives tend to be more viscous, they also prove to be much more shear thinning than the base slurry. This is indicated by the reduction in the flow behavior index (n) for slurries with additives. The addition of 0.5% nanomaterial to the base slurry made the slurry design more shear thinning. The addition of 30% fly ash and 1 gal/sack of latex also made the cement slurry more shear thinning. However, adding 0.5% nanomaterial to the slurry design with 30% fly ash and 1 gal/sack of latex increased the 'n' value, drawing it closer

to a Newtonian fluid. Table 2.9 shows the rheological properties of all the slurry designs that were tested.

Table 2.9. Rheological properties of tested cement slurries

	Neat Class H	Class H cement, 30% Fly ash and 1% latex	Class H, 0.5% nanomaterial	Neat Class G	Class H, 30% fly ash, 1 gal/sack latex 0.5% nanomaterial	Class H, 1.5 liters/100 kg commercial additive
Shear Rate (1/s)	**Shear Stress (Pa)**					
1021.3809	161.32	107.60	131.58	58.32	120.34	105.66
510.9969	82.32	71.44	76.38	40.40	70.28	70.56
340.6986	53.64	57.50	58.14	34.24	53.74	55.84
170.2982	38.64	44.58	44.22	27.10	38.90	42.32
10.2138	7.98	14.26	9.840	8.68	13.36	12.98
5.1069	6.14	10.94	6.90	4.14	10.30	7.64
Apparent Viscosity Profile (255.4 s-1) from Room Temperature to 102°F						

2.5.2 Gas Transit time

Gas transit time is the period during which the cement slurry changes from a true hydraulic fluid capable of providing hydrostatic pressure to a highly viscous material showing solid characteristics. The gas transit time starts when the cement slurry develops enough static gel strength (SGS) to restrict transmission of full hydrostatic pressure and ends when the cement is solid enough to prevent gas flow. SGS is measured using a cement consistometer. It is calculated by the geometry and slow motion of the consistometer paddle (10°). This slow movement allows SGS to be measured but does not inhibit gel strength development. Sabins et al. (1982) estimated that transition time ends when the cement slurry has developed an SGS exceeding 250 Pa (522 lbf/100ft^2). Generally, gas transit time is the time it takes for the SGS of a cement slurry to rise from 100 lbf/100ft^2 to 500 lbf/100ft^2.

The gas transit time of the slurry designs are displayed in Figure 2.44. The shorter gas transit times in the new slurry mixtures show higher potential for mitigating gas flow through the cement slurry. With the addition of 30% flyash and 1 gal/sack latex, the gas transit time was reduced by almost 1 hour, making the new slurry design desirable. The new slurry design with 30% flyash and 1 gal/sack latex proved to be a better substitute to neat Class H. It had a leak time of 21 minutes and 26 seconds in a 2-inch pipe, while neat Class H proved to prevent gas flow for only 5 minutes.

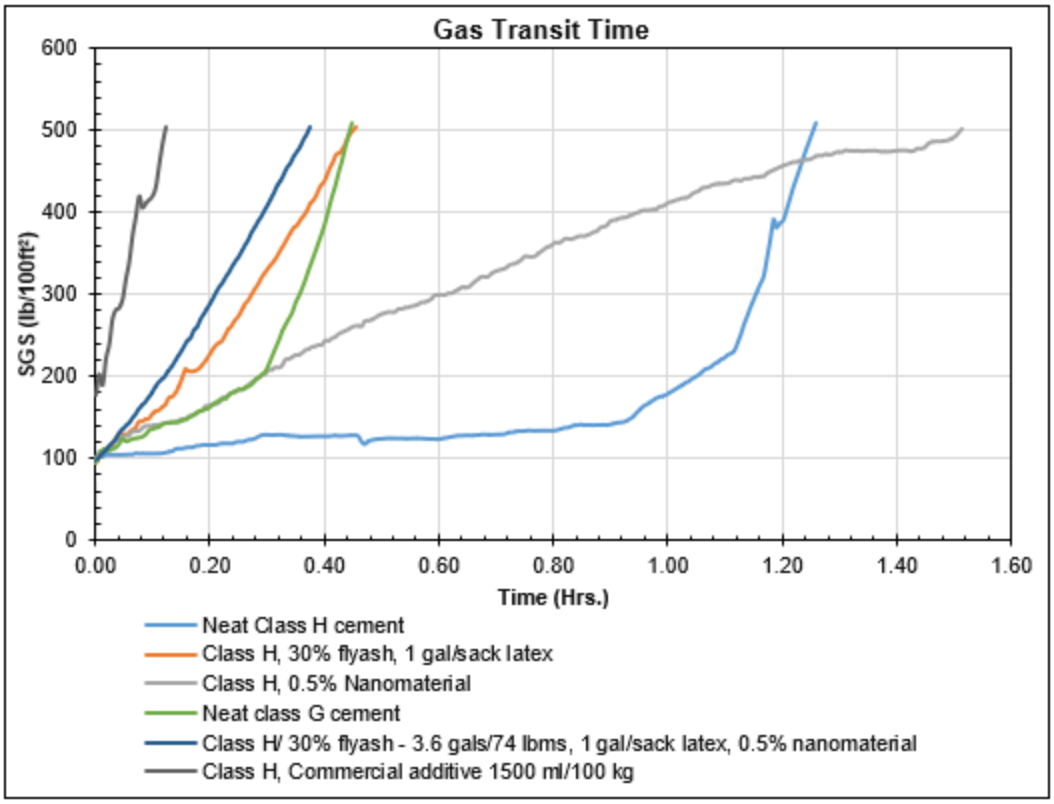

Figure 2.44: Gas transit time for various cement slurry samples.

Class H with 0.5% nanomaterial had a better gas transit time compared to neat Class H. This slurry design showed better performance with an improved leak time of 9 minutes and 54 secs. A cautious inference can be made that a slurry with a shorter gas transit time has a good potential to mitigate gas migration. However, this may not always hold for all slurry designs, especially when different additives are mixed. For instance, the slurry design with neat Class H, 30% BWOC flyash, 1 gal/sack latex, and 0.5% BWOC nanomaterial took 12.5 minutes (0.2089 hrs.) to attain 100 lbf/100 ft^2 and 35 minutes to attain 500 lbf/100 ft^2. The gas transit time was 22 minutes and 30 seconds. Although this slurry design had a short gas transit time, the leak time when it was used in small setup I experiment 8 was within 1 minutes and 14 seconds after 24 hours WOC. This is attributed to the properties of some of the additives which tends to impede early UCS development. This will be discussed in the next subsection. With the addition of 1.5 liters/100 kg of commercial additive, the gas transit time reduced to 7 minutes 19 seconds, this was the least recorded time. This slurry had no leaks occur throughout the testing period proving to be completely gas tight.

2.5.3 Unconfined Compressive Strength and Ultrasonic Testing

Unconfined compressive strength (UCS) is the maximum axial compressive stress that a right-cylindrical or cubic material can withstand under unconfined conditions (zero confining stress). The materials used for UCS test were set cement samples. UCS is also known as the uniaxial compressive strength of a material (cement cubes) because the application of compressive stress

is only along one axis — the longitudinal axis — of the sample. In an ultrasonic compressive-strength test, a high-frequency sound pulses through a set cement sample and measures the time required for the sound wave to travel completely across the lateral dimension of the sample. This generates an ultrasonic pulse velocity (UPV). As the cement sets with time, the sound wave travels faster; thus, taking a shorter time to reach the other end of the sample.

In this study, both the ultrasonic cement test and unconfined compressive strength tests were carried out on the slurry designs which were cured for 1 and 3 days, and have been used in the big and small setups I. This was done to provide a holistic picture of the performance of cement slurries used for testing. Using the API RP10B-2 (2013) procedures, cubical cement samples were prepared for both UPV and UCS testing. The preparation of the cement samples are as follows: i) the molds were put together and greased, ii) the right slurry was selected, and iii) the appropriate mixing procedure was used for each cement slurry. The cement slurries were then poured into the molds, each cube in a mold was filled to half of its capacity, followed by the next cube, and finally the third cube. After filling the third cube to half of its capacity, the first cube was topped up to the brim, followed by the second cube, and finally the third cube to complete one mold.

After curing the samples in a water bath for the appropriate number of days (1 or 3 days) at atmospheric temperature and pressure, the samples were taken out of the water bath and dried shortly. For each test, three samples were prepared to provide more accurate data. Before each test, the dimensions of the samples were recorded (Figure 2.45). Three values for length and width were taken and averaged out to provide the final length and width of the sample. This was done for each of the three samples to be used for the test. The Ultrasonic test was conducted first since it is a nondestructive test. The probes were placed on both ends of the cubic cement sample and high frequency sounds were propagated through the cement sample. The time it takes for the sound frequencies to propagate through the sample was recorded. Figure 2.46 shows an ultrasonic test being conducted on a cement sample. The same procedure was followed for each slurry design and Table 2.10 shows the ultrasonic pulse velocity (UPV) readings obtained from the ultrasonic cement tests.

Figure 2.45: Dimensions of cement samples (Class H and Class G) measured.

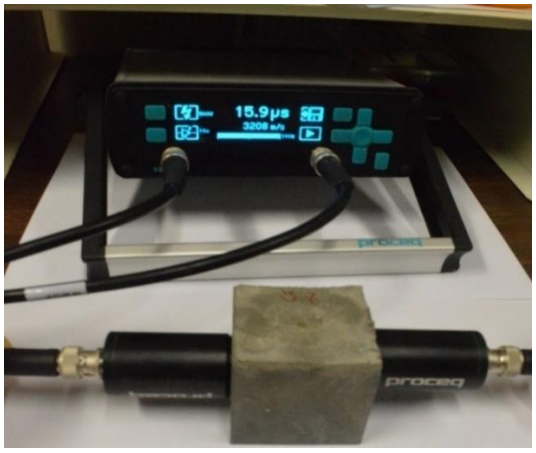

Figure 2.46: Ultrasonic cement test being carried out.

Table 2.10: Ultrasonic pulse velocity (UPV) and unconfined compressive strength (UCS) test results.

Cement slurry type	Day	UPV	UCS
Neat Class H	1	2191.69	4.00
	3	2972.17	15.36
Neat Class G	1	2915.39	15.34
	3	3406.41	28.36
Class H, Nanomaterial	1	2369.56	6.09
	3	3123.44	19.66
Class H, Flyash, latex Nanomaterial	1	1888.46	1.69
	3	2686.24	6.41

For the unconfined compressive strength (UCS) tests, a Test Mark Compressive Strength machine was used. A uniaxial force was applied to the cement matrix till it failed by shearing. The value at which the maximum stress is applied on the body is termed as the UCS of the sample. UCS tests were performed on all the samples with the same curing day(s) and the average of the values was considered the strength of the set cement. Figure 2.47 shows an unconfined compressive strength test being conducted and the shear failure of the cement sample. The 1-day and 3-day compressive strengths of various samples are reported in Table 2.10. From this table, an increase in UCS for neat Class H cement sample was observed. This increase was in the range of 220% and 285% for a period of 1 day to 3 days. The addition of additives like nanomaterial and fly ash impaired compressive strength development in the samples.

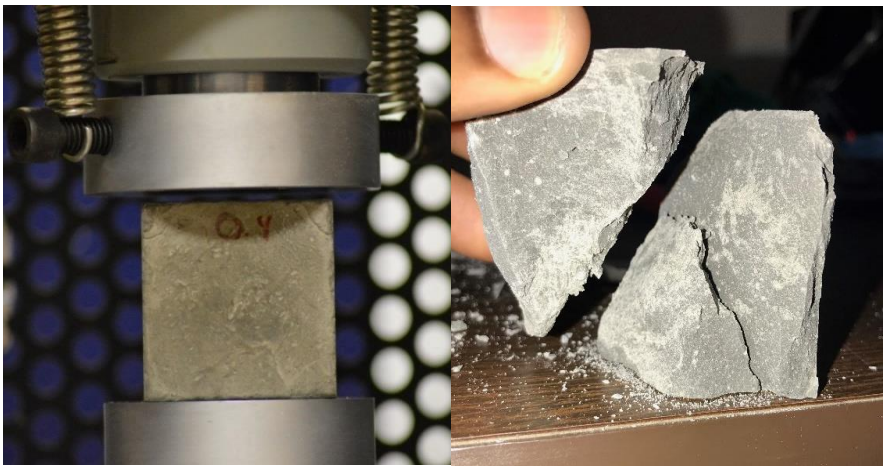

(a) **(b)**

Figure 2.47: Unconfined Compressive Strength conducted

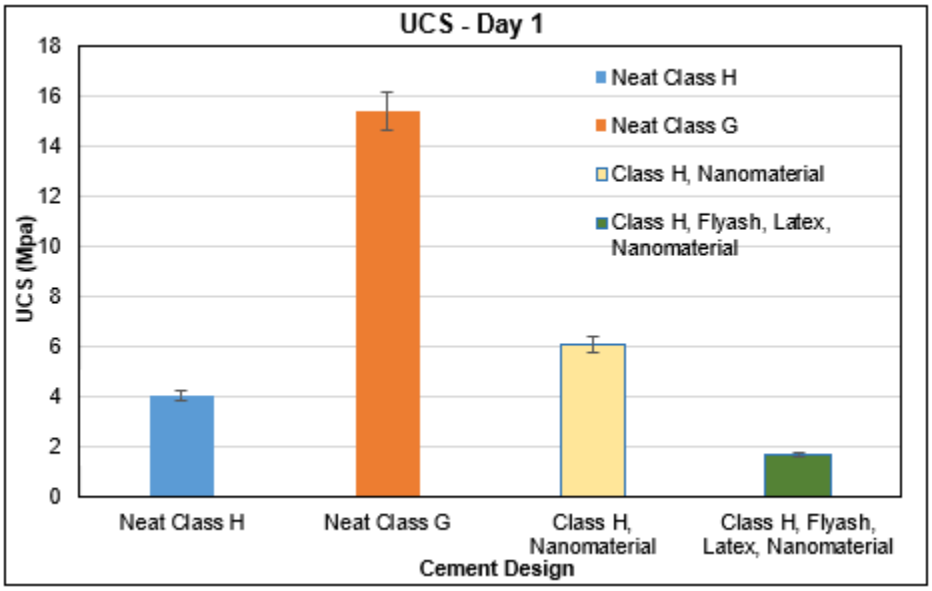

Figure 2.48: Day 1 results for unconfined compressive strength (UCS) tests.

From Figure 2.48, it can be observed that adding 0.5% nanomaterial to the slurry design improved the initial compressive strength of the new slurry. A 52.3% increase in day-1 compressive strength was recorded. However, Figure 2.49 shows that the late time effect of nanomaterial is not as significant as the early time improvement. An increase in 28% was recorded in the nanomaterial cement slurry design for day 3 UCS test. This increase is related to the neat Class H cement slurry after the third day of UCS test. The addition of latex, nanomaterial, and fly ash did not improve the UCS test values. The light weight of fly ash and latex are plausible factors that impeded compressive strength development. Apart from the recorded decrease in density, this slurry design showed a decrease in compressive strength by 57.75% on the first day and 58.27% on the third day of testing. Comparing Class H and Class G cement samples, Class G revealed better

compressive strength development in both the first and third day of UCS test. A 283.5% increase in UCS was recorded in the first day.

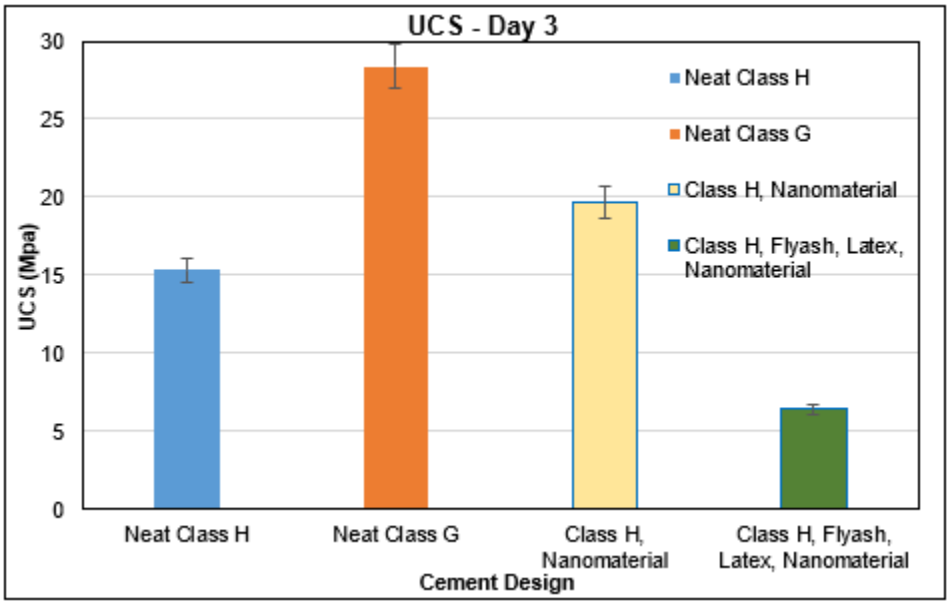

Figure 2.49: Day 3 results for unconfined compressive strength (UCS) tests.

2.6 SUMMARY AND CONCLUSIONS

In this section of the report, the findings from the cement tests (big setup I and small setup I) are summarized. It highlights the conclusions drawn from the theoretical, experimental, and analytical studies as follows:

- Neat Class H and Class G cement slurry (without gas migration additives) is inadequate to serve as a primary well barrier.
- The combined permeability of annular cement increases as cement age increases.
- The leakage time increases as the combined annular cement permeability decreases.
- The leakage scenario results reveal that 62% of the total leakage time falls under the liner-casing overlap range between 50 and 250 ft. This overlap range may not permit longer duration for detecting and controlling gas influx, when the cement sheath is faulty.
- The leakage scenario results suggest that 35% of the leakage times are between 1 and 30 minutes. The current casing pressure test duration of 30 minutes may not be enough to verify the integrity of the cement sheath in the liner hanger overlap.
- Partially densified and densified microsilica both behave as inert materials in cement. They do not exhibit superior performance for adequate zonal isolation.
- Besides the commercial additive cement slurry, the slurry designs with the longest leakage times (21 minutes and 21 minutes 7 seconds) both had latex in their formulation. Cement

formulation with latex can have superior performance at temperatures above the ambient temperature.

- Nanomaterial in low concentrations of 0.5% BWOC improved 1-day compressive strength.
- A slurry design with short gas transit time shows a good potential for mitigating gas migration. This depends on the additives added. Other tests such as the UCS and pressure tests can be used to confirm their gas migration mitigation ability.
- The inclusion of nanomaterial improves the property of set cement which mitigates gas migration.
- 1.5 liters/100 kg of the commercial additive used in this study is enough to mitigate gas migration in the cement column completely.

3 ELASTOMER AGING CELL TESTS USING SET UP III

3.1 INTRODUCTION

Elastomers are materials that have randomly distributed chains which are connected by cross links in their molecular structure (Visakh et al. 2013). Walker (2011) argued that elastomers are the most versatile engineering material of the 21st century with multiple uses including: noise reduction and dampening in the mechanical engineering discipline and thermal insulation in the electrical engineering discipline. In the oil and gas industry, elastomers are used as hydraulic seals, O-rings, packers, liner hangers, and in other downhole equipment. Elastomer seals are essential for zonal isolation in vertical and deviated wells. As production packers and in liner hanger systems, they act as a strong seal, preventing influx and channeling of hydrocarbon between the production casing and tubing (Davis and McCrady 2008; Gavioli and Vicario 2012). As such, setting up elastomeric sealing systems are a routine procedure applied in drilling and completions. Properly installed elastomeric sealing systems can effectively isolate formation zones. Adequate zonal isolation allows for production of oil and gas from the producing formations without leaks into the surface and other subsurface formations (Ahmed et al. 2009). This is what qualifies an elastomer to be fit for service.

3.1.1 Overview

There are many elastomers used in the oil and gas industry. Some of these include but are not limited to: acrylonitrile butadiene rubber (NBR), ethylene propylene diene rubbers (EPDM), hydrogenated nitrile-butadiene (HNBR), fluoroelastomers (FKM), perfluoro-elastomers (FFKM), and tetrafluoro ethylene/propylene rubber (FEPM). The deterioration or degradation of any elastomer during use would render the elastomer not “fit for service”. Elastomer degradation can occur because of physical, chemical, or both physical and chemical processes. Physical degradation can occur when an elastomer is exposed to extreme stress loading conditions for a prolonged period. In downhole conditions, elastomers are often in a compressed state, especially when used in liner hanger systems, BOPs, gaskets, and seals. These conditions tend to alter the physical structure of the elastomer. Pressure, temperature, ultra-violet rays, atmospheric ozone, and moisture are all factors that can alter the physical structure of an elastomer. In addition, surrounding downhole gas molecules tend to permeate the pores of the compressed elastomer. A sudden release of the surrounding gases causes the gas molecules within the pores to escape in what is known as rapid gas decompression (RGD) or explosive decompression. These conditions could cause the elastomer to lose its physical sealing abilities. Although most physical changes of an elastomer are reversible, there are few exceptions. Not all physical changes occurring in an elastomer are reversible. Extreme physical and non-physical compression of elastomers can break the London dispersion forces (instantaneously induced dipole forces) existing in an elastomer. This causes an irreversible physical change in the elastomer.

Elastomers are also susceptible to chemical attacks. A good elastomer for oil and gas application is one that exhibits both chemical and heat resistance, while maintaining properties of

resilience and rebound in aggressive chemical media, including H_2S, hydrocarbon, and polar solvents (Parker Hannifin, 2002). Elastomer sealing properties vary with time as it interacts with the surrounding fluid under downhole conditions. Depending on the nature and abundance of the fluid interacting with the elastomer, severe degradation can occur, accompanied with significant changes in tensile strength, swelling, ultimate elongation, and hardness of the elastomer. Limited laboratory studies (Cong et al. 2013; Fernández et al. 2016; Tynan 2016; Dajiang et al. 2017) have been conducted to access the degradation behavior of elastomer under acidic wellbore environments.

3.1.2 Statement of the Problem

Exploration and production of oil and gas wells has witnessed a progressive change over the years. From producing conventional sands to exploring unconventionals in harsh environments, shallow gas kicks and blowouts still pose a wellbore drilling challenge to the industry. The substantial presence of CO_2, H_2S, and methane gas has complicated the art and design of well construction. Typically, these gases are first encountered during drilling. Therefore, it is imperative that a wellbore design procedure incorporates careful selection of suitable elastomers that would not degrade when exposed to these gases, combined with other downhole conditions.

Oil field elastomers are vulnerable to acid attacks and harsh downhole environments. Different physical and chemical mechanisms are involved in deteriorating the properties of an elastomeric. There are limited available studies that have been conducted to study the effects of H_2S, CO_2, and other harsh downhole conditions on elastomers. Published research on elastomer degradation mechanisms when exposed to these conditions are scarce (Cong et al. 2013). Thus, more studies are needed to ensure that elastomers are "fit for service" in the environments they are used.

3.1.3 Objectives

Elastomer seals are essential for zonal isolation in vertical and deviated wells. They are often used either as O-rings (static seals) or as energized seals (packers). O-rings fit a predetermined sealing configuration with specific grove depth, width, and clearance. Packers act as a strong seal, preventing influx and channeling of hydrocarbon between the production casing and tubing (Davis and McCrady 2008; Gavioli and Vicario 2012). For elastomers to perform their functions effectively over an extended period, it is essential that the elastomers withstand the deleterious effects of pressure, prolonged loading effects, severe temperatures, corrosive fluids, and acidic gases. This study aims to provide a better understanding of the role of acidic gases and corrosive fluids in the degradation of elastomers. The study focuses on following elastomers which frequently used in the oil and gas industry: Nitrile butadiene rubber (NBR), Ethylene propylene diene monomer (EPDM), Fluoroelastomers (FKM), and Polytetrafluoroethylene (PTFE). The investigations concentrate on examining the effects of acidic and corrosive fluids on the physical properties (hardness, volumetric swelling, and compression) of the elastomer. The possible failure of elastomers in a wellbore makes it imperative to understand the various elastomer degradation

mechanisms and develop methods to reduce the degradation. Hence, the objectives of this section of the report are:

- To investigate if elastomers are "fit for service" in shallow well construction applications.
- Determine elastomer performances under downhole corrosive conditions (temperature, pressure, and corrosive gases).

3.2 LITERATURE REVIEW ON ELASTOMER DEGRADATION

Harsh and challenging reservoir environments are driving the need for compatible elastomers. Elastomers are viscoelastic materials which implies that they exhibit both elastic and viscous properties when undergoing deformation. This viscoelastic feature makes them responsive to compressive forces that are critical to their sealing efficiency. Wang et al. (2017) studied the sealing ability of elastomers using pressure-extrusion curves and suggested that elastomers could have four modes of failure. The first is known as the front-end crack, which is initiated in front of the seal, and propagates through the length of the seal. The second failure mode is the local crack, which occurs when a crack forms at the end of the elastomer and cuts the extruded elastomer. The third failure mode exists when the elastomer is not damaged but allows fluid to penetrate through the interface between the elastomer and the wall, causing fluid leakage. The final mode of failure is when the elastomeric seal escapes through the sealing site because of deformation and pressure.

Elastomers require a comprehensive standard set of tests before obtaining approval. These tests are necessary to determine the seal performance at high pressures, wide temperature fluctuations, loading conditions, and exposure to corrosive environments. Despite the wide use of elastomers in many oil field applications, their performance in high pressure high temperature (HPHT) corrosive conditions is not well understood. In HPHT acidic environments, elastomer seals can degrade considerably in a short period of time. In harsh environments, elastomers quickly lose their performance because of thermal degradation and chemical attacks. Selecting a suitable elastomer for an onshore or offshore operation requires evaluation of many inter-dependent elastomer characteristics. It is often a challenge to predict the life of an elastomer seal under a harsh borehole environment, because of the physical and chemical changes that occur in the elastomer. Table 3.1 lists some of the acclaimed properties of typical elastomers used in the oil and gas industry. The ability of an elastomer to seal effectively depends on its physical and mechanical properties in downhole conditions. In most cases, elastomers are required to exhibit excellent performance while retaining their physical properties at high and low temperature conditions respectively. A good description would be the Joule-Thompson effect, which occurs when there is a sudden pressure release in a subsea wellhead and blow out preventer (BOP); thus, leading to rapid changes in temperature (Chen et al. 2016).

In downhole conditions, elastomers are often in a compressed state especially when they are used in liner hanger systems, BOPs, gaskets, and seals. Under these conditions, surrounding gas molecules tend to penetrate the pores of the compressed elastomer. A sudden release of the surrounding gases causes the gas molecules within the pores to expend and escape in what is

known as rapid gas decompression (RGD) or explosive decompression. RGD occurs because of trapped-gas expansion when the shear modulus of an elastomer is low. As shown in Figure 3.1, this phenomenon reduces the sealing integrity of elastomers because they experience harsh blistering and cracking when the expanding surrounding gas energy exceeds the physical strength of the elastomer. Elastomers with high temperature sealing performance and excellent rapid-gas-decompression (RGD) resistance tend to have limited low temperature sealing performance due to their high modulus characteristics (Chen et al. 2016). It is often difficult to identify elastomers that have excellent rapid-gas-decompression resistance and are suitable for both high and low temperatures.

Table 3.1: Some of the properties of typical elastomers used in the oil and gas industry.

Elastomer / Property	NBR	HNBR	Viton® (FKM)	Aflas® (FEPM)	Kalrez® (FFKM)
Max. Temperature (°F)	250	300	400	400	620
Tensile Strength (psi)	200-3500	1500-3500	500-2000	1900	2000
Steam Compatibility	Poor	Fair to Good	Poor	Excellent	Excellent
Brine High Density (Na/CaBR)	Poor	Fair to Good	Excellent	Excellent	Excellent
Brine Low Density (Ca/NaCl)	Excellent	Excellent	Excellent	Excellent	Excellent
Crude Oil. Sour (< 2000 ppm H_2S)	Poor	Excellent	Fair to Good	Excellent	Excellent
Drilling Mud (Diesel Based)	Fair to Good	Excellent	Fair to Good	Fair to Good	Excellent
Hydraulic Fluid, Oil/Water (HFA)	Fair to Good	Excellent	Poor	Excellent	Excellent

Figure 3.1: Some examples of elastomer failure caused by RGD (top row) and overload pressure (bottom row).

Under high-pressure, oil-field elastomers can absorb methane, hydrogen sulfide, and carbon dioxide. Subsequently, they swell and lose their strength, depending on the temperature and duration of exposure. When a sudden pressure reduction occurs, the dissolved gasses expand and bubble out quickly, creating blisters and cracks in the material. Elastomers like HNBR are known for absorbing a high level of hydrogen sulfide, which limits its applicability in the oil and gas industry (Cong et al. 2013).

3.2.1 Experimental Studies

Over the years, aging experiments have gained recognition as one of the commonly used methods for evaluating the behavior and performance of elastomers. These tests are conducted in special autoclaves by exposing test samples to corrosive gases and liquid contaminants. Per Schweitzer (2000), the properties of an elastomer can be destroyed only by chain growth or chain rupture. Some of the contributing agents to elastomer aging are atmospheric ozone and moisture, heat, sunlight, CO_2, H_2S, CH_4, drilling fluids, and brine. These agents are used to evaluate the sealing integrity of elastomers.

3.2.1.1 Elastomer Degradation in H_2S Environment

Exposing an elastomer to sour fluid conditions such as H_2S, at elevated temperatures, will accelerate aging and degradation. Thus, it is imperative to have adequate insight on elastomer degradation when exposed to H_2S. Tynan (2016) conducted a study to investigate temperature and corrosive fluid effects on elastomers by comparing the reactivity of various elastomers to H_2S with their glass transition temperature (T_g) and high temperature performance (as shown in Table 3.2). It was suggested that low temperature and H_2S resistance are two properties that can exist for the same elastomer type. This was like one of the author's previous observations in which an elastomer seal was selected with the combined qualities of high performance at low temperatures, excellent resistance to sour gas (H_2S), and a good amine corrosion inhibitor. Low temperature FFKM elastomer was chosen against FKM because the design allowed for a life of 20+ years, while maintaining a good low temperature resistance. Furthermore, the study recommended FFKM as the most viable option for low temperature and H_2S conditions.

Table 3.2: H_2S resistance of various elastomers, at their respective glass transition and high temperature performance (Tynan 2016).

Elastomer Type	Resistant to H_2S	Glass Transition (T_g) °F	Upper Service Temp. °F
NBR	Most reactive	-22	248
Low Temp. HNBR	Most reactive	-40	320
HNBR	Less reactive	-22	356
FEPM (TFE/P)	Non-reactive	41	482
Low Temp. FKM	Less reactive	-40	437

FKM	Most reactive	1.4	437
Low Temp. FFKM	Non-reactive	-22	464
FFKM	Non-reactive	32	500

Cong et al. (2013) published the experimental results of an aging cell study for HNBR samples in aqueous solutions of H_2S and HCl. The authors used nuclear magnetic resonance, infrared spectroscopy, and X-ray photoelectron to analyze the samples. The H_2S experiment was carried out at 1000±100 psi and 212°F, while the HCl experiment was carried out at 284°F. They observed that exposing HNBR to HCl solution resulted in a slight reduction of tensile strength and ultimate elongation because of the hydrolysis of the C≡N group to —OH or O=C—NH_2. Once exposed to the H_2S solution, all the three parameters (tensile strength, ultimate elongation, and hardness) deteriorated significantly. Given the high reaction activity of H_2S, homolysis and heterolysis are two reactions of H_2S that may take place during elastomer degradation. Heterolysis coverts H_2S into H^+ and HS^-. H^+, causing the acidic hydrolysis of the C≡N group, while HS^- attacks C=O because of its strong nucleophilicity, giving rise to C=S and C—C=S groups (Figure 3.2). During homolysis, H_2S can alter into mercapto radicals of $H^\cdot$ and $HS^\cdot$. $HS^\cdot$ reacts with the macromolecule radicals of the elastomer that forms at high temperatures. It then forms mercapto compounds. These compounds undergo further pyrolysis to form macromolecule radicals which reacts with the mercapto radicals ($HS^\cdot$) in a continuous reaction cycle. This chain of reactions increases the C—S—C bonds. The breakdown of the triple bond in the CN group, to double and single bonds, as shown by these reactions, is responsible for the deteriorating properties of the elastomer. Studies have shown that when exposed to H_2S solution, the structure of HNBR would change because of formation of new chemical compounds.

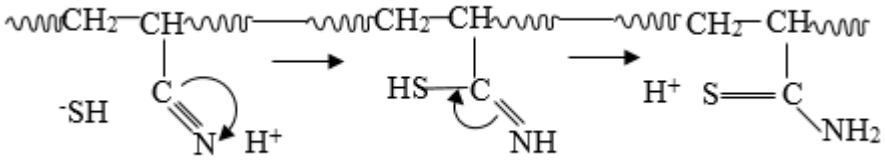

Figure 3.2: Nucleophilic reaction mechanism showing the breakdown of the acrylonitrile group in HNBR (redrawn after Cong et al. 2013).

Fernández and Castaño (2016) studied the elastomeric properties of two NBR's (high and low ACN) using two separate autoclave tests in liquid and gas contaminants respectively. They varied the concentrations of crude oil compositions to obtain three liquid contaminants, while using H_2S and CO_2 as the gas contaminants. In their experiments, the H_2S concentration was increased from 714 ppm to 5000 ppm. A reduction in the elastic properties was observed, causing the elastomers to be less retractable. Tensile strength and elongation at break properties decreased significantly with an increase in H_2S concentration. The SEM images in Figure 3.3 show an increase in the brittle fracture surface with increase in H_2S concentration. The authors concluded that permanent deformation of the elastomer is a function of the H_2S concentration.

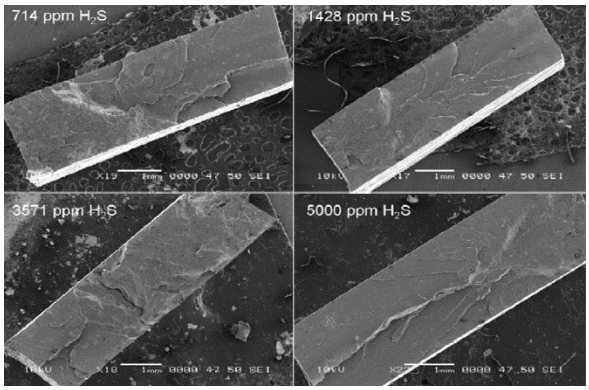

Figure 3.3: SEM images of NBR aged with H_2S (203°F, 168 hrs.) (Fernández and Castaño 2016).

3.2.1.2 Elastomer Degradation in CO_2 Environment

In studying the elastomeric properties of two NBRs (high and low ACN), Fernández and Castaño (2016) recorded an increase in the volumetric swelling and permanent deformation of the elastomers, with increase in CO_2 concentration. The increase in permanent deformation was finite and plateaued at very high concentrations of CO_2. An increase in hardness was recorded for low CO_2 concentration. The SEM image in Figure 3.4 shows a decrease in the brittle fracture surface of the NBR with an increase in CO_2 concentration.

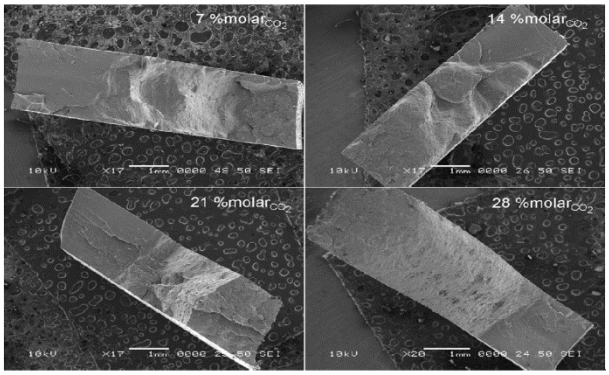

Figure 3.4: SEM images of NBR aged with CO_2 (203°F, 168 hrs.) (Fernández et al. 2016).

Dajiang et al. (2017) characterized NBR and HBNR samples by aging the elastomers in the presence of liquid and gaseous CO_2, under mechanical compression. Their control group samples were compressed in laboratory ambient temperature and pressure. Two separate groups of elastomers were aged in liquid and gaseous CO_2 respectively for 168 hours, at 230°F and CO_2 partial pressure of 145 psi. Compared to the control samples, an increase in elastomer weight was recorded for the aged elastomers. The increase in weight was more pronounced for the elastomers that were aged in liquid CO_2. They also observed that the reduction in elastomer hardness was more severe in the gaseous contaminant, compared to the liquid contaminant. Samples were compressed by 25% of their original height for 24 hours at ambient temperature and left to recover for 30 minutes. The authors recorded compression set results in the range of 9.94% to 17% and 10.33% to 26.02% for NBRs aged in liquid and gaseous CO_2 respectively. They also reported

similar values for the HNBR samples, suggesting that mechanical loading would increase the elastomer's damage in the presence of CO_2.

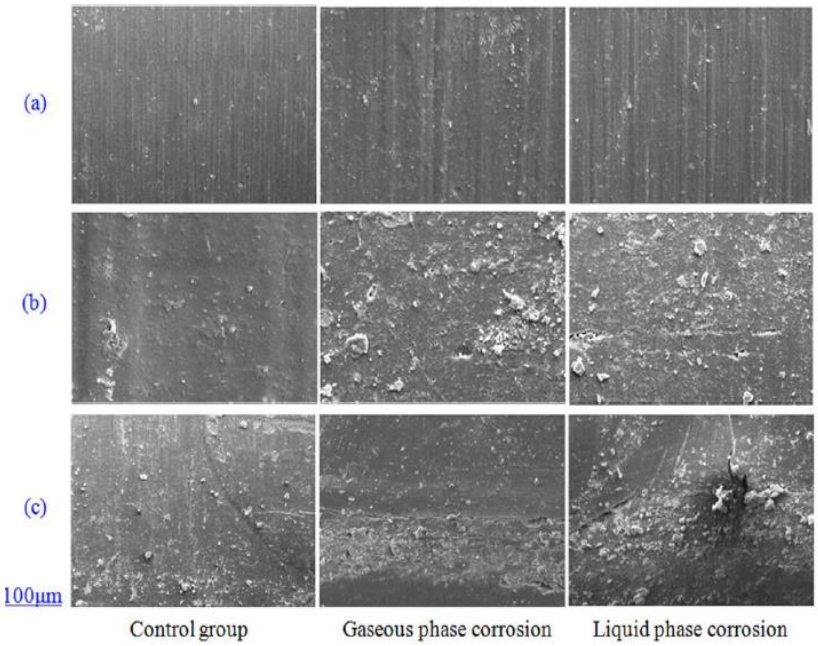

Figure 3.5: SEM image of HNBR after aging at 0lbf (a), 1349lbf (b), and 2698lbf (c) (Dajiang et al. 2017).

In addition, Dajiang et al. (2017) observed slight deformation in the HNBR control group, compared to an obvious swelling and deformation revealed by the aged samples. Figure 3.5 shows HNBR SEM images at various compressional loads. The authors observed holes, fractures, and more damage in the aged HNBR samples. Furthermore, their energy dispersive spectroscopy (EDS) results for the 2698 lbf compressed samples showed a decrease in the weight percent of the main constituent elements (C, O, Si, and Ca). They concluded that the swelling and damage of an elastomer tends to increase with an increase in compressional load in liquid CO_2 corrosion. This appears to be more severe than gaseous CO_2 corrosion.

3.2.1.3 Elastomer Degradation in Other Corrosive Fluids (Crude Oil and Brine)

In addition to corrosive gases, other contaminants such as drilling fluids can deteriorate elastomers. Drilling fluid contamination can impact the behavior and performance of an elastomer. Drilling fluids can alter the physical and chemical properties of elastomers that are used in drilling equipment, severely affecting the equipment's life and function (Bardrak 1994). The degree to which drilling fluid can alter elastomeric properties and/or composition depends on the type of drilling fluid, temperature, pressure, and type of elastomer. For instance, during a drilling operation, positive displacement motors (PDMs) usually experience chunking when the elastomer in the stator has reached its fatigue limit (Guidroz et al. 2011). Kubena et al. (1991) investigated the performance of elastomers that are used in downhole drilling equipment, particularly PDMs. In their study, four elastomers (hydrocarbon, chlorinated, nitrile, and fluorinated elastomers) were contaminated with five non-aqueous fluids (NAF) base liquids (diesel oil, mineral oil, low

aromatic content mineral oil, ester, and glycerol/water mixture). When a PDM is heated above the aniline point (1400°F) of a diesel-base fluid, the aromatic portion of the diesel will penetrate the elastomer compound, causing it to swell. The authors defined the aniline point as the temperature at which a known volume of a clear aromatic compound (aniline) dissolves totally in a specific volume of oil to form a non-cloudy solution. High temperatures tend to accelerate chemical attacks on stator rubbers and reduce its mechanical properties. Previous field studies revealed that PDMs used with mineral/low-toxicity NAF, had twice the service life they would have had, when used with diesel-based NAF. The study concluded that no specific elastomer is best suited for all types of drilling fluids.

Fernández and Castaño (2016) also carried out crude oil tests on elastomers. The tests were conducted at 150°F and 1000psi, for 168 hours. After the crude oil aging, the results from their hardness test revealed no more than 5% change from the original elastomer hardness. A maximum volumetric swelling of 3.1% was recorded. Their compressive set test results showed high permanent deformation values within acceptable limits. A decrease in tensile strength and elongation at break was also recorded. The decrease in tensile strength was more severe with the NBR that was aged in the crude oil, which had the highest percentages of saturates and aromatics.

Other corrosive fluids (such as brine) can potentially influence the performance of an elastomer. Super absorbent polymers (SAP) often swell insufficiently when they are in contact with saline formation water (Bosma et al. 2005). Wang et al. (2015) developed a new water-swellable elastomer that can swell in the presence of high salinity (20+ %) and divalent brines ($CaCl_2$ and $CaBr_2$). They developed these new elastomers by mixing nanocomposite microgels with NBR. Figure 3.6 reveals that the new elastomer showed better swelling ratios compared to SAP (reference 1 and 2) in $CaCl_2$ and $CaBr_2$ at 200°F. A similar performance was observed in the presence of a high level of brine. In addition, other test results revealed that the new elastomer showed better tensile strengths after swelling and enhanced elongation at break properties compared to the current water-swellable elastomers.

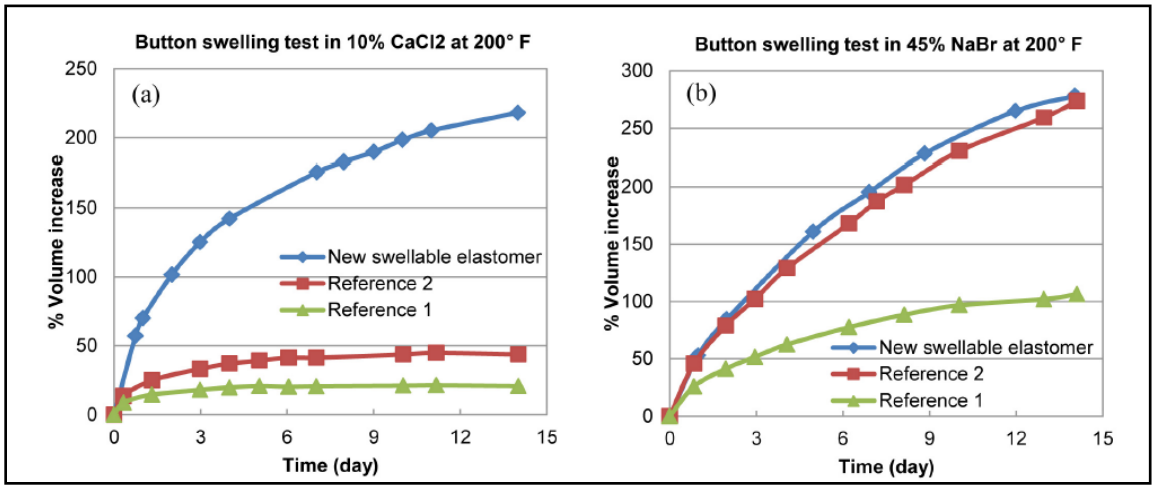

Figure 3.6: Swelling curves of samples of 10% $CaCl_2$ at 200°F (a) 45% NaBr at 200°F (b) (Wang et al. 2015).

Another downhole application of elastomers is in expandable liners and swelling packers. These are used to control oil flow from each lateral to improve total oil recovery. Qamar et al. (2012) conducted longevity tests on a full-scale rig. Table 3.3 shows the test matrix containing packers made from different swelling elastomers, exposed to saline water or crude oil. The tests were conducted at different temperatures and 1000psi. W1 represents low-salinity while W2 and O1 represents high-salinity and oil-swelling elastomers respectively. The authors did not disclose the actual formulation of the elastomers for confidential purposes. However, their results showed that units 1, 2, and 6 failed and did not seal within the first two weeks of the test. Unit 5 sealed then de-sealed after several months of exposure. Unit 7 showed good sealing abilities at lower pressures but failed at a pressure of 1000 psi. Units 3 and 8 had good sealing performance. They concluded that elastomers tend to swell and seal earlier when in contact with low salinity brine at high temperatures, compared to high salinity brine. Additionally, water-swelling elastomers swell and seal faster than oil-swelling elastomers (Qamar et al. 2012; Qamar et al. 2009).

Table 3.3: Experiment design details for the longevity test setup (Qamar et al. 2012).

Unit	Elastomer Type	Swelling Medium	Temperature
	3½-in swell packer inside 7-in casing		
1	W2	12% brine	73°F
2	O1	Crude oil	73°F
3	W2	12% brine	122°F
4	O1	Crude oil	122°F
	4½-in swell packer inside 7-in casing		
5	W2	12% brine	73°F
6	O1	Crude oil	73°F
7	W2	12% brine	122°F
8	W1	0.5% brine	73°F
9	W1	0.5 brine	122°F
	Perspex demonstration unit		
10	W1		73°F

3.2.2 Chemical Changes

When exposed to harsh chemical conditions, elastomers can fail because of changes in their molecular structure. These changes can occur in a continuous reaction cycle depending on the chemical structure of the elastomer. Chemical reactions in elastomers are irreversible due to the

alteration in their molecular structure and the formation of new chemical compounds. The performance of elastomers not only is impacted by their molecular structure, but also by the type and degree of the corrosive conditions. To explain the chemical changes that occur in elastomers, three famous elastomer chemical structures were studied - Acrylonitrile butadiene rubber (NBR), Ethylene propylenediene monomer (EPDM), and Fluoroelastomer (FKM).

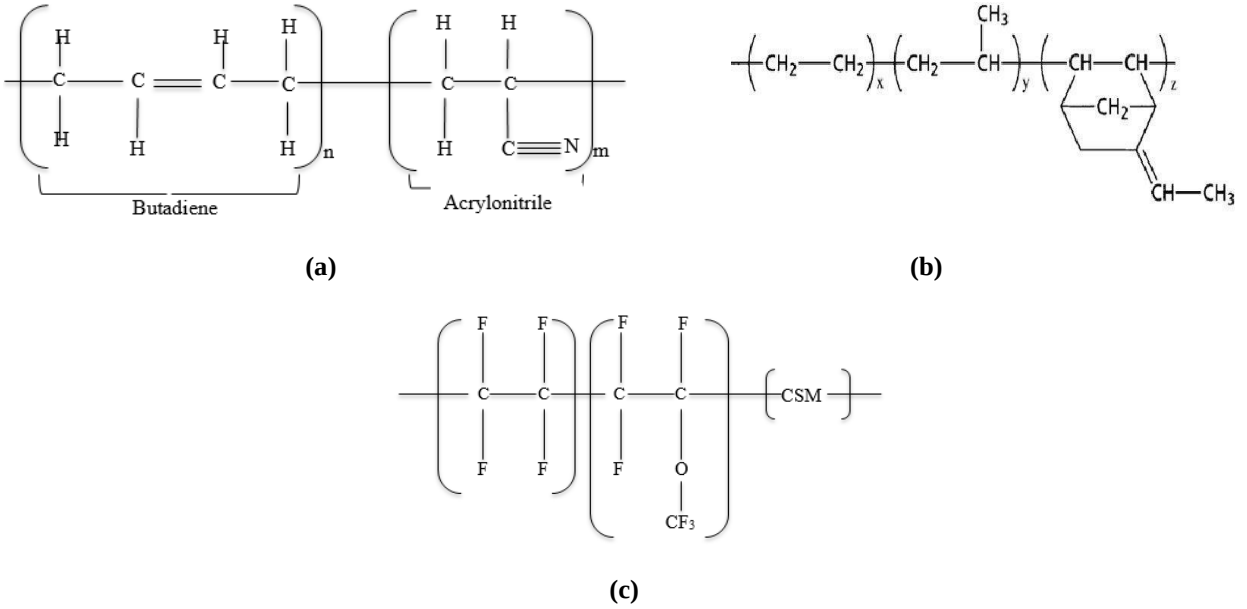

(a) **(b)** **(c)**

Figure 3.7: Chemical structures of: (a) acrylonitrile butadiene rubber (NBR); (b) ethylene propylenediene monomer (EPDM); (c) fluoroelastomer (FKM).

Figure 3.7 shows the repeating terms of the chemical structures (used to explain their chemical degradation) of these elastomers. The NBR structure is made of two parts - Acrylonitrile and Butadiene. The carbon triple bond nitrogen (C≡N) group is what distinguishes NBR from other elastomers. The acrylonitrile content is used to categorize NBR into low, medium, and high. To understand the reaction of elastomers with H_2S, CO_2, and other corrosive media, the concepts of electronegativity and bond dissociation energy should be highlighted. Electronegativity is simply a measure of the tendency of an atom to attract a bonding pair of electrons. Bond dissociation energy is a measure of the strength of an existing chemical bond. It can be well defined as the standard enthalpy change when a bond is cleaved by homolysis, with reactants and products of the homolysis reaction at absolute zero (-459.67 °F). Elastomer degradation under H_2S exposure has been discussed under ***3.2.1.1***.

3.2.2.1 Elastomer Degradation (Chemical Changes) under CO_2 Exposure

CO_2 is a very stable inert gas made up of two carbon-oxygen double bonds (O═C═O). Each of these carbon-oxygen double bonds are very stable; having a bond dissociation energy of 732 kJ/mol. Based on the stability of these bonds, CO_2 has little to no reason to react with any of the elastomers investigated. However, in the presence of brine, CO_2 reacts with water to form a weak

carbonic acid (H_2CO_3). In large quantities, this weak carbonic acid becomes corrosive, and reacts as an acid.

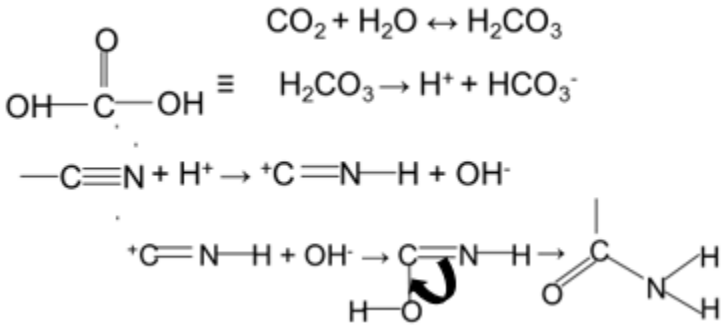

Figure 3.8: Chemical reaction of NBR with CO_2.

Figure 3.8 shows the chemical reaction of CO_2 with brine to form a weak carbonic acid. It also gives detailed reactions of the H^+ with the C≡N group of the NBR elastomer. The C≡N group is made up of two weak pi bonds and one strong sigma bond. The two weak pi bonds contribute to the low bond dissociation energy in C≡N. In addition, carbon and nitrogen are farther from each other on the electronegativity table, making them more susceptible to a chemical reaction compared to the C─H existing in the butadiene section of the NBR. The product of this reaction is an amine group. After this reaction has occurred, the chemical structure of the elastomer has been altered, as such this change is irreversible. In the ethylene propylene diene monomer, the carbon to carbon double bond has a bond dissociation energy of 611 kJ/mol. They are also made up of solely hydrogen and carbon elements, which are two elements close to each other in the electronegativity series. High bond dissociation energy and close electronegativity create a high stability in the EPDM structure. With the FKM, despite the large electronegativity difference between carbon and fluorine, the C─F has a bond dissociation energy of 450 kJ/mol because fluorine is a highly stable halogen. Of all the carbon single bonds on hydrogen, nitrogen, oxygen, and florin, C─F has the largest bond dissociation energy; thus, the stability of FKM.

3.2.2.2 Elastomer Degradation (Chemical Changes) under CH_4 Exposure

The chemical structure of methane in Figure 3.9 shows that it has four single (sigma) carbon-hydrogen bonds. These bonds have a bond dissociation energy of 410 kJ/mol each. Carbon and hydrogen are close elements in the electronegativity series, meaning that they are more stable and less likely to react with any substance until they are burnt in the presence of light or oxygen. This stability causes methane not to react chemically with any of the elastomers investigated.

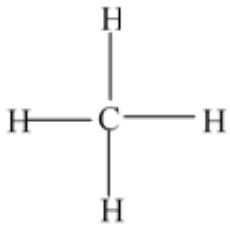

Figure 3.9: Chemical structure of methane.

3.2.3 Physical Changes

Unlike regular metals that have Young's modulus property, the viscoelastic properties of elastomers cause them to have a "modulus", which is the stress at any given strain. Per Schweitzer (2000), the modulus of elastomers is generally measured at a specific elongation (such as at 300% or lower). The stress, strain, and compression changes that occur within an elastomer can change its physical properties. Pressure, temperature, ultra-violet rays, weathering, oxygen, and ozone, amongst others are all factors that can affect the physical structure of an elastomer (Schweitzer 2000). The author claimed that when an elastomer is subjected to such unfavorable conditions, a physical change could occur. The elastomers may shrink or swell then change size again depending on the conditions. Jin et al. (2008) explained that mobility and crosslinking of the elastomer molecular chains (chain growth) causes the elastomer hardness to increase with an increase in temperature (Figure 3.10). Schweitzer (2000) also suggested that during elastomer aging, chain growth will usually decrease elongation, and increase the hardness and tensile strength. The author further explained that chain breakage or chain rupture will have the reverse effect on these properties.

It should be noted that most physical changes are reversible, except for a few. London dispersion forces are temporary attractive forces that arise when the electrons in two adjacent atoms occupy positions that make the atoms form temporary dipoles. They are the weakest intermolecular forces of attraction that exist in long chain polymers or compounds with similar electronegativity. When an elastomer is subjected to physical or non-physical compression after a certain threshold, the London dispersion forces become weak and tend to break. In some cases, when these compression forces are expelled, the elastomer never regains its original shape and size.

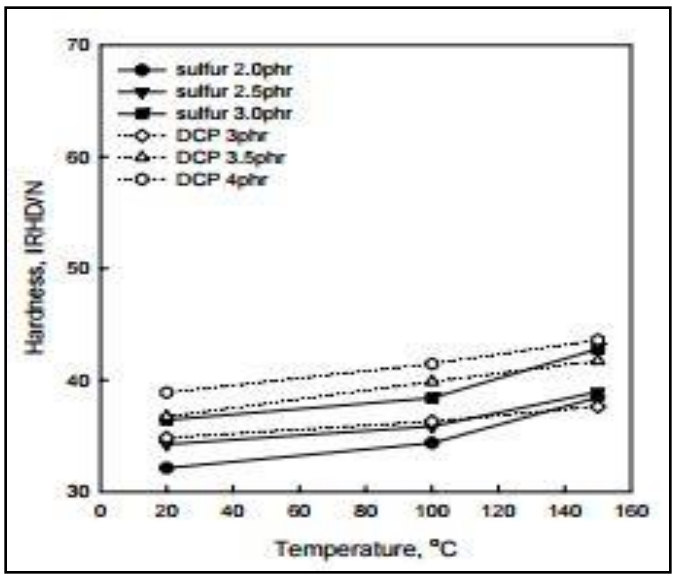

Figure 3.10: Hardness vs. temperature (Jin et al. 2008).

3.3 RESEARCH METHODOLOGY

To achieve the objectives in this section of the report, both theoretical and experiment approaches were considered. A comprehensive literature review has provided a road map for the theoretical and experimental studies of the selected elastomers. Elastomer degradation strongly depends on the elastomer's chemical structure as well as the composition and abundance of the liquid and gaseous phases they are in contact with. In this section of the project, the relationship between elastomer degradation and downhole conditions such as temperature, exposure time, and acid gas variations were studied. The outcome of the theoretical analyses provided useful information in understanding the mechanisms that are involved in the elastomer degradation process.

In addition to the theoretical analyses, experimental investigations were conducted to study the degrading behavior of elastomers in acidic environments. The degree of degradation was measured from the change in intrinsic properties of the elastomer such as hardness, volumetric swelling, and compression. These investigations were used to determine whether the elastomers are “fit for service” for a given set of downhole conditions.

3.3.1 Scope of Work

Elastomers are sensitive to downhole conditions (temperature, pressure, acid gas variations, and acid gas concentration). To perform the tests under simulated wellbore conditions, elastomer-aging experiments were carried out at varying temperatures of 120°F and 180°F. Pressure was kept constant at 1000 psi, with two fluid phases - a vapor and brine phase. For each experiment, the same types of elastomers were used. Half of them were immersed in the brine phase and the other half exposed to the vapor from the brine (vapor phase). The gas variations included: methane (CH_4), hydrogen sulfide (H_2S), and carbon dioxide (CO_2). Some experiments were conducted with 100% CH_4, 100% H_2S (500 ppm) with methane carrier, and 100% CO_2. Subsequent experiments

were conducted with a mixture of the three gases (50% CO_2 and 50% 500ppm H_2S with methane carrier). The aging duration which was used to quantify the effects of time on elastomer degradation was 1 and 7 days. Some experiments were also conducted with an aging duration of 3 days to study the patterns in the changing properties. Four different elastomers (NBR, EPDM, FKM, and PTFE) were considered in the investigation.

To quantify the level of degradation, elastomer properties (hardness, volumetric swelling, and compression) were measured and compared before and after aging. In addition, a Dino-Lite Digital Microscope was used in observing the morphology and blistering of severely damaged elastomers. Two types of elastomer sizes were prepared to carry out the experiments. Cylindrical samples of thickness (height) 0.33-inch and 1-inch were selected based on preliminary tests and results. The 0.33-inch thick elastomer was prepared for compression measurements based on ASTM D575-91, while the 1-inch thick elastomer was prepared for volumetric swelling and hardness measurements. All the elastomers had a constant diameter of 0.75-inch.

3.3.2 Test Materials

Elastomers

Four elastomers were used: NBR, EPDM, FKM, and PTFE. These elastomers were selected because they are widely used in oil and gas applications such as blowout preventers (BOP), packers, liner hangers, heat exchanger gaskets, paper mill rolls, rotary shaft seals, hoses and cable jacketing in hydraulic/pneumatic systems. The behavior of these elastomers was studied when exposed to harsh conditions to determine whether they are “fit for service”.

Brine

Two percent brine was used for the experiments. This is because the salt concentration averages from 14 to 36 ppt in the Gulf of Mexico (LaMourie et al. 2005). This approximates to 2.5% brine concentration. In this study, brine was used as the liquid corrosive medium to provide more information on elastomer degradation in the presence of liquid and vapor media. The presence of brine creates the opportunity to explain why elastomers would degrade differently based on their surrounding medium.

Gases

H_2S, CO_2, and CH_4 were the gases used for conducting the experiments. These gases were selected based on the tasks and deliverables in the project proposal. In addition, they are predominant gases associated with shallow wells in the Gulf of Mexico. Furthermore, these gases are known to be commonly used in elastomer aging experiments, based on the materials and methods from previous studies. The pressure supply for each test was 1000 psi.

3.3.3 Test Matrix

Nine test categories consisting of 288 experimental samples were conducted to examine the effects of temperature, aging, and the presence of H_2S, CO_2, and CH_4 on the degradation of oilfield elastomers. Table 3.4 and Table 3.5 summarizes all test parameters of the experiments. The nine aging tests are distinguished by nine different text-box highlight colors. The yellow text box represents aging test 1 (AT1), peach text box represents aging test 2 (AT2), green text box represents aging test 3 (AT3), and blue text box represents aging test 4 (AT4). Aging test 5 (AT5) was conducted with 100% CH_4. Aging test 6 (AT6) was conducted with 100% CO_2, and aging test 7 (AT7) was conducted with 100% 500ppm H_2S with methane carrier. Aging test 8 (AT8) is represented by the purple text box, while aging test 9 (AT9) is represented by the red text box. There are five independent variables: 1) Type of elastomer: NBR, EPDM, FKM, and PTFE, 2) Aging period: one and seven days, 3) Liquid contaminant: brine phase and vapor phase, 4) Sample length: 0.33-inches and 1-inch, 5) Temperature: 120°F and 180°F. Each test sample is given a unique nomenclature, which is discussed in **3.3.5**.

Table 3.4: Test parameters for aging experiments conducted for one and three days.

Age (Days)	Phase	Length	T1 (120°F)	T3 (180°F)	Age/Phase	T8 (120°F)	T9 (180°F)
One	Vapor Phase	L1 (0.33-in)	N1V1T1	N1V1T2	Three Days/Vapor Phase	N3V1T1	N3V1T2
		L1 (0.33-in)	E1V1T1	E1V1T2		E3V1T1	E3V1T2
		L1 (0.33-in)	V1V1T1	V1V1T2		V3V1T1	V3V1T2
		L1 (0.33-in)	P1V1T1	P1VIT2		P3V1T1	P3VIT2
		L2 (1.0-in)	N1V2T1	N1V2T2		N3V2T1	N3V2T2
		L2 (1.0-in)	E1V2T1	E1V2T2		E3V2T1	E3V2T2
		L2 (1.0-in)	V1V2T1	V1V2T2		V3V2T1	V3V2T2
		L2 (1.0-in)	P1V2T1	P1V2T2		P3V2T1	P3V2T2
	Brine Phase	L1 (0.33-in)	N1B1T1	N1B1T2	Three Days/Brine Phase	N3B1T1	N3B1T2
		L1 (0.33-in)	E1B1T1	E1B1T2		E3B1T1	E3B1T2
		L1 (0.33-in)	V1B1T1	V1B1T2		V3B1T1	V3B1T2
		L1 (0.33-in)	P1B1T1	P1BIT2		P3B1T1	P3BIT2
		L2 (1.0-in)	N1B2T1	N1B2T2		N3B2T1	N3B2T2
		L2 (1.0-in)	E1B2T1	E1B2T2		E3B2T1	E3B2T2
		L2 (1.0-in)	V1B2T1	V1B2T2		V3B2T1	V3B2T2
		L2 (1.0-in)	P1B2T1	P1B2T2		P3B2T1	P3B2T2

Table 3.5: Test parameters for aging experiments conducted for seven days.

Age (Days)	Phase	Length	T2 (120°F)	T4 (180°F)	T 5 (100% CH_4 @120 °F)	T 6 (100% CO_2 @120 °F)	T 7 (100% H_2S @120 °F)
Seven	Vapor Phase	L1 (0.33-in)	N7V1T1	N7V1T2	N7V1T1M	N7V1T1C	N7V1T1H
		L1 (0.33-in)	E7V1T1	E7V1T2	E7V1T1M	E7V1T1C	E7V1T1H
		L1 (0.33-in)	V7V1T1	V7V1T2	V7V1T1M	V7V1T1C	V7V1T1H
		L1 (0.33-in)	P7V1T1	P7V1T2	P7V1T1M	P7V1T1C	P7V1T1H
		L2 (1.0-in)	N7V2T1	N7V2T2	N7V2T1M	N7V2T1C	N7V2T1H
		L2 (1.0-in)	E7V2T1	E7V2T2	E7V2T1M	E7V2T1C	E7V2T1H
		L2 (1.0-in)	V7V2T1	V7V2T2	V7V2T1M	V7V2T1C	V7V2T1H
		L2 (1.0-in)	P7V2T1	P7V2T2	P7V2T1M	P7V2T1C	P7V2T1H
	Brine Phase	L1 (0.33-in)	N7B1T1	N7B1T2	N7B1T1M	N7B1T1C	N7B1T1H
		L1 (0.33-in)	E7B1T1	E7B1T2	E7B1T1M	E7B1T1C	E7B1T1H
		L1 (0.33-in)	V7B1T1	V7B1T2	V7B1T1M	V7B1T1C	V7B1T1H
		L1 (0.33-in)	P7B1T1	P7B1T2	P7B1T1M	P7B1T1C	P7B1T1H
		L2 (1.0-in)	N7B2T1	N7B2T2	N7B2T1M	N7B2T1C	N7B2T1H
		L2 (1.0-in)	E7B2T1	E7B2T2	E7B2T1M	E7B2T1C	E7B2T1H
		L2 (1.0-in)	V7B2T1	V7B2T2	V7B2T1M	V7B2T1C	V7B2T1H
		L2 (1.0-in)	P7B2T1	P7B2T2	P7B2T1M	P7B2T1C	P7B2T1H

3.3.4 Elastomer Properties Testing Equipment's and Protocols

Degradation of elastomers can significantly change its properties and performance. To assess the extent of elastomer degradation after exposure to an acidic environment, different tests were conducted to measure the changes in their physical properties. Measurements included: hardness, volumetric swelling, and compression.

3.3.4.1 Hardness

To measure the hardness of the elastomer, each elastomer was placed on a firm, flat surface. The hardness readings are taken with a Shore 'A' durometer (Figure 3.11). Shore A durometer measures how much a material indents when a standardized amount of pressure is applied. The indentation hardness is inversely related to the indenter's penetration and is dependent on the material's viscoelastic behavior and elastic modulus (PennCoat Inc. 2014).

The durometer is tuned to zero before using it for any reading. The needle at the bottom of the durometer is pressed onto the surface of the elastomer until the round bottom part of the durometer touches the elastomer surface. The durometer reading decreases gradually and is observed until a constant value is reached for three to five seconds. This reading is recorded and documented. The hardness is measured on two different spots on one flat surface and repeated at two other different spots on the second flat surface. The average of these four readings is then

taken to be a representation of the hardness of the elastomer sample. After each aging test, the hardness measurement is conducted immediately after removing the elastomer samples from the aging cell. The same procedure is followed. Table 3.6 shows the hardness measurements.

Table 3.6: Durometer readings for three days aging test.

Sample	Before					After				
	Duro 1	Duro 2	Duro 3	Duro 4	Avg. Duro	Duro 1	Duro 2	Duro 3	Duro 4	Avg. Duro
T1	76.2	75.5	76.1	75.8	**75.9**	67.5	67.9	69.1	69.6	**68.5**
T2	76.5	76.1	75.3	75.5	**75.9**	69	68.7	68	68.8	**68.6**
T3	75.8	75.3	76.4	76	**75.9**	68.7	68.1	68.4	68.6	**68.5**
T4	76	74.8	76.2	75.4	**75.6**	68.6	67.3	67.3	69.5	**68.2**
T5	75.6	75.8	75.1	76.2	**75.7**	68.5	68.2	69	69.2	**68.7**
T6	76.5	75.2	75.5	76	**75.8**	68.3	69.6	67.7	69.2	**68.7**

Figure 3.11: Digital Durometer Model DD-4.

3.3.4.2 Volumetric Swelling

The diameter and length of each elastomer sample are measured before and after the aging test. A Vernier caliper (Figure 3.12) is used in taking the readings. Before aging, one diameter reading is taken and recorded. After aging, three diameter readings are taken for each sample. The first reading is obtained from the point where the elastomer sample reveals the most diameter swelling. This will be the midpoint for most samples, except a few. The second and third readings are obtained from the edges of the sample. They may vary but are usually the same. The average of

these three readings represents the diameter reading of the sample after aging. All readings are taken immediately after removing the elastomer from the aging cell. Table 3.7 shows the diameter and length measurements.

Table 3.7: Diameter and length readings for three days test.

Sample	Before			After					
	Length	Diameter	Volume	Length	Dia. M	Dia. E1	Dia. E2	Avg. Dia.	Volume
T1	0.515	0.759	0.233	0.59	0.886	0.875	0.874	0.878	0.358
T2	1.033	0.759	0.467	1.167	0.883	0.874	0.874	0.877	0.705
T3	1.504	0.759	0.681	1.7	0.875	0.876	0.876	0.876	1.024
T4	0.505	0.759	0.229	0.571	0.89	0.875	0.877	0.881	0.348
T5	0.985	0.759	0.446	1.128	0.885	0.879	0.879	0.881	0.688
T6	1.503	0.759	0.68	1.719	0.88	0.8766	0.875	0.877	1.039

Figure 3.12: Digital Vernier Caliper.

3.3.4.3 Compression Test

The compression test was conducted using the compression machine in Figure 3.13, before and immediately after each aging test. The ASTM D 575-91 specimen standard was followed, and the ratio of specimen diameter to thickness (2.3) was kept constant. To maintain this ratio, the specimen diameter was maintained at 0.75 inches, while the specimen thickness was 0.33 inches. "Test Method B - Compression Test at Specified Force" in ASTM D575-91 was the compression test procedure followed. A specified minor mass is applied for a period long enough to adjust the deflection gauge. After this, major forces (15lbf, 30lbf, 45lbf, 60lbf, 75lbf, 90lbf) are applied for three seconds. The deflection on the dial gauge at the end of the three-second period is read. This reading does not include any deflection caused by the minor force. The percent deflection or strain based on the extension and original thickness of the specimen is calculated. The stress based on the applied force and area of the elastomer sample is also calculated. The median of the values taken from three specimens of one elastomer type or aging condition is reported. The six major forces were selected based on preliminary tests conducted and the limitations of the machine. Table 3.8 shows an example of compression test values.

Figure 3.13: Compression machine setup.

Table 3.8: Stress vs. strain relationship of NBR before and after three days aging.

NBR 1						NBR 1 After (Vapor)		
Force (Lb)	Area (in^2)	Exten. (in)	Length (in)	Stress (psi)	Strain	Exten. (in)	Length (in)	Strain
15	1.692	0.038	0.34	8.87	0.112	0.035	0.339	0.103
30	1.692	0.047	0.34	17.73	0.138	0.045	0.339	0.133
45	1.692	0.051	0.34	36.6	0.15	0.06	0.339	0.177
60	1.692	0.06	0.34	35.46	0.176	0.067	0.339	0.198
75	1.692	0.066	0.34	44.33	0.194	0.076	0.339	0.225
90	1.692	0.074	0.34	53.19	0.218	0.085	0.339	0.251

3.3.5 Elastomer Sample Preparation

Elastomer samples were cut into the appropriate sizes (0.33-inch and 1-inch length) from 10 feet elastomer rods. Sample sizes are kept with a 15% margin of error before they are accepted to be used for any test. All measurements including hardness, compression, diameter, length, and weight are taken and recorded in a Microsoft excel file. The sample nomenclature or sample identification code follows the independent variable listing in the order from 1 to 5 found in section **3.3.3.** (Test Matrix). Table 3.9 describes the nomenclature used in identifying the samples.

Table 3.9: Nomenclature of elastomer sample.

N1V1T1				
N	**1**	**V**	**1**	**T1**
NBR sample	1-day aging period	Vapor phase contaminant	First sample length	First temperature

This nomenclature is written on each test sample bottle, after which the elastomer sample is placed in its corresponding sample bottle. For each elastomer aging test, a total of 32 samples were prepared and grouped into their sections (4), based on their type. Upon completion, the elastomers were ready to be moved to the autoclave for testing.

3.3.6 Elastomer Aging Experiment

3.3.6.1 Experimental Setup

To simulate elastomer aging under corrosive downhole conditions, a test setup was developed. The schematic of the setup is shown in Figure 3.14. The setup consists of four components. The first is an aging cell with a 3-liter capacity. The second component comprises of three gas cylinders filled with test gases (CO_2, CH_4, and H_2S with CH_4 carrier). The third component is a gas injection cylinder (250 ml capacity) for accurate control of the composition of the gas inlet to the aging cell. Finally, there are measuring instruments and a data acquisition (DAQ) system. The cylinder is separated into two chambers via an injection cylinder equipped with a floating piston. The upper chamber of the cylinder is connected to an oil pump and reservoir, while the lower chamber is used to meter and inject the gas phase into the aging cell. The hydraulic oil flows back to the oil reservoir when the lower chamber is refilled with gas coming from one of the test gas cylinders. The piston location is determined from the liquid-level measured in the oil tank. During the aging test, elastomer samples were placed in the cell using round multilayer-racked shelves. The cell is partially filled with brine and the elastomers to be exposed to the liquid phase are immersed in the brine. The cell lid is put in place and the gas inlet line is connected. Gas injection begins by opening the valve between the injection cylinder and aging cell. Gas is injected into the cell repeatedly (in a selected sequence) until the cell pressure (P2) reaches the desired value.

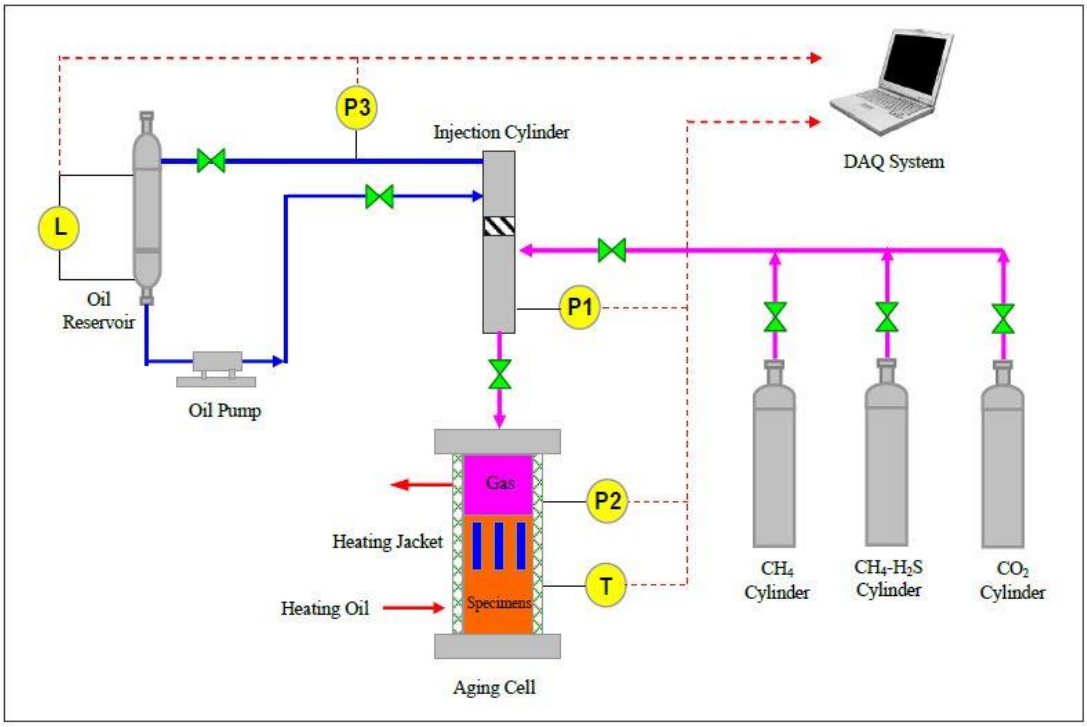

Figure 3.14: Schematic of autoclave cell setup.

3.3.6.2 Test Procedure

Figure 3.15 (a) and Figure 3.15 (b) shows the arrangement of the elastomers before and after lowering the elastomers in the autoclave cell respectively. Table 3.10 shows the elastomer type and their arrangements in the shelves. The autoclave cell is equipped with a sample racking system that has 12 shelves, out of which the bottom two shelves are kept empty during aging experiments. The full length (inside) of the aging cell is 30-in. Prior to lowering the rack, the cell is filled with a 2% NaCl (by weight) solution up to 15-in. The samples are arranged on the racking system, 4 samples per shelf as shown in Figure 3.15 (a), and then lowered carefully into the cell. As shown in Figure 3.15 (b), 16 samples were completely immersed in the brine, while the remaining 16 were exposed to any vapor from the brine phase. The remaining 15-in space in the autoclave was to all gas entrance. The autoclave was sealed and heated to the desired temperature by circulating heating oil through the heating jacket. During temperature ramp-ups, the autoclave cell was flushed twice with nitrogen, 15 minutes for each flush. The goal of the nitrogen flush is to remove any trapped air within the system. When the autoclave temperature reaches the selected test matrix temperature, the gas injection was initiated. The gas compositions are: 50% CO_2 and 50% H_2S with a CH_4 carrier. The combined target pressure is 1000psi. First, the CO_2 is injected up to 500psi, followed by the H_2S with CH_4 carrier until 1000 psi is achieved.

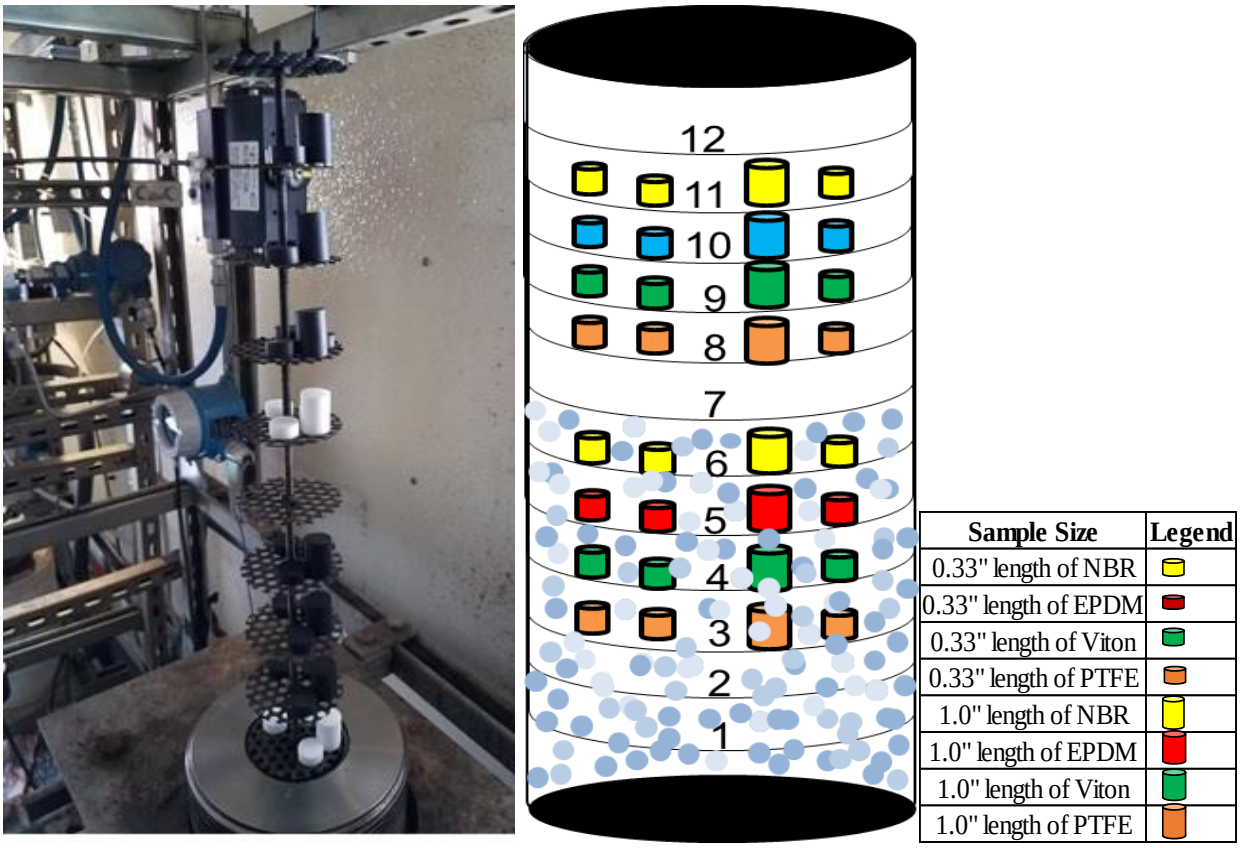

(a) **(b)**

Figure 3.15: (a) Samples arranged in different shelves before lowering into the aging cell. (b)Schematic of sample arrangement inside the aging cell with legend. Shelves 1 to 6 are submersed inside brine, while shelves 7 to 12 are not, but still exposed to vapor from the brine.

Table 3.10: Elastomer arrangement in autoclave shelves

Shelf	Sample
12	Empty
11	NBR in vapor phase
10	EPDM in vapor phase
9	Viton in vapor phase
8	PTFE in vapor phase
7	Empty
6	NBR in brine phase
5	EPDM in brine phase
4	Viton in brine phase
3	PTFE in brine phase
2	Empty
1	Empty

3.4 RESULTS

This section summarizes the results from the experiments conducted during the project. The results comprise of all the useful data collected during the elastomer aging studies. It shows elastomer degradation in terms of change in the performance of three indications: hardness, compression, and volumetric swelling. The parameters varied include: days (1, 3, and 7 days), temperature (120 °F and 180 °F), and corrosive gases (CO_2, H_2S, and CH_4).

3.4.1 Performance of Elastomers

An elastomer's performance in oil and gas wells is determined by its sealing integrity. Elastomer seals are essential for zonal isolation in both vertical and deviated wells. The ability of an elastomer to perform this function is determined by its hardness, volumetric swelling, and compression.

3.4.1.1 Hardness

Elastomer hardness is defined as the resistance of an elastomer surface to indentation by a Shore A durometer. Adequate knowledge of elastomer hardness is important because O-rings made of harder materials may be required for sealing very high-pressure fluids in oil and gas wells. In addition, when sealing delicate objects - like thin plastics - an elastomer made of a softer material is desired. In this study, the hardness of the elastomers was measured and reported as highlighted in ***3.3.4.1.***

Effects of Days

A general observation is that after one, three, and seven days, elastomer hardness tends to drop from its original value. This observation was consistent for the two temperatures (120^{o}F and 180^{o}F). This is because of exposure to temperature, pressure, and corrosive gas conditions. However, from one to three days and from three to seven days, there is a general increase in hardness irrespective of the temperature. This happens because of chain growth or cross-linkage. Jin et al. (2008) showed that elastomer hardness tends to increase with temperature. However, from the experiments performed in this project, it was discovered that if the temperature is kept constant, but the time of exposure is increased, this could compensate for a slow but steady increase in temperature within the elastomer. Thus, resulting to more cross linking and chain growth. This conclusion was drawn because an increase in exposure time of an elastomer to high temperatures, leads to more chain growth within the elastomer. With an increase in chain growth, there is an increase in elastomer hardness and tensile strength.

At 120°F (Figure 3.16a), the decrease in elastomer hardness is greater than 5% and up to 15% from the original hardness. This behavior was not observed in all PTFE (both brine and vapor phase) and all Viton (FKM) in the brine phase. At 180°F (Figure 3.16b), there was a 5% to 10% decrease from original hardness, excluding PTFE (brine and vapor). In addition, the 7-day samples of NBR, EPDM, and Viton aged in brine did not follow this general observation.

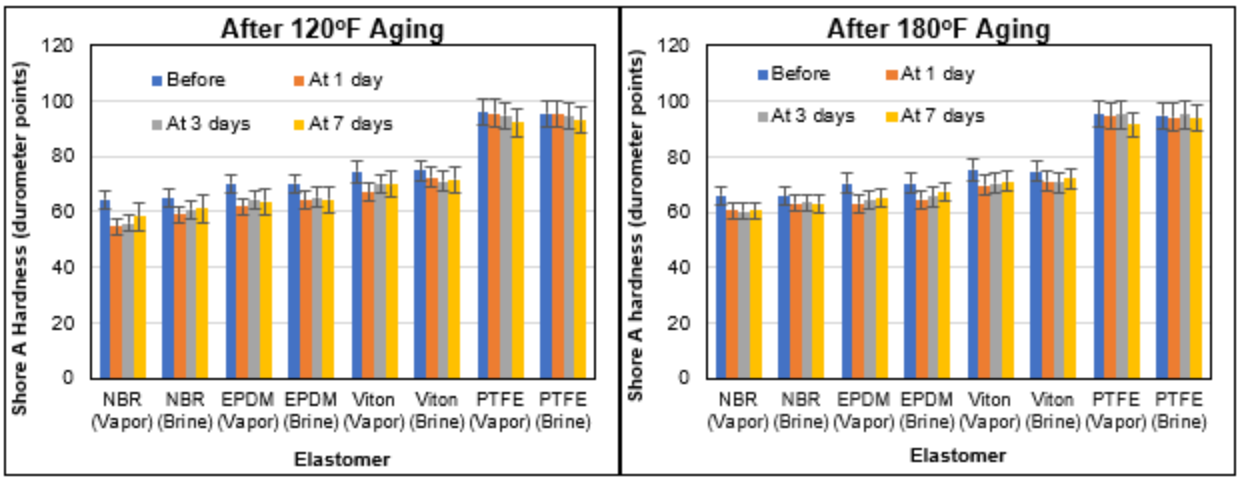

(a) (b)

Figure 3.16: Effects of days on hardness of elastomer samples aged at 1000 psi, and at (a) 120°F, (b) 180°F.

Effects of Temperature

An increase in temperature concurrently increases an elastomer's hardness. The initial exposure of the elastomer to aging conditions (temperature, pressure, and corrosive gas conditions) causes it to soften. Keeping all other conditions in an aging test (1 day or 7 days) constant and altering the temperature from 120°F to 180°F, results in an increase in hardness. This is because of chain growth or cross-linking of the polymer chains within the elastomer.

Figure 3.17 (a) shows 1-day aging for 50% CO_2 and 50% H_2S with a CH_4 carrier. A decrease of more than 5% and up to 15% from the original hardness is observed. This excludes all the PTFE's (vapor and brine phase) and Viton's in the brine phase. A slight increase in hardness is observed when shifting from 120°F to 180°F. After a 7-day test at the same aging conditions (Figure 3.17 (b)), a decrease of more than 5% and up to 10% from the original hardness is was recorded. In addition, a slight increase in hardness was observed with an increase in temperature. In the three-day test (Figure 3.18), the results were like those from the 1 and 7-day tests. Both Figure 3.17 and Figure 3.18 show that the reduction in elastomer hardness was more severe in the vapor phase (gaseous contaminant) compared to the brine phase (liquid contaminant). This observation is supported by the study carried out by Dajiang et al. (2017). One way to quantity the significance of the variables is by performing hypothesis tests using analysis of variance (ANOVA).

ANOVA is a statistical tool that is used in analyzing experimental data. It is a collection of statistical models developed by Ronald Fisher, and used to analyze the variances among group means and their associated procedures (Fisher 1966). This is done to compare the means between groups and determine whether any of these means are significantly different from others. Using a 95% confidence interval ANOVA, age, temperature, and fluid medium variation (vapor or brine phase) significantly affect elastomer aging.

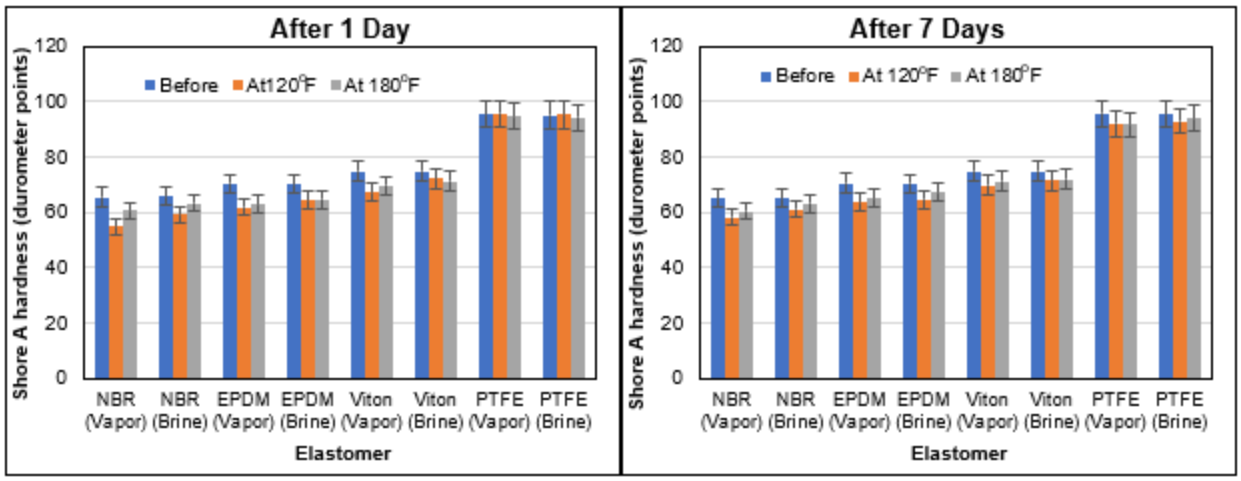

(a) (b)

Figure 3.17: Effects of temperature on hardness of elastomer samples aged at 1000 psi, and after (a) 1 day, (b) 7 days.

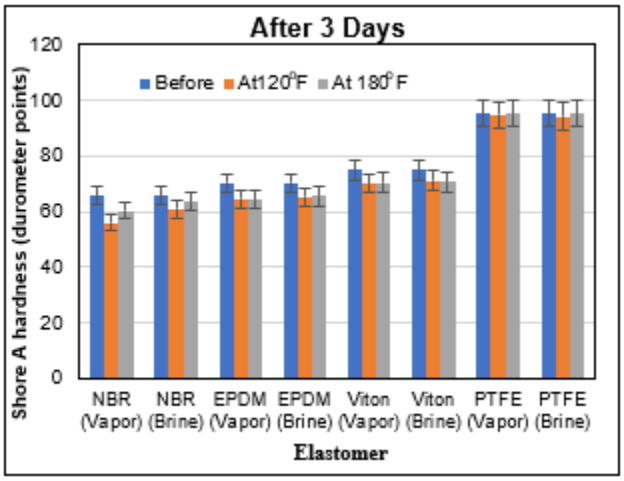

Figure 3.18: Effects of temperature on hardness of elastomer samples aged at 1000 psi, and after 3 days.

In actual downhole conditions, it is impractical to keep all factors affecting aging constant while varying one at a time. Each of these factors are constantly varying. Thus, the interaction effect is used to investigate the effect varying one factor while keeping others constant. In practice, an interaction effect exists when the effect of one factor on the response varies across the levels of another factor. For example, when the effect of days on hardness varies across the various levels of temperature. From the ANOVA, a combination of the effect of days and fluid medium variation presented an insignificant variation for NBR and EPDM. However, there is a significant change in hardness between the Viton in the vapor phase and brine phase, from one to seven days. When fluid medium variation and temperature are combined, the effect was also insignificant for NBR and EPDM. Viton showed a significant change in hardness with fluid contaminant and temperature interaction. The results showed that the Viton samples immersed in brine had an average drop in

hardness of about 3.2 durometer points, while those in the vapor phase dropped by 6.2 durometer points. This implies that the 3.0 durometer points difference is statistically significant. However, Viton does not exhibit a significant change in hardness with aging period and temperature interaction. This is because of its toughness and resistance to temperature. A combination of all the three parameters (days, fluid medium variation, and temperature) has an insignificant effect in elastomer aging. It can be inferred that with respect to the hardness of elastomers under corrosive downhole conditions; the time of exposure and the temperature downhole would affect the sealing integrity of the elastomer significantly.

Effects of Gas Variation

For the CO_2 and CH_4 tests, 100% of each of the gases were exposed to the elastomers. For the H_2S test, 0.05% H_2S in CH_4 carrier was exposed to the elastomers. High bond dissociation energy (410 kJ/mol) and close electronegativity values of carbon and hydrogen in the electronegativity series causes CH_4 to have little to no effect on the aging of elastomers. From Figure 3.19, CH_4 causes less than 5% decrease in hardness from the original hardness in all the elastomers. This decrease is attributed to physical changes in the elastomer under exposed corrosive conditions. More than 5% and up to 15.6% decrease from original hardness is observed when the elastomers were exposed to CO_2. Figure 3.19 also shows approximately 5% decrease from original hardness in NBR and EPDM when exposed to H_2S. However, it is to be noted that a conspicuous change was not observed in the subsequent elastomer samples. This is because of the low H_2S concentration (500 ppm or 0.05%) compared to previous studies, with little to no reactivity of the CH_4 carrier gas on the elastomers. A combined effect of CO_2, H_2S, and CH_4 showed more than 5% and up to 9.6% reduction from original hardness. In conclusion, gas degradation on elastomers hardness is in the order of CO_2>All gases>H_2S>CH_4.

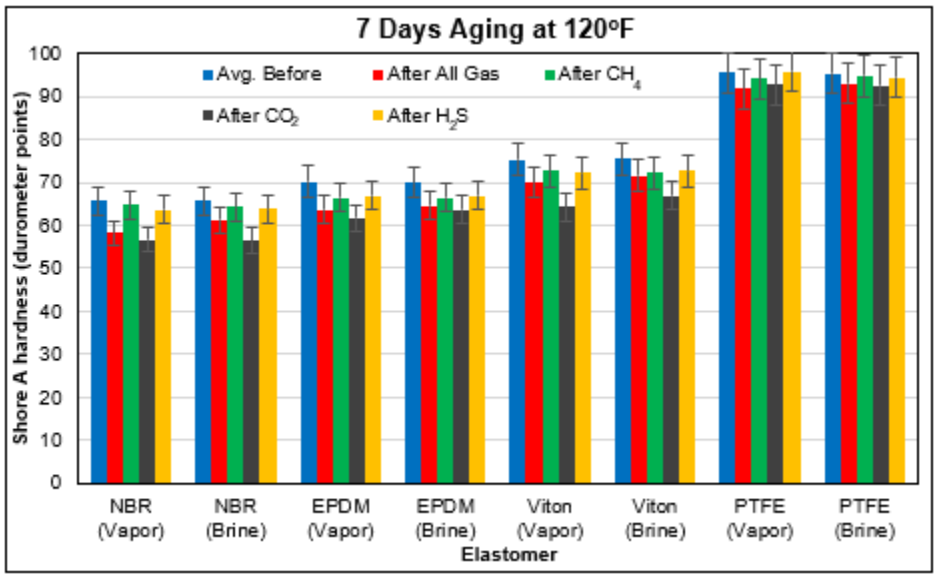

Figure 3.19: Effects of gas variation on hardness of elastomer samples aged at 1000 psi after 7 days.

3.4.1.2 Compression

The compression tests (compressive stress-strain) conducted was to measure the strain of the elastomers at a given compressive stress (psi). The procedure has been highlighted in ***3.3.4.3.*** The goal is to observe the deformation (strain change) due to aging of the elastomer. This knowledge is important to well sealing integrity because an elastomer in a compressed state under downhole conditions begins to alter its compression abilities, which can lead to leakage paths created between the elastomer and the contact surface. This will compromise the sealing integrity of the elastomer and allow fluid migration.

Effects of Days

According to Schweitzer (2000), an elastomer chain rupture reverses the effects of cross-linkage or polymer chain growth. This implies that when an elastomer chain ruptures, the elastomer decreases in hardness and tensile strength. Chain rupture also increases elastomer elongation. For the same stress applied on the elastomers before and after aging, Figure 3.20 shows an increase in strain from original values. The increase in strain was recorded for all the elastomers (NBR, EPDM, and FKM) except PTFE. This is because PTFE is a thermoset plastic and thus resistant to heat. PTFE had consistent strain before and after aging, irrespective of the aging conditions (Figure 3.21). A closer look at the graphs show that 120°F has the most strain change among the four plots in Figure 3.20. Comparing (a) with (b) and (c) with (d), it is observed that for the same temperature, an increase in the aging period causes less strain. This is because extended exposure of an elastomer to the same temperature causes chain growth to occur.

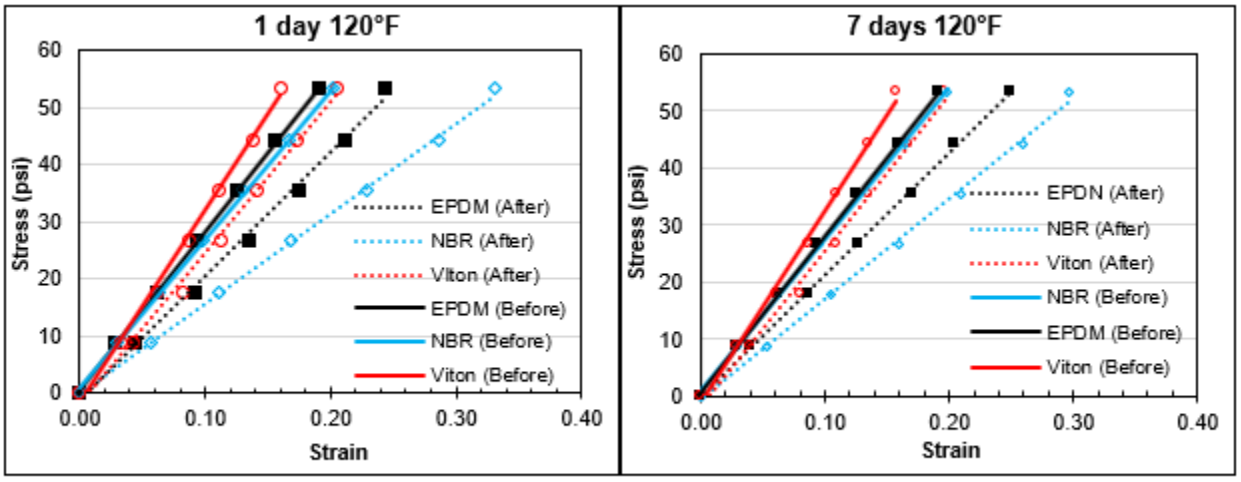

(a) (b)

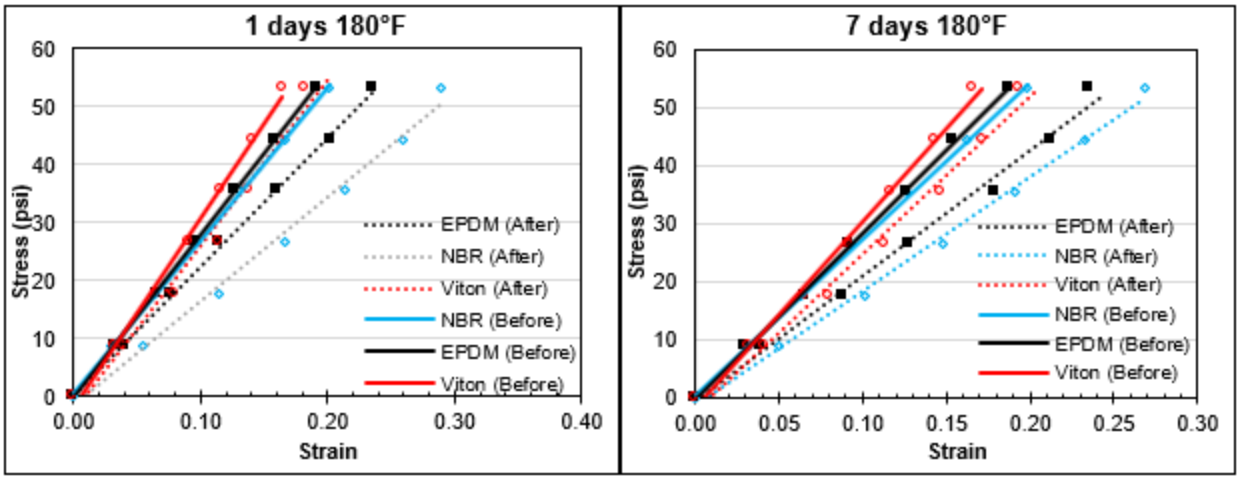

(c) (d)

Figure 3.20: Elastomer compression measurement at: 120°F (a) after 1 day, (b) after 7 days, and 180°F (c) 1 day, (d) 7 days.

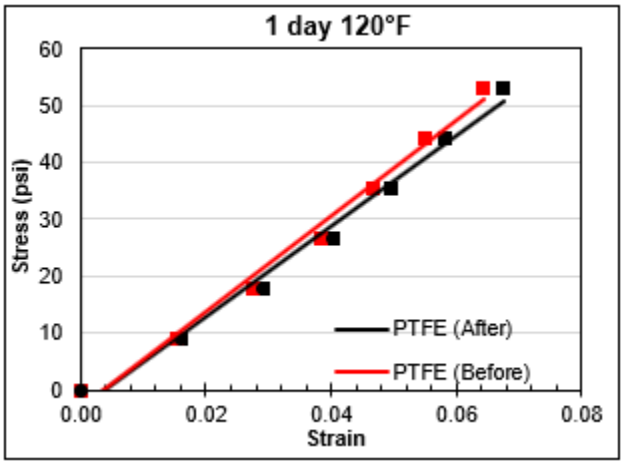

Figure 3.21: PTFE compression measurement at after 1 day at 120°F.

Effects of Temperature

Figure 3.22 shows the results for 3 days aging and the temperature from 120°F to 180°F. The increase in temperature causes a decrease in strain for the same number of days. These changes are because of polymer chain growth within the elastomers at higher temperatures. Chain growth decreases the elongation of the elastomer, which makes it stiffer and allows for less strain to occur when compressed.

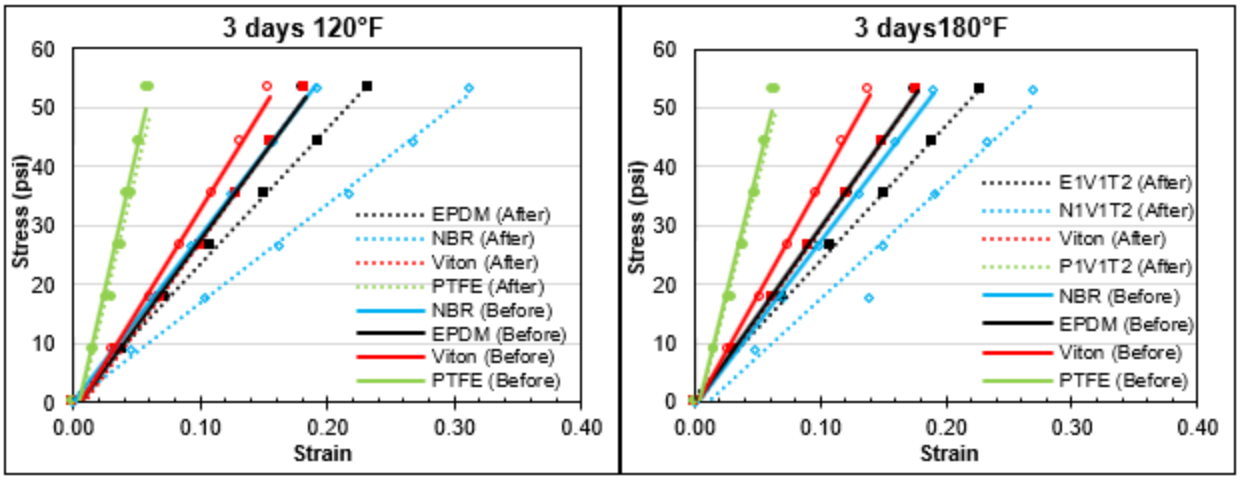

(a) (b)

Figure 3.22: Effects of temperature on compression of elastomer samples after 3 days aging at 1000 psi, and at (a) 120°F, (b) 180°F

3.4.1.3 Compression at Maximum Stress of 53.2 psi

To understand the effect of aging on the compression of elastomers, the maximum stress (53.2 psi) from the compression machine was selected, and its behavior on each elastomer was investigated.

Effects of Days

At 120 °F, for both 1 and 7-day tests, there was an increase in strain at 53.2 psi applied stress. This increase was more than 5% and up to 39% from original strain (Figure 3.23b). This observation does not include all PTFEs (vapor and brine phases). The initial rise in strain, irrespective of the aging period, is due to an increase in elastomer elongation. Moving from 1 to 7 days, extended exposure of the elastomer samples to corrosive conditions causes chain growth, thereby increasing the hardness of the elastomer and decreasing its strain deviation.

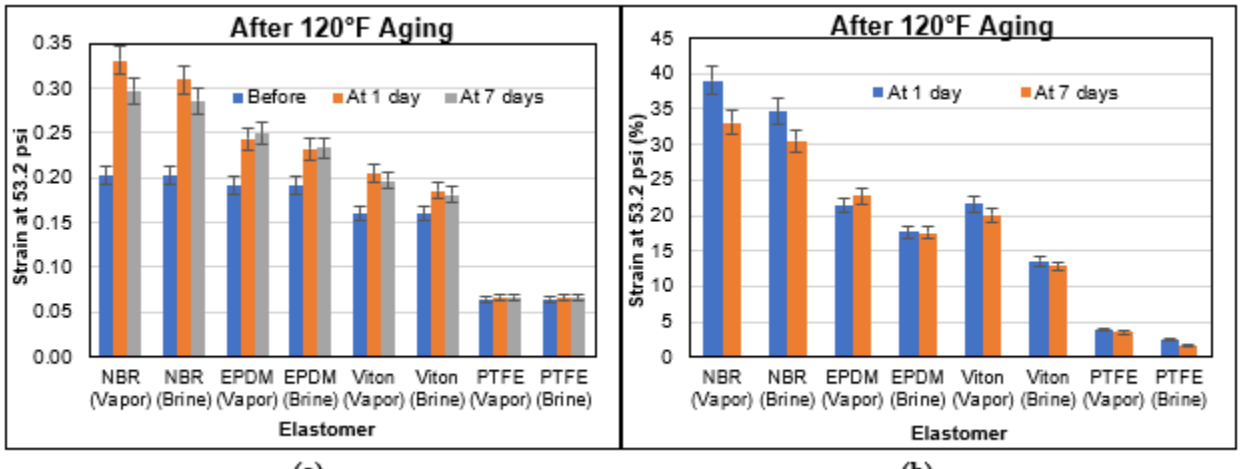

(a) (b)

Figure 3.23: Effects of days on compression of elastomer samples aged at 1000 psi and 120 °F (a) actual strain values, (b) percentage increase in strain values.

After aging at 180°F, for both 1 and 7-day tests (Figure 3.24), there was an increase in strain at 53.2 psi. This increase was more than 5% and up to 30% from the original strain, except all PTFEs (vapor and brine phases). The initial rise in compression is due to increase in elastomer elongation. Increase in the number of days causes chain growth, which increases the hardness of the elastomer and decreases its strain deviation. The maximum increase in strain at 120°F was 39%, while the maximum increase in strain at 180°F was recorded as 30%. This observation is explained further in the succeeding section.

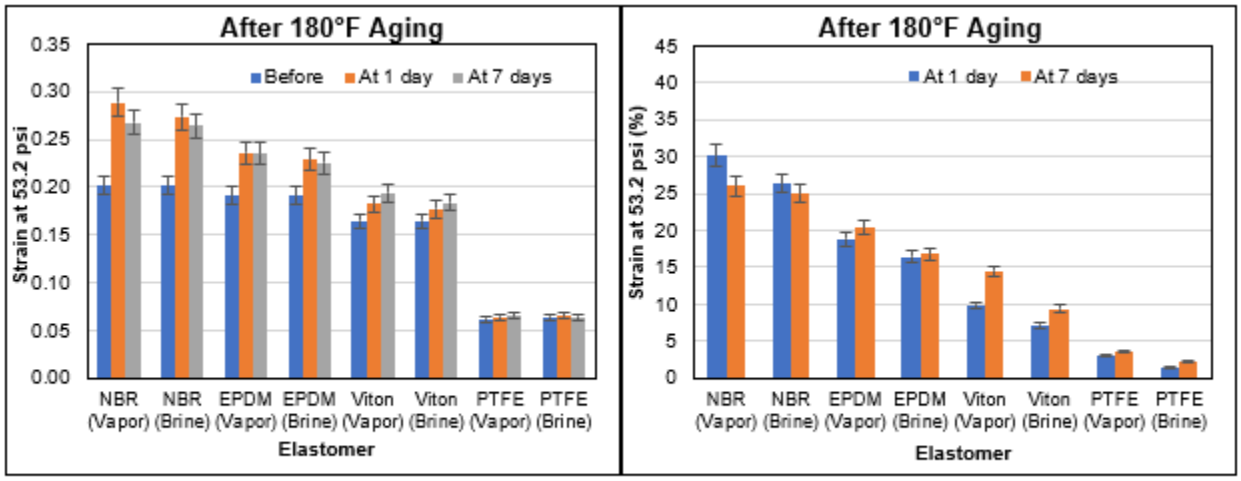

(a) (b)

Figure 3.24: Effects of days on compression (percentage strain) of elastomer samples aged at 1000 psi and 180°F (a) actual strain values, (b) percentage increase in strain values.

Effects of Temperature

To understand the effects of temperature on elastomer compression, a constant aging period is selected (one or seven days) and the temperature is altered. After 1 day of aging, all the elastomers displayed more than 5% and up to 39% increase from original strain, besides PTFE in both vapor and brine phase. This is shown in Figure 3.25b. After 7 days of elastomer aging, all samples except all PTFEs demonstrated more than 5% and up to 33% increase from original strain at 53.2 psi (Figure 3.26b). From the graphs, it is observed that for both 1 and 7 days, all elastomer samples exposed at 180°F have lower strain increase compared to those exposed at 120°F. The decrease in percentage strain change at higher temperatures is once again linked to the chain growth that occurs in the elastomers upon exposure to higher temperatures. Irrespective of the aging period, exposing the elastomer to higher temperatures diminishes its sealing abilities.

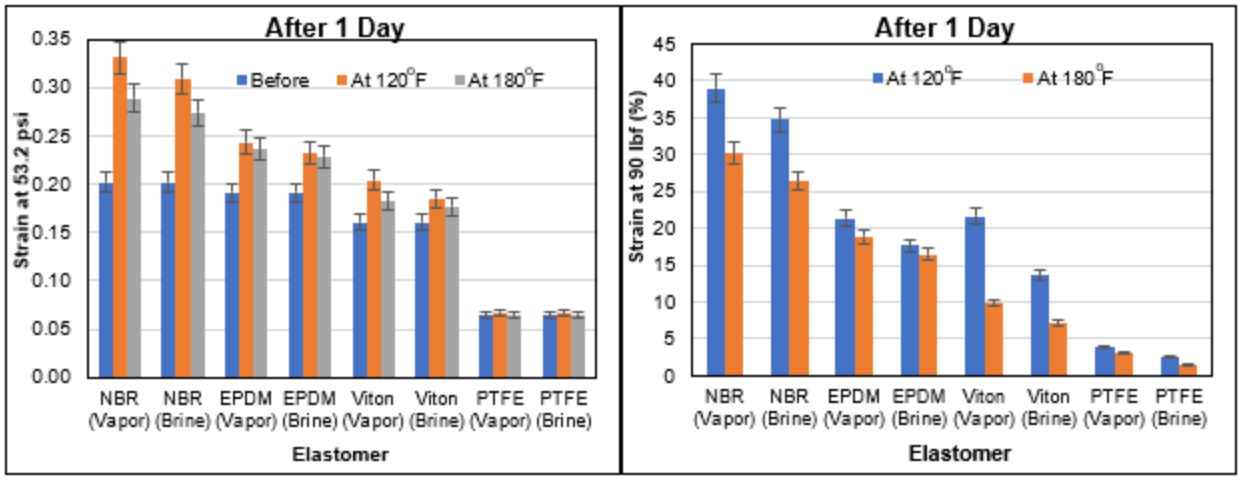

(a) (b)

Figure 3.25: Effects of temperature on compression of elastomer samples aged for 1 day at 1000 psi (a) actual strain values, (b) percentage increase in strain values.

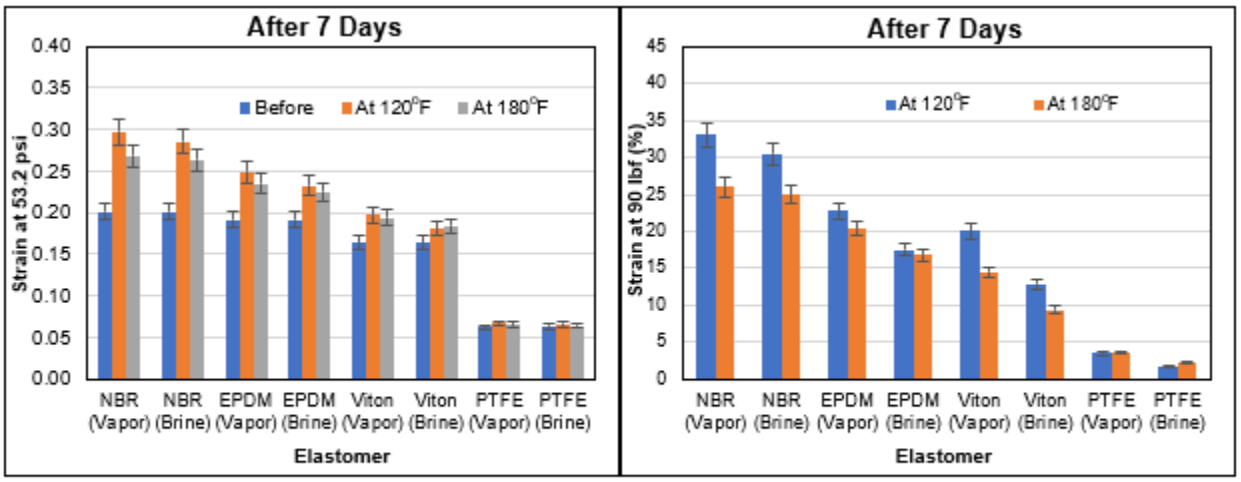

(a) (b)

Figure 3.26: Effects of temperature on compression of elastomer samples aged for 7 days at 1000 psi (a) actual strain values, (b) percentage increase in strain values.

Performing ANOVA with a 95% confidence interval, none of the elastomer samples (NBR, EPDM, FKM, and PTFE) showed significant changes in compression, shifting from one temperature to another or from one aging medium to another. Considering all the three parameters (days, fluid medium variation, and temperature) individually, compression of elastomers was insignificant with a change in any of these parameters. This implies that aging an elastomer for 1 day and for 7 days does not show any significant change. Neither does a change in temperature from 120°F to 180°F nor a shift from the vapor to the brine phase significantly affect the compression of an elastomer. The ANOVA results also provides evidence that the combined effect of the parameters does not affect elastomer compression significantly. With the forgoing, exposing an elastomer to the least corrosive condition (1 day in vapor phase at 120°F) is enough to cause its

sealing integrity to be compromised appreciably. Changing any of these aging conditions afterward is redundant since the elastomer has already been damaged.

Effects of Gas Variation

Compression changes in the elastomers due to gas attack are shown in Figure 3.27. Figure 3.27 (a) shows the actual increase in strain values for each elastomer after aging with a particular gas, while Figure 3.27 (b) shows the percentage increase in strain for each elastomer after aging with a particular gas. For CH_4, more than 5% and up to 13.8% increase from the original strain was recorded at 53.2 psi, except for PTFE (vapor and brine). For CO_2, more than 5% and up to 36.3% increase from original strain was recorded at 53.2 psi, while an increase from 5% to 17.7% in strain was recorded for H_2S. A combination of the all gases revealed more than 5% increase but no more than 33.1% increase from the original strain at 53.2 psi. These observations exclude all the PTFE's. The order of elastomer degradation from compression, with respect to corrosive gases is in order of CO_2 > All gases > H_2S > CH_4. This order is similar to the order for hardness degradation.

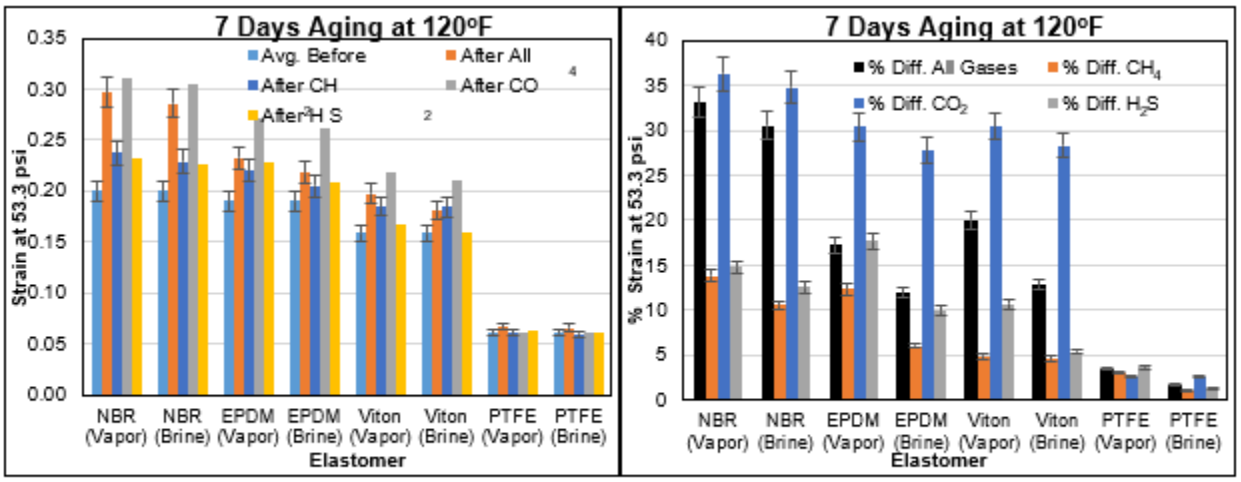

(a) (b)

Figure 3.27: Effects of gas variations on compression of elastomer samples aged at 1000 psi and 120 °F (a) compression measurement (b) percentage difference in compression measurements.

3.4.1.4 Volumetric Swelling

Volumetric swelling is the volume increase of an elastomer. The volume of the elastomer is calculated before and after aging. The change in these two values is the volumetric swelling. The procedure for measuring and calculating the volumetric swelling highlighted in ***3.3.4.2***.

Effects of Days

Figure 3.28 shows the volumetric swelling after aging at 120°F. Figure 3.29 also show the volumetric swelling after aging at 180°F. These two graphs show a general increase in volumetric swelling after 1 day, a peak in swelling after 3 days, and a gradual decline in swelling after a week. According to Schweitzer (2000), "some elastomers will continue to harden, and some soften, and

some will show an initial hardening followed by softening." In the volumetric test except for the PTFE's, the elastomer samples reached a maximum point of softening, then began to harden. Figure 3.28b show more than 5% and up to 59% increase from the original volume except the PTFE's and 1-day Viton (brine phase). After aging at 180°F, more than 5% and up to 43% increase from the original volume was recorded except for the PTFEs and all Viton (Brine). These changes in elastomeric properties are linked to the initial chain rupture in the elastomer followed by chain growth within the elastomer. Chain rupture increases the elastomers size (swelling) while chain growth causes the elastomer to shrink.

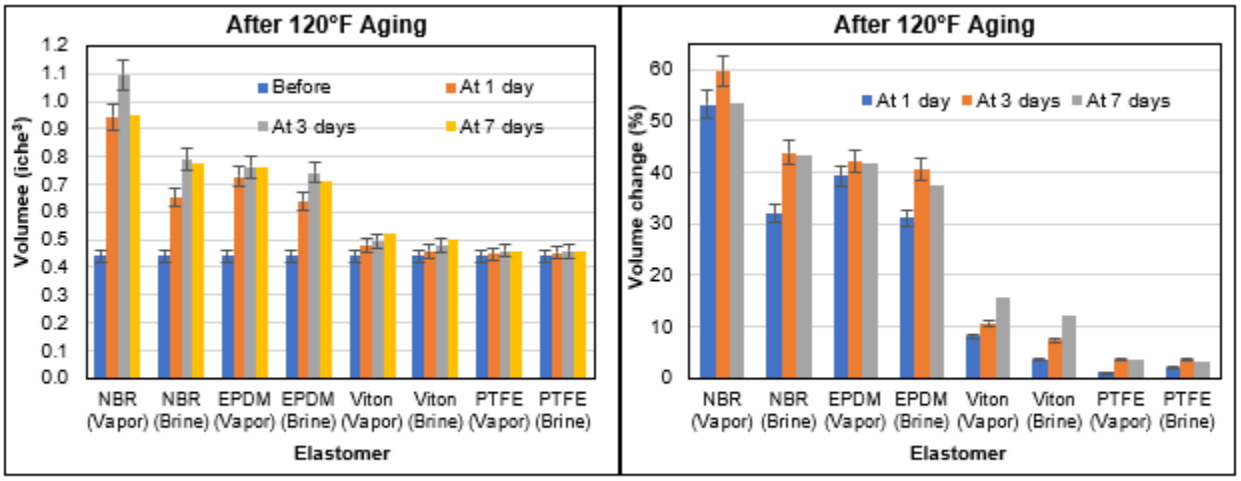

(a) (b)

Figure 3.28: Effects of days on volumetric swelling of elastomer samples aged at 120°F and 1000 psi, (a) compression measurement (b) percentage difference in compression measurements.

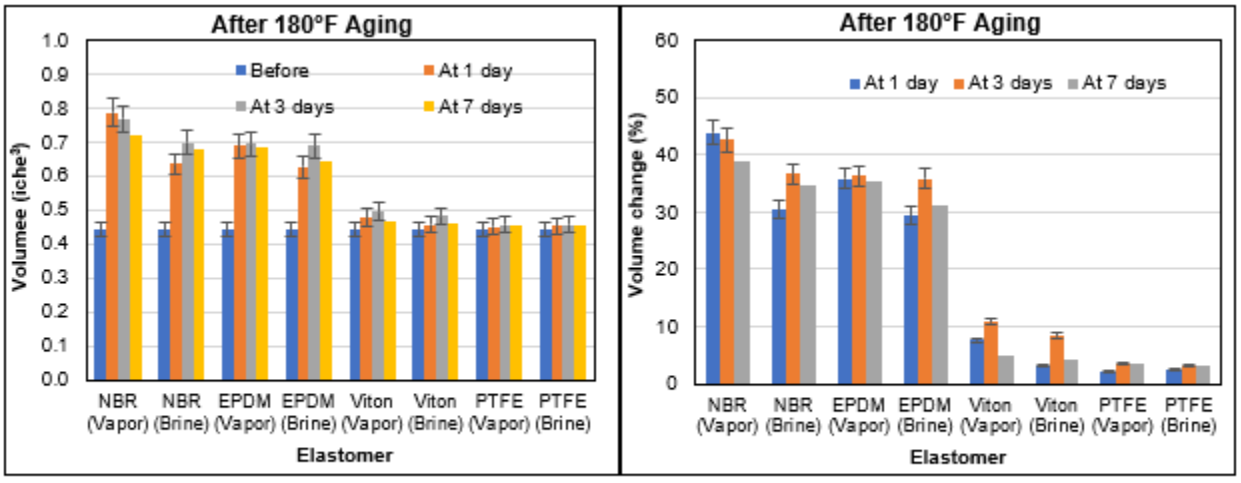

(a) (b)

Figure 3.29: Effects of days on volumetric swelling of elastomer samples aged at 180°F and 1000 psi, (a) compression measurement (b) percentage difference in compression measurements.

Effects of Temperature

Based on visual observations and measurements shown in Figure 3.30 (a) and (b), NBR in the vapor phase appears to have shown maximum swelling amongst its counterparts (EPDM and Viton). This observation was consistent after aging at 120°F and 180°F. For all the elastomers, the swelling was more predominant in the samples exposed to the vapor phase compared to those exposed to the brine phase. For example, the NBR samples in Figure 3.30 (a) clearly shows more swelling at the ends of the elastomer in the vapor phase, compared to NBR exposed to the brine. An increase in temperature results to a decrease in swelling. All the three samples showed a decrease in swelling from 120°F and 180°F. Viton, however, at higher temperatures does not only experience swelling but also blistering.

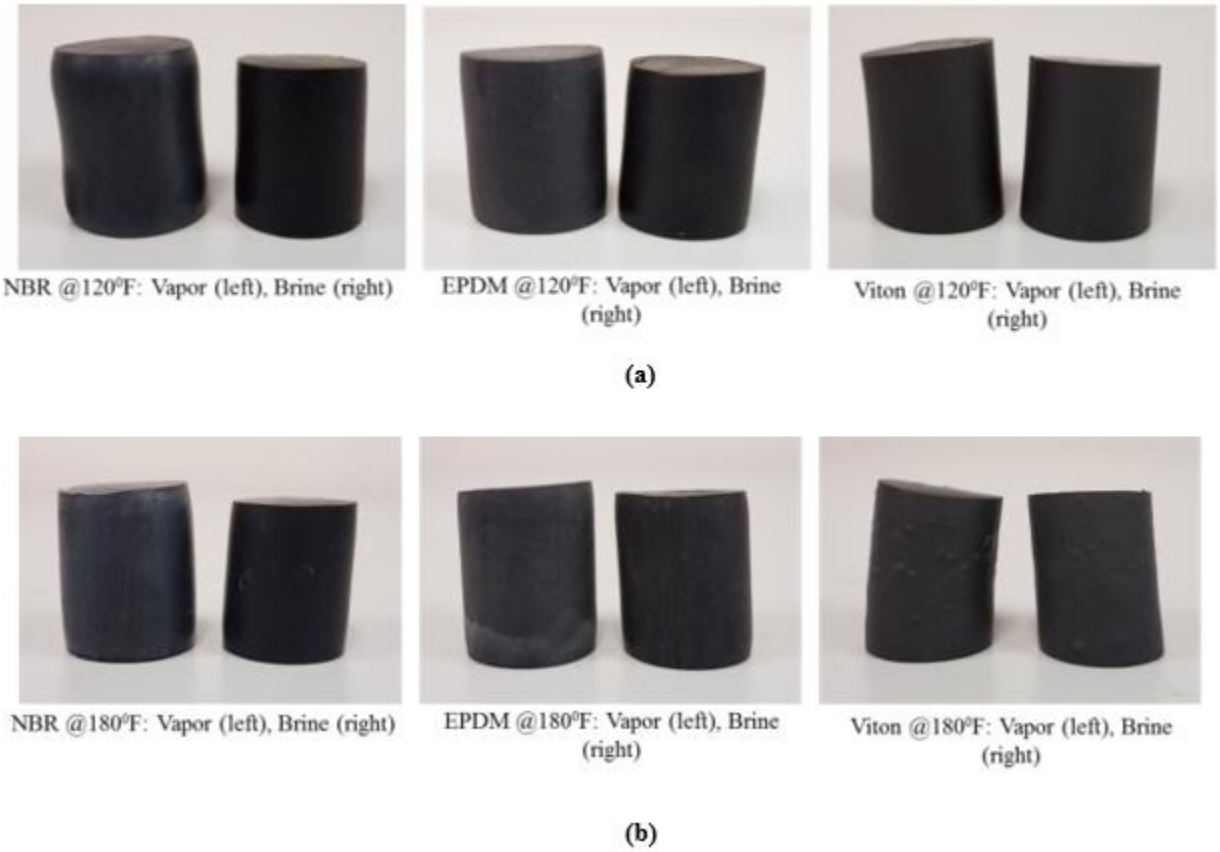

Figure 3.30: After 1-day aging in CO_2 and H_2S with CH_4 carrier at 1000 psi. (a) 120°F and (b) 180°F.

Blisters refer to bubbles or raised defects that appears on the surface of an elastomer. They are caused by the high energy which the trapped gases within the elastomer pores tend to escape after decompression. It should be noted that the decompression performed after each test was rather gradual, not rapid. Blistering causes delamination and breakage of the elastomer-lining layer, resulting in a loss of its corrosive protection (Van Dinh and Kubouchi 2012). Viton's poor decompression resistance causes this blistering at high temperatures. The test samples showed that blistering occurred in one, three, and seven-day tests, and was consistent for aging tests performed

at 180^{o}F. Figure 3.31 shows the blistering on the FKM elastomer surface. All the images were taken with the Dino-Lite Digital Microscope. Keeping aging period constant and varying temperature from 120°F to 180°F, a decrease in volumetric swelling for all the elastomers was recorded. This is because elastomers tend to undergo cross-linkage at elevated temperatures; thus, decreasing their elongation.

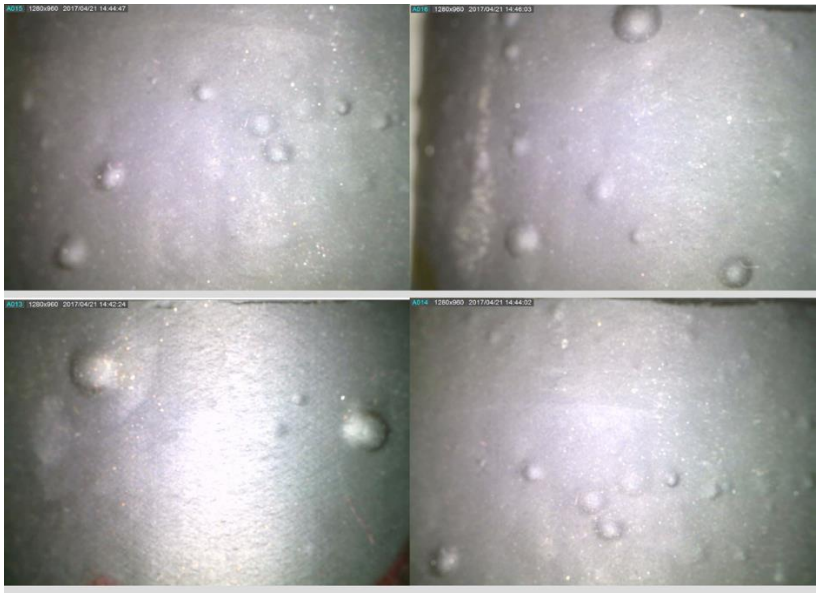

Figure 3.31: Viton blistering image taken with a Dino-Lite Digital Microscope.

Figure 3.32 shows the plots of volumetric increase (percent) after one, three, and seven days of aging. These aging tests were conducted at 1000 psi and at two temperatures 120°F and 180°F. All the tests were conducted with 50% CO_2 and 50% 500 ppm H_2S with CH_4 carrier. After 1-day, volumetric swelling of more than 5% and up to 53% increase from the original values were recorded. After 7 days, the volumetric swelling was also between 5% and 53% increase from the original volume. These observations exclude the PTFE's in both vapor and brine phase. The 3-day aging tests showed the highest recorded volumetric swelling readings - more than 5% and up to 59.7% volumetric swelling. Using these numbers, Figure 3.32 suggests that irrespective of the aging period and elastomer type (except PTFE), an increase in temperature tends to decrease volumetric swelling.

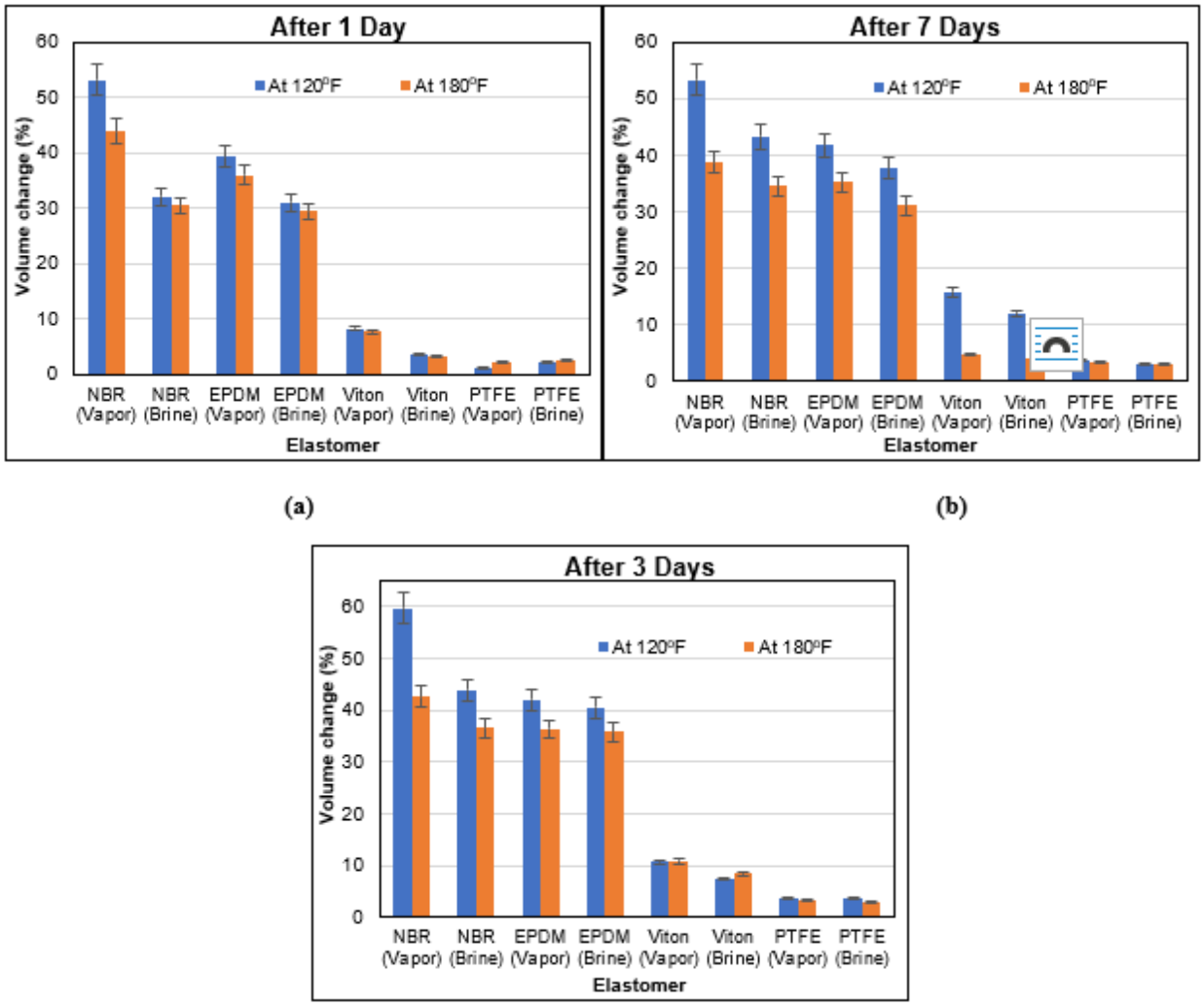

Figure 3.32: Effects of temperature on percentage volumetric change in elastomer samples aged at 1000 psi, after (a) 1 day (b) 7 days (c) 3 days.

ANOVA results suggest that the volumetric swelling of elastomer samples is not significant with changes in temperature, aging period, and the aging medium. Varying one parameter in the aging test while keeping all others constant, gives an insignificant effect. However, this is impractical given that multiple aging parameters can change simultaneously in actual downhole conditions. The interaction effects for volumetric swelling was insignificant. With these results, it can be cautiously concluded that exposing an elastomer to the least corrosive condition (1 day in the vapor phase at 120°F) is enough to cause its sealing integrity to be compromised. A change in aging conditions after this is considered redundant since the elastomer has already been compromised appreciably.

Effects of Gas Variation

Figure 3.33 compares the effects of gas variation on volumetric swelling of elastomers. The least effect of volumetric swelling was experienced with CH_4. The chemistry of methane (high bond dissociation energies and close electronegativity) explains its stability and low reactivity. Thus, it is less likely to react with any elastomer sample. Aging in the presence of 100% methane shows volumetric swelling of more than 5% and up to 32.6% from the original values. This swelling is mainly because of physical changes of the elastomer rather than a chemical reaction. H_2S caused a 5% to 34.2% increase in volume after aging the elastomer. From Figure 3.33b, aging in 100% CO_2 shows more than 5% and up to 53.2% volumetric increase in all elastomers except for some PTFE. PTFE aged in 100% CO_2 had an average swelling of 5.3%. For combined gases, the elastomers experienced more than 5% and up to 53.3% increase from the original volume. It is difficult to put all gases in order of corrosion for volumetric swelling. This is because 100% CO_2 showed a more detrimental effect on EPDM compared to NBR, while a combination of CO_2, H_2S, and CH_4 had a more detrimental effect on NBR compared to EPM. However, CH_4 had the least effect on elastomer volumetric swelling.

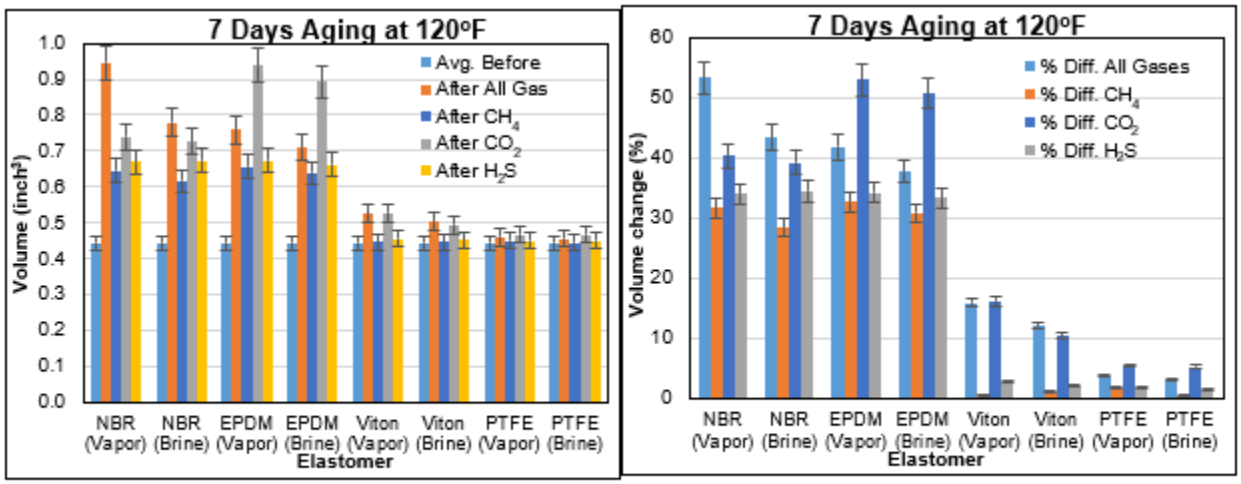

Figure 3.33: Effects of gas variation on percentage volume measurements of elastomer samples aged at 1000 psi and after 7 days (a) volume measurement (b) percentage volumetric change.

3.5 SUMMARY AND CONCLUSIONS

The following conclusions and summaries have been drawn from the theoretical and experimental investigations, results, and analyses conducted in this section of the report:

- Physical and chemical degradation of elastomers occur when exposed to testing conditions.
- The degree of chain growth and chain rupture depends on the temperature and degree of chemical exposure.

- NBR exhibited the most significant deterioration.
- Viton showed the least amount of degradation but has poor decompression resistance.
- CO_2 showed the most damaging effect of all the corrosive gases used in this study.
- Elastomer hardness is inversely proportional to volumetric swelling and compression.
- For all the elastomer samples, the general order of corrosive gas effect on elastomer degradation is CO_2 > All gases > H_2S > CH_4.
- Statistical analyses indicate that exposing an elastomer to the least corrosive condition (1 day in vapor phase at 120°F) is enough to cause its sealing integrity to be compromised appreciably. However, this cannot be extended to higher temperature conditions (greater than 180°F) because of unavailability of experimental data.

4 SEALING ASSEMBLIES TESTS USING SET UP II

4.1 INTRODUCTION

The release of uncontrolled fluids from a reservoir, particularly in shallow formations is one of the most challenging risks in oil and gas exploration. Uncontrolled fluid leakage and migration can take place at any phase in the life cycle of a well starting with drilling, completion, production, and plug and abandonment. Several factors can influence the influx and migration of formation fluids to the surface facilities or shallow formation. These include but not limited to: rock properties, reservoir fluids properties, well pressure and temperature, loss of hydrostatic from drilling or completion fluids, type of production or injection, tubular corrosion, abandonment procedure, and the type of barriers that are installed to maintain the well's integrity. Identification of potential leak paths provides information on how leaks can be managed, as well as planning operations, inspections, and maintenance of barrier systems. Leakage models can be used in identifying leak sources, potential pathways, and the pressure differential (Davies et al. 2014; Watson and Bachu 2007). After identifying potential leak paths, well barrier plans should be developed. According to API RP 96 (2013), a barrier plan should include the potential leak flow paths and identify the barriers required to prevent the flow through each path specifically during the well construction.

4.1.1 Overview

Drilling operations, particularly in an offshore environment, require special tools and equipment. Liners and liner hangers are commonly used in offshore drilling applications instead of full string casings. They are cost effective, require shorter time for running into the hole, improve cement job, and provide more space to accommodate completion equipment's above the liner (Mohamed and Al-Zuraigi 2013). When a well section is drilled, liner hanger and cement are used to engage and seal off the liner, connecting it to the previous casing. After this, a formation strength test such as leak-off test (LOT), extended leak-off test (XLOT), and formation integrity test is performed. Typically, the liner hanger sealing assembly is placed up-stream to the cement column. This arrangement prevents the evaluation of both the cement and liner hanger sealing assembly independently, since the sealing element isolates the cement sheath and there is no direct or indirect way of assessing its integrity. Moreover, Pleasants et al. (2012) highlighted that it is difficult to evaluate the performance of liner hanger seals and cement independently through the pressure test when both cement and mechanical barriers (seal) are used in series. This concern was also outlined in BSEE internal QC-FIT report #2014-02.

Statistical records have shown that a majority of the incidents associated with drilling operations in offshore shallow sections are attributed to gas migration and failure of liner hanger and cement sheath (Moore et al. 2002; Walvekar and Jackson 2006). This has jeopardized the integrity of many wells and there are no direct methods or standards that may be used to identify which of them (cement sheath or liner hanger sealing element) failed. When uncontrolled gas migrates through the wellbore, the liner hanger and cement acts as a barrier system to prevent the

gas from flowing through. The liner hanger sealing system consists of an elastomeric material and its sealing performance depends on the elastomer type, design specifications, and compatibility with the wellbore environment. Elastomers are commonly used rubber materials in oilfield operations because of the unique set of properties they possess, particularly in high-temperature/high-pressure environments (Dolog et al. 2017). Nitrile elastomers (NBR, HNBR), fluoroelastomers (FKM, FEPM), and Neoprene (EPDM) are among the most common materials used in downhole oilfield applications (Dolog et al. 2017; Campion et al. 2005). They are used to provide the sealing and hanging mechanisms in the liner hangers (Williford and Smith 2007; Wardak et al. 2010). In addition to the elastomeric material, the cement sheath also acts as a barrier. Slurries used in gas migration prone zone are typical mixed with gas migration additives. This has been discussed in detail in section 1 of this report (cement tests using setup I).

4.1.2 Statement of Problem

Well integrity can be compromised when a barrier or multiple barriers fail to prevent formation fluid influx and migration. The integrity of elastomeric seals must be maintained and not compromised by any failure mode over their service life. Failure in seals can be identified by excessive fluid leakage that is caused by a loss of seal interference (seal contact stress) or a loss of seal integrity, which is generally referred to as physical damage (James 2017). The physical and chemical degradation of elastomers have been discussed in detail in the section 3 of this report. In this section (4), elastomers are investigated as barrier elements expected to fulfil specific performance requirements. Barrier acceptance criteria needs to be evaluated to ensure that the barrier performance requirements are met, and their integrity verified. Barrier verification can be performed directly by conducting a pressure test or through other observations (API RP 96 2013). When liner hangers are deployed in the field, they are sealed off by cement and elastomers. Some of the key questions raised in this situation include: i) Which of these materials (elastomer seal or cement) is considered to be the primary barrier? ii) Should both barriers be tested independently? iii) If this is possible, how can these tests be conducted in the field? iv) Is it necessary to increase the pressure test duration for conductor, surface casing, and liners from 30 minutes to 60 minutes with less than 10 percent pressure decline?

To address these questions, two stages of experiments were conducted to evaluate the sealing capacity of elastomers and cement recipes using setup II. In the first stage, pressure tests were conducted on elastomer samples that are commonly used in liner hanger application. In this case, the elastomer seals were considered a single barrier system and the pressure tests were conducted considering three different experimental conditions. In the second stage (methodology and results are presented in the final report), experiments were conducted to test both elastomer seals and cement as a dual barrier considering different scenarios. The details of all the experiments are discussed in the methodology. In addition, pressure cycling tests were also performed because the sealing assembly (elastomer and cement sheath) can be influenced by the pressure cycling that usually occur over the life cycle of a well. During these cycles, an elastomer can damage from

explosive decompression because of gas expansion when there is a sudden pressure decline (AP1 RP 96 2013).

4.1.3 Objectives

The primary objective in this section of the project is to study and evaluate the performance a liner hanger sealing assembly and cement sheath and determine which of them acts as a primary barrier to prevent the migration of uncontrolled fluids during drilling operations. The specific objectives include:

- Identify the primary barrier when a liner hanger seal assembly and cement are used as a dual barrier system to seal off a liner.
- Evaluate the elastomers performance, particularly EPDM and NBR in sealing uncontrolled gas migration when used as barrier element.
- Evaluate the performance of elastomers under mechanical failure mode (due to improper setting and/or manufacturing defect).
- Evaluate the performance of elastomers when they are exposed to chemical degradation (degradation with surfactant).
- Assess the effect of pressure cycling upon the elastomers performance.
- Assess the effect of the pressure cycling when elastomer and cement sheath are used as a dual barrier system.
- Assess the effect of prolonging the pressure test duration from 30 minutes to 60 minutes on the seals and cement performance.

4.2 LITERATURE REVIEW

4.2.1 General Overview on Leak and Mechanism in Various Applications

A leak is defined as unintended movement of fluid to or from a system (ISO16530-2 2013). Although a leak can be well defined, and a variety of sealing systems developed to prevent fluid leakage, the exact mechanism of roughness induced leakage is not well understood (Persson and Yang 2008). Watson and Bachu (2007) and Davies et al. (2014) stated that three main factors should co-exist for fugitive emissions or leakage to take place. These factors are: a leakage source, a driving force such as buoyancy or head differential, and a leakage pathway. Bauer (1965) claimed that leakage flow paths occur through the interconnection of void spaces formed by the topographical variations of the static mating surfaces.

Over the years, leaks have been considered a critical challenge in sealing systems. Some of the well-known catastrophic disasters resulting from sealing system failure include but not limited to: The Challenger disaster in the aerospace industry, the Chernobyl disaster in the nuclear industry, and the Macondo incident in the oil and gas industry. Results of these events have increased the technical and operation safety requirements, creating more awareness to challenges resulting from leaks in various operations (Ràfols 2016). The failure of a sealing system can occur because of many interrelated key factors. The supplier in some cases may not comply with

customer specifications and not aware of the actual operating condition(s). On the other hand, an end-user may not have accurately followed the operating instructions or disregarded the design and material limitations. In some cases, both the manufacturer and end-user misunderstand the implications and constrains of significant factors in the assembly process, testing, operating conditions, storage, a spike in temperature, pressure fluctuations, and properties of the fluid to be sealed (Flitney 2014).

The assembly process of a sealing system is usually performed by joining two or multiple parts of different materials such as metal to metal, rubber to metal, rubber to glass, and rubber to porous material. The most common connection sealing techniques are metal to metal and rubber to metal. A general overview of these techniques, including their applications and mechanisms are briefly discussed herein. Figure 4.1 shows a typical topography of a metal-to-metal seal that is commonly used in high temperature high pressure environments, where the use of rubber seals may not be completely effective. Metal-to-metal connections are a common practice in aerospace, cryogenic systems, nuclear power plants, and oil and gas applications. Although a metal-to-metal sealing system can withstand severe temperature and pressure conditions, the complexity of the system components can be a detrimental factor. The contact face morphology and roughness are a spiral groove that consists of two profiles: a bottom part of the groove called valleys and an upper part called peaks. During a leak, the pressure gradient leads the flow in the radial direction, perpendicular to spiral groove rather than the circumferential direction as depicted in Figure 4.1. The radial flow direction is preferred since it is the direction of the pressure drop (Ràfols et al. 2015). Therefore, sealing can only be achieved by fully blocking the channels in the radial direction (Amyot et al. 2007).

To prevent flow across a seal, the metal-to-metal surfaces must be effectively tight. The tightness requires the connection of two metallic surfaces by welding, threading, or pressing processes. The surface profiles are normally rough, and the degree of roughness depends on the manufacturing process. The roughness provides potential leakage pathways in case the applied load to perform the boning/connection is insufficient to reach the geometrical percolation threshold (Amyot et al. 2007). Ràfols (2016) developed a model for metal to metal leakage which delivers a quantitative prediction of seal, accomplished by including the stochastic nature of the surface of the topography in a two-scale method. The main objective was to obtain the gap between two surfaces when they are pressed against each other with a certain load. The model was also used to investigate the seal behavior when the applied load is gradually reduced (unload) after plastic deformation. This was done to assess the seal performance when subjected to a certain load cycle.

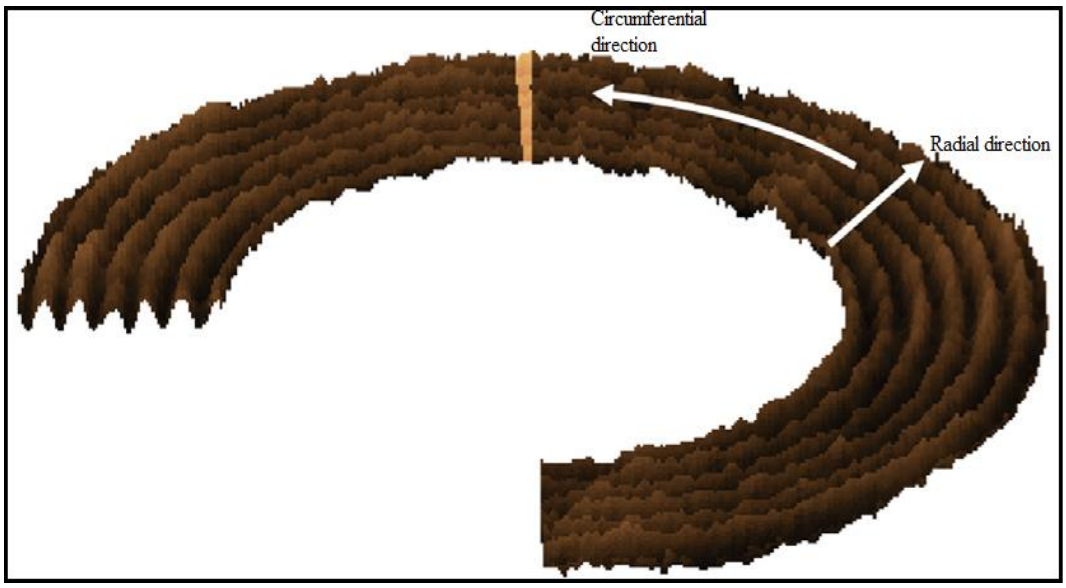

Figure 4.1: Schematic of a typical topography encountered in a metal-to-metal seal, with the two main directions (after Ràfols 2016)

In oil and gas well completion equipment's, metal to meal sealing connections are still commonly used. Metal sealing systems tend to be a more viable option where the mating seal surface finishes have very good morphology. In this situation, there is no movement between the mating seal surfaces, and high setting loads can be applied easily. However, in situations where these factors are not practical for the intended application, rubber sealing systems should be considered as an alternative solution (Kelly and Theiss 1989).

Elastomers are a viable alternative and are been used in the oil and gas industry as wellbore isolation/intervention devices (Hoff 2012). Although the rubber industry has been around for over 150 years, it is only in the last 75 years that design engineers have been able to combine the strength of metals with the elasticity of rubber to form integrated sealing systems. The first commercial successful bonding process was executed in the 1920's, using a technique called brass plating. This technique was replaced by bonding with chemical agents, which were introduced after the end of the Second World War (Chandrasekaran 2010). Rubber to metal bonding is used extensively in the automotive and oil industry. The failure mechanisms of bonded rubber to metal in marine environments have not been deeply investigated. Corrosion is the main contributor to bonding failure. It impacts the performance of the adhesive joint at the bonded interface or adjacent to it (Ismail and Harun 2013). The authors categorized three failure modes that can occur in the adhesive joint as: interfacial failure according to water hydrolysis of the adhesive from the substrate, the degradation of the adhesive itself when exposed to harsh environments, and the interfacial failure from cathodic or anodic reactions of the substrate. In rubber to metal bonding, the bond strength is generally greater than the strength of the elastomer; thus, the failure mode is usually within the elastomer. Although these failure modes exist, elastomeric seals are still one of the most important components in pressure control devices for oilfield applications. Elastomers

have significant advantages in terms of processability, versatility, and cost when compared with metal-to-metal sealing systems (Chen et al. 2016).

4.2.2 Well Control Barriers

Maintaining a well under control is a primary and essential safety requirement during drilling operations. Well control is defined as activities implemented to prevent or mitigate unintentional release of formation fluids and gases from the well to its surroundings (API RP 96 2013). Well surroundings could be external (the sea in a subsea well, the platform deck in a topside X-mas tree) or some components of the system (the flowline from a subsea well) (Torbergsen et al. 2012). Thorogood (2017) considers hydrocarbon influx into the wellbore a "top event". The author defined a "top event" to be the deviation from a normal activity or procedure before an adverse effect emerges. In this case, having a well and operation under control before formation fluid migrates to the surface uncontrolled is a "top event". There are many principles for well control set by regulatory agencies and industrial standards. Most of them agreed on a common rule for well control barriers which is: "at least, two tested independent barriers should be in place between the hydrocarbons in the reservoir and the environment at all times" (NORSOK D-010 2014; API RP 96 2013; ISO 16530-2 2013). This rule is also recognized by the Bureau of Safety and Environmental Enforcement (BESS) and Norwegian Petroleum Safety Authority (PSA) regulations. Oil and gas operators and service providers are expected to adhere to the concept of two well barriers during all well operation activities. However, investigations from many well control related accidents have revealed that most of the two well barriers were inadvertently maintained by the crew during the incidents (Strand 2017).

Barrier analysis and management have received more attention over the years from operating and services companies, contractors, and regulators to ensure that they are properly identified, in place, and functional. The focus on barrier performance requirement verification increased after the significant blowouts in Montara and Macondo (Aggelen 2016), as well as the shallow gas migration event in the Main Pass Block 295. Well barriers are used to prevent leakages and reduce the risk associated with drilling, production, and intervention activities. Torbergsen et al. (2012) summarized the essential objectives of a well barrier into the following:

- Prevent a major wellbore fluid leakage to the surrounding environment.
- Shut in the wellbore on direct command during an emergency shutdown scenario to prevent formation fluid influx and migration in the well.

To fulfill these objectives, a barrier must meet certain performance requirements such as functionality, availability, reliability, capacity, effectiveness, integrity, ability to withstand loads, robustness, accessibility and response time (ISO/TS 16530-2 2013; PSA 2013; Hauge and Øien 2016). In addition to these, the following should be considered as part of the performance standards according to ISO/TS 16530-2 2013:

- Failure mechanisms.

- Failure consequences.
- Operating conditions.
- Interactions with other systems.

4.2.3 Barrier Failure Modes

There are different failure modes by which a wellbore barrier can fail. The study conducted by Davies et al. (2014) showed that the percentage of wells that have had issues on well barrier or integrity failure is highly variable (1.9%-75%). This range variation is based on the number of wells surveyed, their type, age, geological location, regulatory policies as well as design, operation and maintenance procedures (Davies et al. 2014; King and King 2013). Offshore wells had the higher barrier failure and ranked at the end of range (King and King 2013). During the life cycle of a well, well barrier and integrity failures are undesirable. They can occur during drilling, production, and/or after plug and abandonment. King and King (2013) defined well integrity failure as a situation when all the well barriers fail to prevent a leak, leading to loss of well control. The major contributors of well integrity issues are leaks in tubular or valves and reservoir issues that lead to loss of zonal control (Torbergsen et al. 2012)

According to King and King (2013), well barrier failure occurs when individual or multiple well barriers fail to perform their function, however the well is kept under control. Many studies have been conducted to investigate the root causes of the barrier failures. Barrier failure during the well construction, particularly during drilling and completion phase, is more probable rather than failures expected during production or plug and abandonment. The main causes of barrier failure associated with drilling are: inadequate cementing, leaking tubular, corrosion, degradation, cyclic loads, thermal extremes, earth stresses, wear/abrasion, seals that isolate the top of tubulars, seals between the hangers, and valves amongst others (King and King 2013; Aggelen 2016). One of the well failure mechanisms is pressure cycling which can lead to barrier degradation. The hydraulic fracturing process is a typical example where fluid migration pathways can be created due to the cyclic pressures associated with the stimulation process (Wu et al. 2016). In addition to these causes, Gustafson (2014) and Tinmannsvik et al. (2011) claimed that complexity is a major issue for barrier failure, particularly in offshore drilling. The authors defined complexity in terms of technical and organizational contexts, specifically with respect to technological advancement in deep wells and complex reservoirs that involves many parties. They concluded that the interaction, coordination, communication, and organization between the parties is very crucial, and failure of these aspects can increase the degree of complexity. Finally, human factors are a prime contributor to barrier failure. Studies have shown that the human factor accounts for up to 70%-97% of the incidents related to failure or weakening of barriers (Aggelen 2016).

There are several measures that can be taken to prevent the incidents that arise from barrier failures. Predicting the causes of barrier failure under various operating scenarios, awareness of the barrier system components as well as detecting leakage at an early stage are important proactive steps for risk control and prevention (Torbergsen et al. 2012; King and King 2013). The barrier

systems must be thoroughly analyzed by conducting hazard and operability (HAZOP) review to ensure that barriers are "fit for service" for all the expected conditions of operation (Thorogood 2017).

4.2.4 Types of Elastomeric Materials Used in Liner Hangers

A liner hanger is a device that is positioned at the top of the liner string to attach or hang a liner from the internal wall of a previously set casing string. It supports the weight of the liner and is set by engaging the slip and cone (conventional versions) or set by external expansion (expandable liner hangers). In addition to supporting the liner load, liner hangers seal off the annulus above and below the packer when an external packer is energized (API RP 96 2013; API RP 65-2 2010).

Table 4.1*: Comparison between different liner hanger mechanisms (Mohamed and Al-Zuraigi 2013).*

	Mechanical Set Liner Hanger	**Hydraulic Set Liner Hanger**	**Balanced Cylinder Hydraulic Liner Hanger**	**Expandable Liner Hanger**
Setting Depth	Limited	Unlimited	Unlimited	Unlimited depending on Manufacturer
Well Deviation	Limited	Unlimited	Unlimited	Unlimited depending on Manufacturer
Integrity of the System	High	Potential Leak Paths	Potential Leak Paths	High
Available Metallurgy and Material Grades	Un-Limited	Unlimited	Unlimited	Limited
Circulation Pressures While Running in Hole	Unlimited	Limited	Unlimited	Unlimited depending on Manufacturer
Rotating While Running in Hole	No (very limited)	Yes	Yes	Yes
Rotating While Cementing	Available	Available	Available	Available only with the risk of keeping the running tool attached to the liner while cementing
Reaming with Liner Application	No	Limited	Yes	Yes
Drilling with Liner Application	No	Limited	Limited	Yes
Cost	Low	Average	High	High

Note: This comparison is relative to different manufacturers and locations.

The evolution of liner hanger technology started with the mechanical-set liner hangers, evolving through to the hydraulic-set liner hangers, balanced cylinder hangers, and expandable liner hangers (Mohamed and Al-Zuraigi 2013). A comparison between different liner hangers, setting mechanisms, advantages, and limitations are illustrated in Table 4.1. The liner hanger sealing system consists of an elastomeric material and its sealing performance depends on the elastomeric element, design specifications, and compatibility with the wellbore environment. Types and properties of elastomers have been discussed in section **3**. The major elastomers used in liner hangers are summarized in Table 4.2.

Table 4.2: Comparison between elastomers used in liner hangers (James 2009; DuPont 2017).

Type	Family	Applications	Working Conditions	Manufacturer
NBR	Nitrile	**RS**: Petroleum oils and fuels, water and glycols **Not RS**: Ketones, H2S esters and amines	-For lower duties -Low to medium down-hole temperature	James Walker
HNBR	Hydrogenated Nitrile,	**RS**: Petroleum oils &fuels, water and glycols **Not RS**: Strong acids and halohydrocarbons	-Slightly better tolerance than standard nitrile	James Walker
Viton®	Fluoroelastomer (FKM),	**RS**: Petroleum oils & fuels, acids, halohydrocarbons and phosphate esters **Not RS**: Ketones, amines, hot water and steam	-Medium to high down-hole temperature, 200°C to 315°C -Resistant to H2S -Economical solution in high-temperature and harsh-chemical environments	James Walker DuPont
Aflas®	Tetrafluoroethylene (FEPM),	**RS**: Sour petroleum oils &fuels, acids, bases, amines and steam **Not RS**: Halohydrocarbons	-Medium to high down-hole temperature -Resistant to H2S -Swellable when used in oil-based fluids	James Walker AFLAS
Kalrez®	Perfluoroelastomer (FFKM),	**RS**: Sour petroleum, acids, bases, MTBE and ketones **Not RS**: Alkali metal solutions	-HP/HT applications -Tubing-to-packer seals -DD, LWD and MWD tools	James Walker DuPont

Note: RS = Recommended Service.

EPDM is used by Rigger Engineering for substituting the lead-in-lead seal liner hanger that is used in gravel packing operations where a slotted liner is to be hung in a producing zone. EPDM is usually not recommended by most suppliers. Viton® has been used in oil and gas exploration,

production, and refining industries for over 30 years. They are used as sealing elements in packers, mud motors, pumps, valves, and blowout preventers. They offer best solution for critical sealing problems where elastomers such as NBR or EPDM fail to provide adequate sealing performance. Kalrez® has an outstanding chemical resistance and thermal stability in aggressive environments. They offer excellent explosive decompression resistance, extrusion resistance in high-pressure applications, and excellent chemical resistance to drilling muds, sour gas, and amines. Seal application in oil tools includes packer elements, slip-joint seals, and casing tie-back seals (DuPont 2013 and 2017).

4.2.5 Failure Mode of Liner Hangers

Well integrity can be compromised because of single or multiple barrier element(s) failure. Major barrier elements whose failure can compromise well integrity include but not limited to: cement, tubular, seals that isolate the top of tubulars, seals between the hangers, and valves (Lauridsen et al. 2016; Aggelen 2016). Liner hanger problems which are related to well integrity failure have a growing concern and is given more attention.

In deep and complex offshore drilling, deploying liner strings have become more demanding. Running a string can result to major challenges in the installation tools and cementing technologies. These tools often operate in some of the most critical wellbore temperatures, pressures, borehole solids, and deviation (Ron 2005). Despite the significant advantages of liners, the failure of liner-top is still a challenging issue. In the conventional system that utilizes the cone and slip technique, the failure rate of the top packers exceeds 40% (Ron, 2005; Walvekar and Jackson 2006). The outcomes of an informal survey conducted in 1999 over several GoM operators revealed that 30% to 50% of pressure seals in overlaps failed (Moore et al. 2002). The major failure modes identified by Williford and Smith (2007) are:

- Completion tools (packer and hanger) and centralization issues, preset or failure from inadequate set, as well as seal failure.
- Casing shoe integrity and squeeze.
- Top of liner (TOL) integrity and liner lap squeeze.

Ron (2005) and Walvekar and Jackson (2006) stated that liner top and liner installations fail because of a variety of reasons that can be attributed to liner top cement integrity failure, inability to run the liner to the predefined depth, and tools failure such as darts, plugs, running/ setting tools, etc. In addition, Ron (2005) presented the following issues in relation to liner hangers:

- The configuration of hanger slips and cones represents a trap for cuttings and debris to accumulate. This can lead to increase in the equivalent circulating density (ECD) which eventually results in lost circulation.
- Setting tools that get stuck because of debris that enter the setting tool and extension sleeve gap, as well as improper tool assembly at the shop.
- Preset hanger or packer that results from debris trapped in the slips or packer elements and the effect of surge from running tool into the hole.

Regarding the elastomer element failure, the following modes are the most predominant (Hoff 2012):

- Gasification or rapid gas decompression (RGD).
- Temperature and chemical degradation.
- Shearing and deformation across an extrusion gap.
- Fatigue under dynamic pressure cycles.
- Catastrophic failures from compression loads.

Over the years, most of the liner hanger problems have been encountered with the conventional versions. Thus, the expandable liner hanger system was introduced in 1999 to overcome these troubles. It is simple and does not contain moving parts such as the slips and cones (Moore et al. 2002; Ron 2005; Williford and Smith 2007; AlMusa et al. 2017). In addition to solving the conventional liner hanger system limitations, the expandable liner hanger technology improves the cement job quality because it can rotate and reciprocate while cement pumping is ongoing. Good cement job quality provides better sealing and zonal isolation; hence, cement issues such as channeling and micro-annuli are eliminated by the rotating process. The stress over the preceding casing is evenly distributed, which eliminates potential corrosion sites (Ron 2005; Jackson and Smith 2007). Although, the expandable liner hanger technology has considerable advantage over the conventional version, it has some limitations such as: longer installation and setting time, complexity of the running tools (require longer manufacturing lead time), very limited selections for the materials, and higher cost (Mohamed and Al-Zurigi et al. 2013).

Cement is used to seal the liner/casing overlap in the conventional liner hanger system (Williford and Smith 2007). However, gas migration through the cement sheath creates problematic issues such as high annular pressures at the surface, poor zonal isolation, and blowouts. Gas migration through the cement sheath can be caused because of improper cement design, poor mud cake removal, high cement shrinkage, and poor bonding (Pour and Moghadasi et al. 2007). Well integrity can also be impacted by prolonged waiting of the cement on the top of liner (TOL). This is because the conventional retarders improve the thickening time to a range of 6-8 hours; however, the compressive strength at TOL is reduced (Al-Yami et al. 2017).

4.3 RESEARCH METHODOLOGY

4.3.1 Scope of Work

Sealing assembly and cement sheath are used to seal off the liner hanger. It is difficult to differentiate which of the barriers passes the pressure test because of the presence of elastomeric material ahead of the cement column. The scope of this study is to identify a test method that allows for evaluating the performance of seals and cement independently. Indeed, to identify whether the seals or cement sheath is the primary barrier.

The scope also covers evaluating the impact of manufacturing defects, chemical degradation and pressure cycling upon seals performance. EPDM and NBR were selected for the

tests because they are commonly used in down hole sealing systems. The pressure tests were conducted at 40 psig for safety precautions because the setup was fabricated from an acrylic material and cannot withstand higher pressures. The tests were performed at room temperature similar to the tests from setup I (cement tests).

4.3.2 Experimental Setup Description

The setup consists of 10 inch (OD) outer acrylic pipe and 8 inch (OD) inner acrylic pipe, the annular space between the pipes is 0.7 in (18 mm). The length of each pipe is 3 ft (setup length). Figure 4.2 shows two elastomers with cord thickness of 0.75 inch (19mm). Both elastomers were inserted in the annular space between the pipes and mechanically energized with three aluminum rings and six threaded rods as illustrated in Figure 4.3.

Figure 4.2: Elastomers for sealing the annulus between the outer and inner pipes

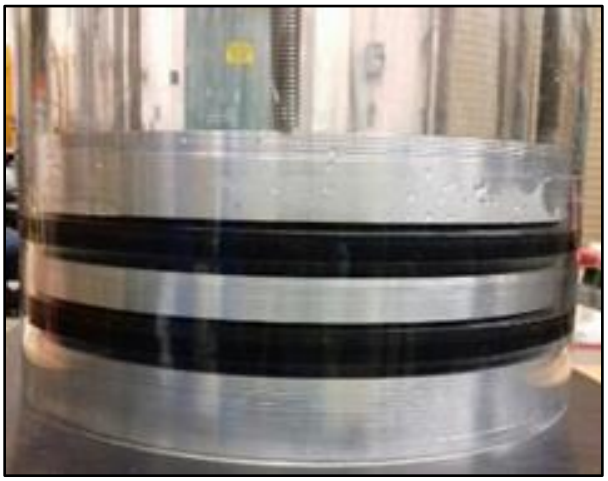

Figure 4.3: Two elastomers placed in between aluminum ring during energization

The upper and lower sides of the pipes were closed with acrylic plates which were connected by four outer threaded roads. A hole was drilled on the upper cap to inject the nitrogen gas into the inner pipe. The inner pipe was perforated to disperse the gas flow underneath the bottom of the lower elastomer. To help detect the gas leakage in the case where the elastomers fail, a portion of the annular was filled with water to observe and track the gas bubbles. In addition, two to three cameras were distributed around the setup for continuous surveillance of the gas bubbles when there is a leak. The setup components are illustrated in Figure 4.4 (a).

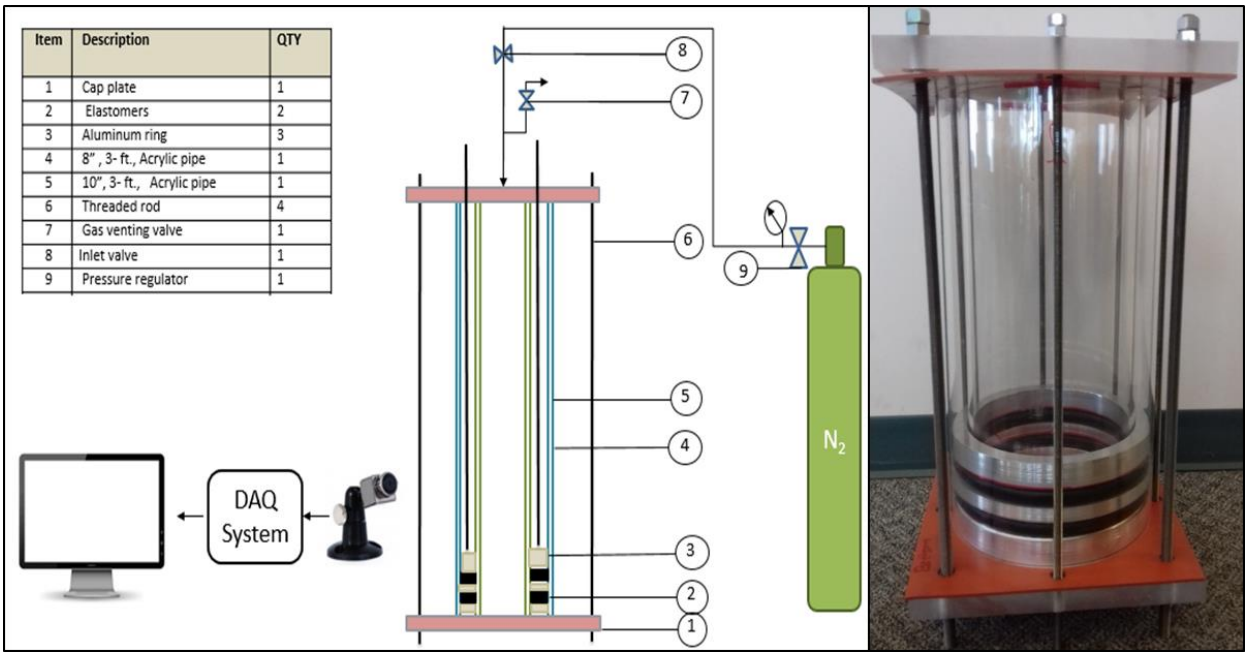

(a) **(b)**

Figure 4.4: Schematic showing the arrangements of setup II components (a) and an actual setup II (b)

4.3.3 Test Description

The experimental work was divided into two main parts: the first part aims at testing the elastomers independently whereas the second part focuses on testing the elastomer seals and the cement as a dual barrier.

4.3.3.1 Elastomer Tests as Independent Barrier

The pressure tests for elastomers were performed to evaluate their sealing capacity by investigating gas leakage through the elastomers. EPDM and NBR were tested under three different experimental conditions. The first experiments for both elastomers were performed under normal condition. The normal condition in this case implies that the elastomers were not exposed to any physical or chemical damage, properly set/energized, and perfectly manufactured (defect free). The second experiments were performed after chemical failure of the elastomers. A surfactant which is commonly used as a non-aqueous fluid (NAF) additive was used to degrade the elastomers. The third experiments were conducted after mechanical failure of the elastomers. In

this condition, a physical/mechanical defect was intentionally created on some part of the elastomer surface. This was achieved by creating seams that can result in non-uniform surface which can provide gas leakage pathways. Table 4.3. shows the tests matrix for the elastomer tests as an independent barrier system.

Table 4.3: Test matrix for testing elastomers as an independent barrier

Experimental parameters		First experiments under normal condition	Second experiment after chemical degradation	Third experiment after physical degradation
Testing Pressure (psig)		40	40	40
Elastomer Type	EPDM	E1T1	E2T1	E3T1
	NBR	E1T2	E2T2	E3T2

First Experiment: Under Normal Condition

After the elastomers were placed in the annulus, they were energized by applying a torque of 180 in-Ibf. A preliminary test was conducted followed by 3 major tests. The objective of the preliminary test was to establish the maximum test pressure limit that the setup can handle for safety precautions. The test began with a low pressure (10 psig) for 15 minutes which showed no leaks around the elastomers or within the setup. The pressure was increased by 5 psig every 15 minutes, up to 40 psig for each test. It was concluded that beyond 40 psig, it would be unsafe to run pressure tests because the setup rods, nuts, caps, and pipes were tightened to an upper limit above which they may break.

The first and second major tests under normal conditions were performed at 40 psig with 30 minutes and 60 minutes respective holding times. Nitrogen was injected for 5 minutes into the setup after which the gas cylinder valve was closed. During this time, the pressure gauge was observed for 30 minutes to monitor any pressure drop. At the end of the test, the setup was vented. After the test, the total torque was reduced from 180 in-lbf to 120 in-Ibf and to 0 in-Ibf. The same test procedure was followed for each change in torque condition. This was done to assess the influence of torque on the elastomers contact pressure. The tests were also performed after the elastomers were relaxed for one week without applying any torque. The same procedure (pressure test, change in torque, and one-week relaxation) was repeated for the 60 minutes test (second test). Each elastomer sample was subjected to 16 tests and a total of 32 tests were conducted under the normal experiment condition.

The third major test was the pressure cycling test. Frequent cycling may lead to the de-bonding of the cement sheath and a reduction in contact pressure at the sealing element interface. This can create a micro-annulus within the cement and micro-cracks within the elastomer which can provide pathways for gas migration (Al-Yami et al. 2017). A series of ten pressure cycles was conducted for each elastomer energization (180 in-lbf, 120 in-Ibf, 0 in-Ibf, and one-week relaxation with 0 in-lbf) to assess the elastomers performance under pressure cycling conditions.

In each cycle, the pressure was raised to 40 psig within 5 minutes, the injection valve was shut-off, and the sealing system (elastomers) was kept under this pressure for 10 minutes (holding time). At the end of the holding time, the vent valve was opened suddenly to reduce the pressure to 10 psig, then closed within 1 second. After closing the vent valve, the injection valve was opened very quickly to fill the setup to 40 psig**.**

Second Experiment: After Chemical Degradation

The objective of the second experiment was to investigate the elastomer's performance when exposed to a surfactant which is typically used in non-aqueous fluids (NAF) for drilling. The test procedure used for normal condition was used in the second experiment. After one-week of exposure to a surfactant, EPDM elastomer swelled with the diameter increasing from 8.74 inches to 8.82 inches and thickness increasing from 0.75 inches to 0.78 inches. Conversely, their hardness reduced from 75 durometer points to 63.7 durometer points. The elastomers were not torqued in the annulus because the dimension expansion provided more friction that raised the pre-compression force. Figure 4.5 shows EPDM elastomer before and after it was immersed in a surfactant for one week.

Figure 4.5: EPDM elastomers before (left) and after (right) degradation with surfactant.

The EPDM elastomers were also subjected to CO_2 degradation to evaluate their sealing capacity. This was done based on one of the conclusions from the elastomer aging tests (setup III) that CO_2 showed the most detrimental effect out of all the gases that were tested. The samples were placed in an autoclave cell (setup III) and exposed to CO_2 at room temperature and 600 psi for three days. Cracks and blisters were visually observed over the elastomers surface as shown in Figure 4.6, and this can compromise the elastomers sealing integrity.

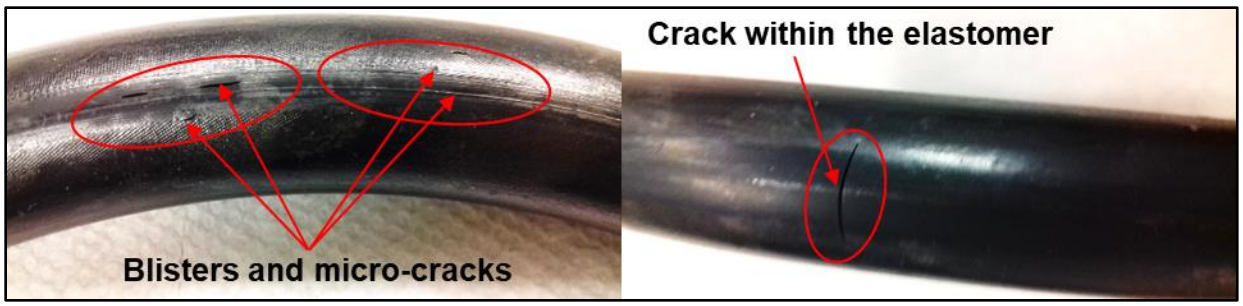

Figure 4.6: Blisters and cracks on surface of the elastomers after chemical degradation with CO_2.

The NBR elastomers were subject to only surfactant degradation for one week. Their diameter increased from 8.74 inches to 8.94 inches and thickness increased from 0.75 inches to 0.87 inches. The elastomers became very soft with hardness decreasing from 66 durometer points to 44 durometer points. The high volumetric swelling shown in Figure 4.7 (a) made the elastomers installation very difficult process. After placement, Figure 4.7 (b) shows the apparent deformation as a result of the volumetric swelling.

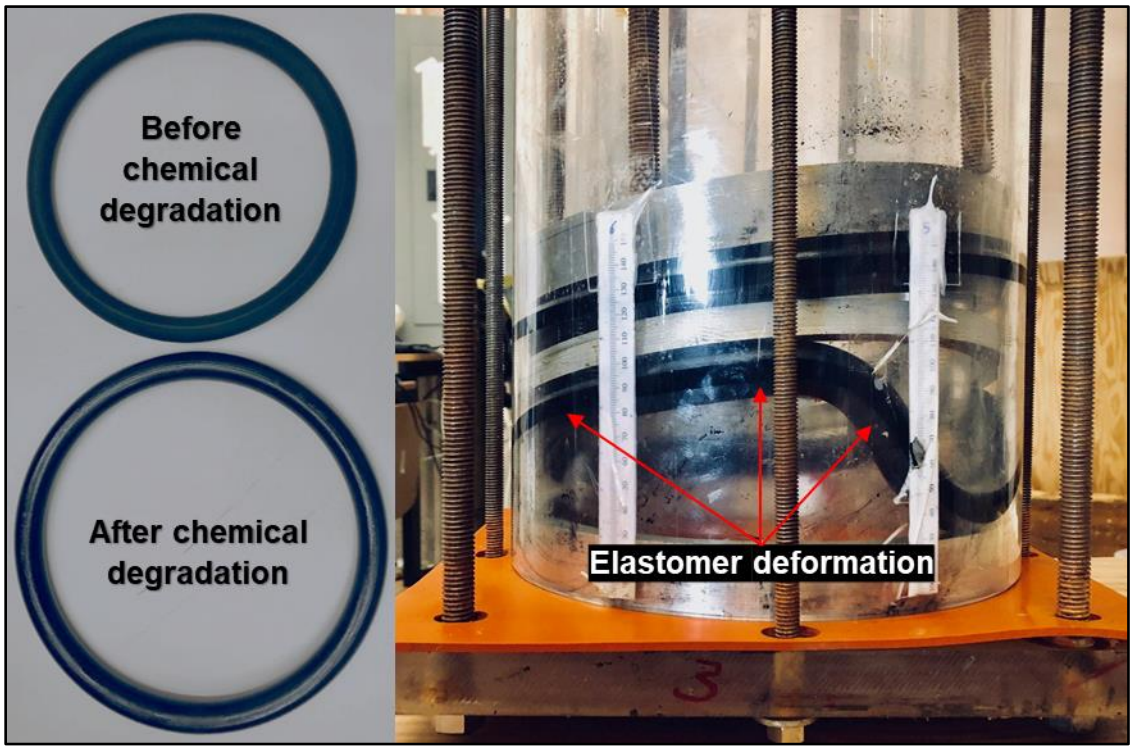

(a) **(b)**

Figure 4.7: NBR elastomers before and after degradation with surfactant (a) and deformation after swelling and installation in the annulus (b).

Third experiment: After Physical (Mechanical) Defect

In this experiment, the elastomers were intentionally defaced (Figure 4.8**)** to assess the effect of the surface imperfection upon their sealing integrity. The same test procedure was used for all the tests performed in this experiment.

Figure 4.8: Elastomer after creating a seam as an intentional physical defect

4.4 RESULTS

The results obtained from the experiments were analyzed to evaluate the performance of different elastomer samples, as well as verify their conformance with the technical requirements. Pressure tests were performed to determine the elastomer's sealing capacity independently under various operating conditions such as normal, after mechanical failure, and after chemical failure.

4.4.1 Elastomer Tests

4.4.1.1 Pressure Tests Under Normal Condition

Normal conditions in this case implies that the elastomers have not been exposed to any form of chemical degradation or mechanical damage such as manufacturing defect, cracks, setting and installation problems. A preliminary test was conducted on EPDM and NBR samples. Figure 4.9 and Figure 4.10 shows the test results for EPDM and NBR respectively at different torques. No leaks were recorded during the tests and 40 psig was established as the maximum pressure test limit.

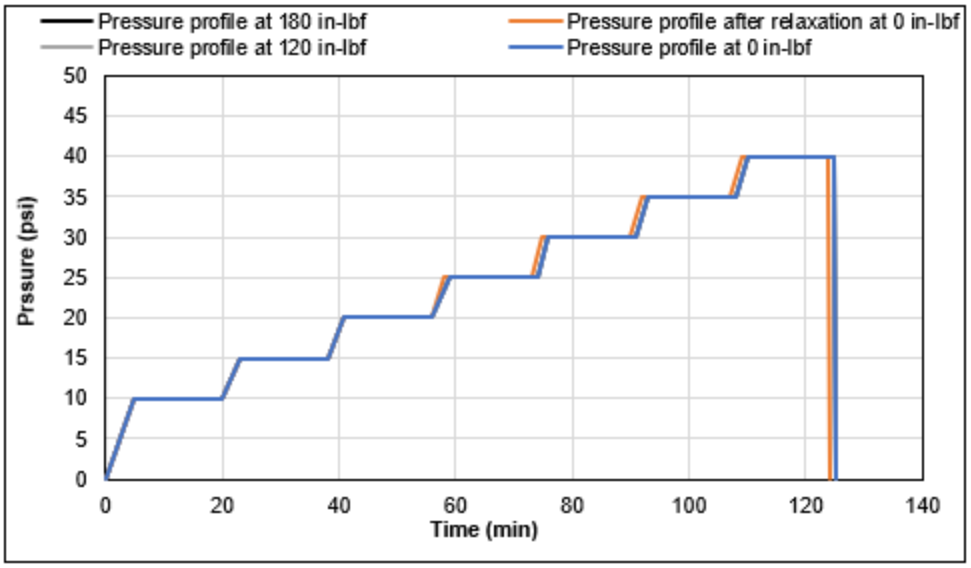

Figure 4.9: EPDM preliminary pressure test at different torques.

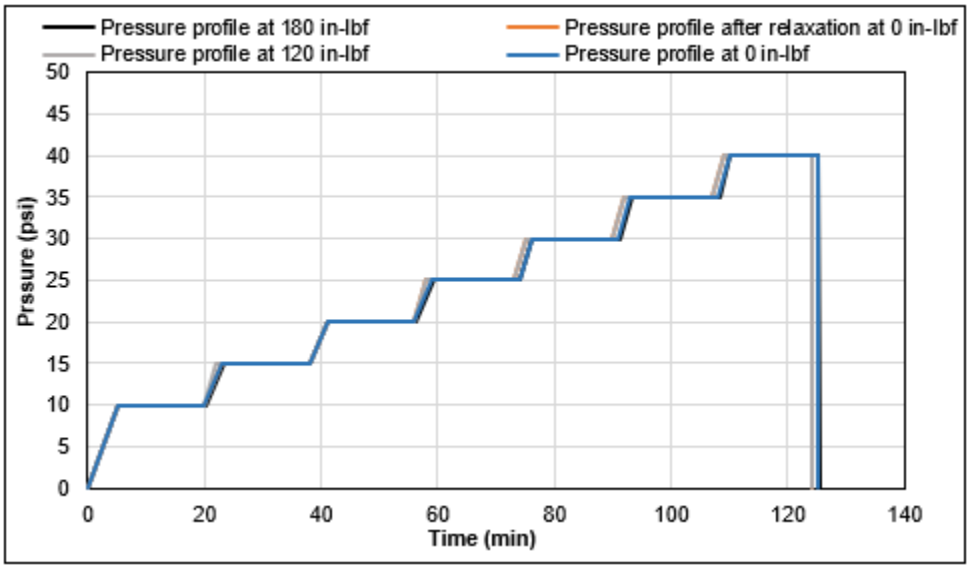

Figure 4.10: NBR preliminary pressure test at different torques.

EPDM Pressure Tests for 30 and 60 Minutes Holding Times

Following the preliminary assessment pressure tests, EPDM samples were tested at 40 psig for 30 minutes at 180 in-Ibf and no leak (pressure drop) was observed. The test was repeated after the torque was reduced to 120 in-lbf and 0 in-Ibf to evaluate the effect of energization on the elastomers' performance. The test was repeated after the elastomers were allowed to relax for one week and no torque was applied. The goal of the one-week relaxation was to assess the friction force between the pipes and elastomers upon their energization. Figure 4.11 shows that for all the energization conditions and under normal condition, no leaks were recorded within 30 minutes of pressure test. The elastomers exhibited good sealing capacity up to 40 psig.

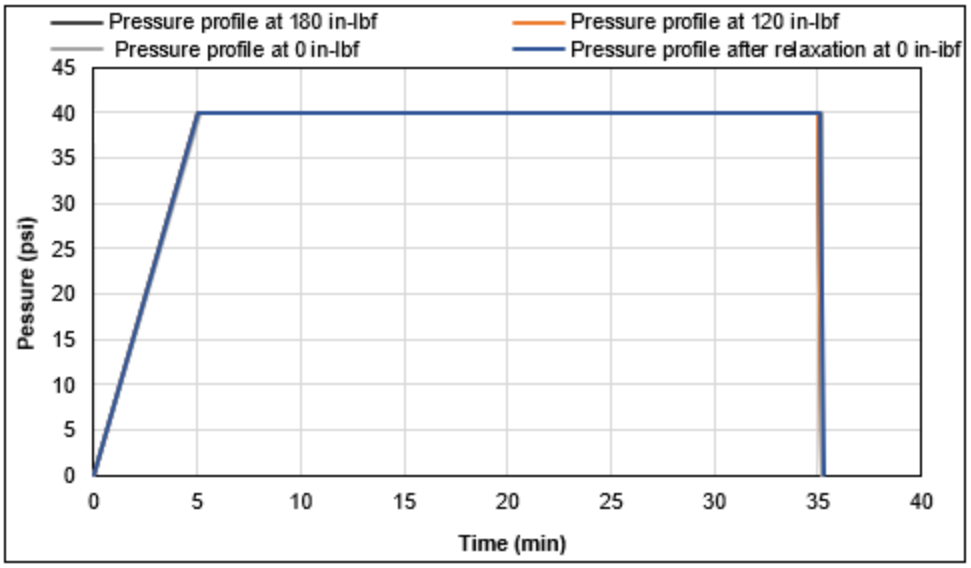

Figure 4.11: EPDM pressure test at different torques and 30 minutes

The same tests using similar procedure was conducted for 60 minutes. Figure 4.12 shows that for all the energization conditions and under normal condition, no leak was recorded within 60 minutes of pressure test. The elastomers exhibited good sealing capacity up to 40 psig. The result obtained from this test confirmed the claim made by Hopkins (2016). The author suggested that overall, expanding the test holding time to 60 minutes does not improve leak detection and safety because in field operations, pressure test failures can be detected very quickly. While this may be true, the analytical results from setup I supports increase in pressure test time as liner-casing overlap length increases. This has been discussed in the section 2 of this report and in the draft recommendation document.

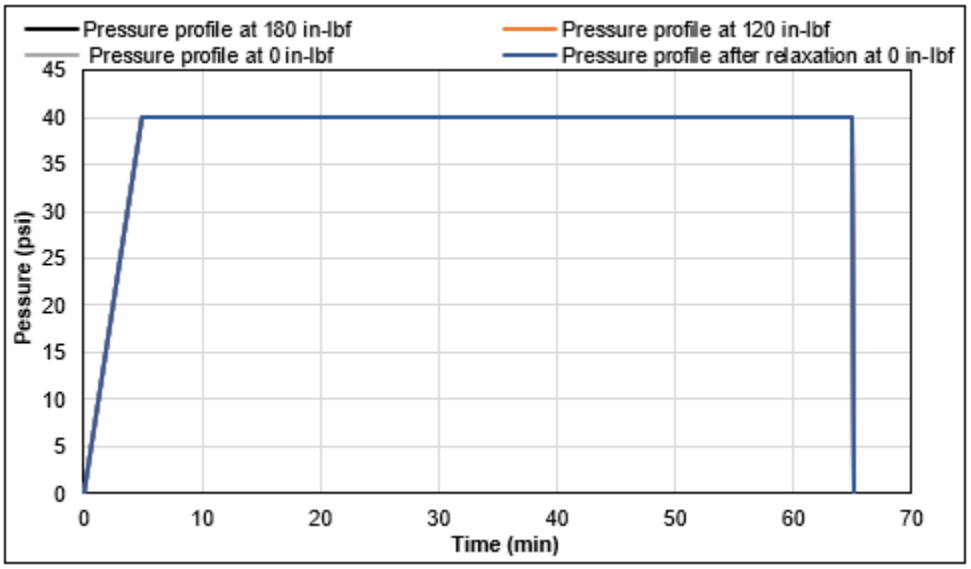

Figure 4.12: EPDM pressure test at different torques and 60 minutes.

EPDM Pressure Cycling Test

The objective of exposing the elastomers to a pressure cycling test was to assess their sealing capacity and failure modes when they encounter high pressure shifts and cycles in field applications. Dusseault et al. (2014) claimed that production, injection, stimulation, and other operations may result in cyclic pressure and/or thermal stresses. Four pressure cycling tests were conducted after the following torque/energization: 180 in-lbf, 120 in-Ibf, 0 in-Ibf, and one-week relaxation with 0 in-lbf. In each test, the cycle was repeated 10 times and the pressure profiles are shown in Figure 4.13. No leak was observed during these tests as shown from the stability of the pressure profiles over the holding periods (10 minutes), which implies proper sealing.

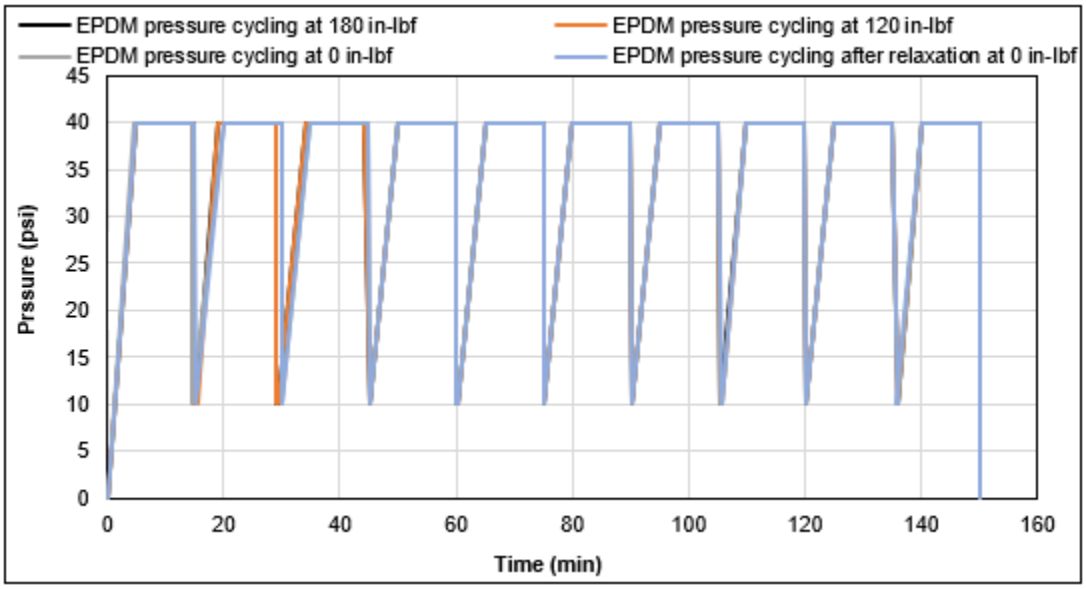

Figure 4.13: EPDM pressure cycling test at different torques.

NBR Pressure Tests for 30 and 60 Minutes Holding Times

NBR samples were subjected to 30 and 60 minutes pressure test using the same energization from the EPDM tests. Figure 4.14 shows that from 5 minutes to 35 minutes, there was no pressure fluctuation nor decline. This result holds for all the energization conditions. No leak was recorded which confirmed that the NBR samples provided good sealing up to 40 psig. The same tests were repeated for 60 minutes holding period. The pressure profiles shown in Figure 4.15 appeared to be steady throughout the holding time. No leak was recorded which implies that the NBR samples provided good sealing for the test conditions.

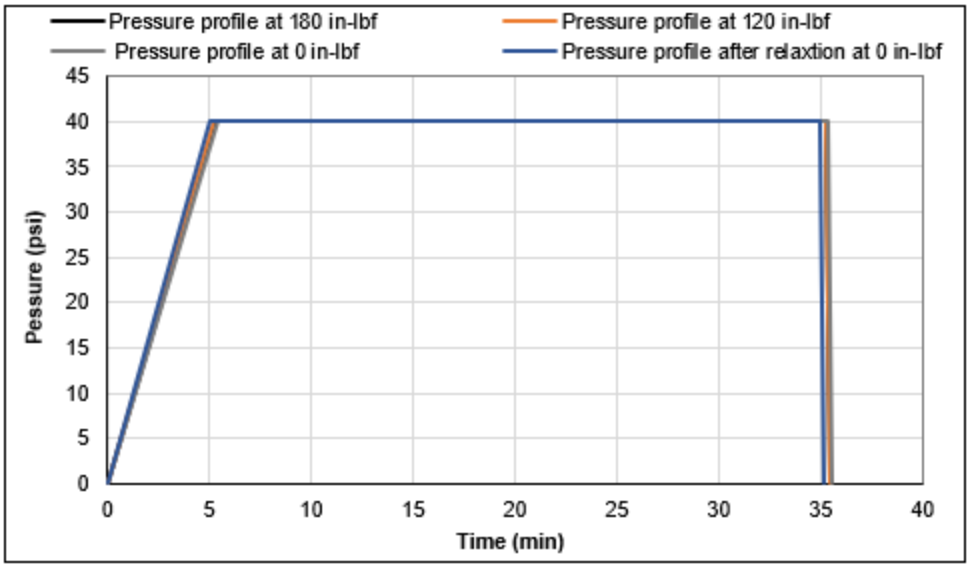

Figure 4.14: NBR pressure test at different torques and 30 minutes

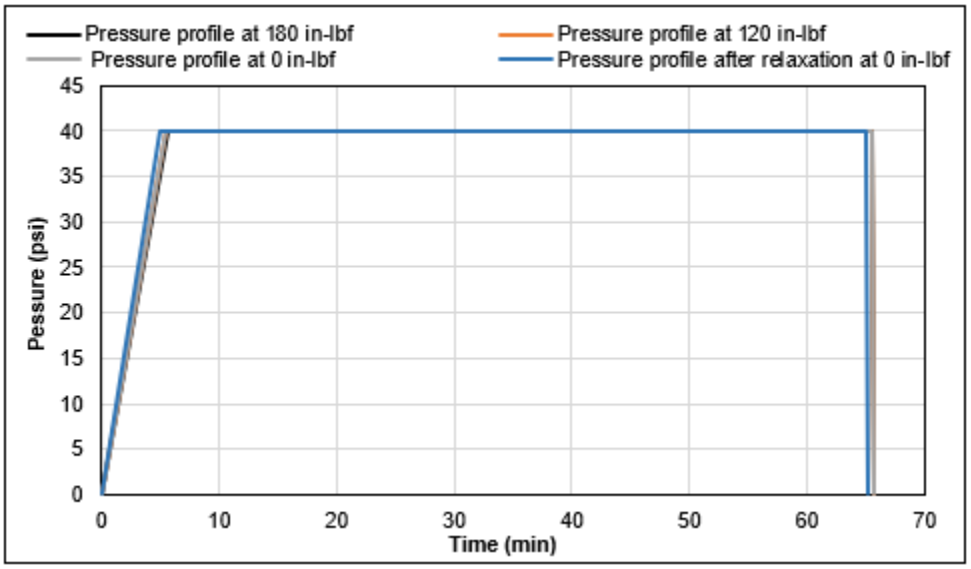

Figure 4.15: NBR pressure test at different torques and 60 minutes

NBR Pressure Cycling Test

NBR samples were subjected to pressure cycling tests. Figure 4.16 shows no leak was recorded during the first and second tests (180 in-lbf and 120 in-Ibf). The minor deviations in the 8th and 9th cycles were from pressuring up and pressure release, which had no effect on the elastomers sealing performance. However, a leak appeared in the form of a blowout during the zero-torque test condition. This is shown in Figure 4.17 (b). The sealing integrity was first compromised at the end of the 3rd cycle (first leak) as shown in Figure 4.18. Although the last three cycles in this figure showed a stable pressure profile, the four subsequent cycles before these last three cycles further compromised the elastomers sealing performance, with 4.5 minutes as the minimum holding time.

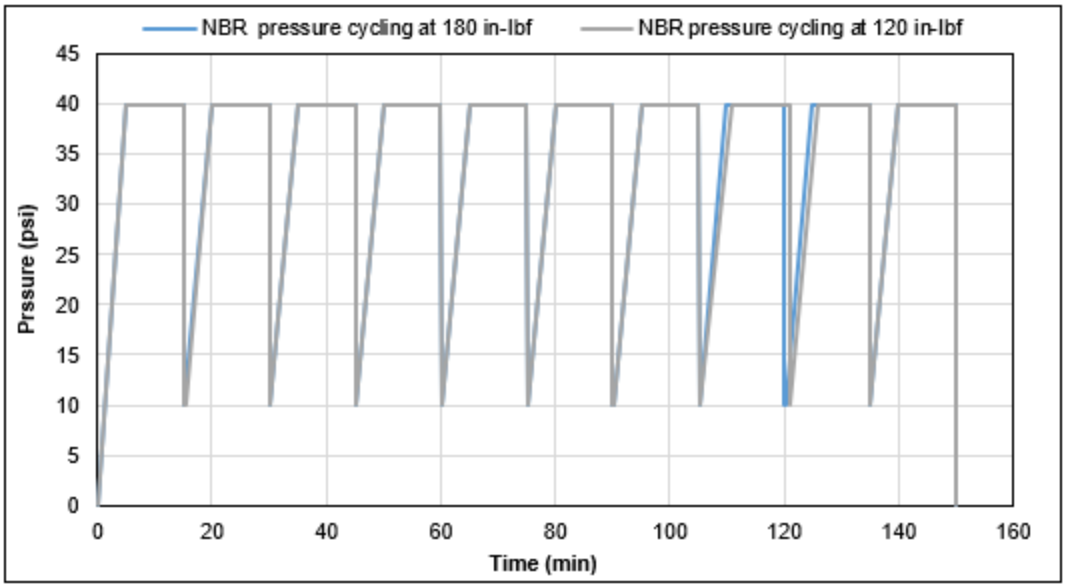

Figure 4.16: NBR pressure cycling test at 180 in-lbf and 120 in-lbf (successful tests).

(a) **(b)**

Figure 4.17: NBR before (a) and after (b) failure during pressure cycling

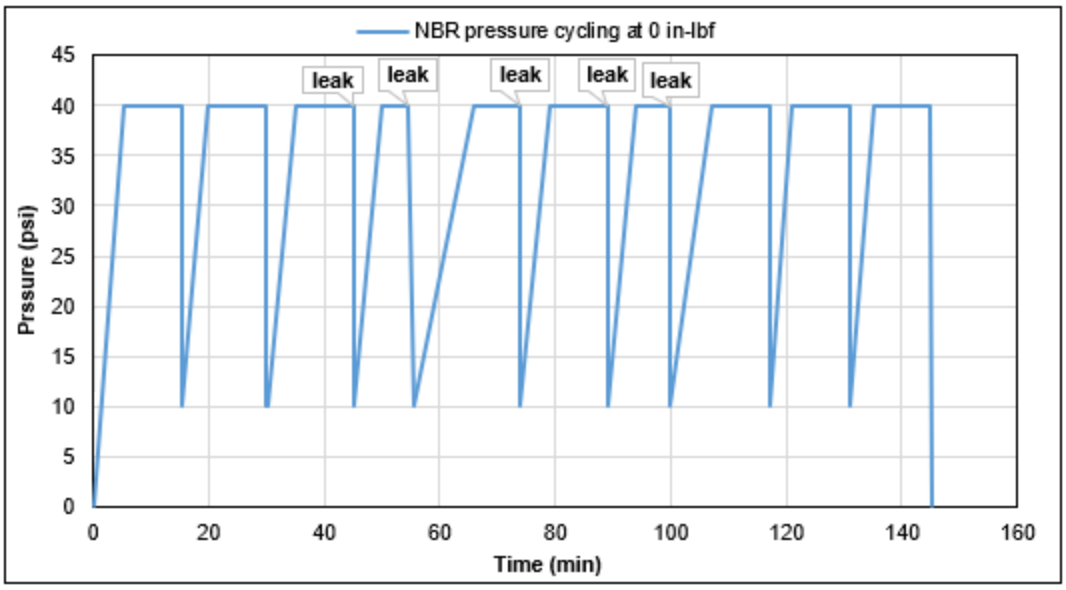

Figure 4.18: NBR pressure cycling test at zero torque (failed test).

After one week of relaxation, pressure cycling tests were performed without torque and as expected, NBR's sealing performance was much inferior. Figure 4.19 shows that the elastomers failed within 2.5 minutes of the second cycle. Other subsequent cycles were incomplete because leaks kept appearing. The sealing integrity worsened towards the end of the pressure cycling test. The practical implication is that at low or no energization, elastomer seals can lose their contact pressure with the casing/liner during pressure cycling activities. This can allow formation fluid influx. To verify this, the torque was increased to 60 in-lbf and the number of failed cycles reduced. The leak completely stopped after the torque was increased to 120 in-Ibf. Overall, the EPDM samples exhibited better sealing properties than the NBR samples and the influence of energization was more evident in the NBR performance.

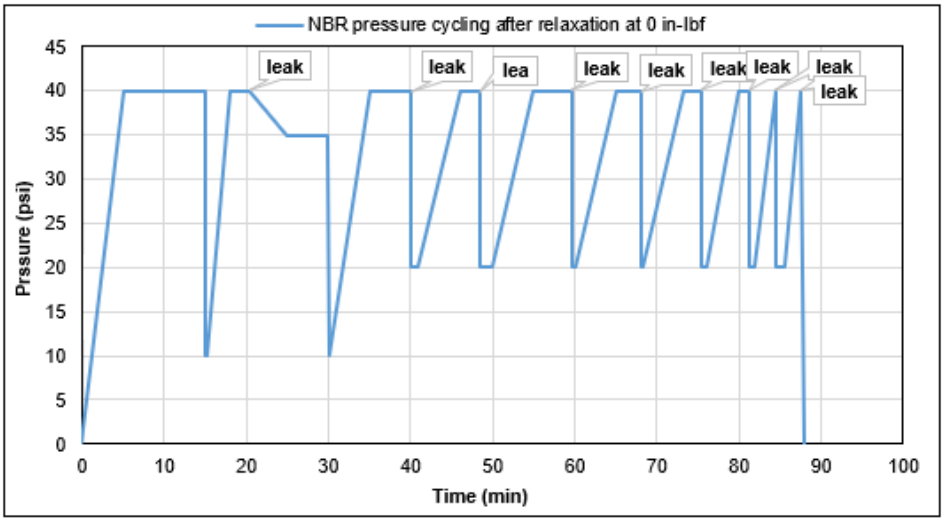

Figure 4.19: NBR pressure cycling test after one-week relaxation (failed test).

4.4.1.2 Pressure Tests After Chemical Degradation

The objective of performing the tests under this section was to evaluate the effect of chemical degradation on the elastomers sealing performance. Both elastomers were exposed to a surfactant that is typically used in non-aqueous fluid for one week at atmospheric temperature and pressure. No torque was applied during elastomer installation because of their significant swelling after been removed from the surfactant. The elastomers swelling added to the difficulty experienced during the installation and their contact pressure was increased because of the high friction force between them and the pipes walls. In addition, EPDM samples were also degraded with CO_2.

EPDM Tests for 30 and 60 Minutes Holding Times

EPDM elastomers were tested at 40 psig and 30 minutes holding time after surfactant exposure. The test was repeated for two consecutive days and the pressure profiles shown in Figure 4.20 revealed no leak or pressure drop. The test was repeated for 60 minutes as shown in Figure 4.21 and the same trend of no leak was observed. Although, a decrease in hardness from 75 durometer points to 63.75 durometer points was recorded, the elastomers diameters increased from 8.74 inches to 8.82 inches and thickness increased from 0.75 inches to 0.78 inches. One plausible explanation for their sealing performance is the increase in contact pressure between the sealing interfaces (elastomer and pipe walls) because of the volumetric swelling.

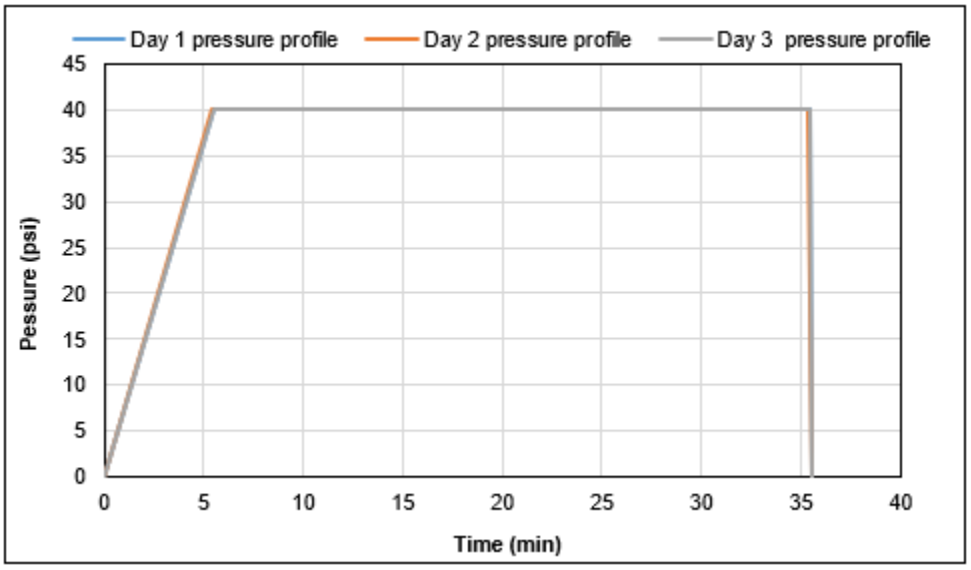

Figure 4.20: EPDM pressure test at Day 1, Day 2 and Day 3 after exposure to a surfactant (30 minutes).

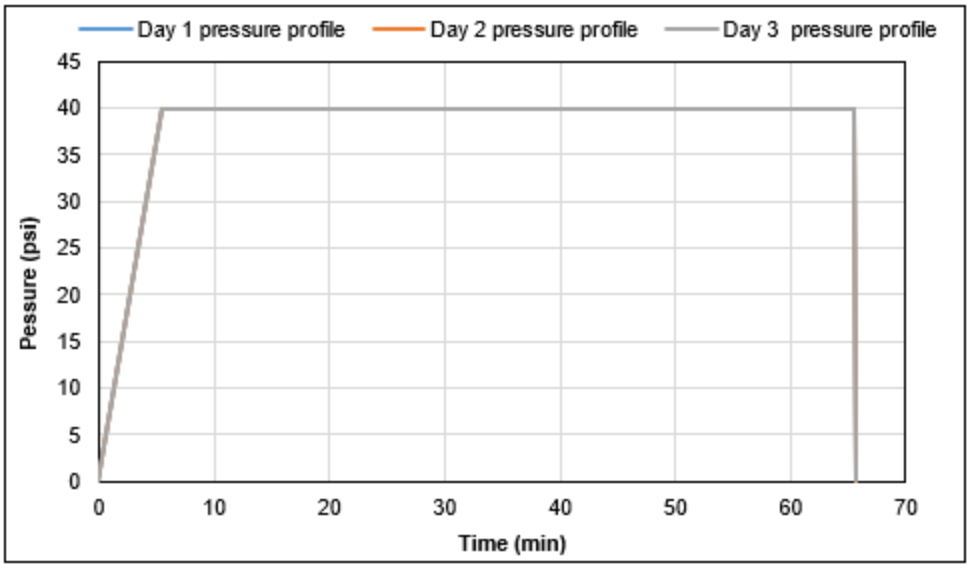

Figure 4.21: EPDM pressure test at Day 1, Day 2, and Day 3 after exposure to a surfactant (60 minutes)

EPDM Pressure Cycling Test

Pressure cycling tests were performed at day 1, day 2, and day 3 to assess its impact on EPDM performance. The results shown in Figure 4.22 reveals the stability and sealing performance of EPDM for the 10 cycles.

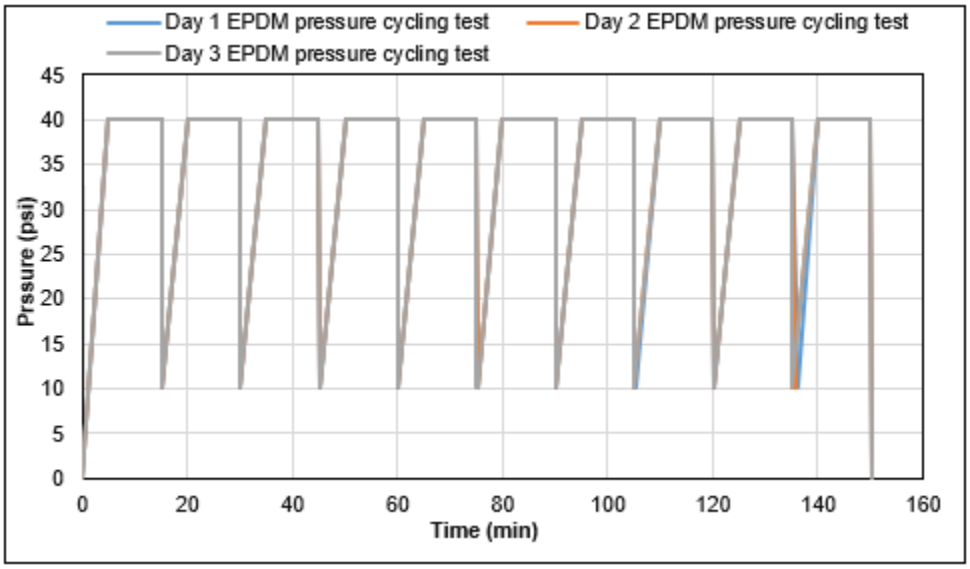

Figure 4.22: EPDM pressure cycling test at Day 1, Day 2, and Day 3 after exposure to surfactant.

NBR Pressure Tests for 30 and 60 Minutes Holding Times

Pressure tests were conducted on NBR samples for 30 minutes and 60 minutes using the same procedure and consecutive intervals (days) for EPDM. No torque was applied because of the

volumetric swelling of NBR which was more significant than EPDM. The NBR samples diameters increased from 8.74 inches to 8.94 inches and thickness increased from 0.75 inches to 0.87 inches Figure 4.23 and Figure 4.24 shows the pressure profiles for 30 minutes and 60 minutes pressure tests respectively. No leaks were recorded and the increase in duration did not have any effect on NBR's sealing performance.

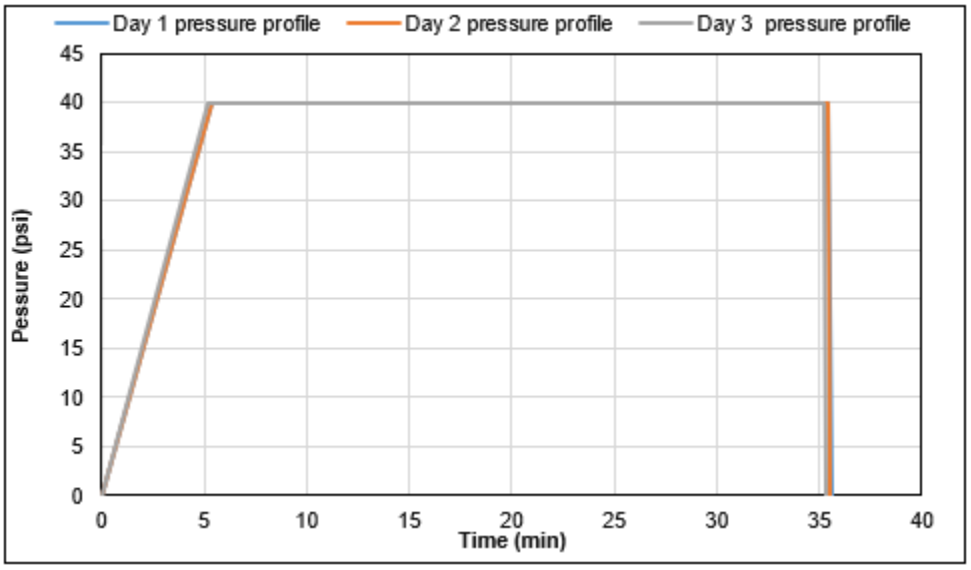

Figure 4.23: NBR pressure test at Day 1, Day 2, and Day 3 exposure to a surfactant (30 minutes).

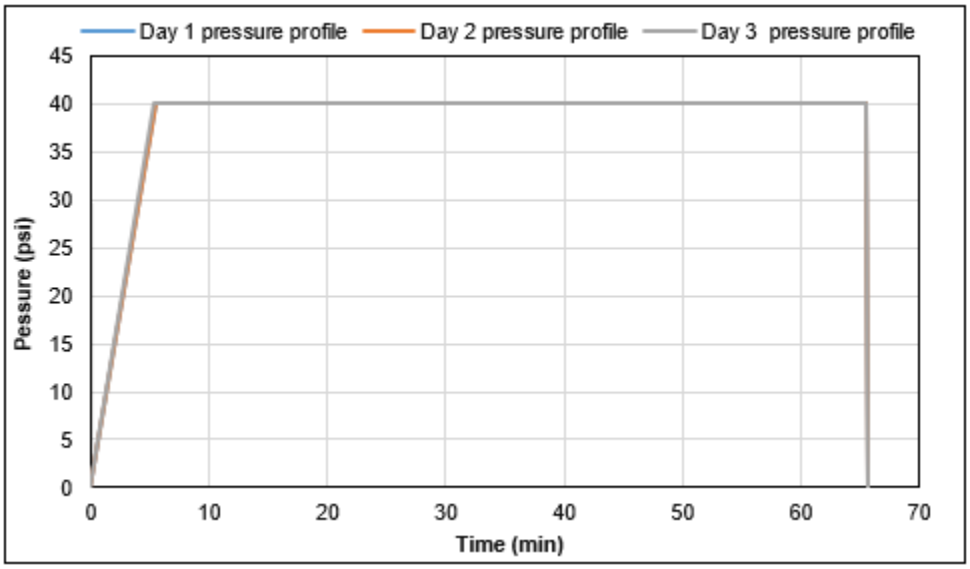

Figure 4.24: NBR pressure test at Day 1, Day 2, and Day 3 after exposure to a surfactant (60 minutes).

NBR Pressure Cycling Test

NBR Pressure cycling tests were performed on day 1, day 2, and day 3 to evaluate its performance after exposure to a surfactant. The surfactant decreased NBR's hardness from 66 durometer points to 44 durometer points; however, their contact sealing was improved because of better energization

created from the elastomer and pipe high friction force. Figure 4.25 shows that no leak was recorded during the pressure cycling test.

It is worthy to mention that while the volumetric swelling of the elastomers may appear to be good as it provided adequate contact between the sealing interfaces that prevented leaks, it should be noted that the pressure tests were performed at room temperature. In addition, the elastomers were exposed to the surfactant at room temperature and pressure. Chemical attacks on elastomers can be accelerated at temperatures beyond ambient. These attacks and alteration of molecular structure can be exacerbated at elevated temperatures; thus, reducing the elastomers sealing performance. In addition, the inert nature of N_2 may have also masked the impact of surfactant degradation at room temperature. Other downhole corrosive gases such as H_2S can have more detrimental impact. These have been discussed in the elastomer aging tests section (3) of the report.

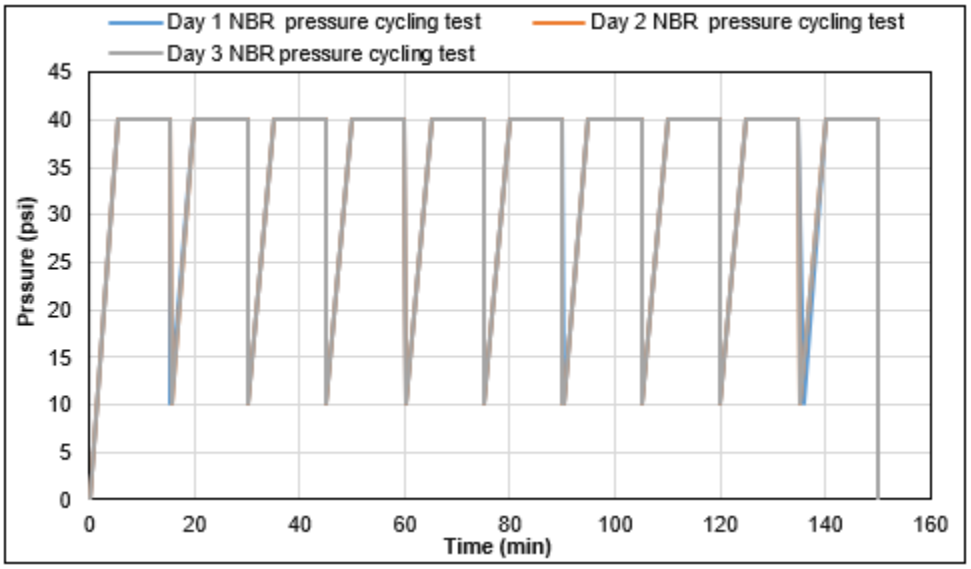

Figure 4.25: NBR pressure cycling test at Day 1, Day 2 and Day 3 after exposure to a surfactant.

EPDM Pressure Tests After CO_2 Degradation

To evaluate the sealing performance of elastomers when they are exposed to other forms of chemical degradation besides a surfactant, EPDM samples were aged for three days with CO_2 at room temperature and 600 psig. After aging, blisters and cracks were created on the elastomers surface. Two pressure tests were conducted: without torque and at 180 in-lbf. In both tests, the elastomers lost their sealing integrity and a leak was observed within few seconds of commencing each test. Figure 4.26 and Figure 4.27 illustrates the EPDM failed pressure tests (no torque) after CO_2 exposure and degradation. After 5 minutes of pressuring up, Figure 4.26 shows an instantaneous pressure decline (within 5 to 6 seconds), which becomes more evident as pressure increases. This is supported by Figure 4.27 which shows that as pressure increase, the first bubble leak time decreases. Figure 4.28 and Figure 4.29 indicates that increasing the torque had little to

no effect in preventing the leaks. Similar instantaneous pressure decline was recorded at 180 in-lbf. The effect of torque may have been slightly observed as the first bubble time (10 psig) in Figure 4.29 was later than the first bubble time (10 psig) in Figure 4.27. However, this time difference (0.017 seconds) is quite small, in addition to the small pressure at which this difference was recorded. Overall, the results from these pressure tests validates the detrimental effect of CO_2 degradation compared to surfactant degradation. While both chemical degradations revealed an increase in volumetric swelling because of elastomer chain rupture, CO_2 degradation created visible cracks and blisters. Its molecular structure allows it to penetrate the elastomer chains more (compared to surfactant) such that during decompression (normal or explosive), it results in physical damages shown on the elastomers surface. This explains EPDM's inferior performance during the pressure tests performed under this section.

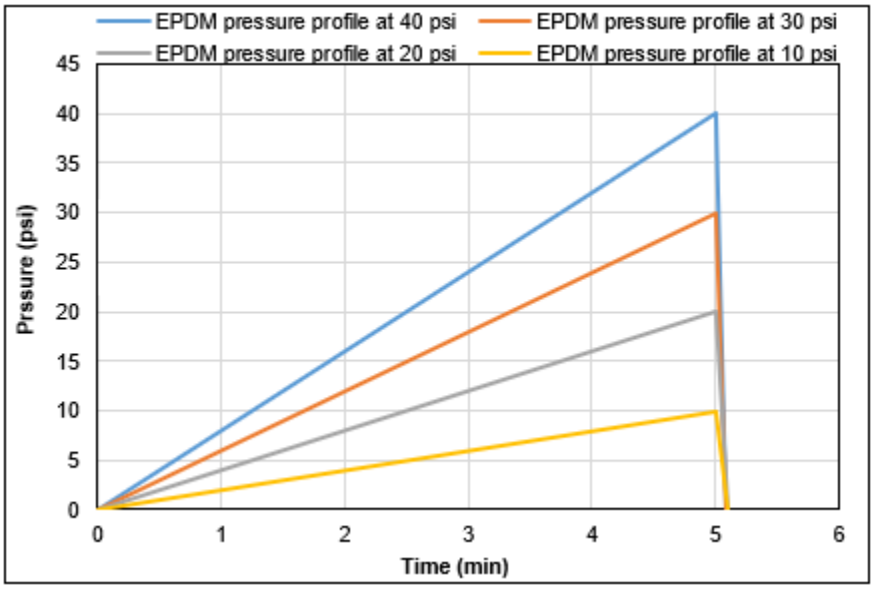

Figure 4.26: EPDM 30-minutes pressure test after CO_2 degradation without applying torque.

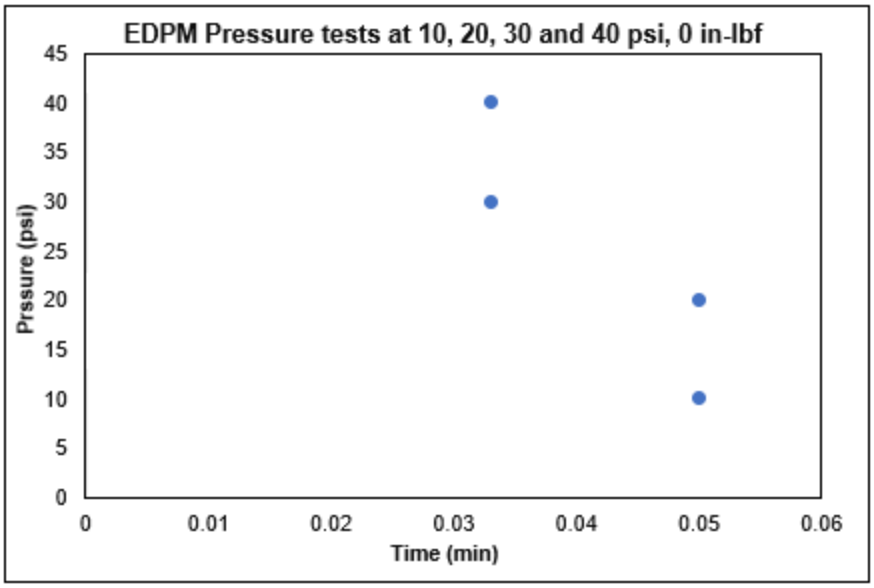

Figure 4.27: First bubble times for EPDM pressure test after CO_2 degradation without applying torque.

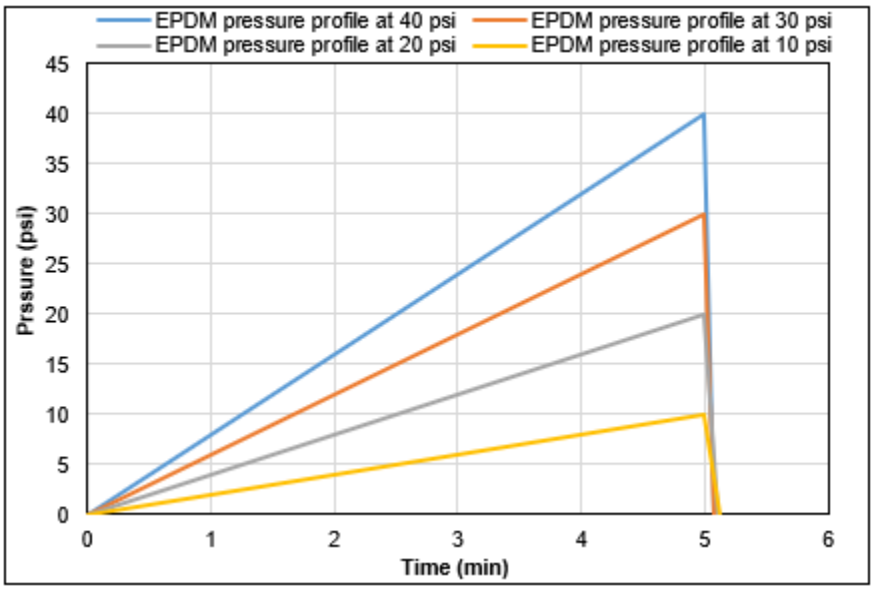

Figure 4.28: EPDM 30-minutes pressure test after CO_2 degradation and applying 180 in-lbf

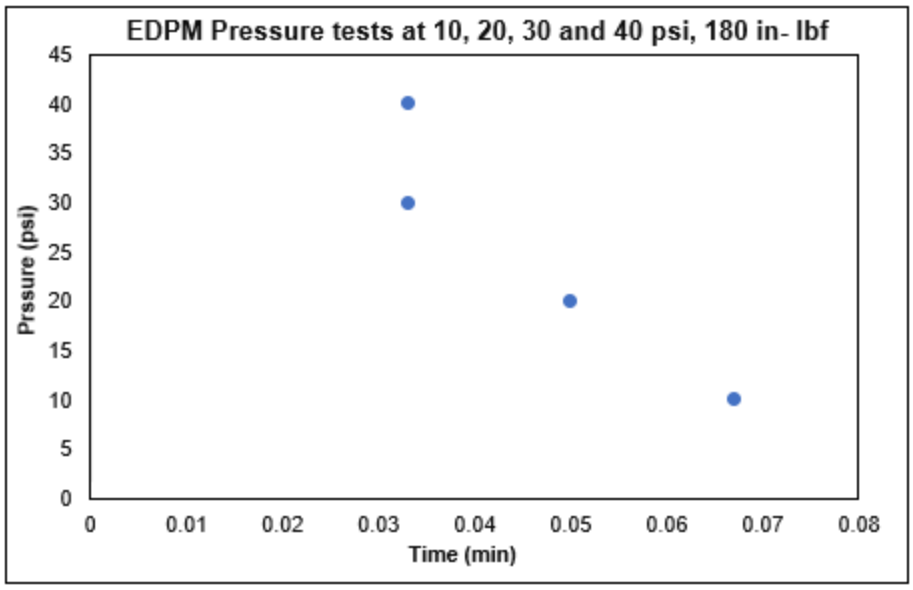

Figure 4.29: First bubble times for EPDM pressure test after CO_2 degradation and applying 180 in-lbf

4.4.1.3 Pressure Tests After Physical (Mechanical) Defect

In this section, seams were intentionally created on the elastomers surface to assess the influence of defects or imperfections that may arise from manufacturing, handling, and/or installation. For both the EPDM and NBR samples, the seams were created similarly in terms of size and area as shown in Figure 4.8. The elastomers were torqued up to 180 in-lbf and the pressure tests were performed at 10, 20, 30, and 40 psig.

EPDM Pressure Tests for 30 Minutes

To improve the leak surveillance, the tests were conducted at different pressures beginning with 10 psig (considered as low pressure). Besides, the results from the pressure tests after CO_2 degradation informed the decision to test at different pressures and only for 30 minutes. Figure 4.30 is the pressure profile for the 30 minutes test. It reveals pressure decline because the physical defects on the EPDM samples compromised their sealing integrity. The figure also shows that this pressure decline is more evident as pressure increases. Figure 4.31 shows the time of the first bubble leak which was approximately 12 seconds into the 40-psig test. This figure also validates the evident pressure decline with an increase in pressure (Figure 4.30), because the first bubble leak time (Figure 4.31) increases as pressure decreases.

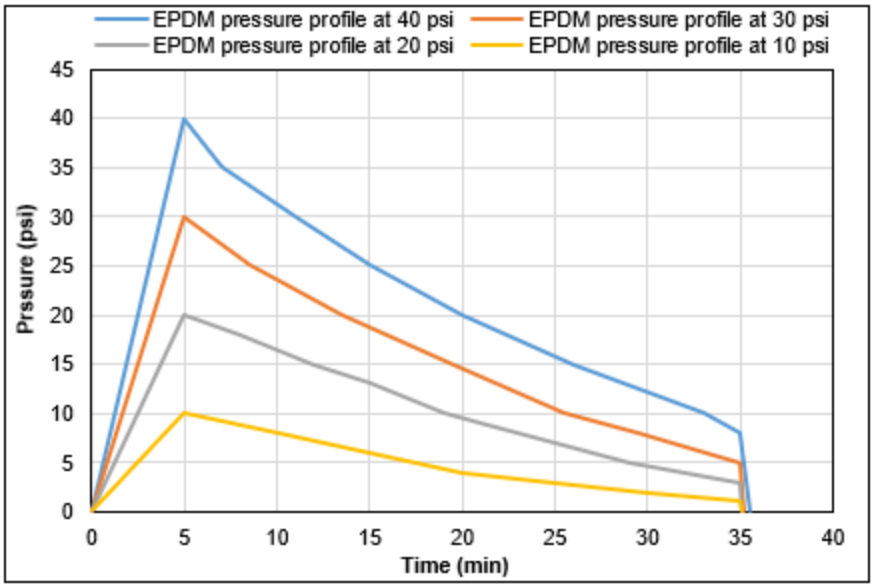

Figure 4.30: EPDM pressure test after physical defects.

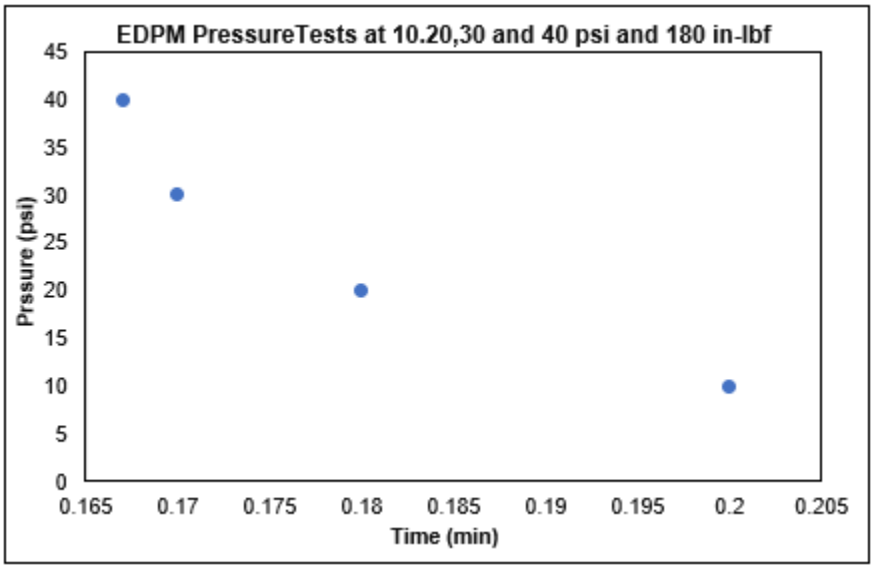

Figure 4.31: First bubble leak times for different pressure tests on EPDM samples after physical defects.

NBR Pressure Tests for 30 Minutes

The NBR samples were subjected to the same pressure tests and methods used for the EPDM samples. Figure 4.32 shows that the elastomers did not hold pressure and that pressure declines become obvious with an increase in pressure. Figure 4.33 shows that the first leaks for 20, 30, and 40 psig tests appeared approximately after 5 seconds.

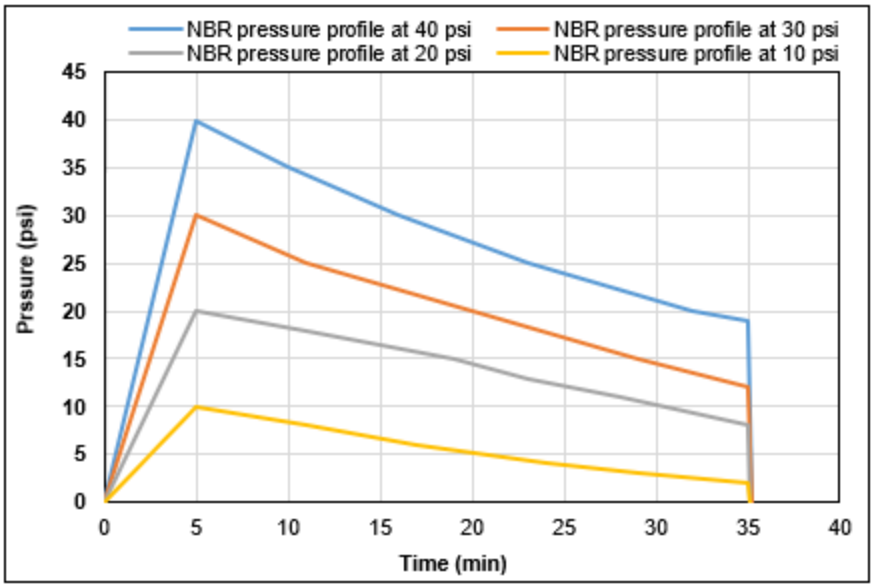

Figure 4.32: NBR pressure test after physical defects.

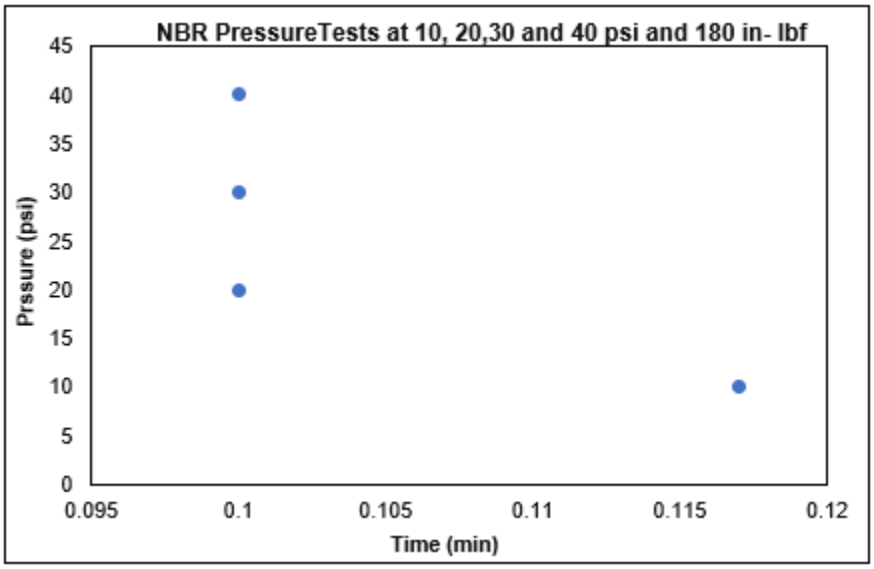

Figure 4.33: First bubble leak times for different pressure tests on NBR samples after physical defects

Comparing the pressure test performances of both elastomers after physical defects, it can be inferred that NBR showed better performance than EPDM. Although, it is possible to argue that the first bubble leak times at 40 psig for EPDM and NBR were 12 and 6 seconds respectively. In addition, the first bubble leak times from the NBR tests were generally smaller (first bubble appear faster) that those from the EPDM test. While the first bubble leak times are important for leak identification, the pressure decline appears to be of much greater concern. Figure 4.34 compares the 40-psig pressure tests of both samples under similar conditions (identical seams, heights, and diameters). The pressure decline from the EPDM test was steeper compared to the decline from the NBR test. This is attributed to its improved energization with an approximate displacement of

0.1 inch compared to 0.06 inch for EPDM under the same torque. The practical implication of this is that gas migration rate may be faster through a mechanically defaced EPDM barrier compared to NBR.

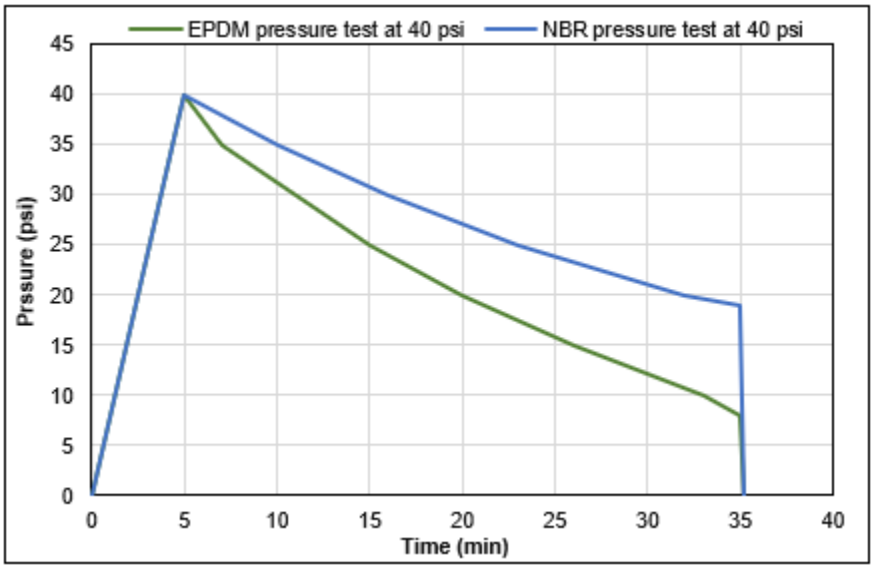

Figure 4.34: Comparison between EPDM and NBR 40 psig pressure tests after physical defects.

Figure 4.35 compares all the 30-minutes and 40-psig tests for all the conditions (normal, surfactant degradation, physical degradation) at 180 in-lbf. The elastomer samples performed well under normal conditions and after surfactant degradation. However, the EPDM test after CO_2 degradation showed instantaneous failure of the elastomer; thus, it was not included in this figure. Both elastomers' performances were compromised from the physical defect. Practically, all sealing elements used in liner hangers should be tested for the anticipated wellbore conditions before they are deployed.

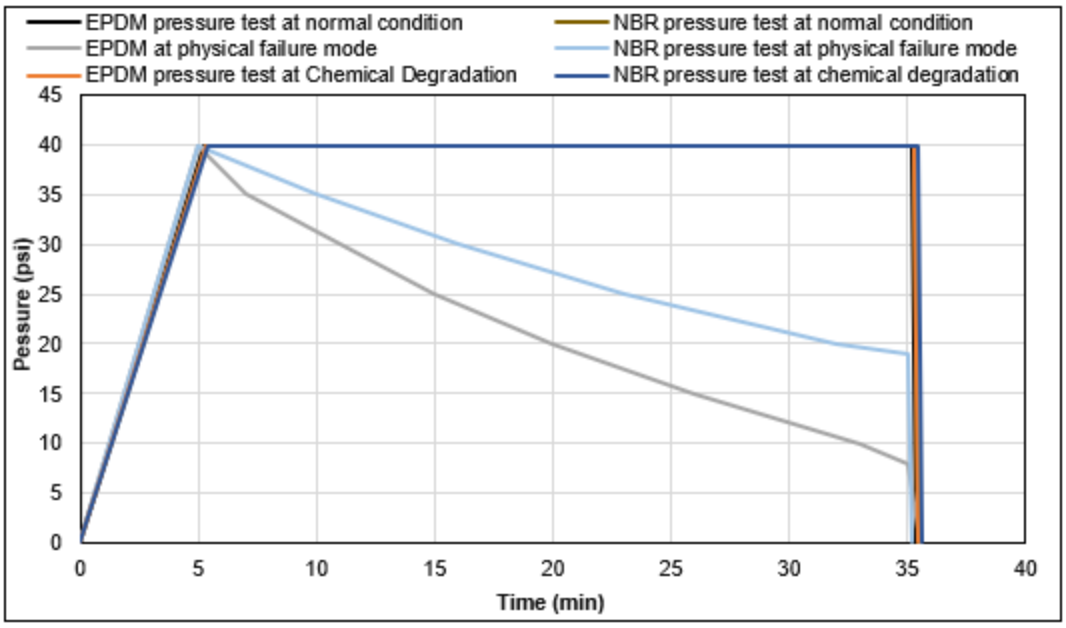

Figure 4.35: Comparison of EPDM and NBR 40 psig pressure test performances at different conditions (normal, surfactant degradation, and physical defect) at 180 in-lbf.

4.5 SUMMARY AND CONCLUSIONS

The following conclusions and summaries have been drawn from the theoretical and experimental investigations, results, and analyses conducted in this section of the report:

- Pressure tests are an effective tool to evaluate and compare the performance of the seals. Under normal condition, both EPDM and NBR elastomers exhibited good sealing capacity for 30 minutes holding time.
- Prolonging the pressure test duration from 30 minutes to 60 minutes may not assist in better evaluation of elastomers as an independent barrier.
- The independent sealing performance of EPDM and NBR after surfactant degradation was not impaired for the test conditions used in this study.
- The independent sealing performance of EPDM was completely compromised after CO_2 chemical degradation. The pressure tests showed instantaneous decline with no sealing effect.
- Physical damage from a manufacturing, handling and/or installation process impacts elastomers sealing performance. EPDM and NBR failed the pressure test after physical defects were created intentionally.
- Elastomer energization plays a critical role in maintaining their seal integrity. EPDM and NBR showed good performance at 180 in-lbf and 120 in-lbf during the pressure cycling test. EPDM performed better than NBR without torque. Pressure cycling showed that pre-compression of EPDM was enough to maintain the elastomers seal performance compared to NBR.

ACKNOWLEDGEMENTS

We thank BSEE for funding this work and providing research team with valuable feedback.

NOMENCLATURE

Acronyms

ACN		Acrylonitrile
API		American Petroleum Institute
ASTME		American Society of Tool and Manufacturing Engineers
AT		Aging test
BOP		Blow out preventer
BSEE		Bureau of Safety and Environmental Enforcement
DAQ		Data Acquisition
EDS		Energy dispersive spectroscopy
EPDM		Neoprene ethylene propylene diene monomer
FEPM		Fluorocarbon/ Tetrafluoro ethylene/ Propylene rubber
FFKM		Perfluoroelastomer
FKM		Fluoroelastomer
HFA		Hydraulic fluid
HNBR		Hydrogenated Nitrile Butadiene Rubber
ID		Internal diameter
NAF		Non-aqueous fluid
NBR		Nitrile Butadiene Rubber
NCS		Norwegian Continental Shelf
NVR		Network Video Recorder
OD		Outer Diameter
PDM		Positive displacement motor
PTFE		Polytetrafluoroethylene
RGD		Rapid gas decompression
SAP		Super absorbent polymer
SEM		Scanning electron microscope
W/C	–	Water to cement ratio
WOC	–	Wait on cement
WT	–	Wall thickness (cm)

Symbols

A	Annulus area (cm^2 in equation 1.3 and m^2 in equation 1.4)
A_m	Area involved in the flow (m^2)
atm	Atmospheric
cc	Cubic centimetre
C_g	Gas compressibility (cm^2/dyne)
cP	Centi-Poise
°F	Degree Fahrenheit
ft	Foot
h	Hydraulic aperture (m)
hp	Horsepower
hrs	Hours
in	inch
K	Permeability (mD in equation 1.3 and m^2 in equations 1.4 and 1.8)
˚K	Degree Kelvin
L	Length of cement column (cm in equation 1.3 and m in equation 1.4)
L_c	Liner- casing overlapping length (m)
lbf	pound force
M	Molecular weight (kg/mol)
m^2	Square meters
mD	millidarcy
ml	millilitre
mol	Mole
N_2	Nitrogen Gas
n_j	Number of bubbles at position j
P_1	Inlet pressure (psi)
P_2	Cell pressure (psi)
P_a	Pascal
P_b	Base pressure (atm)
P_d	Downstream pressure (psig)
P_i	Inlet pressure (atm)
P_o	Outlet pressure (atm)
ppg	Pound per gallon
ppm	parts per million
ppt	parts per thousand
psia	Pound per square inch absolute
psig	Pound per square inch gauge
P_u	Upstream pressure (psi)
$P_{u\,(i)}$	Initial upstream pressure (psi)
$P_{u\,(t)}$	Upstream pressure at time t (psi)

q_g	Gas flow rate (cc/sec in equations 1.1, 1.2, and 1.3 and m^3/sec in equation 1.4)
q	Gas flow rate (m^3/sec)
R	Universal gas constant (m^3. Pa/mol.˚K)
r_1	Radius of the inner pipe
r_2	Radius of the annular gap
t	Time (sec)
T	Temperature (˚K)
T_g	Glass transition temperature
V	Upstream volume (cc)
V_j	Volume of bubbles at position j (cc)
Z	Gas compressibility factor

GREEK SYMBOLS

σ	shear stress
$\dot{\gamma}$	shear rate
K	flow consistency index
n	flow behavior index
μ	Gas viscosity (cP in equation 1.3 and Pa-sec in equation 1.4)
β	Inertial coefficient (m)
ρ	Gas density (kg/m^3)
ω	Length of hydraulic aperture (m)

REFERENCES

1. Abbas, G., Irawan, S., Kumar, S. et al. 2013. Gas Migration Prevention Using Hydroxypropylmethylcellulose as a Multifunctional Additive in Oil Well Cement Slurry. Prese ted at SPE/PAPG Annual Technical Conference, Islamabad, Pakistan, 26-27 November. Society of Petroleum Engineers. SPE-169643-MS. https://doi.org/10.2118/169643-MS
2. Adams, N. J. and Kuhlman, L. G. 1990. Case History Analyses of Shallow Gas Blowouts. Presented at the IADC/SPE Drilling Conference, Houston, Texas, 27 February - 2 March. IADC/SPE 19917. SPE-19917-MS. http://dx.doi.org/10.2118/19917-MS
3. Aggelen, A. 2016. Functional Barrier Model-A Structural Approach to Barrier Analysis. Presented at the SPE Annual Technical Conference and Exhibition on Heath, Safety, Security, Environment, and Responsibility, Stavanger, Norway, 11-13 April. SPE-179214-MS. https://doi.org/10.2118/179214-MS
4. Ahmed, R. M., Takach, N. E., Khan, U. M. et al. 2009. Rheology of Foamed Cement. *Cement and Concrete Research*: **39**(4), 353-361. http://dx.doi.org/10.1016/j.cemconres.2008.12.004
5. Al-Buraik, K., Al-Abdulqader, K., and Bsaibes, R. 1998. Prevention of Shallow Gas Migration Through Cement. Presented at IADC/SPE Asia Pacific Drilling Technology, Jakarta, Indonesia, 7-9 September. SPE-47775-MS. https://doi.org/10.2118/47775-MS

6. AlMusa, A. S., Obi, I. I., and Garcia, J.S. 2017. Expandable Liner Deployment Remedies Premature Casing Point in an Offshore Gas Well. Presented at the Abu Dhabi International Petroleum Conference & Exhibition, Abu Dhabi, USE, 13-16 November. SPE-188721-MS. https://doi.org/10.2118/188721-MS.
7. Amyot, O., Flukiger. F, Geoffory, S. et al. Critical Point Network for Drainage between Rough Surfaces. 2007.*Transport in Porous Media* **70** (2): 257-277. DOI: 10.1007/s11242-007-9098-3.
8. Al-Yami, A., Mukherjee, T. S., Riskiawan. A. et al. 2017. Optimum Practices to Mitigate Gas Migration Problems in Deep Gas Wells. Presented at the SPE Russian Petroleum Technology Conference, Moscow, Russia, 16-18 October. SPE-187700-MS.
9. https://doi.org/10.2118/187700-MS.
10. Al-Yami, A. S., Nasr-El-Din, H. A., and Al-Humaidi, A. S. 2009. An Innovative Cement Formula to Prevent Gas-Migration Problems in HT/HP Wells. Presented in SPE International Symposium on Oilfield Chemistry, The Woodlands, Texas, 20-22 April. SPE-120885-MS. https://doi.org/10.2118/120885-MS
11. *API RP 19 LH, Recommended Practice for Liner Hangers*, First Draft.
12. *API RP 96, Recommended Practice for Deepwater Well Design and Construction*, first edition .2013. Washington, DC: API.
13. *API RP 10B-2, Recommended Practice for Testing Well Cements,* second edition. 2013. Washington, DC:
14. API. *API RP 10A, Specification for Cements and Materials for Well Cementing,* 24th edition. 2010. Washington, DC: API.
15. *API RP 65-Part 2, Standard for Isolating Potential Flow Zones During Well Construction* second edition .2010. Washington, DC: API.
16. *API STD 65, Standard for Cementing Shallow Water Flow Zones in Deepwater Wells* first edition .2002. Washington, DC: API.
17. API *BULLETIN E3, Environmental Guidance Document: Well Abandonment and Inactive Well Practices for U.S. Exploration and Production Operations,* First Edition. 1993. Washington, DC: API.
18. *ASTM D575-91, Standard Test Methods for Rubber Properties in Compression* .2012. West Conshohocken, PA: ASTM International.
19. Badrak, R. P. 1994. Effects of New Generation Drilling Fluids on Drilling Equipment Elastomers. Presented at SPE/IADC Drilling Conference, 15-18 February, Dallas, Texas. SPE-27452-MS. http://dx.doi.org/10.2118/27452-MS
20. Bauer, P. 1965. Investigation of Leakage and Sealing Parameters. Technical Report AFRPL - TR-153, IIT Research Institute, Air Force Propulsion Laboratory, Air Force System Command, Edwrads, Califiornia (August 1965).
21. Bannister, C. E., Shuster, G. E., Wooldridge, L. A. et al. 1983. Critical Design Parameters to Prevent Invasion During Cementing Operations. Presented at SPE Annual Technical Conference and Exhibition, San Francisco, California, 5-8 October. SPE-11982-MS. https://doi.org/10.2118/11982-MS

22. Beirute, R. M. and Cheung, P. R. 1990. Method for Selection of Cement Recipes to Control Fluid Invasion after Cementing. *SPE Prod Eng*. SPE-19522-PA. https://doi.org/10.2118/19522-PA
23. Bogaerts, M., De Bruijn, G. G., Khalilova, P. R. et al. 2012. Identifying and Mitigating the Risks of Shallow Flow in Deepwater Cementing Operations. Presented at SPE Deepwater Drilling and Completions Conference, Galveston, Texas, 20-21 June. SPE-155733-MS. https://doi.org/10.2118/155733-MS
24. Bois, A., Vu, M., Galidiolo G. et al. 2017. Use of Advanced Gas Migration Model to Optimize Zonal Isolation. AADE-17-NTCE-104. http://www.aade.org/technical-papers/2017-national-technical-conference-papers/
25. Bois, A.P., Garnier, A., Rodot, F. et al. 2011. How to Prevent Loss of Zonal Isolation Through a Comprehensive Analysis of Microannulus Formation. *SPE Drilling & Completion* **26** (1): 13-31. SPE-124719-PA. https://doi.org/10.2118/124719-PA
26. Bortsov V. P., Baluev A. A., and Bastrikov S. N. 1997a. Plugging solution for oil and gas wells – contains portland cement, aluminium powder, fish scale, anionic and nonionic surfactant, plasticiser and water, assigned to Sibe Oil Ind. Res. Inst. 1997. RU patent 2 078 906.
27. Bortsov V. P., Baluev A. A., and Bastrikov S. N. 1997b. Plugging solution for oil and gas wells – contains portland cement, expanding additive, water and additionally aluminium powder, surfactants and plasticiser, assigned to Sibe Oil Ind. Res. Inst. 1997. RU patent 2 082 872.
28. Bosma, M. G. R., Cornelissen, E. K., Cuijpers, J. et al. 2005. System for sealing a space in a wellbore, Patent No. WO2005012686; IPC No. E21B 43/ 10 A I. https://data.epo.org/publicationserver/rest/v1.0/publicationdates/20061018/patents/EP1649136NWB1/document.pdf
29. Bour, D. L. and Wilkinson, J. G. 1992. Combating Gas Migration in the Michigan Basin. *SPE Drill Eng*. SPE-19324-PA. https://doi.org/10.2118/19324-PA
30. Brace, W. F., Walsh, J. B., and Frangos, W. T. 1968. Permeability of Granite Under High Pressure. *Journal of Geophysical Research*. **73** (6): 2225–2236. https://doi.org/10.1029/JB073i006p02225
31. BSEE 2015a, Investigation into the January 30, 2014 Loss of Well Control Lease OCS-G 17921, Vermilion Block 356, Well A-007. OCS report BSEE 2015-01. U.S. Department of the Interior, Bureau of Safety and Environmental Enforcement.
32. BSEE 2015b, Investigation of Loss of Well Control and Fire South Timbalier Area Block 220, Well No. A-3, OCS-G 24980, July 2013. OCS report BSEE 2015-02. U.S. Department of the Interior, Bureau of Safety and Environmental Enforcement.
33. Bureau of Safety and Environmental Enforcement (BESS), Office of Offshore Regulatory Programs.2014. OC-FIT Evaluation of Seal Assembly & Cement Failures Interim Summary of Findings. Internal QC-FIT Report #2014-02 (December 2014). https://www.bsee.gov/sites/bsee_prod.opengov.ibmcloud.com/files/memos/public-engagement/qc-fit-bp-bolts-report-final.pdf

34. Calloni, G., Moroni, N., and Miano, F. 1995. Carbon Black: A Low Cost Colloidal Additive for Controlling Gas-Migration in Cement Slurries. Presented at SPE International Symposium on Oilfield Chemistry, San Antonio, Texas, 14-17 February. SPE-28959-MS. https://doi.org/10.2118/28959-MS
35. Campion, R.P., Thomson, B. and Harris, J.A.2005. Elastomers for Fluid Containment in Offshore Oil and Gas Production: Guidelines and Review. Research Report 320, MERL Ltd, Tamworth Road, Hertford, SG12 7DG.
36. Carey, J. 2013. Geochemistry of Wellbore Integrity in CO_2 Sequestration: Portland Cement-Steel-Brine-CO_2 Interactions. *Reviews in Mineralogy and Geochemistry* **77** (1): 505–539. https://doi.org/10.2138/rmg.2013.77.15
37. Carroll, S., Carey, J., Dzombak, D. et al. 2016. Review: Role of Chemistry, Mechanics, And Transport on Well Integrity in CO2 Storage Environments. *International Journal of Greenhouse Gas Control* **49:** 149-160. https://doi.org/10.1016/j.ijggc.2016.01.010
38. Carroll, T. 2016. Successful selection of oil and gas seals. *World Pumps*: **2016**(9), 28-30. http://dx.doi.org/10.1016/S0262-1762(16)30235-8
39. Carter, L. G., Cook, C., and Snelson, L. 1973. Cementing Research in Directional Gas Well Completions. Presented at the SPE European Meeting, London, United Kingdom, 2-3 April. SPE-4313-MS. https://doi.org/10.2118/4313-MS
40. Chandrasekaran, V. C. 2010. *Rubber Seals for Fluid and Hydraulic Systems*, First edition. Elsevier
41. Chen, X., Bartos, J., Salem, H. et al. 2016. Elastomers for High Pressure Low Temperature HPLT Sealing. Presented at Offshore Technology Conference held in Houston, USA, 2-5 May 2016. OTC-27227-MS. http://dx.doi.org/10.4043/27227-MS
42. Cheung, P. R. and Beirute, R. M. 1985. Gas Flow in Cements. *J Pet Technol*. SPE-11207-PA http://dx.doi.org/10.2118/11207-PA
43. Cheung, P. R. and Myrick, B. D. 1983. Field Evaluation of an impermeable Cement System for Controlling Gas Migration. Presented at the SPE Annual Technical Conference and Exhibition, San Francisco, California, 5-8 October. SPE-11983-MS. http://dx.doi.org/10.2118/11983-MS
44. Christian, W. W., Chatterji, J., and Ostroot, G. W. 1976. Gas Leakage in Primary Cementing–A Field Study and Laboratory Investigation. *J Pet Technol.* SPE-5517-PA. https://doi.org/10.2118/5517-PA
45. Cong, C., Cui, C., Meng, X. et al. 2013. Degradation of hydrogenated nitrile-butadiene rubber in aqueous solutions of H2S or HCl. *Chemical Research in Chinese Universities*: **29**(4), 806–810. http://dx.doi.org/10.1007/s40242-013-2401-7
46. Cook, C. and Cunningham, W. C. 1977. Filtrate Control - A Key in Successful Cementing Practices. *J Pet Technol*. SPE-5898-PA. https://doi.org/10.2118/5898-PA
47. Cooke, C. E., Kluck, M. P., and Medrano, R. 1983. Field Measurements of Annular Pressure and Temperature during Primary Cementing. *J Pet Technol*. SPE-11206-PA. https://doi.org/10.2118/11206-PA

48. Dajiang, Z., Yuanhua, L., Huali, Z. et al. 2017. Experimental studies on CO2 corrosion of rubber materials for packer under compressive stress in gas wells. *Engineering Failure Analysis*: 80, 11-23. https://doi.org/10.1016/j.engfailanal.2017.01.012
49. Danenberger, E. P. 1993. Outer Continental Shelf Drilling Blowouts, 1971-1991. Presented in thte Offshore Technology Conference, Texas, Houston, 3-6 May. OTC-7248-MS. http://dx.doi.org/10.4043/7248-MS
50. Daou, F. and Piot, B. M. 2009. Cement-Slurry Performance and Set-Cement Properties vs. Microsilica Densification. *SPE Drill & Compl*. SPE-112701-PA. http://dx.doi.org/10.2118/112701-PA
51. Davies, R. J., Almond, S., Ward, R. S. et al. 2014. Oil and gas wells and their integrity: Implications for shale and unconventional resource exploitation. *Marine and Petroleum Geology*, **56**: 239-254. http://dx.doi.org/10.1016/j.marpetgeo.2014.03.001
52. Davis, T. W., and McCrady, D. D. 2008. Using Swellable Packers to Provide Annular Isolation for Multistage Fracture Treatments. Presented at SPE Annual Technical Conference and Exhibition, 21-24 September, Denver, Colorado, USA. SPE-115775-MS. http://dx.doi.org/10.2118/115775-MS
53. Dean, G. D. and Brennen, M. A. 1992. A Unique Laboratory Gas Flow Model Reveals Insight to Predict Gas Migration in Cement. Presented in the SPE Western Regional Meeting, Bakersfield, California, 30 March-1 April. SPE-24049-MS. http://dx.doi.org/10.2118/24049-MS
54. Dolog, R., Ventura, D., Khabashesku, V. et al. 2017. Nano-Enhanced Elastomers for Oilfield Applications. Presented at Offshore Technology Conference, Houston, Texas. 1-4 May. OTC-27609-MS. https://doi.org/10.4043/27609-MS.
55. DuPont. 2017. Oil and Gas Product Selector Guide.http://www.dupont.com/content/dam/dupont/products-and-services/plastics-polymers-and-resins/parts-and-shapes/kalrez/documents/KZE-A40042-00-A0217.pdf.
56. DuPont. 2013. Putting Science to Work, High Performance Materials: Oil and Gas Industry.http://www2.dupont.com/Oil_and_Gas/en_CA/assets/downloads/DuPont_High_Performance_Materials.pdf.
57. Dusseault, M. B., Jackson. R. E., and MacDonald. D. 2014.Towards a Road Map for Mitigating the Rates and Occurrences of Long-Term Wellbore Leakage. University of Waterloo and Geofirma Engineering Ltd. (May 22, 2014). http://geofirma.com/wp-content/uploads/2015/05/lwp-final-report_compressed.pdf.
58. Dylan Moore. 2015. http://www.cementkilns.co.uk/images/cem_psd.png
59. Eilers, L. H., Nelson, E. B., and Moran, L. K. 1983. High Temperature Cement Compositions – Pectolite, Scawtite, Truscotite or Xonoloite: Which Do You Want? *J Pet Technol* 35 (7): 1373-1377. SPE-9286-PA. https://doi.org/10.2118/9286-PA
60. Federal Highway Administration. 2017. Fly Ash Facts for Highway Engineers. *U.S. Department of Transportation, Federal Highway Administration,* 06.27.2017. https://www.fhwa.dot.gov/pavement/recycling/fach01.cfm

61. Fernández, C., and Castaño, P. 2016. Compatibility Behavior of Elastomers for PCP Applications. *NACE International*: NACE-2016-7106. https://www.onepetro.org/conference-paper/NACE-2016-7106.
62. Fisher, R.A. *The Design of Experiments. 8th edition*. Hafner Publishing Company, New York (1966).
63. Flitney, R. K. 2014. *Seals and Sealing Handbook*, sixth edition. Elsevier.
64. Garcia, J. A. and Clark, C. R. 1976. An Investigation of Annular Gas Flow Following Cementing Operations. Presented in the SPE Symposium on Formation Damage Control, Houston, Texas, 29-30 January. SPE-5701-MS. https://doi.org/10.2118/5701-MS
65. Gavioli, P., and Vicario, R. 2012. The Evolution of the Role of Openhole Packers in Advanced Horizontal Completions: From Novel Technology to a Critical Key to Success. *SPE Drill & Compl:* **27**(01), 75-93. SPE-132846-PA.http://dx.doi.org/10.2118/132846-PA
66. Grabowski, E. and Gillott, J. E. 1989. Effect of Replacement of Silica Flour with Silica Fume on Engineering Properties of Oil Well Cements at Normal and Elevated Temperatures and Pressures. *Cement and Concrete Research, Vol. 19*, pp 333-344. https://doi.org/10.1016/0008-8846(89)90023-9
67. Grinrod, M., Vassoy, B., and Dingsoyr, E. O. 1988. Development and Use of a Gas-Tight Cement. Presented at the SPE/IADC Drilling Conference, Dallas, Texas, 28 February-2 March. SPE-17258-MS. http://dx.doi.org/10.2118/17258-MS
68. Guidroz, B. C., Barton, S. P., and Hussain, M. 2011, January 1. Can You Protect Your Motor Without Sacrificing Performance? Presented at SPE/IADC Middle East Drilling Technology Conference and Exhibition, 24-26 October, Muscat, Oman. SPE-146576-MS. http://dx.doi.org/10.2118/146575-MS
69. Gustafson, S., 2014. Barrier management within the oil and gas industry: A comparison Study of the Implementation of Norway's and EU's Regulations with Focus on the Environment. Report No. 5465, Division of Risk Management and Societal Safety, Lund University, Lund, Sweden (May 2014).
70. Hauge, S and Øien, K. 2016. Guidance for Barrier Management in the Petroleum Industry. SINTEF Technology and Society, Safety Research. Report No. SINTEF A27623, Trondheim, Norway (September 2016).
71. Hoff, K., 2012. *Slender Well Design.* MS thesis. Norwegian University of Science and Technology (NTNU), Trondheim, Norway (June 2012).
72. Hopkins, H.A.2016. API Response to BSEE Report 2014-02, QC-FIT Evaluation of Seal Assembly and Cement Failures Interim Summary of Findings (dated December 2014). API Energy, Washington, DC (November 3, 2016). https://www.bsee.gov/sites/bsee.gov/files/seal-assembly-and-cement-failure-report-api-response-11032016.pdf.
73. Huerta, N., Hesse, M., Bryant, S. et al. 2012. Experimental Evidence for Self-Limiting Reactive Flow through a Fractured Cement Core: Implications for Time-Dependent Wellbore Leakage. *Environmental Science & Technology 47* (1): 269-275. https://dx.doi.org/10.1021/es3013003

74. Huerta, N. J., Checkai, D., and Bryant, S. L. 2009. Utilizing Sustained Casing Pressure Analog to Provide Parameters to Study CO_2 Leakage Rates Along a Wellbore. Presented at the SPE International Conference on CO2 Capture, Storage, and Utilization, San Diego, California, 2-4 November. SPE-126700-MS. https://doi.org/10.2118/126700-MS
75. Hyun-Ho, J., Hong C. K., Dong-Lyun, C. et al. 2008. Effects of Temperature on Hardness of Rubber Materials with Different Curing System. *Elastomers and Composites:* **43** (4), 213-220.
76. International Association of Drilling Contractors (IADC). 2017. Liner. *IADC*. 1 December 2017, http://www.iadclexicon.org/liner/ (Accessed 14 April 2018).
77. Ismail, I. and Harun. M. K. 2013. Evaluation of Rubber/Mid Steel Bonds Failure after Expose in Marine Environment. *International Journal of Chemical Engineering and Applications,* **4** (3): 119-123. DOI: 10.7763/IJCEA. 2013.V4.276.
78. *ISO/TS 16530-2:2013, Petroleum and natural gas industries -Well Integrity-Part 2: Well integrity for the operational phase,* first edition. 2013. Geneva, Switzerland: ISO.
79. Jackson, J and Smith, P. 2006. Development of an Expandable Drill-In Liner Hanger for Use in Problem-Well Scenarios: Case History. Presented at the 2006 Offshore Technology Conference, Houston, Texas, 1-4 May. OTC-18158-MS. https://doi.org/10.4043/18158-MS.
80. James Walker. 2017. Elastomer Engineering Guide. https://www.jameswalker.biz/de/pdf_docs/148-elastomer-engineering-guide.
81. James Walker. 2009. Elastomeric Seals & Components for the Oil & Gas Industry. 29 July 2009. https://www.jameswalker.biz/docs/jw_and_co/Oil_and_gas_guide.pdf.
82. Jassal, M., Chattopadhyay, R., and Ganguly, D. 2004. Synthesis and Characterization of Sodium Acrylate and 2-Acrylamido-2- Methylpropane Sulphonate (AMPS) Copolymer Gels. *Journal of Fibers and Ploymers*, **5** (2): 95-104. https://doi.org/10.1007/BF02902921.
83. Jin, H., Hong, C., Cho, D. et al. 2008. Effects of Temperature on Hardness of Rubber Materials with Different Curing System. *Journal of Elastomers and Composites,* **43** (4): 213-220.
84. Jones, R. R. and Carpenter, R. B. 1991. New Latex, Expanding Thixotropic Cement Systems Improve Job Performance and Reduce Costs. Presented in SPE International Symposium on Oilfield Chemistry, Anaheim, California, 20-22 February. SPE-21010-MS. https://doi.org/10.2118/21010-MS
85. Kelly, T. P. and Theiss, D. H., 1989. Rationale for Sealing Systems for Subsea Production Systems. Presented at 21st Annual Offshore Technology Conference, Houston, Texas. 1-4 May. OTC-6083-MS. https://doi.org/10.4043/6083-MS.
86. King, G.E. and King, D.E. 2013. Environmental Risk Arising from Well-Construction Failure - Differences between Barrier and Well Failure and Estimates of Failure Frequency across Common Well Types, Locations and Well Age. Presented at the SPE Annual Technical and Exhibition Conference, New Orleans, Louisiana, 30 September –2 October. SPE 166142. https://doi.org/10.2118/166142-MS.
87. Kiran, R., Teodoriu, C., Dadmohammadi, Y. et al. 2017. Identification and evaluation of well integrity and causes of failure of well integrity barriers (A review). *Journal of Natural Gas Science and Engineering* **45**: 511-526. ISSN 1875-5100, https://doi.org/10.1016/j.jngse.2017.05.009

88. Kubena, E., Ross, K. C., Pugh, T., and Huycke, J. 1991. Performance Characteristics of Drilling Equipment Elastomers Evaluated in Various Drilling Fluids. Presented at SPE/IADC Drilling Conference, 11-14 March, Amsterdam, Netherlands. SPE-21960-*MS*. http://dx.doi.org/10.2118/21960-MS
89. Kucyn, P. V. 1997. Prevention des manifestations du gaz entre le tubage et les parois du puits et de l'eruption incontrolee au cours du forage. *Gazovaja Promyshlennost.* Translated from Russian
90. Kuksov A. K., Krezub A. P., Mariampolskij N. A. et al. Oil and gas borehole plugging solution reagent – contains brown coal treated with alkali, organic silicon compound and lignosulphonate. Assigned to Borehole Consolidation Mu. 1992. SU patent 1 719 618.
91. LaMourie, M. J., Broadus J. M., and Geyer R. A. 2005. Gulf of Mexico. Gulf, North America. *Encyclopaedia Britannica*, 06 October 2005, https://www.britannica.com/place/Gulf-of-Mexico#ref408394 (Accessed 23 March 2017)
92. Lauridsen, O. Lootz, E., Husebo. T. et al. 2016. Barrier Management and the Interaction between Technical, Operational and Organizational Barrier Elements. Presented at the SPE Annual Technical Conference and Exhibition on Heath, Safety, Security, Environment, and Responsibility, Stavanger, Norway, 11-13 April. SPE-179364-MS. https://doi.org/10.2118/179364-MS.
93. Lea, F.M. 1971. *The Chemistry of Cement and Concrete*, third edition, Chemical Publishing Co., New York City, 177-202.
94. Lécolier, E., Rivereau, A., Ferrer, N. et al. 2010. Durability of Oilwell Cement Formulations Aged in H2S-Containing Fluids. *SPE Drill & Compl*: **25**(01). SPE-99105-PA. http://dx.doi.org/10.1007/10.2118/99105-PA
95. Levine, D. C., Thomas, E. W., Bezner, H. P. et al. 1979. Annular Gas Flow after Cementing: A Look at Practical Solutions. Presented at SPE Annual Technical Conference and Exhibition, Las Vegas, Nevada, 23-26 September. SPE-8255-MS. http://dx.doi.org/10.2118/8255-MS
96. Matthew, S. M. and Copeland, J. C. 1986. Control of Annular Gas Flow in the Deep Anadarko Basin. Presented at the SPE Deep Drilling and Production Symposium, Amarillo, Texas, 6-8 April. SPE-14980-MS. http://dx.doi.org/10.2118/14980-MS
97. MMS Safety Alert. U.S. Department of the Interior Minerals Management Service, Gulf of Mexico OCS Region. Safety Alert No. 216. October 22 2003. https://www.bsee.gov/sites/bsee.gov/files/safety-alerts/safety/safety-alert-no-216.pdf
98. Mohamed, A.O. and Al-Zuraigi, A. 2013. Liner Hangers Technology Advancement and challenges. Presented at the SPE Middle East Oil and Gas Show and Conference, Manama, Bahrain.10-13 March. SPE-164367-MS. https://doi.org/10.2118/164367-MS.
99. Moore, M. J., Campo, D. B., Hockaday, J.et al. 2002. Expandable Liner Hangers: Case Histories. Presented at Offshore Technology Conference, Houston, Texas. 6-9 May. OTC 14313-MS. https://doi.org/10.4043/14313-MS.
100. Moore, B., and Hamilton, T. A. P. 1993. Shallow Gas Hazard - The HSE Perspective. The Institute of Petroleum, London, UK.

101. Murray, S. J., Williamson, M. D., Gilham, S. et al. 1995. Well Design for Shallow Gas. Presented at SPE/IADC Drilling Conference, Amsterdam, Netherlands, 28 February-2 March. SPE-29343-MS. http://dx.doi.org/10.2118/29343-MS
102. Nelson B. E. and Guillot D. 2006. *Well Cementing*. Second Edition. Schlumberger, Sugar Land, Texas 77478.
103. Nishikawa, S. 1999. *Mechanism of Gas Migration after Cement Placement and Control of Sustained Casing Pressure*. Master's Thesis, Louisiana State University, Baton Rouge, Louisiana (May 1999).
104. NORSOK Standard D-010. 2014. Well integrity in drilling and well operations. (Rev. August 3, 2014) http://www.standard.no/pagefiles/1315/d-010r3.pdf
105. Omosebi, O. A. 2016. *Mechanical Degradation of Well Cement in HPHT Carbonic Acid Environment: Experimental Studies and Mathematical Modeling.* PhD dissertation, University of Oklahoma, Norman, Oklahoma (June 2016).
106. Parker Hannifin. 2002. Specialty Elastomers for Energy, Oil and Gas Industries. *Parker Hannifin Corporation Product Fact Sheet*, 1 October 2002, https://www.parker.com/literature/O-Ring%20Division%20Literature/EOGFactSheet.pdf. (Accessed July 3, 2017).
107. Parrott, L. J. 1995. Influence of cement type and curing on the drying and air permeability of cover concrete. *Magazine of Concrete Research* **47** (171): 103-111. https://doi.org/10.1680/macr.1995.47.171.103
108. PennCoat Inc. 2014. http://www.penncoatinc.com/blog/materialhardness/. Published October 10, 2014. (Accessed July 15, 2017).
109. Persson, B. N. J and Yang, C. 2008. Theory of the Leak-rate of Seals. *Journal of Physics: Condensed Matter* **20** (31): 315011(11pp). doi:10.1088/0953-8984/20/31/315011.
110. Petroleum Engineer's Guide - Chapter 10 - Cement additives, In *Petroleum Engineer's Guide to Oil Field Chemicals and Fluids (Second Edition)*, ed. Johannes Fink, Gulf Professional Publishing, Boston, 2015, Pages 317-367, ISBN 9780128037348, https://doi.org/10.1016/B978-0-12-803734-8.00010-2
111. Pinto G. H., Martins, A. L., Rocha J. M., et al. 2012. New Methodology for Gas Migration Prediction after Oilwell Cementing. AADE-12-FTCE-40. Presented in Houston, Texas, April 10 -11 2012.
112. Pleasants, C. W., Joseph, B. J., and Farrar, A. L. 2012. Reliable Completion System for Gas Migration Prevention. Presented at the SPE Annual Technical Conference and Exhibition, San Antonio, Texas, 8 –10 October. SPE-160217-MS. https://doi.org/10.2118/160217-MS.
113. Pour, M.M. and Moghadasi, J. 2007. New Cement Formulation That Solves Gas Migration Problems in Iranian South Pars Field Condition. Presented at the 15th SPE Middle East Oil & Gas Show and Conference, Bahrain International Exhibition Centre, Kingdom of Bahrain. 11-14 March. SPE-105663-MS. https://doi.org/10.2118/105663-MS.
114. Prince, P. K. 1990. Current Drilling Practice and the Occurrence of Shallow Gas. Presented in the Safety in Offshore Engineering: Proceedings of an international conference, London, UK, 25-26 April. SUT-AUTOE-v25-003. https://www.onepetro.org/conference-paper/SUT-AUTOE-v25-003

115. PSA. Norwegian Petroleum Safety Authority.2013. Principles for Barrier Management in the Petroleum Industry. http://www.ptil.no/getfile.php/1319891/PDF/Barrierenotatet%202013%20engelsk%20april.pdf.
116. Qamar, S. Z., Hiddabi, S. A., Pervez, T. et al. 2009. Mechanical Testing and Characterization of a Swelling Elastomer. *Journal of Elastomers and Plastics:* **41**(5), 415-431. http://dx.doi.org/10.1177/0095244309105248
117. Qamar, S. Z., Pervez, T., van de Velden, M. et al. 2012. Design and Fabrication of Test Facility for Longevity Testing of Elastomer Seals. Presented at International Mechanical Engineering Congress and Exposition in Houston, Texas, USA, 9-15 November 2012. IMECE2012-93145. http://dx.doi.org/10.1115/IMECE2012-93145
118. Rae, P. 1987. Cementing: Preventing Gas Migration during Setting. *Noroil No. 3*, 31
119. Rae, P., Wilkins, D., and Free, D. 1989. A New Approach to the Prediction of Gas Flow after Cementing. Presented in the SPE/IADC Drilling Conference, New Orleans, Louisiana, 28 February-3 March. SPE-18622-MS http://dx.doi.org/10.2118/18622-MS
120. Ràfols, F. P., 2016. *Modelling and Numerical Analysis of Leakage Through Metal -to-Metal Seals.* Licentiate thesis. Luleå University of Technology, Luleå, Sweden (March 2016).
121. Ràfols, F. P., Larsson, R. and Almqvist, A. 2015. Modelling and Numerical Analysis of Leakage on Metal-to-Metal Seals. *Tribology International* **94** (2016): 421-427. http://dx.doi.org/10.1016/j.triboint.2015.10.003 .
122. Rocha-Valadez, T., Hasan, A. R., Mannan, S. et al. 2014. Assessing Wellbore Integrity in Sustained-Casing-Pressure Annulus. *SPE Drilling & Completion* **29** (1): 131-138. SPE-169814-PA. https://doi.org/10.2118/169814-PA
123. Ron Nida. 2005. Liner Hanger System Increases Installation Success. Hallburton Energy Services (March/April 2005). http://iadc.org/dcpi/dc-maraprl05/March05-expand.pdf.
124. Rupak K. K. 2007. Leakage behind Casing. Norwegian University of Science and Technology, Trondheim, Norway
125. Sabins, F. L. and Sutton, D. L. 1986. The Relationship of Thickening Time, Gel Strength, and Compressive Strength of Oilwell Cements. *SPE Prod Eng*. SPE-11205-PA.http://dx.doi.org/doi:10.2118/11205-PA
126. Sabins, F. L., Tinsley, J. M., and Sutton, D. L. 1982. Transition Time of Cement Slurries between the Fluid and Set States. *SPE J*. SPE-9285-PA. http://dx.doi.org/10.2118/9285-PA
127. Salehi, S. 2013. Modelling Near Wellbore Leakage Pathways in Shale Gas Wells: Investigating Short and Long Terms Wellbore Integrity. Presented at US EPA Technical Workshop on Well Construction/Operation and Subsurface Modelling, Research Triangle Park, North Carolina, April 16-17.
128. Schweitzer P. A. 2000. *Mechanical and Corrosion-Resistant properties of Plastics and Elastomers*, First Edition, Boca Raton, Florida, USA: CRC Press.
129. Shakirah, S. 2008. A New Approach for Optimizing Cement Design to Eliminate Microannulus in Steam Injection Wells. Presented in the International Petroleum Technology Conference, Kuala Lumpur, Malaysia, 3-5 December. IPTC-12407-MS. https://doi.org/10.2523/IPTC-12407-MS

130. Seidel, F.A. and Greene, T.G., 1985. Use of Expanding Cement Improves Bonding and Aids in Eliminating Annular Gas Migration in Hobbs Grayburg-San Andres Wells. SPE Annual Technical Conference and Exhibition, Las Vegas, Nevada, 22-26 September. SPE-14434-MS. http://dx.doi.org/10.2523/14434-MS
131. Skalle, P. and Sveen, J. 1991. Emulsion Cement. Presented in the Offshore Europe, Aberdeen, United Kingdom, 3-6 September. SPE-23075-MS. http://dx.doi.org/10.2118/23075-MS
132. Smith M. Louis, 2012. A Review of Offshore Blowouts and Spills to Determine Desirable Capabilities of a Subsea Capping Stack. MS Thesis, LSU, May 2012. http://etd.lsu.edu/docs/available/etd-04232012-211924/unrestricted/Smith_Thesis.pdf.
133. Stiles, D. A. and Baret, J. F. 1993. Sedimentation and Free Water of Cement Slurries: Mathematical Models and Practical Solutions. Presented in the Low Permeability Reservoirs Symposium, Denver, Colorado, 26-28 April. SPE-25866-MS. https://doi.org/10.2118/25866-MS
134. Stone, W. H. and Christian, W. W. 1974. The Inability of Unset Cement to Control Formation Pressure. Presented at the SPE Symposium of Formation Damage Control, New Orleans, Louisiana, USA, February 7-8. SPE-4783-MS. http://dx.doi.org/10.2118/4783-MS
135. Stormont, J. C., Fernandez, S. G. Taha, M. R. et al. 2017. Gas flow through cement-casing microannuli under varying stress conditions. *Geomechanics for Energy and the Environment* **13**: 1-13. https://doi.org/10.1016/j.gete.2017.12.001
136. Strand, G., 2017. *Well Safety: Risk Control in the Drilling Phase of Offshore Wells.* PhD Thesis. Norwegian University of Science and Technology (NTNU), Trondheim, Norway (June 2017).
137. Sutton, D. L., Sabins, F. L., and Paul, R. 1984. New Evaluation for Annular Gas-Flow Potential. *Oil Gas Journal* (December 17 1984) No. 51, 109-112. http://www.worldcat.org/title/new-evaluation-for-annular-gas-flow-potential/oclc/4434501598&referer=brief_results
138. Talabani, S., Hareland, G., and Islam, M. R. 1997. Gas Migration Eliminated Through Correct Cement Design Including Elastomers. Presented in the SPE/IADC Middle East Drilling Technology Conference, Bahrain, 23-25 November. SPE-39279-MS. http://dx.doi.org/10.2118/39279-MS
139. Tao, Q., Checkai, D., and Bryant, S. L. 2010. Permeability Estimation for Large-Scale Potential CO2 Leakage Paths in Wells Using a Sustained-Casing-Pressure Model. Presented at the SPE International Conference on CO_2 Capture, Storage, and Utilization, New Orleans, Louisiana, 10-12 November. SPE-139576-MS. https://doi.org/10.2118/139576-MS
140. Tarco, J. C. and Asghari, K. 2010. Experimental Study of Stability and Integrity of Cement in Wellbores Used for CO_2 Storage. *Journal of Canadian Petroleum Technology* **49** (10): 37-44. SPE-142004-PA. https://doi.org/10.2118/142004-PA
141. Technology Assessment and Research Study Number 195: "Analysis of Platform Vulnerability to Cratering Induced by a Shallow Gas Flow."
142. Technology Assessment and Research Study Number 27: "Study of Cementing Practices Applied to the Shallow Casing in Offshore Wells."

143. Thorogood, J. L. 2017. Systems Approach to Well Control Barrier Management During Drilling Operations. Presented at the IADC/SPE Drilling Conference and Exhibition, Hague, The Netherland. 14-16 March. SPE/IADC-184668-MS. https://doi.org/10.2118/184668-MS.
144. Tinmannsvik, R. K., Albrecthsen, E. B., Bråtveit, M. et.al. 2011. The Deepwater Horizon accident: Causes, learning points and recommendations for the Norwegian continental shelf. Report No. SINTEF A19148, SINTEF, Norway (May 2011). http://www.ptil.no/getfile.php/1314694/Tilsyn%20p%C3%A5%20nettet/vrige/Deepwater%20Horizon%20-%20SINTEF%20-%20Executive%20summary.pdf.
145. Tinsley, J. M., Miller, E. C., Sabins, F. L. et al. 1980. Study of Factors Causing Annular Gas Flow Following Primary Cementing. *J Pet Technol*. SPE-8257-PA. http://dx.doi.org/10.2118/8257-PA
146. Torbergsen, H. B., Haga, H. B., Sangeslan, S. et al. 2012. An Introduction to Well Integrity. Document Rev 0, 04 December 2012. Norwegian Oil and Gas Association's, Norwegian University of Science and Technology and University of Stavanger. https://www.norskoljeoggass.no/Global/2013%20Dokumenter/Andre%20vedlegg/INTRODUCTION%20TO%20WELL%20INTEGRITY%20-%2004%20December%202012.pdf
147. Tynan, C. 2016. Successful selection of oil and gas seals, World Pumps, Volume 2016, Issue 9, September 2016, Pages 28-30, ISSN 0262-1762, http://dx.doi.org/10.1016/S0262-1762(16)30235-8
148. Van Dinh, C., and Kubouchi, M. 2012. An Approach for the Prediction of Blistering on Polymer- Steel Lining Systems Exposed to an Aqueous Environment. *Industrial & Engineering Chemistry Research*: **51**(36), 11681-11687. http://dx.doi.org/10.1021/ie202975s
149. Visakh, P. M., Thomas, S., Chandra, A. K. et al. (Eds.). 2013. *Advances in Elastomers I Blends and Interpenetrating Networks*, Volume 11, Advanced Structured Materials, Berlin Heidelberg: Springer-Verlag. http://dx.doi.org/10.1007/978-3-642-20925-3
150. Walker. 2011. *Elastomer Engineering Guide*. 10 November 2011, https://www.jameswalker.biz/de/pdf_docs/148-elastomer-engineering-guide (Accessed 23 June 2017)
151. Walvekar, S. and Jackson, T. 2006. Expandable Technology Improves Reliability of Conventional Liner Hanger Systems. Presented at the IADC/SPE Drilling Conference, Miami, Florida. 21-23 February. SPE-99186-MS. https://doi.org/10.2118/99186-MS.
152. Wang, Z., Chen, C., Liu, Q. et al. 2017. Extrusion, slide, and rupture of an elastomeric seal. *Journal of the Mechanics and Physics of Solids*: 99, 289–303. https://doi.org/10.1016/j.jmps.2016.12.007
153. Wang, X., Sadana, A. K., and Mathur, V. 2015. Water-Swellable Elastomers for Heavy Brine Environments. Presented at SPE Annual Technical Conference and Exhibition, 28-30 September, Houston, Texas, USA. SPE-174825-MS. http://dx.doi.org/10.2118/174825-MS
154. Wang W. J. 1996. The Development and Applications of CX-18 Anti-channelling Agent. *J Xi'an Pet Inst*, **11**(5):6-7,50-53.
155. Wardak, A., Williford, J., Walker, A. et al. 2010. Ensuring Success on an Extended-Reach Well with Expandable Liner Hangers and Advanced Software Modeling. Presented at the IADC/SPE Asia Pacific Drilling Technology Conference and Exhibition, Ho Chi Minh City, Vietnam 1-3 November. IADC/SPE-136300. https://doi.org/10.2118/136300-MS.

156. Watson, T.L. and Bachu, S. 2007. Evaluation of the Potential for Gas and CO_2 Leakage along Wellbores. Presented at the SPE E&P Environmental and Safety Conference, Galveston, Texas, 5–7 March. SPE 106817. https://doi.org/10.2118/106817-PA.
157. Watters, L. T. and Sabins, F. L. 1980. Field Evaluation of Method to Control Gas Flow Following Cementing. Presented in the SPE Annual Technical Conference and Exhibition, Dallas, Texas, 21-24 September. SPE-9287-MS. http://dx.doi.org/10.2118/9287-MS
158. Webster, W. W. and Eikerts, J. V. 1979. Flow After Cementing: A Field and Laboratory Study. Presented in the SPE Annual Technical Conference and Exhibition, Las Vegas, Nevada, 23-26 September. SPE-8259-MS. https://doi.org/10.2118/8259-MS
159. Williford, J and Smith, P. 2007. Expandable Liner Hanger Resolves Sealing Problems and Improves Integrity in Liner Completion Scenarios. Presented at the SPE 2007 Production and Operations Symposium, Oklahoma City, Oklahoma, 31 March-3 April. SPE-106757-MS. https://doi.org/10.2118/106757-MS.
160. Wu, B., Doble, R., Turnadge, C. et.al. 2016. Well Failure Mechanism and Conceptualisation of Reservoir-Aquifer Failure Pathways. Presented at the SPE Asia Pacific Oil & Gas Conference and Exhibition, Perth, Australia, 25-27 October. SPE-182460-MS. https://doi.org/10.2118/182460-MS.
161. Xu, R. and Wojtanowicz, A.K. 2001. Diagnosis of Sustained Casing Pressure from Bleed-off/Buildup Testing Patterns. Presented at the SPE Production and Operations Symposium, Oklahoma City, Oklahoma, 24–27 March. SPE-67194-MS. http://dx.doi.org/10.2118/67194-MS
162. Xu, R. 2002. *Analysis of Diagnostic Testing of Sustained Casing Pressure in Wells*. PhD Dissertation, Louisiana State University, Baton Rouge, Louisiana (December 2002).
163. Xu, R. and Wojtanowicz, A. K. 2003. Diagnostic Testing of Wells with Sustained Casing Pressure-An Analytical Approach. Presented at the Canadian International Petroleum Conference, Calgary, Alberta, 10-12 June. PETSOC-2003-221. https://doi.org/10.2118/2003-221
164. Xu, R. and Wojtanowicz, A.K. 2016. Pressure buildup test analysis in wells with sustained casing pressure. *Journal of Natural Gas Science and Engineering* **38**: 608-620. https://doi.org/10.1016/j.jngse.2016.12.033